Qualitative and quantitative assessment of peripheral neurotoxicity

Dissertation zur Erlangung

des akademischen Grades eines

Doktors der Naturwissenschaften

(Dr. rer. nat.)

vorgelegt von

Anna-Katharina Holzer

an der

Universität Konstanz

Mathematisch-Naturwissenschaftliche Sektion

Fachbereich Biologie

Konstanz, 2022

Tag der mündlichen Prüfung: 03.06.2022

1. Referent: Prof. Dr. Marcel Leist

2. Referent: apl. Prof. Dr. Aswin Mangerich

Danksagung

Zu Beginn möchte ich mich bei Marcel für das Überlassen dieses spannenden und fordernden Projekts, wie auch für die kritischen Diskussionen und das Vertrauen über die vielen Jahre hinweg bedanken.

Außerdem möchte ich Herrn apl. Prof. Dr. Aswin Mangerich für die Übernahme des Zweitgutachtens, wie auch für die Unterstützung als Mitglied meines Thesiskomitees danken. Bedanken möchte ich mich auch bei Herrn Prof. Dr. Alexander Bürkle für die Übernahme des Vorsitzes meiner Prüfungskommission.

Ich möchte ich mich von Herzen bei allen Freunden und Kollegen in der AG Leist bedanken, für die gemeinsame Zeit an der Uni und auch darüber hinaus. Neben all den faszinierenden Themen und klugen Köpfen dieser Arbeitsgruppe hat mich in den letzten Jahren vor allem das Miteinander begeistert und durch die Zeit der Doktorarbeit getragen. Vielen Dank für viele hilfreiche Diskussionen, aufmunternde Worte und die produktive Zusammenarbeit an verschiedensten Projekten. An die gemeinsamen Weihnachtsfeiern, Ausflüge, Kaffee- und Eispausen, den Klatsch und Tratsch zwischen Tür und Angel, ja, sogar an die Bastel- und Sing-Sessions werde ich immer wieder gerne zurückdenken!

Ein spezieller Dank geht hier vor allem auch an Christiaan. Ohne seine unermüdliche Unterstützung mit immerneuen CaFFEE-Versionen und allerlei anderer Expertise wäre vieles in diesem Projekt so nicht möglich gewesen. Danke für all die ausgiebigen Diskussionen, sei es über Ca^{2+}-Imaging, NGN1 oder Essen.
Bedanken möchte ich mich auch bei Marion für ihre Unterstützung im Labor und ihr immer offenes Ohr.
Ganz besonders möchte ich Xenia, Sophie und Steffi für die letzten Jahre danken. Mit ihnen wurde es in der Stammzellkultur nie langweilig, und auch für einen gelungenen Ausgleich zur Arbeit mit Wein, Trash-TV, Bergausflügen, Bouldern und zuletzt auch über Skype war mit ihnen immer gesorgt.

Für das geduldige Korrekturlesen der Manuskripte und meiner Dissertation möchte ich mich bei Sandra, Karina, Steffi und Christiaan bedanken.

Allen meinen Freunden, die meine Zeit in Konstanz unvergesslich gemacht haben, gilt ein herzliches Dankeschön. Erwähnen möchte ich hier natürlich auch die Heimat, die mir in den letzten zehn Jahren so viele tolle neue Freunde und Begegnungen beschert und meine Jugend in bester Blüte erhalten hat.

Karina und Sandra, die mich mein ganzes Studium über begleitet und unterstützt haben, möchte ich von Herzen danken. Solche wunderbaren Freunde zu haben ist nicht selbstverständlich und ihr bedeutet mir unglaublich viel.

Der größte Dank gilt meiner Familie. Danke für eure bedingungslose Unterstützung und euren Rückhalt. Ohne euch wäre das alles so nicht möglich gewesen. Ich bin unbeschreiblich froh ein Teil der besten Herde der Welt zu sein.

Zu guter Letzt möchte ich mich bei Michael bedanken. Danke, dass du mit mir durch Sturm und Verderben segelst, Gipfel erklimmst und auch die kleinen Dinge des Lebens genießt. Danke, dass du mich immer unterstützt, mich motivierst und einfach für mich da bist.

Abstract

Peripheral neurotoxicity represents a key challenge in drug development. Particularly with chemotherapeutic agents, peripheral neurotoxicity is a commonly observed side effect that can be dose-limiting and can affect patients' quality of life beyond therapy. Drug development, as well as risk assessment would benefit from a better understanding of such peripheral neuropathies, but the lack of human-relevant experimental models limits further research. The aim of this work was to develop new approaches to assess peripheral neurotoxicity *in vitro* by using peripheral neurons derived from human induced pluripotent stem cells (iPSCs). The establishment of a method to assess toxicant-induced impairments in neuronal signaling was of particular interest, since peripheral neuropathies manifest primarily as sensory symptoms, including aberrant pain perception. In a first step, the fate specification of a conventional protocol for the differentiation of human peripheral neurons was directed toward nociceptive neurons by exploiting the principle of transcriptional programming, in this case by controlled overexpression of an NGN1-transgene. Comprehensive functional characterization confirmed that the resulting neurons were peripheral neurons with nociceptor features (PNN) capable of stable pain receptor signaling via transient receptor potential-V1 (TRPV1) receptors and the purinergic receptor P2X3. In a next step, functional PNN were explored regarding their capacity to model chemotherapy-induced peripheral neuropathy (CIPN)-related alterations in pain signaling. For the evaluation of such signaling responses detected in Ca^{2+}-imaging experiments, a dedicated software was developed. It enabled the image-based quantification of changes in intracellular Ca^{2+}-concentration of hundreds of individual cells simultaneously. PNN were found to be capable of displaying CIPN-related functional impairments upon exposure to the chemotherapeutic drug oxaliplatin. Altered signaling through TRPV1 as well as the development of allodynia-like mechanical hypersensitivity were detected. This proves the usefulness of PNN as an *in vitro* model to study CIPN. Finally, the relevance of PNN for pre-clinical evaluations of chemotherapeutic agents was strengthened by a study on the substance class of proteasome inhibitors, which are associated with painful CIPN *in vivo*. Specific attenuation of purinergic P2X3 pain receptor signaling and cytoskeletal reorganization were identified as early indicators of cellular stress induced by non-cytotoxic concentrations of proteasome inhibitors. PNN exhibited superior sensitivity towards proteasome inhibitor-induced alterations compared to immature peripheral

neurons. This demonstrated the importance of test methods that are specific to the target cell type and developmental stage *in vivo*. The studies presented in this thesis expand the panel of test methods for identifying peripheral neurotoxicants, thus improving risk assessment. Moreover, new avenues are opened for a better understanding of peripheral neuropathies. This may allow future improvements of drug development in terms of chemotherapeutic agents with fewer side effects, but also pharmacological countermeasures for CIPN.

Zusammenfassung

Die periphere Neurotoxizität stellt eine große Herausforderung in der Arzneimittelentwicklung dar. Insbesondere bei Chemotherapeutika ist die periphere Neurotoxizität eine häufig beobachtete Nebenwirkung, die dosis-limitierend sein kann und die Lebensqualität der Patienten nach der Therapie beeinträchtigen kann. Die Entwicklung und die Risikobewertung von Medikamenten würden von einem besseren Verständnis solcher peripheren Neuropathien profitieren, aber der Mangel an human-relevanten Versuchsmodellen schränkt die weitere Forschung ein. Ziel dieser Arbeit war die Entwicklung neuer Konzepte zur Bewertung der peripheren Neurotoxizität *in vitro* unter Verwendung peripherer Neuronen, die aus humanen induzierten pluripotenten Stammzellen (iPSCs) gewonnen werden. Die Erarbeitug einer Methode zur Evaluierung toxikologisch bedingter Beeinträchtigungen der neuronalen Signalübertragung war von besonderem Interesse, da sich periphere Neuropathien vor allem als sensorische Symptome, einschließlich einer gestörten Schmerzwahrnehmung, manifestieren. In einem ersten Schritt wurde das Entwicklungsziel eines konventionellen Protokolls für die Differenzierung humaner peripherer Neuronen auf nozizeptive Neuronen ausgerichtet. Dafür wurde das Prinzip der transkriptionellen Programmierung, in diesem Fall durch kontrollierte Überexpression eines NGN1-Transgens, ausgenutzt. Eine umfassende funktionelle Charakterisierung bestätigte, dass es sich bei den resultierenden Neuronen um periphere Neuronen mit Nozizeptor-Eigenschaften (PNN) handelte, die zur stabilen Schmerzrezeptor-Signaltransduktion über TRP (englisch „transient receptor potential) V1-Rezeptoren und den purinergen Rezeptor P2X3 fähig sind. In einem nächsten Schritt wurden funktionelle PNN auf ihre Fähigkeit hin untersucht, Veränderungen der Schmerzsignalübertragung zu modellieren, die mit der Chemotherapie-induzierten peripheren Neuropathie (CIPN) zusammenhängen. Für die Auswertung solcher Signalreaktionen, die in Ca^{2+}-Bildgebungsexperimenten ermittelt werden, wurde eine spezielle Software entwickelt. Diese ermöglichte die bildgestützte Quantifizierung von Veränderungen der intrazellulären Ca^{2+}-Konzentration von Hunderten von Einzelzellen gleichzeitig. Es wurde gezeigt, dass PNN in der Lage sind, CIPN-ähnliche funktionelle Beeinträchtigungen zu entwickeln, wenn sie dem Chemotherapeutikum Oxaliplatin ausgesetzt sind. Eine veränderte Signalübertragung durch TRPV1 sowie die Entwicklung einer allodynie-ähnlichen mechanischen Überempfindlichkeit wurden festgestellt. Dies belegte die Nützlichkeit der PNN als *in vitro*-Modell zur Erforschung von CIPN.

Abschließend wurde die Relevanz von PNN für die präklinische Prüfung von Chemotherapeutika durch eine Studie über die Substanzklasse der Proteasom-Inhibitoren untermauert, die *in vivo* mit schmerzhafter CIPN verbunden sind. Eine spezifische Abschwächung der purinergen P2X3-Schmerzrezeptor-Signalübertragung und eine Reorganisation des Zytoskeletts wurden als frühe Indikatoren für zellulären Stress identifiziert, der durch nicht-zytotoxische Konzentrationen von Proteasom-Inhibitoren ausgelöst wird. PNN zeigten im Vergleich zu unreifen peripheren Neuronen eine höhere Empfindlichkeit gegenüber durch Proteasom-Inhibitoren hervorgerufenen Veränderungen. Dies verdeutlichte, wie wichtig Testmethoden sind, die auf den Ziel-Zelltyp und das Entwicklungsstadium *in vivo* abgestimmt sind. Die in dieser Arbeit vorgestellten Studien erweitern das Spektrum der Testmethoden zur Identifizierung peripherer neurotoxischer Stoffe und optimieren damit die Risikoanalyse. Darüber hinaus wurden neue Wege zu einem besseren Verständnis der peripheren Neuropathien eröffnet. Dies könnte künftige Verbesserungen bei der Arzneimittelentwicklung im Hinblick auf Chemotherapeutika mit geringeren Nebenwirkungen, aber auch auf pharmakologische Behandlungsmöglichkeiten für CIPN ermöglichen.

List of publications

Publications integrated in this thesis

Results chapter 2.1.:

Generation of human nociceptor-enriched sensory neurons for the study of pain-related dysfunctions

Holzer A-K, Karreman C, Suciu I, Furmanowsky LS, Wohlfarth H, Loser D, Dirks WG, González EP, Leist M (2022) *bioRxiv.* doi: 10.1101/2022.02.19.480828

Results chapter 2.2.:

Specific attenuation of purinergic signaling during bortezomib-induced peripheral neuropathy

Holzer A-K, Suciu I, Karreman C, Goj T, Leist M (2022) *bioRxiv.* doi: 10.1101/2022.02.17.479688

Results chapter 2.3.:

CaFFEE: A Program for evaluating time courses of Ca^{2+} dependent signal changes of complex cells loaded with fluorescent indicator dyes

Karreman C, **Holzer A-K**, Klima S, Leist M (2020) *ALTEX* 37, 332–336. doi: 10.14573/altex.2003191

Publications not integrated in this thesis

Neurodevelopmental toxicity assessment of flame retardants using a human DNT in vitro testing battery

Klose J, Pahl M, Bartmann K, Bendt F, Blum J, Dolde X, Förster N, **Holzer A-K**, Hübenthal U, Keßel HE, Koch K, Masjosthusmann S, Schneider S, Stürzl LC, Woeste S, Rossi A, Covaci A, Behl M, Leist M, Tigges J, Fritsche E (2021) *Cell Biol Toxicol.* doi: 10.1007/s10565-021-09603-2

Establishment of an a priori protocol for the implementation and interpretation of an in-vitro testing battery for the assessment of developmental neurotoxicity
Masjosthusmann S, Blum J, Bartmann K, Dolde X, **Holzer A-K**, Stürzl LC, Keßel EH, Förster N, Dönmez A, Klose J, Pahl M, Waldmann T, Bendt F, Kisitu J, Suciu I, Hübenthal U, Mosig A, Leist M, Fritsche E (2020) *EFSA Support Publ* 17. doi: 10.2903/sp.efsa.2020.EN-1938

The EU-ToxRisk method documentation, data processing and chemical testing pipeline for the regulatory use of new approach methods
Krebs A, van Vugt-Lussenburg BMA, Waldmann T, Albrecht W, Boei J, ter Braak B, Brajnik M, Braunbeck T, Brecklinghaus T, Busquet F, Dinnyes A, Dokler J, Dolde X, Exner TE, Fisher C, Fluri D, Forsby A, Hengstler JG, **Holzer A-K**, Janstova Z, Jennings P, Kisitu J, Kobolak J, Kumar M, Limonciel A, Lundqvist J, Mihalik B, Moritz W, Pallocca G, Cediel Ulloa AP, Pastor M, Rovida C, Sarkans U, Schimming JP, Schmidt BZ, Stöber R, Strassfeld T, van de Water B, Wilmes A, van der Burg B, Verfaillie CM, von Hellfeld R, Vrieling H, Vrijenhoek NG, Leist M (2020) *Arch Toxicol* 94, 2435-2461. doi: 10.1007/s00204-020-02802-6

Lapachol acetylglycosylation enhances its cytotoxic and pro-apoptotic activities in HL60 cells
Marques LB, Ottoni FM, Pinto MCX, Ribeiro JM, de Sousa FS, Weinlich R, de Victo NC, Kisitu J, **Holzer A-K**, Leist M, Alves RJ, Souza-Fagundes EM (2020) *Toxicol In Vitro* 65, 104772. doi: 10.1016/j.tiv.2020.104772

Time and space-resolved quantification of plasma membrane sialylation for measurements of cell function and neurotoxicity
Kranaster P, Karreman C, Dold JEGA, Krebs A, Funke M, **Holzer A-K**, Klima S, Nyffeler J, Helfrich S, Wittman C, Leist M (2020) *Arch Toxicol* 94, 449-467. doi: 10.1007/s00204-019-02642-z

The influence of structural gradients in large pore organosilica materials on the capabilities for hosting cellular communities
Bronner H, **Holzer A-K**, Finke A, Kunkel M, Marx A, Leist M, Polarz S (2020) *RSC Adv* 10, 17327-17335. doi: 10.1039/D0RA00927J

Development of a neural rosette formation assay (RoFA) to identify neurodevelopmental toxicants and to characterize their transcriptome disturbances
Dreser N, Madjar K, **Holzer A-K**, Kapitza M, Scholz C, Kranaster P, Gutbier S, Klima S, Kolb D, Dietz C, Trefzer T, Meisig J, v Thriel C, Henry M, Berthold MR, Blüthgen N, Sachinidis A, Rahnenführer J, Hengstler JG, Waldmann T, Leist M (2020) *Arch Toxicol* 94, 151-171. doi: 10.1007/s00204-019-02612-5

A structure-activity relationship linking non-planar PCBs to functional deficits of neural crest cells: new roles for connexins
Nyffeler J, Chovancova P, Dolde X, **Holzer A-K**, Purvanov V, Kindinger I, Kerins A, Higton D, Silvester S, van Vugt-Lussenburg BMA, Glaab E, van der Burg B, Maclennan R, Legler DF, Leist M (2018) *Arch Toxicol* 92, 1225-1247. doi: 10.1007/s00204-019-02612-5

Stem cell transcriptome responses and corresponding biomarkers that indicate the transition from adaptive responses to cytotoxicity
Waldmann T, Grinberg M, König A, Rempel E, Schildknecht S, Henry M, **Holzer A-K**, Dreser N, Shinde V, Sachinidis A, Rahnenführer J, Hengstler JG, Leist M (2017) *Chem Res Toxicol* 30, 905-922. doi: 10.1021/acs.chemrestox.6b00259

Table of contents

1 Introduction

1.1 The peripheral nervous system

The peripheral nervous system (PNS) is the mediator between the brain and spinal cord, i.e., the central nervous system (CNS), and the muscles, organs, and skin. It transfers information from other parts of the body to the CNS, allowing us to recognize a diverse range of stimuli. Furthermore, it enables us to react to such stimuli by transmitting information from the CNS to the periphery, e.g., the limbs. The PNS is divided into two main systems based on the type of signals they convey: the somatic nervous system and the autonomic nervous system (Catala and Kubis 2013). The autonomic nervous system unconsciously controls smooth muscles of the viscera and glands and is in turn divided into three sections: the sympathetic, parasympathetic and enteric divisions (Gabella 2001). The somatic nervous system, in contrast, is in charge of transmitting all conscious signals. It consists, on the one hand, of efferent motor nerves that control voluntary movements and, on the other hand, of afferent sensory nerves that form the (somato-) sensory nervous system (SNS) and convey signals from sensory receptors distributed throughout the body (Catala and Kubis 2013). Highly coordinated developmental processes are required to give rise to this broad spectrum of subtypes of peripheral neurons with all their different functions and tissue targets.

1.1.1 Development of the peripheral nervous system

Embryonic development starts with the fertilization of the oocyte. The resulting zygote undergoes cell division until the stadium of the multicellular morula is reached. Then, cells start to differentiate into the outer and the inner cell mass, thereby forming the blastocyst (Elshazzly et al. 2021; O'Rahilly and Müller 2010). The embryo develops from the inner cell mass. During gastrulation, the inner cell mass forms the three germ layers: the ectoderm, mesoderm and endoderm. Different tissues and organs develop from each of the three germ layers. The liver, gut and bladder develop from the endoderm, while, e.g., skeleton, heart, and kidneys are formed by the mesoderm (Elshazzly et al. 2021; Ferretti and Hadjantonakis 2019; Grapin-Botton and Melton 2000). The ectoderm is further divided into the non-neural or surface ectoderm, giving rise to the skin, and the neural ectoderm (Elshazzly et al. 2021; O'Rahilly and Müller 2010).

The neural ectoderm undergoes neurulation. During this process, the neural ectoderm gives rise to the neural plate, which forms the neural tube by bending upwards until the neural folds fuse and close the neural tube (Nikolopoulou et al. 2017). At the neural plate border, which is the dorsal-most part of the neural tube, neural crest cells (NCCs) are formed in response to inductive signals from the non-neural ectoderm and the underlying mesoderm (Selleck and Bronner-Fraser 1995). They undergo epithelial-to-mesenchymal transition and start to delaminate from the neural tube. NCCs can be classified according to their origin along the neuraxis: cranial, cardiac, vagal, trunk, and sacral (Marmigère and Ernfors 2007). Specific pathways of migration and differentiation capacities are attributed to the single groups, with the trunk NCCs giving rise to cells of the PNS, comprising the autonomic and the somatic nervous system. The delaminated trunk NCCs migrate along a ventral pathway (Fig. 1.1A). NCCs that differentiate towards cells of the autonomic lineage, including enteric and sympathetic neurons, migrate further ventral than NCCs that produce cells of the sensory lineage. These sensory neurons form the dorsal root ganglia (DRG) in close proximity to the spinal cord (Fig. 1.1B,C).

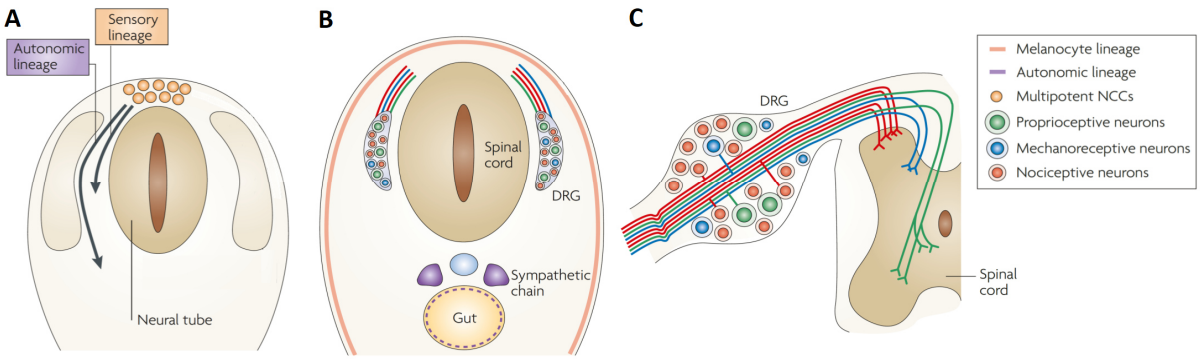

Figure 1.1: The development of the peripheral nervous system

(A) Trunk neural crest cells (NCCs) of the autonomic and the sensory lineage delaminate from the dorsal part of the neural tube and start to migrate ventrally. **(B)** NCCs with autonomic lineage commitment differentiate into neurons that form the sympathetic chain or innervate the gut. The NCCs of the sensory lineage coalesce into the dorsal root ganglia (DRG) where they specify into three main types of sensory neurons: proprioceptive (green, large), mechanoreceptive (blue) and nociceptive (red, small) neurons. **(C)** Cell bodies of sensory neurons reside in the DRGs. The neurons are pseudo-unipolar with only one process, the axon, extending from each cell body. This axon bifurcates and extends to the periphery innervating target tissues such as organs, skin or joints, and to the spinal cord, where it connects to the CNS. Figure adapted and modified based on (Marmigère and Ernfors, 2007)

1.1.2 Development of the sensory nervous system

The sensory neurons can be grouped into three subclasses: proprioceptors, mechanoceptors and nociceptors. These sensory neuronal cell types develop during different waves of trunk sensory neurogenesis (Fig. 1.2). These waves are characterized by the expression of distinct basic helix-loop-helix transcription factors, the neurogenins, which bias NCCs to the sensory lineage (Bhatt et al. 2013; Ma et al. 1999; Marmigère and Ernfors 2007). During the first wave, the subset of early migratory NCCs transiently expresses neurogenin 2 (NGN2) and migrate into the coalescing DRG (Ma et al. 1999). Next, the postmigratory NCCs down-regulate the expression of NGN2, while BRN3A expression is induced. NCCs of this first wave particularly develop into mechanoreceptors and proprioceptors. At early stages of development, these types of sensory neurons are characterized by the expression of the Runt related transcription factor RUNX3 and the tropomyosin receptor kinase (Trk) C, which is the receptor for neurotrophin-3 (Chen AI et al. 2006; Kramer et al. 2006; Levanon et al. 2001; Tessarollo et al. 1993). Expression of both factors is maintained in proprioceptors, while RUNX3 is down-regulated during the development of mechanoreceptors. The latter are characterized by distinct expression patterns of tyrosine receptor kinase (Trk) B, the receptor for the brain-derived neurotrophic factor (BDNF) and TrkC (Chen AI et al. 2006; Klein et al. 1991; Kramer et al. 2006; Tessarollo et al. 1993).

The second wave of sensory neurogenesis is initiated by the expression of neurogenin 1 (NGN1) (Ma et al. 1998; Ma et al. 1999). After migration into the coalescing DRG, multipotent NCCs, which are positive for the NCC-characteristic transcription factor SOX10, express NGN1. They give rise to the major part of the nociceptor population, which is, at early developmental stages, characterized by the expression of the nerve growth factor (NGF) receptor TrkA and the transcription factor RUNX1 (Snider and McMahon 1998).

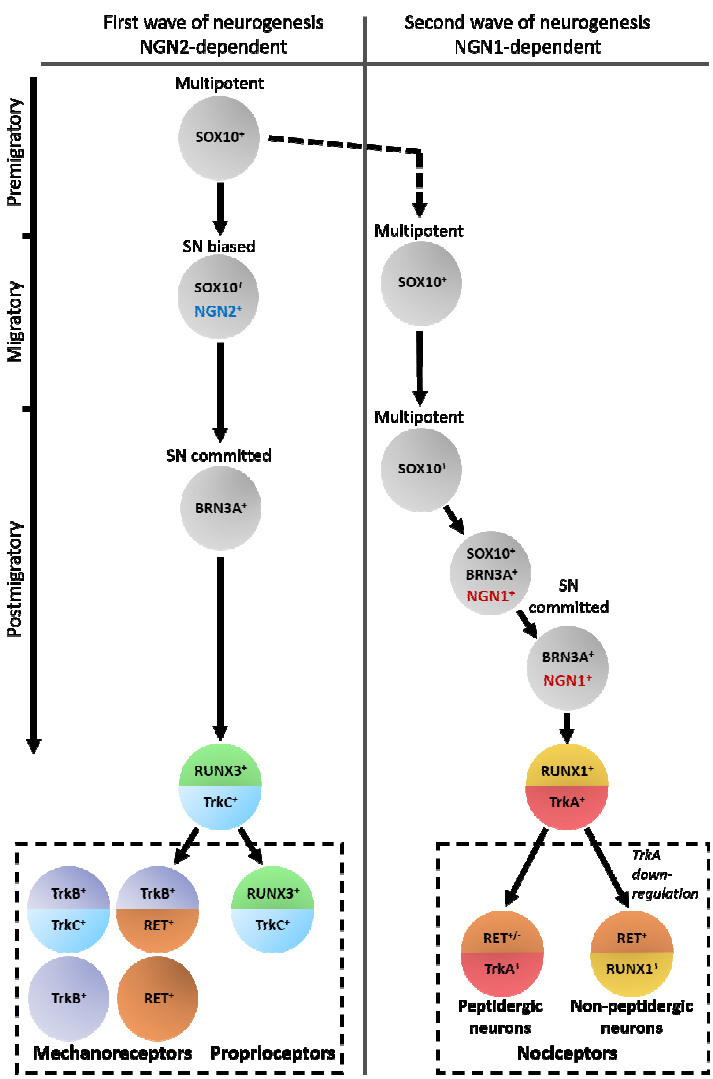

Figure 1.2: Waves of trunk sensory neurogenesis and subtype specification
Schematic representation of the two waves of neurogenesis from trunk NCCs. The axis on the left depicts the dorsoventral position and the corresponding migratory status of the neural crest cells (NCCs). During the first wave of neurogenesis, multipotent SOX10-positive (SOX10$^+$) cells migrate and express NGN2. NGN2-expression induces a sensory neuron (SN) bias and is followed by the expression of BRN3A in the postmigratory state. Cells of the first wave then differentiate into mechanoreceptors and proprioceptors, which express RUNX3 and TrkC at early developmental stages. Proprioceptors maintain the expression of both factors, while RUNX3 is down-regulated during the development of mechanoreceptors (TrkB$^+$, TrkC$^+$ and/or Ret$^+$). During the second wave of sensory neurogenesis, all migratory NCCs maintain SOX10 expression. Sensory commitment and the specification into nociceptors is induced by the expression of NGN1 and BRN3A in postmigratory NCCs in the DRG. All early nociceptors express RUNX1 and TrkA. However, during development, only about half of the nociceptors maintain TrkA expression (peptidergic nociceptors), while the other half down-regulate TrkA and upregulate Ret (non-peptidergic nociceptors). Figure adapted and modified based on (Marmigère and Ernfors 2007, Bhatt et al. 2013).

1.1.3 Nociceptors – the pain-sensing neurons

The sensory neuronal subclass of nociceptors is, in turn, divided into two main nociceptor classes that undergo distinct differentiation pathways - the peptidergic and the non-peptidergic nociceptors (Fig. 1.2). During development, the aforementioned NGF-receptor TrkA is down-regulated again in about half of the nociceptors (Chen C-L et al. 2006; McMahon et al. 1994). These TrkA-negative cells constitute the class of non-peptidergic nociceptors, which maintain the expression of RUNX1 and up-regulate the expression of RET, the glia-derived neurotrophic factor (GDNF) receptor (Franck et al. 2011; Snider and McMahon 1998; Takaku et al. 2013). They are further characterized by isolectin B4 binding and the expression of the purinergic receptor subtype P2X3 (Chen et al. 1995; Chen C-L et al. 2006; Snider and McMahon 1998). Peptidergic neurons, which

maintain the expression of TrkA but down-regulate RUNX1, express and release the neuropeptides calcitonin gene-related peptide (CGRP) and substance P (Snider and McMahon 1998). A subpopulation of the TrkA-positive neurons co-expresses RET and exhibits a mixed phenotype of peptidergic neurons with P2X3 expression (Rostock et al. 2018).

Furthermore, nociceptors can be distinguished according to their responsiveness to different stimuli. Nociceptors possess a high activation threshold, which is why they respond only to potentially tissue-damaging stimuli (Sherrington 1903). They detect noxious thermal, chemical, and mechanical stimuli via ion channels that respond specifically to certain environmental features. The responsible ion channels are described in the following and include but are not limited to transient receptor potential (TRP) channels, purinergic receptors and voltage-gated sodium channels.

TRP channels

The majority of heat-sensing nociceptors display an activation threshold of 42°C, which allows us to recognize and avoid potentially harmful temperatures (Basbaum et al. 2009). The TRP ion channel vanilloid-1 (TRPV1) is a prominent transducer of this noxious range of warm temperatures (>42°C) (Basbaum et al. 2009; Caterina et al. 2000). However, it is not only activated by increased temperatures but also by the TRPV1 specific compound agonist capsaicin (Caterina et al. 1997). This polymodality of TRPV1 activation also includes other agonists such as H^+ and metabolites of polyunsaturated fatty acids, e.g., the endocannabinoid anandamide (Dhaka et al. 2007; Ramsey et al. 2006). TRPV1 activation leads to the opening of the non-selective cation channel pore. The subsequent influx of cations depolarizes the neurons resulting in a burning pain sensation. Further thermo-sensitive TRPs (thermoTRPs) activated by distinct ranges of warm temperatures are TRPV2-4 (see table 3.1) (Levine and Alessandri-Haber 2007).

Nociceptors are not restricted to heat-sensation, but can also detect cold stimuli. A cold-activated thermoTRP channel expressed in nociceptors is TRPM8 (melastatin-8). TRPM8 is gated by temperatures of 25°C or below but can also be activated by compound agonists like menthol (Bautista et al. 2007; Colburn et al. 2007; Dhaka et al. 2007; Peier et al. 2002). A second cold-sensitive channel of the TRP family is TRPA1 (ankyrin-1), which is activated by noxious cold at temperatures below 17°C (Karashima et al. 2009). This channel shares the TRP family feature of polymodal activation and also functions as a ligand-gated non-

selective cation channel. Specific activation of TRPA1 can be elicited by allyl isothiocyanate (mustard, wasabi) and cinnamaldehyde (cinnamon), which are known to cause a pungent burning sensation (Bandell et al. 2004). Table 3.1 provides a comprehensive but not exhaustive overview of human thermoTRPs and respective activating stimuli.

Table 1.1: ThermoTRPs and the respective activating stimuli

thermoTRP	*Thermal activation*	*Chemical agonists*
TRPV1	>42°C	Capsaicin, protons, resiniferatoxin, piperine, olvanil, anandamide
TRPV2	>52°C	2-aminoethoxydiphenyl borate
TRPV3	>33°C	Camphor, thymol, carvacrol
TRPV4	>25-34°C	Bisandrographolide
TRPM8	<25°C	Menthol, icilin, eucalyptol, geraniol
TRPA1	<17°C	Cinnamaldehyde, mustard oil, acrolein, allicin

Purinergic receptors

In addition to the channels of the TRP family, there are many other receptors and channels characteristic of nociceptors and involved in pain sensation. In 1977, it was reported that ATP applied to a blister base elicited the sensation of pain (Bleehen and Keele 1977). Nowadays, it is known that the purinergic receptor P2X3 is involved in such ATP-induced pain sensations (Jarvis et al. 2002; North 2004). ATP can be released from endothelial and epithelial cells upon shear stress or distension (Bodin and Burnstock 2001; Ferguson et al. 1997; Schwiebert et al. 2002) or simply by (mechanically) lysed cells (Cook and McCleskey 2002). This points towards a potential role of P2X3 in mechanical pain sensation (Nakamura and Strittmatter 1996; North 2004), and also in chronic inflammatory pain conditions (Jarvis 2003).

Voltage-gated sodium channels

Other channels contributing to pain sensation are voltage-gated sodium (Na_V) channels. Up to five Na_V channels are found on cells of the DRG. Three of them, $Na_V1.7$, $Na_V1.8$, and $Na_V1.9$, are exclusively expressed in the PNS. Other Na_V channel subtypes not only expressed in the DRG but also in the CNS are $Na_V1.3$ and $Na_V1.6$ (Dib-Hajj et al. 2010; Wood et al. 2004). Na_V channel subtypes can be distinguished based on their sensitivity

to blocking by the neurotoxin tetrodotoxin (TTX). While $Na_V1.3$, $Na_V1.6$, and $Na_V1.7$ are blocked by TTX, $Na_V1.8$ and $Na_V1.9$ are resistant to it. Altered expression and activity of sodium channels are associated with inflammatory and neuropathic pain. Such alterations could lead to enhanced neuronal excitability, which is discussed as the main pain-triggering mechanism in such conditions (Kim et al. 2001; Sleeper et al. 2000).

1.1.4 Nociceptor sensitization

Inflammation and tissue injury induce hypersensitivity to stimuli in the surrounding area, described as allodynia and hyperalgesia. Hyperalgesia refers to the sensation of enhanced pain in response to noxious stimuli, i.e., an increase in the magnitude of response, whereas allodynia describes a decrease in the activation threshold. Thus, under allodynic conditions, stimuli normally perceived as innocuous are now transmitted by the nociceptive pathway and induce pain sensation. These phenomena result from nociceptor sensitization and lead to a nocifensive behavior towards the injured site, protecting it from further damage (Dubin and Patapoutian 2010). Specific factors that induce sensitization include neurotrophins (e.g., NGF), neurotransmitters (e.g., substance P, CGRP), prostaglandins (e.g., PGE_2), kinins (e.g., bradykinin), protons and ATP, collectively called the "inflammatory soup" (Fig. 1.3) (Basbaum et al. 2009; Bonnington and McNaughton 2003; Chuang et al. 2001; Namer et al. 2015; Tominaga et al. 1998; Woolf and Ma 2007; Yam et al. 2018).

Given this variety of sensitizers, the proposed mechanisms of sensitization are similarly diverse. One of the mechanisms contributing to NGF-induced sensitization is the increase in membrane incorporation of pain-related TRPV1 channels by exocytotic insertion from intracellular stores (Zhang et al. 2005). Up-regulation of the TRPV1 *de novo* synthesis is also a known sensitization process (Fig. 1.3) (Ji et al. 2002). Another proposed contributor to nociceptor sensitization is the release of TRPV1 from endogenous inhibition by phosphatidylinositol 4,5-bisphosphate (PIP_2) through the metabolism of PIP_2 induced by phospholipase C signaling (Chuang et al. 2001). These examples emphasize that TRPV1 is one of the main pain receptors affected by sensitization and plays a key role, especially in thermal hyperalgesia (Caterina et al. 2000; Davis et al. 2000). Another aforementioned TRP channel, TRPA1, is also known to contribute to thermal but also to mechanical hypersensitivity (Bautista et al. 2006; Kwan et al. 2006). Nociceptive thresholds may also

be modulated by voltage-gated sodium channels as shown by mutations in $Na_V1.7$ channels associated with increased nociceptor-excitability (Choi et al. 2006).

As nociceptor sensitization plays an essential role in pain pathogenesis, targeting the underlying mechanisms appears to be a valuable strategy for pain management. Therefore, TRP channel antagonists and selective Na_V channel blockers are considered as good candidates to treat (inflammatory) pain conditions (Fujii et al. 2008; Honore et al. 2005; Jarvis et al. 2007). In addition, direct targeting factors of the inflammatory soup using anti-NGF or -PGE_2 antibodies or blockers of PGE_2-synthesis could also address the problem at its source by preventing sensitization rather than attenuating pain signaling (Jarvis et al. 2007; Portanova et al. 1996; Woolf and Ma 2007).

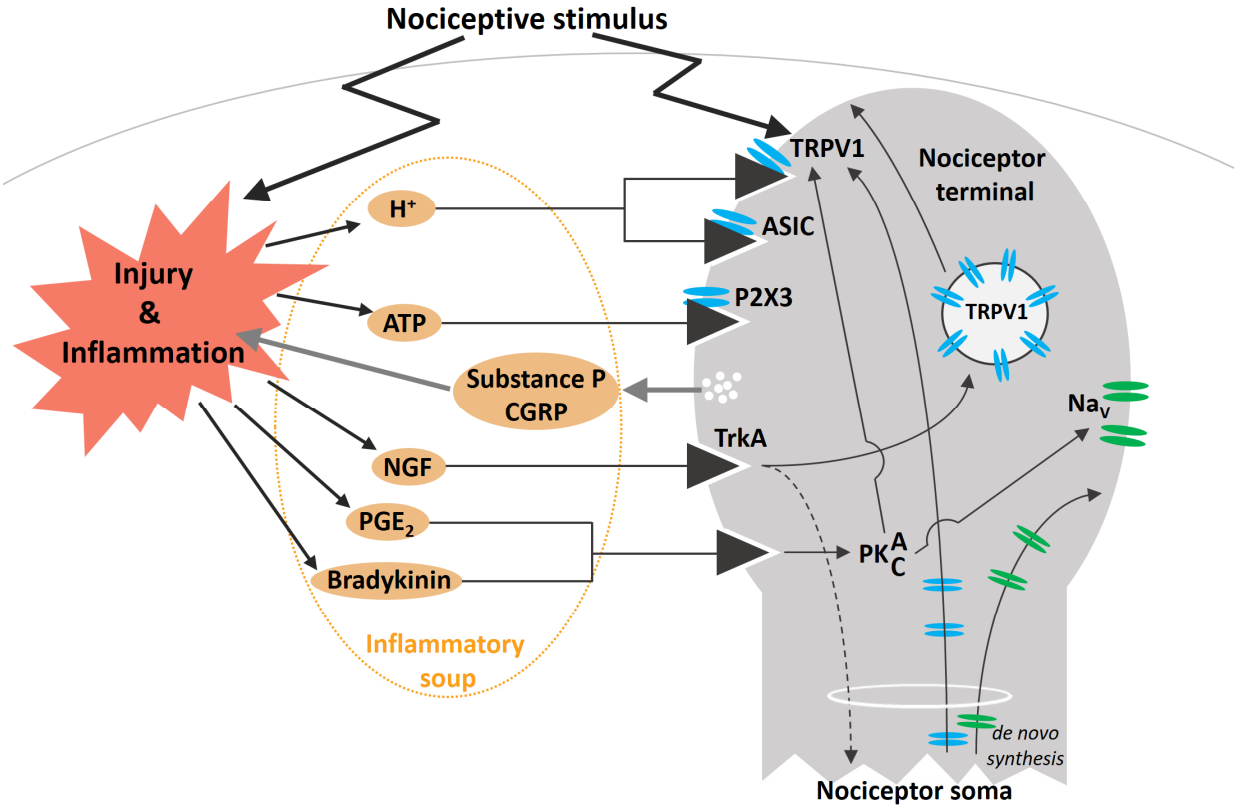

Figure 1.3: Key players in nociceptor sensitization

In conditions of injury or inflammation, factors that can activate and/or sensitize nociceptive neurons are released (yellow). These factors constitute the inflammatory soup. Protons (H^+) can directly activate and sensitize TRPV1 channels and acid-sensing ion channels (ASICs), while ATP activates P2X3 receptors. NGF, PGE_2 and bradykinin are pure nociceptor-sensitizers, not activators. NGF binds to its high-affinity receptor, TrkA, inducing *de novo* synthesis of TRPV1 and Na_V channels in the soma. These channels are then transported to the nociceptor terminals, where they are enriched in the plasma membrane. NGF also increases TRPV1 incorporation into the membrane by exocytotic insertion from intracellular, TRPV1-bearing vesicles. PGE_2 and bradykinin bind to specific receptors and induce phosphorylation of protein kinase A and C (PKA, C), respectively. This leads to enhanced Na_V channel activity and lowered activation thresholds of TRPV1. In addition, substance P and calcitonin gene-related peptide (CGRP) are released by nociceptors upon activation and can, in turn, enhance inflammatory processes or act directly on the nociceptors themselves. Figure adapted and modified based on (Coutaux et al. 2005).

1.2 Peripheral neuropathies

Peripheral neuropathies are a heterogeneous group of diseases affecting peripheral nerves. They can involve autonomic and motor symptoms. However, the first and, therefore, most important signs of neuropathy are usually the sensory symptoms. These comprise numbness, tingling, pins and needles, as well as burning sensations and pain in the extremities (McLeod 1995). It appears typically in a glove-and-stocking distribution, which means that sensory impairments are first noticed in hands and feet, the most distal regions of the PNS (Fig. 1.4). Peripheral neuropathies can have various causes, e.g. diabetes, infections, inflammation, or tumors (Croft and Wilkinson 1965; Fuller et al. 1993; Govoni et al. 1996; Partanen et al. 1995). In addition, neuropathic diseases can have hereditary causes, like in the Charcot-Marie-Tooth disease (Jeong et al. 2013). Neuropathies can further be induced by hazardous substances since the PNS is always in direct contact with the environment (Morgan 1982). This can lead to so-called toxic neuropathies induced by drugs, heavy metals, or industrial agents, whereby the latter is rather uncommon (Karam and Dyck 2015).

Generally, peripheral neuropathies are classified into three main groups based on their structural target affected: (i) axonopathies, with axonal degeneration affecting predominantly long fibers; (ii) neuronopathies, which involve initial effects on the cell bodies, particularly of the DRG; and (iii) myelopathies characterized by segmental demyelination, in which the axon remains intact, but the myelin sheath is destroyed (McLeod 1995). However, many pharmacological and toxic agents do not cause such structural damage but affect synaptic function, e.g., by modulating ion channels, which is not considered in the classification of peripheral neuropathies (Valentine 2020).

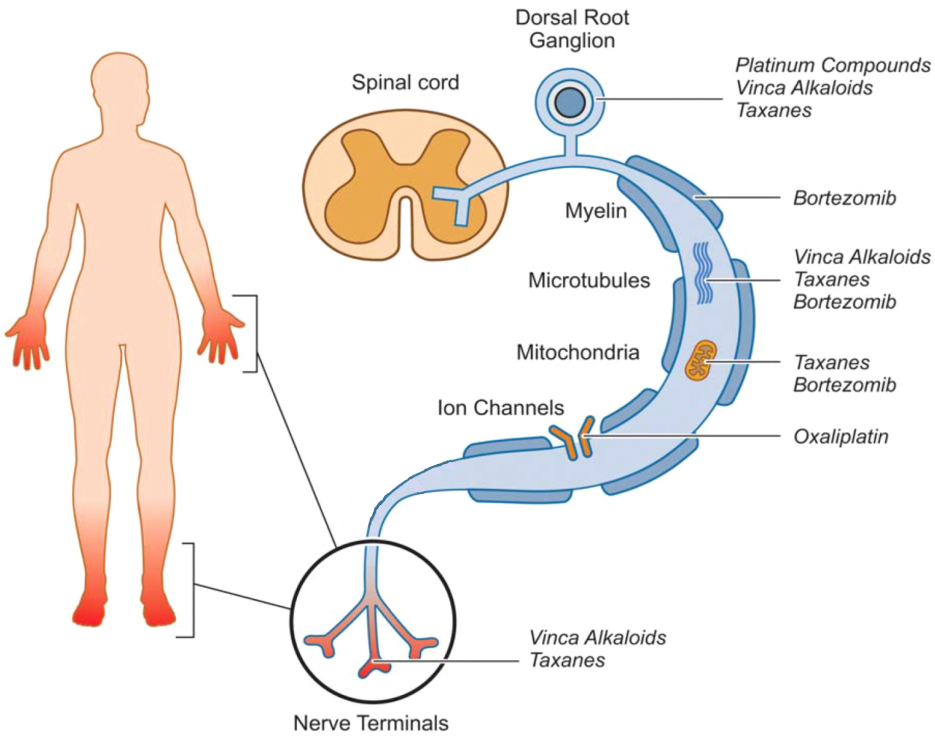

Figure 1.4: Typical glove-and-stocking distribution of peripheral neuropathy symptoms and presumable toxicity targets

First peripheral neuropathy symptoms typically appear in the hands and feet, the so-called glove-and-stocking distribution. A schematic sensory neuron displays the potential target sites for specific classes of chemotherapeutic agents (platinum compounds, vinca alkaloids, taxanes, Bortezomib): the cell body residing in the dorsal root ganglion, the long axon with its myelin sheath, microtubules and ion channels, and the distal nerve terminals. Figure adapted from (Park et al. 2013).

1.2.1 Possible targets affected in toxic neuropathies

Peripheral neurons depend on numerous highly coordinated and therefore, susceptible processes that can be affected by toxicants. The most apparent vulnerability comes with the length of peripheral axons. In humans, they may be about a meter long and therefore provide an excessive surface area for contact with toxic agents. Since the cell soma is the primary biosynthesis source of components of the axon and synapse, well-functioning transport mechanisms are required that cover the enormous length of the axon (Lasek et al. 1984). In addition, axonal transport in either direction, anterograde or retrograde, is crucial for maintaining overall viability and is, therefore, a susceptible mechanism in peripheral neurons (Smith et al. 2016).

Tracks for cargo transport are formed by linearly arranged microtubules (Niwa et al. 2013). Microtubules are dynamic structures composed of α,β-tubulin heterodimers and are subject to constant and controlled assembly and disassembly. This so-called dynamic instability represents another mechanism that is, in turn, also very susceptible to perturbations, such as drug binding to tubulin via hydrogen bonds (Fig. 1.4) (Sharma et al. 2013). Disruption of microtubule function in the tips of axons impairs proper innervation of the epidermis, which is in constant turn-over (Siau et al. 2006).

In peripheral neurons, a wealth of such constantly occurring, dynamic processes is found, such as the aforementioned microtubule dynamics and axonal transport, but also the maintenance of the membrane potential, which is required for functional signaling. All these processes account for an enormous energy demand of peripheral neurons, which is also reflected by a large number of mitochondria in the neuronal synapses (Ly and Verstreken 2006). As mitochondria are the main supplier of energy in the form of adenosine triphosphate (ATP), this implies that mitochondrial dysfunction has severe implications on signal transduction and neuronal maintenance (Summers et al. 2014). Additionally, mitochondria accumulate Ca^{2+} upon stimulation of neurons thereby functioning as a buffer system for intracellular Ca^{2+}, which contributes to the maintenance of proper neuronal signaling (Ly and Verstreken 2006; Rizzuto et al. 1998). Taken together, this highlights that mitochondria may play a key role in peripheral neuropathies (Fig. 1.4).

Neuronal signaling can further be compromised by the modulation of ion channels, which are responsible for the stimulus sensation or the transmission of electrical signals (Marrs and Maynard 2013). As mentioned before, modulation of ion channels can occur either on the level of expression and plasma membrane incorporation or by (de)sensitization, which changes the ion channel response threshold (Fig. 1.3, 1.4) (Choi et al. 2006; Ji et al. 2002; Zhang et al. 2005).

1.2.2 Chemotherapy-induced peripheral neuropathy

Drug toxicity is the most common cause of toxic neuropathies and is especially induced by chemotherapeutic agents (Fig. 1.4) (Karam and Dyck 2015). Among patients receiving chemotherapy, the prevalence of chemotherapy-induced peripheral neuropathy (CIPN) is more than 60% and continues to increase (Seretny et al. 2014). CIPN is often the dose-

limiting side-effect of chemotherapeutic drugs. In most cases, it is reversible, but CIPN can also be long-lasting, even permanent (Brouwers et al. 2009; Richardson et al. 2006). Sometimes a phenomenon called “coasting” is observed, which means the worsening of symptoms after treatment termination (Albany et al. 2021; Park et al. 2013).

Coasting is particularly common for platinum derivates used in chemotherapy, such as cisplatin, carboplatin, and oxaliplatin (Albany et al. 2021; Karam and Dyck 2015). Neuropathies induced by platinum compounds are mainly sensory and fall into the class of neuronopathies. The DRGs are damaged due to the crosslink of the platinum compounds with the DNA, thereby inhibiting DNA repair and synthesis, which ultimately leads to apoptosis. In the particular case of oxaliplatin, also acute symptoms can be observed. These manifest themselves in the form of cold-induced paresthesia in the hands and feet, tightness of the throat and jaw, and muscle cramps. Such acute symptoms are not linked to structural effects of oxaliplatin but to hyperexcitability of the neurons (Adelsberger et al. 2000; Lehky et al. 2004; Webster et al. 2005; Wilson et al. 2002).

Vinca alkaloids are another group of chemotherapeutics accounting for CIPN, with vincristine as the most neurotoxic agent of this drug class (Karam and Dyck 2015). They interfere with the microtubule system by hindering the assembly of tubulins. This has severe implications for axonal transport and the general maintenance of the neuronal structure, resulting in distal axonopathy. Furthermore, vincristine is discussed to induce mitochondrial dysfunction leading to altered Ca^{2+} efflux and uptake, thus impairing intracellular signaling and neuronal excitability (Canta et al. 2015). The first symptoms of vincristine-induced peripheral neuropathy are paresthesia in hands and feet, and loss of tendon reflexes (Casey et al. 1973). However, CIPN is often reversible and, due to its dose-dependency, dose adjustment can limit the extent of neuropathy (Legha 1986).

Instead of preventing tubulin assembly in order to interfere with microtubule dynamic instability, chemotherapeutic agents can also rely on the principle of microtubule stabilization. One example is the taxane class, which binds to the β-subunit of tubulin from the inside of the microtubules, thereby stabilizing them (Horwitz 1994). Taxanes, such as paclitaxel, and docetaxel, are often used as post-operative adjuvant treatment of breast cancer patients (Shimozuma et al. 2012). Taxol is associated with sensory neuropathic symptoms, with pain observed in up to 40% of the patients (Winer et al. 2004). In neurons, taxanes act directly on the distal axon and cause a length-dependent

polyneuropathy affecting primarily sensory but also motor neurons (Gornstein and Schwarz 2017).

Proteasome inhibitors (PIs) are used clinically to treat multiple myeloma (Kane et al. 2003; Richardson et al. 2003). As the name indicates, these drugs target the proteasome, which is responsible for the degradation of more than 80% of proteins in eukaryote cells (Craiu et al. 1997). As neurons have a high protein turnover and metabolic rate due to the wealth of constantly ongoing, dynamic processes, it is not surprising that PIs can induce neurotoxicity (Alé et al. 2014). The PI bortezomib induces peripheral neuropathies, which are exclusively sensory and often painful, affecting up to 64% of patients (Jagannath et al. 2004; Richardson et al. 2006; Richardson et al. 2009; San Miguel et al. 2008; Velasco et al. 2010). The underlying mechanisms of neuropathy induction are still unknown for the class of PIs. Besides cytoskeletal alterations due to increased tubulin polymerization and DNA damage, also aggresome formation, mitochondrial dysfunction, and neuroinflammation are discussed as causes of PI-induced neuropathies (Alé et al. 2014; Poruchynsky et al. 2008; Staff et al. 2013).

As the number of cancer survivors increases, so does the number of people suffering from CIPN (Mols et al. 2014). This fact highlights the need to understand better the mechanisms underlying peripheral neuropathies induced by chemotherapeutic drugs. Research and new insights in this direction essentially form the basis for the development of antineoplastic drugs with fewer side effects.

1.3 Assessment of peripheral neurotoxicity

In clinics, peripheral neurotoxicity is often assessed using clinician-guided, standardized classification scales, called the Common Toxicity Criteria. However, this strategy is associated with significant inter-observer variations and could lead to misinterpretations due to undifferentiated evaluation of impairments, disability, and quality of life (Cavaletti et al. 2010). Quantitative sensory testing is applied to assess hyperalgesia or allodynia conditions using heat, cold, and pressure as stimuli. Furthermore, a skin biopsy is used as a standard method to investigate intraepidermal nerve fiber density providing evidence of possible nerve fiber loss (Argyriou et al. 2019; Kanzawa-Lee et al. 2019).

The latter two methods are also used in *in vivo* CIPN research mainly performed in rodents. Rodent models offer a broad spectrum of readout possibilities with functional sensory and motor tests as standard methods. The rotarod test, for example, assesses sensory-motor function and coordination of animals balancing on a rotating stick, whereas hyperalgesia can be assessed in the pin-prick test, measuring paw-withdrawal triggered by pressing but not penetrating the skin. (Bruna et al. 2020). Functional alterations of the nerves, e.g., in the action potential amplitude, can be assessed in *in vivo* electrophysiological nerve conduction studies via electrodes inserted into the tail or muscles of the animals (Boehmerle et al. 2014).

Rodents are complex organisms with metabolism, where interactions between different cell types come into play, and behavioral changes can be assessed (Bruna et al. 2020). However, such complex systems often reveal only specific symptoms, but do not allow a clear distinction between primary and secondary effects. Furthermore, studies on rodents are always associated with ethical concerns, as the animals often must undergo painful and distressing scientific procedures.

To overcome such ethical issues in CIPN research, *in vitro* cell culture models are increasingly used nowadays. However, the cell-based systems most commonly used as models for the PNS are still based on non-human cells, such as cultured dorsal root ganglia of rodents (Alé et al. 2015; Meregalli et al. 2014; Staff et al. 2013). Such systems have the major disadvantage that the obtained results can only be transferred to humans to a limited extent due to the differences between sensory neurons of humans and other model organisms (Chen et al. 2008; Davidson et al. 2014; La Roche et al. 2013; Serrano et al. 2012).

The use of stem cells was a turning point in the availability of cell systems relevant to humans. Targeted differentiation of human stem cells *in vitro* enables the generation of cell types otherwise inaccessible for toxicity testing, such as peripheral neurons (Chambers et al. 2012; Hoelting et al. 2016). General advantages of *in vitro* cultures are the controlled physico-chemical environment and the fast replication of experiments. At the same time, the simplicity of cell culture models, as only the cell type of interest is studied, can be seen as an advantage or disadvantage (Lehmann et al. 2020). However, the most important positive aspect of the simplicity is that mechanistic studies can be performed. Single aspects of the cultured cells, such as the cytoskeletal structure, general

morphology of the neurons (e.g., neurite length, branching, integrity), and functional features (e.g., receptor function, network formation), can be investigated simultaneously. Such deconstructed *in vitro* approaches could reveal, for example, de-regulations of distinct pain receptors that could contribute to the CIPN symptoms observed *in vivo*. Therefore, *in vitro* cell systems allow both the testing of known neurotoxicants to uncover the underlying mechanisms of neurotoxicity as well as the rapid and simple testing of unknown substances to identify potentially harmful neurotoxicants.

1.4 Future strategies in toxicology

The primary means for toxicological studies have ever been animal models, especially in rodents. However, already in 1959, Russel and Burch presented a vision for overcoming such inhumane techniques used in animal experimentation (Russell and Burch 1959). On the one hand, they acknowledged that animal experimentation was the basis for numerous scientific knowledge and modern medicine achievements. On the other hand, they have highlighted the ethical concerns and defined the 3Rs principle as a basis and guideline for future developments in science. The principles of Refinement, Reduction and Replacement of animal experimentation constitute the 3Rs. Whenever possible, experiments using live, sentient animals should be replaced by non-animal models or other non-sentient material such as tissue slices. When complete replacement is not possible, consideration should be given to reducing the number of experimental animals used to the minimum number necessary to reliably answer a particular research question. Any animal experimentation method still required should be refined to minimize pain, suffering and any kind of distress for the animals. This approach was intended to improve the animal wellfare and the quality of scientific and medical research.

Switching experimental systems from sentient animal models to, e.g., tissue slices would still require the use of animals. Therefore, the complete replacement of animal material with human cell systems would be of great interest to minimize ethical concerns while improving the quality of science since, as previously mentioned, it is generally questionable to what extent animal-derived data is relevant for human risk assessment (Hartung 2008). Differences between animals and humans cannot be denied and are the greatest challenge in translational research. They vary in terms of bioavailability,

toxicokinetics and toxicodynamics, but also in terms of developmental processes (Hartung 2008; Lin 1995; Sietsema 1989). Further, it is known that the cell type constitution of organs can differ between humans and animals, such as the dorsal root ganglia that exhibit different nociceptor compositions in mice and humans (Rostock et al. 2018). The abundance and distribution of nervous system signaling receptors and channels also vary significantly between species (Chen et al. 2008; Davidson et al. 2014; La Roche et al. 2013; Serrano et al. 2012). This can pose major challenges for the identification of toxic compounds, just as for the development of therapies. Additional problems of risk assessment based on animal models arise from the fact that some human-relevant diseases, such as autism or attention-deficit/hyperactivity disorder, cannot even be studied in animals (Terron and Bennekou 2018). Animal tests can also yield misleading results. Rodents can, for example, die upon oral uptake of a substance that damages the intestinal epithelium, whereas humans would get rid of the substance through vomiting (which rodents cannot do) (Hartung 2008). In animals, it is generally challenging to study disease mechanisms in detail or to determine the primary compound-related effects that lead to the observed overall outcome. However, it is certainly not a realistic option to perform primary toxicity tests on humans rather than animals. In addition, testing on cells of human origin was also not feasible for a long time because most cell types were not available in sufficient quantities for toxicity testing, e.g., peripheral neurons. Strikingly, with the generation of human immortalized cell lines and the advent of stem cell technology, the prerequisites for animal-free research have changed completely (Jennings 2015).

1.4.1 New approach methodologies in peripheral neurotoxicity testing

New approach methodologies (NAMs) for toxicity assessment include *in vitro* assays, e.g., human cell culture systems, *in silico* models, such as quantitative structure-activity reationship (QSAR) models, and computational models of exposure, e.g., *in vitro* to *in vivo* extrapolation (IVIVE) (Parish et al. 2020). They constitute the basis for a paradigm shift in risk assessment towards animal-free testing with enhanced speed and improved data accuracy. However, while a wide range of CNS models are available for toxicity testing, the replacement of animal material in PNS research is not as advanced. For example, less than 15% of *in vitro* studies on CIPN were conducted using human cell lines or induced pluripotent stem cell (iPSC)-derived neurons until 2019 (Lehmann et al. 2020). Among

the cells used in these human cell-based studies, the SH-SY5Y cell line is frequently used. However, it is more of a model for dopaminergic or cholinergic, but not sensory neurons. Especially research regarding CIPN-associated pain is hampered using this cell line, as the cells lack important nociceptor markers such as TRPV1 or CGRP (Yin et al. 2016). Such limitations of cell lines can be overcome by using human stem cell-derived models of peripheral neurons. This is why various differentiation procedures are currently established to generate peripheral neurons (Boisvert et al. 2015; Chambers et al. 2012; Hoelting et al. 2016; Jones et al. 2018; Valensi-Kurtz et al. 2010), but the application of these iPSC-derived cells for *in vitro* testing strategies is rather limited so far.

Only a limited spectrum of endpoints was investigated in the few cases in which iPSC-derived peripheral neurons were used to assess adverse effects of compounds *in vitro*. A commonly investigated endpoint was the overall cell viability. The other endpoints examined were related to the neuronal morphology (Delp et al. 2018; Hoelting et al. 2016; Rana et al. 2017; Schinke et al. 2021; Wing et al. 2017). However, chemotherapy-induced and general peripheral neurotoxicity are not exclusively linked to the length or integrity of neurites. There are, as mentioned earlier, many other processes that may be affected before effects on the neurites occur (see section 3.2.1). Therefore, processes like neuronal signaling should be considered as endpoints when testing for adverse effects of compounds as they may be even more sensitive. Figure 1.5 gives an overview of possible experimental approaches to define neurotoxicity in general.

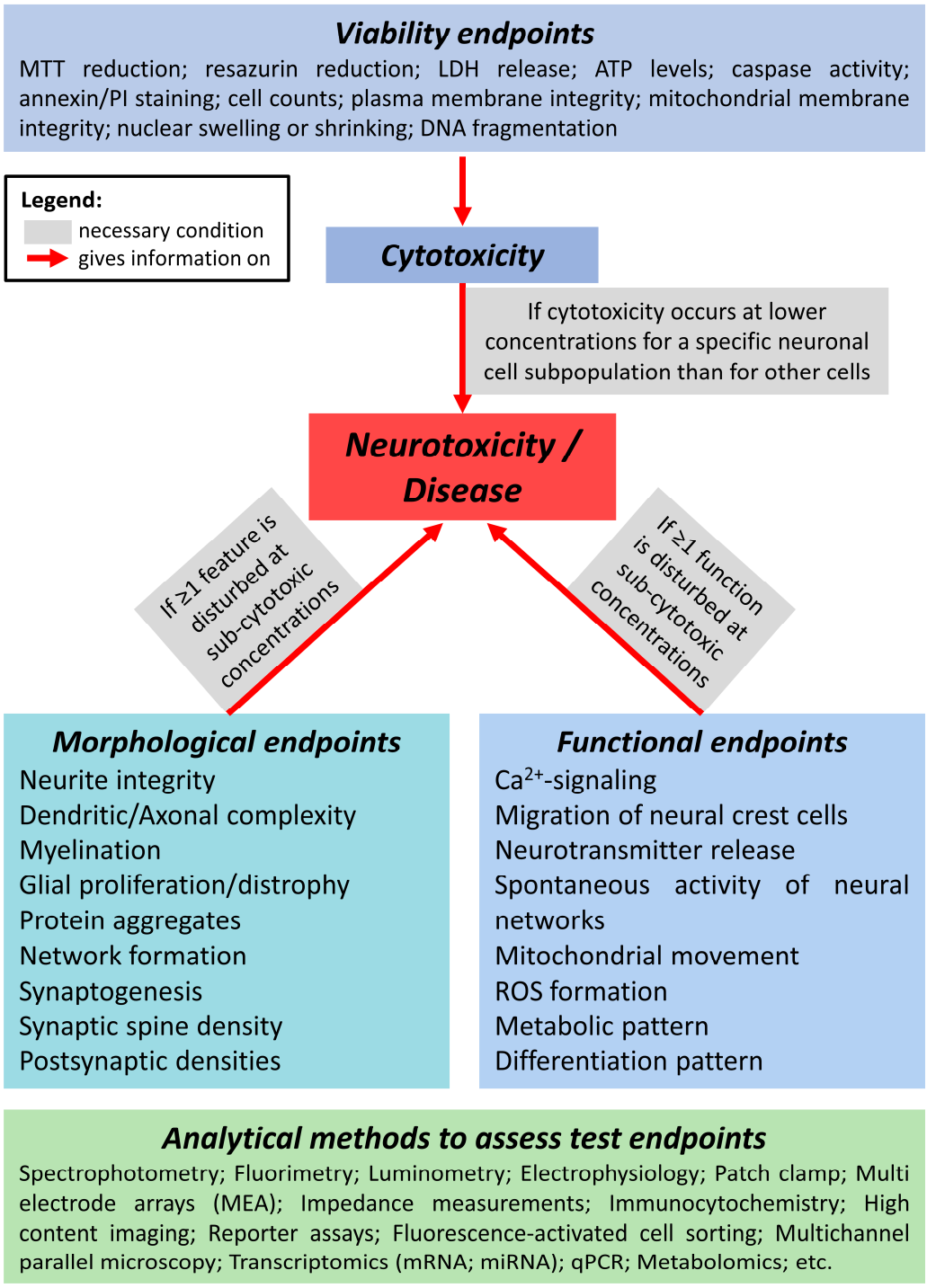

Figure 1.5: Experimental approaches to define neurotoxicity and disease

Viability endpoints, as well as morphological and functional endpoints can indicate neurotoxicity. Examples for test endpoints to be considered are given in the blue boxes; the green box displays possible analytical methods for their assessment. Figure adapted and modified from (Schmidt et al. 2017).

1.4.2 Endpoints to consider for *in vitro* models used for peripheral neurotoxicity assessment

Studies using human peripheral neurons are still scarce, and all studies assessing toxicant effects focus on similar endpoints such as overall cell viability and neurite integrity. Neurite integrity is undoubtedly an important feature to be investigated in CIPN research, as the phenomenon of "dying-back", i.e., the degeneration of the most distal parts of the axon, is a well-known consequence of chemotherapeutic drug toxicity (Bischoff 1967). However, other endpoints could be affected before neurite growth or integrity are impaired as discussed in section 3.2.1 (Siau et al. 2006; Smith et al. 2016). Therefore, the important question arises about how reliable NAMs should be designed to enable *in vitro* studies of CIPN-features observed *in vivo*. The following section presents a range of endpoints eligible for CIPN models and essential considerations regarding their practical implementation.

Cell viability

An endpoint that should always be included in any test method is the viability of the cells (Eldridge et al. 2021). When multiplexed with other assays, it provides valuable insights into the specificity of any other endpoint measured and can be used as an internal control to correct for plating errors, for example (Leist et al. 2010). Viability measurements can also form the basis for comparisons between different cell types to understand whether the observed adverse effects are specific to a particular type of cells. Regarding toxic neuropathies, the viability endpoint is especially interesting for investigating neuronopathy-inducing agents, such as platinum compounds, which induce apoptosis by interference with DNA replication (Gill and Windebank 1998; Staff et al. 2019).

Viability assays are often based on the metabolic activity of the cells (Ramirez et al. 2010). Calcein-AM, for example, is a cell-permeant, non-fluorescent compound that gets converted by esterases in viable, enzymatically-active cells resulting in a fluorescent probe that can be detected. Alternatively, instead of visualizing viable cells, cells with compromised plasma membranes can be visualized by dye exclusion assays (Brüll et al. 2020). Such assays use dyes like propidium iodide, which are rejected by the plasma membrane of healthy cells but can passively diffuse into dying cells, providing a direct measure of cytotoxicity (Krishan 1975). Furthermore, colorimetric assays are widely used

to assess cell viability. Such assays capture the metabolic activity of a cell culture by quantifying the reduction of resazurin or tetrazolium salts (e.g., MTT) (Krug et al. 2014; Pamies et al. 2014).However, they do not distinguish between changes in viability or proliferation of the cells. Consequently, data on cell viability obtained with such assays that do not refer to the overall cell number should therefore be taken with caution. For that reason, possible effects interfering with cell proliferation must be clarified (Mosmann 1983).

Neurite morphology

As mentioned before, a widely used approach to assess peripheral neurotoxicity is the study of neurite-related morphologic features. The "dying-back" phenomenon is a major pathology observed in CIPN presenting as distal nerve degeneration (Bischoff 1967). Therefore, neurite parameters like length, width, area, branching and integrity present *in vivo*-relevant morphologic features that can be investigated *in vitro* (Radio and Mundy 2008). Modeling the "dying-back" phenomenon implies the degeneration of a pre-existing, established neurite network. However, a fully established neurite network requires time and handling expertise, which could affect the robustness of the test system, making it less suitable for use as a high-throughput screening system (Murray and Wigglesworth 2016). An alternative to the study of neurite degeneration is the investigation of neurite outgrowth. For neurite outgrowth studies, young neurons are used, which are in many aspects superior to mature neurons for toxicity testing: (i) testing is more feasible in terms of time and handling (Delp et al. 2018; Hoelting et al. 2016; Wheeler et al. 2015; Wing et al. 2017); (ii) a culture of young, growing neurons is less tangled, facilitating quantitative assessment of parameters like neurite branching; (iii) neurite outgrowth is a highly dynamic process with a high energy demand, which makes growing neurons even more susceptible to perturbation by toxic substances (Schinke et al. 2021).

The neurites can be visualized by immunostaining for the pan-neuronal marker βIII-tubulin or any comparable cytoskeletal protein. In this approach, antibodies against cytoskeletal proteins can be combined with antibodies targeting other organelles, e.g., the mitochondria. This allows to gain insight into any additional aspects of interest, such as a change in mitochondrial shape, which is an indicator of apoptosis induction (Herzig and Martinou 2008). However, immunostaining is laborious, time-consuming and involves many additional steps that potentially compromise reproducibility. Consequently, it is not

an ideal method for screening purposes. An increased throughput can be achieved using fluorescent, membrane-permeable dyes that enable live cell imaging, such as calcein-AM (Brüll et al. 2020; Delp et al. 2018; Hoelting et al. 2016; Krug et al. 2013; Stiegler et al. 2011; Wheeler et al. 2015; Wing et al. 2017). Fluorescent labeling of cells allows quantifying the neurite-related parameters mentioned above, preferably by high-content imaging with subsequent, automated analysis (Stiegler et al. 2011). Another advantage of live cell imaging is the possibility of simultaneously evaluating neurite outgrowth and cell viability or cytotoxicity in the same culture (Fig. 1.6) (Brüll et al. 2020; Hoelting et al. 2016; Stiegler et al. 2011). In conclusion, neurite morphology constitutes a CIPN-relevant endpoint, which is useful for extensive compound screenings as it can be multiplexed with other endpoints in high-content live cell imaging.

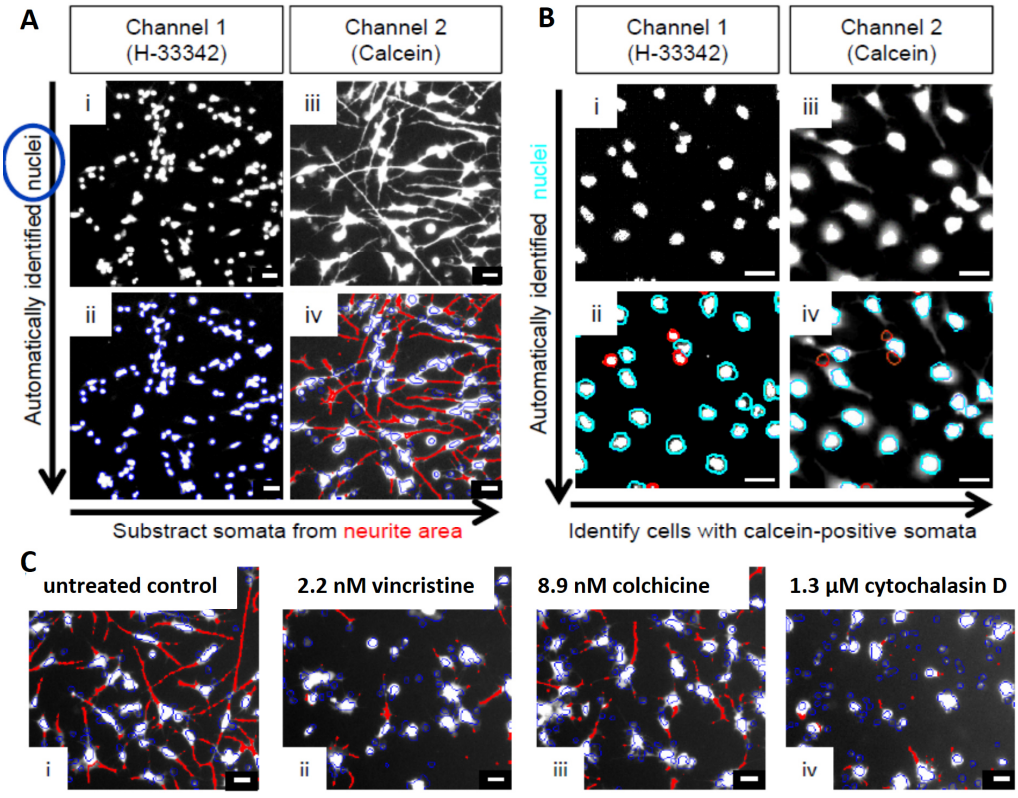

Figure 1.6: Morphology-based evaluation of the neurite area multiplexed with a cell viability readout

The basic principle of the image evaluation algorithm used for the multiplexed quantification of (**A**) neurite area and (**B**) cell viability applied in several *in vitro* test methods is shown (Hoelting et al. 2016; Stiegler et al. 2011). (**A**) Untreated, stem cell-derived peripheral neurons stained with Hoechst-33342 (H-33342) and calcein. (i) Detection of nuclei by their H-33342 staining in channel 1; (ii) automatic identification and marking (indicated by a blue circle); (iii) staining of all viable cells by calcein, which is detected in channel 2; (iv) automatic expanding of the nuclear outline to define a "virtual soma area". All calcein-positive pixels outside the virtual soma area are defined as neurite area (red) and automatically quantified. (**B**) Cells of the example pictures were treated for 24 h with a neuropathy-inducing chemotherapeutic agent. (i) H-33342 staining; (ii) automatic identification of cell nuclei, displayed with a color-coded

outline of their shape (cyan for normal nuclei, red for aberrant objects (e.g., too small, apoptotic nuclei or fragments)); (iii) labeling of viable cells by calcein; (iv) algorithm-based quantification of the calcein intensity in the cells' "virtual soma area". Cells with calcein staining exceeding a threshold value are classified as viable cells (cyan circles). (**C**) Example pictures of neurite area quantifications for either (i) untreated neurons or (ii-iv) neurons treated with the cytoskeleton affecting compounds (ii) vincristine, (iii) colchicine, or (iv) cytochalasin D. Figure adapted and modified from (Hoelting et al. 2016).

Ion channel function

Symptoms of peripheral neurotoxicity are not solely linked to structural alterations of the neurons. Patients receiving chemotherapy can experience sensory impairments like pain while the neurites can still be structurally intact (Ling et al. 2007). Readouts that assess functional aspects of peripheral neurons are therefore not only complementary but essential. Ion channels dysfunction is, for example, a known feature of oxaliplatin-induced peripheral neuropathy (OXAIPN) (Adelsberger et al. 2000; Calls et al. 2020). Such modulations of voltage-gated or ligand-activated ion channels can be studied using the patch-clamp technique, which enables the measurement of membrane potential or current of individual cells (Adelsberger et al. 2000; Loser et al. 2021c). However, patch-clamp procedures are either very time consuming if performed manually, or require a large number of cells if performed automatically. Alternatively, Ca^{2+}-imaging can be used to investigate ion channel function and alterations thereof (Loser et al. 2021c). Ca^{2+} is important for the control of many cellular processes. In neurons, it plays a key role in excitability and signal transduction. Changes in the intracellular Ca^{2+} concentration ($[Ca^{2+}]_i$) mostly result from Ca^{2+} entry via Ca^{2+}-permeable ion channels in the cell membrane (Tsien and Tsien 1990). Such channels open either upon direct activation by an agonist (receptor-operated Ca^{2+} channels) (Fig. 1.7A), or as a secondary reaction, e.g., upon activation by a cytosolic messenger (Fig. 1.7B) or changes in the membrane potential (voltage-gated Ca^{2+} channels, Ca_V) (Fig. 1.7C). Monitoring of the $[Ca^{2+}]_i$ is therefore a direct indicator for receptor-operated Ca^{2+} channel function, but secondarily it also visualizes the function of channels for other ions, such as Na^+ (Gustafsson et al. 2010).

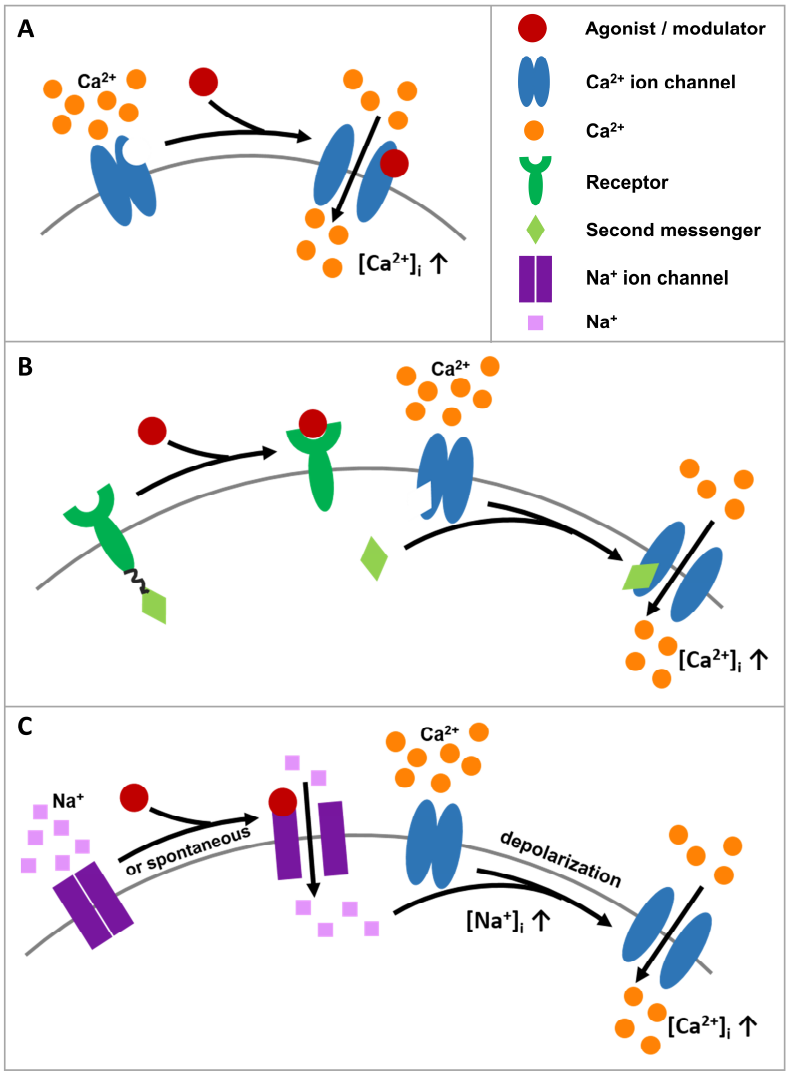

Figure 1.7: Schematic representation of different types of Ca^{2+}-permeable ion channels
(A) Receptor-operated Ca^{2+} channels that open upon direct activation by an agonist. **(B)** Second messenger-operated Ca^{2+} channels that open upon binding of a cytosolic second messenger. Such second messengers can, for example, be released upon agonist-dependent activation of ion channel-independent receptors. **(C)** Voltage-gated Ca^{2+} channels open upon depolarization of the cell membrane. Depolarization can result from Na^+ influx upon targeted or spontaneous opening of Na^+ channels. Opening of Ca^{2+} channels consequently leads to an increased intracellular Ca^{2+} concentration $[Ca^{2+}]_i$.

The availability of fluorescent Ca^{2+} indicator probes facilitated the study of ion channel function and cellular Ca^{2+}-signaling in general (Grynkiewicz et al. 1985). Membrane-permeable acetoxymethyl (AM) ester forms of these Ca^{2+}-indicators allow the non-disruptive loading into cells (Tsien 1981). Fluorescent Ca^{2+} indicators contain a Ca^{2+}-chelating moiety that quenches fluorescence in the absence of Ca^{2+} (Leist and Nicotera 1998; Lock et al. 2015). Rising Ca^{2+} levels inhibit the quenching and result in an increase in fluorescence intensity in the case of single wavelength Ca^{2+} indicators, such as Fluo-4 (Fig. 1.8). Ca^{2+} indicators that emit fluorescence at two different excitation wavelengths, e.g., fura-2, exhibit a shift in the peak excitation wavelength with rising intracellular Ca^{2+} concentrations. However, imaging at two excitation wavelengths also comprises imaging speed and thus the temporal resolution of Ca^{2+} changes.

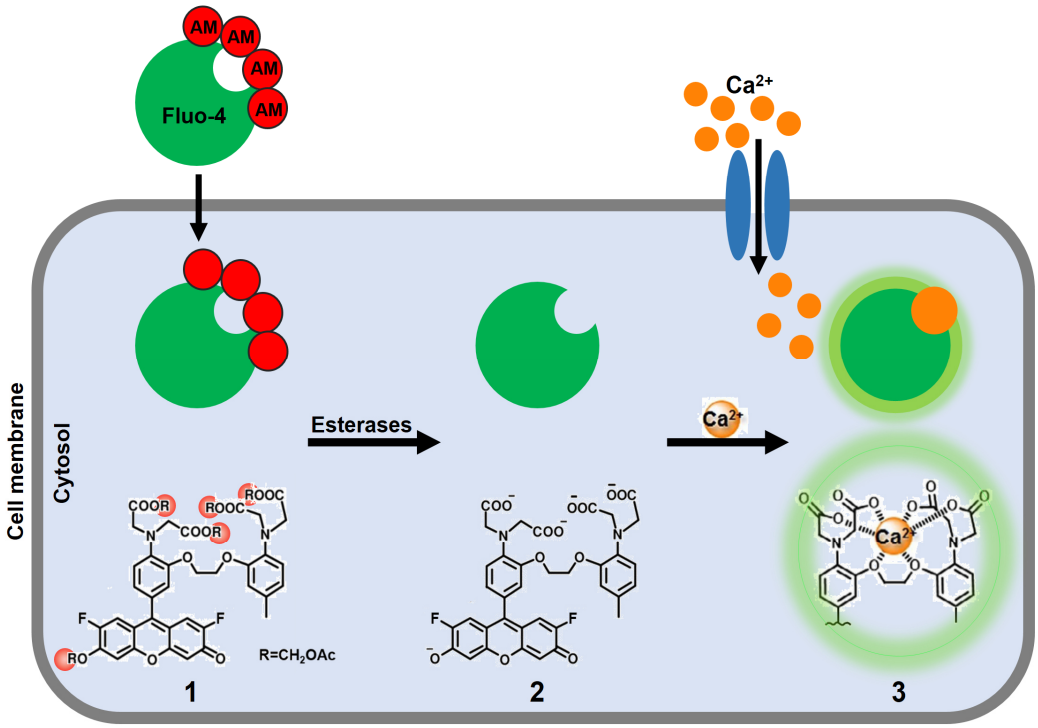

Figure 1.8: Ca^{2+}-imaging using the Ca^{2+} indicator Fluo-4 AM

Processes involved in Ca^{2+}-imaging are depicted. Cells are loaded with the membrane-permeable, acetoxymethyl (AM, red)-modified Ca^{2+} indicator Fluo-4 (green) (structure **1**). In viable cells, esterases cleave the AM-moieties, resulting in the membrane non-permeable Fluo-4 (structure **2**). De-esterification bares the Ca^{2+}-chelating site of Fluo-4. Ca^{2+} entry via ion channels elevates the intracellular Ca^{2+} concentration. Fluo-4 chelates Ca^{2+} (structure **3**), thereby increasing the intensity of the emitted fluorescence. Figure adapted and modified from (Roopa et al. 2019; Rossi and Taylor 2020).

In Ca^{2+}-imaging experiments, whole populations can be investigated, which is especially useful for highly uniform cell cultures (Lilja and Forsby 2004; Loser et al. 2021b; Loser et al. 2021c). Beyond that, also single-cell evaluations are possible, which allows the detailed investigation of cell cultures composed of several subpopulations expressing different receptors or ion channels (Anand et al. 2010; Klima et al. 2021a). Various parameters of ion channel function can be studied using Ca^{2+}-imaging, such as reaction kinetics (transient or persistent) or the extent of Ca^{2+} influx. Thus, this endpoint provides insight into a wide range of processes that may be altered under neurotoxic conditions.

Electrical activity

The electrical activity of neuronal networks can be measured by culturing cells on microelectrode arrays (MEAs). Such MEAs allow the non-invasive recording of extracellular field potentials of whole populations (Shafer 2019). The spontaneous electrical activity of neuronal networks can be studied using MEAs, and therefore, also

changes in the electrical activity in response to acutely or chronically applied pharmacological compounds, such as receptor-specific agonists, can be assessed (Hofrichter et al. 2017; Klima et al. 2021a; Nimtz et al. 2020; Strickland et al. 2018). Furthermore, MEAs can be used to investigate the formation of a functional neuronal network. As this method does not require any modification of the cells, such as staining with fluorescent dyes, the same cell cultures can be measured repeatedly over long periods (Klima et al. 2021a). Therefore, MEA measurements can provide information on the overall developmental status of a neuronal culture and also allow the identification of toxicants that affect the formation of functional networks. Furthermore, washouts can be performed in order to remove treatment compounds from the cell cultures. In this way, possible delayed effects on the electrical activity of the neurons can be detected, and the neuronal cultures can be reused for further tests.

For peripheral neurons, however, the most relevant features that can be studied using MEAs are (i) the spontaneous electrical activity, which, for instance, is known to change upon treatment with distinct chemotherapeutics (Wilson et al. 2002), and (ii) the acute response towards specific pharmacological compounds, which can be impaired under neurotoxic conditions (Anand et al. 2010).

Neurotransmitter release

The release of neurotransmitters is a key process in neuronal signaling. It is the basis of interneuronal communication, but also plays a role in the sensitization of peripheral neurons. The neuropeptides substance P and CGRP serve as neurotransmitters in peripheral neurons (Goodman and Iversen 1986; Konishi et al. 1980). They are also components of the “inflammatory soup” that are locally released at the site of damaged cells, where they contribute to tissue inflammation and sensitization of nociceptive neurons (Fig. 1.3) (Pinho-Ribeiro et al. 2017; Yam et al. 2018). Alterations in neurotransmitter release can therefore also be an indicator for impaired pain perception, and thus peripheral neuropathy (Chen et al. 2015; Jang et al. 2004; Wang et al. 2021). A common method to quantify the release of substance P or CGRP is the enzyme-linked immunosorbent assay (ELISA) (Heidari et al. 2017; Perner et al. 2020). For this assay, only the cell culture supernatant is used. Therefore, the endpoint of neurotransmitter release can be multiplexed with most of the aforementioned functional or morphological readouts.

Transcriptome analysis

The analysis of the transcriptome and changes thereof presents another useful endpoint that can be implemented in *in vitro* test methods (Balmer et al. 2014; Dreser et al. 2015; Rempel et al. 2015; Shinde et al. 2017; Waldmann et al. 2014). Changes in gene expression may provide insights into the mechanisms underlying an observed adverse effect, such as upregulated gene expression of pain receptors, which could be the cause of hyperalgesic conditions (Fischer et al. 2017). Transcriptome studies may also reveal downstream effects of altered neuronal signaling, as Ca^{2+} is a universal second messenger, which is involved in signal transduction but also in gene expression regulation (Finkbeiner and Greenberg 1998). Unbiased transcriptomics approaches investigating the whole transcriptome or large gene sets might therefore give important information on gene expression changes directly or indirectly induced by neurotoxic compounds. This may help identify pathways involved in distinct cell biological processes or a compound's mode of action (Waldmann et al. 2017). Hence, such analyses are also highly relevant for drug development, as potential target pathways for future drugs could be indentified to alleviate neurotoxic disease symptoms. In general, transcriptome analysis also allows the basic understanding and definition of applicability domains of the test system of interest (Waldmann et al. 2017). However, unbiased whole transcriptome analysis approaches have low throughput and are less suitable than morphological readouts for large screenings to identify neurotoxicants, as mentioned above. For such purpose, investigating a limited set of biomarker genes known to be involved in, e.g., pain sensitization, is a more feasible option. This approach allows a cheaper and simplified readout of toxicant-related gene expression changes (Kuegler et al. 2010; Rempel et al. 2015). Thus, the (neuro)toxic potential of unknown compounds can be assessed according to their pattern of induced gene expression changes (Wang et al. 2021).

1.5 Aims of the thesis

In risk assessment of drugs and chemicals, special attention must be paid to the PNS. Unlike the CNS shielded by the blood-brain barrier, the PNS lacks specific protection and has a large contact area, making peripheral nerves particularly susceptible to toxicant-induced damage. To date, risk assessment is still mostly based on animal models. However, pathophysiological differences limit the transferability of insights from animal studies to humans, and labor-intensive animal models restrict the throughput of toxicity assessment. Therefore, the testing strategy is currently changing towards human cell-based *in vitro* test methods, which may allow to overcome these limitations.

This thesis addresses the establishment of alternative test methods specifically dealing with peripheral neuropathy-related toxicity. For that purpose, the first aim was to establish a human iPSC-based *in vitro* model system of peripheral neurons with nociceptor features. The concept of transcriptional programming should be implemented in a standard differentiation protocol to direct the differentiation of iPSCs toward the nociceptor fate. Therefore, an iPSC line should be genetically modified with an inducible NGN1-transgene. After adaptatation of the differentiation protocol to the newly generated iPSC line, comprehensive characterization of the differentiated peripheral neurons should be performed at the level of gene expression, protein expression, and functional pain receptor signaling.

The second objective of this study was to develop a suitable method for quantifying receptor signaling. Neuronal receptors are either coupled to ion channels or are themselves ion channels that, when activated, cause the influx of cations into cells. Thus, the establishment of Ca^{2+}-signaling was envisaged as a test endpoint. Since the neuronal class of nociceptors presents a mixed population of neurons expressing different pain receptors, quantification of receptor responses on the single-cell level should be enabled. Therefore, a dedicated program should be implemented to analyze time-lapse data from hundreds of single cells simultaneously and convert them into accessible numerical data.

The ultimate goal of this study was to establish an advanced *in vitro* method to assess functional impairments indicative of peripheral neurotoxicity. For that purpose, nociceptor cultures that provide pain receptor-related functional endpoints such as P2X3 and TRPV1 signaling should be used to investigate the adverse effects of toxicant

exposure. The relevance of the newly established *in vitro* system of peripheral neurons should be demonstrated by using chemotherapeutic agents known to induce peripheral neuropathy *in vivo*. Finally, it should be investigated whether pain receptor function represents an endpoint associated with increased sensitivity to toxicants, allowing identification of substances with deleterious effects well before signs of cytotoxicity or morphological changes occur.

2 Results

2.1 Generation of human nociceptor-enriched sensory neurons for the study of pain-related dysfunctions

provisionally accepted for publication by *Stem Cells Translational Medicine*
bioRxiv (2022) doi: 10.1101/2022.02.19.480828

Anna-Katharina Holzer[1,2], Christiaan Karreman[1], Ilinca Suciu[1], Lara-Seline Furmanowsky[1], Harald Wohlfarth[1], Dominik Loser[3], Wilhelm G Dirks[4], Emilio Pardo González[3], Marcel Leist[1,5]

[1] In vitro Toxicology and Biomedicine, Dept inaugurated by the Doerenkamp-Zbinden foundation, University of Konstanz, 78457 Konstanz, Germany
[2] Graduate school Biological Sciences (GBS)
[3] NMI Natural and Medical Sciences Institute at the University of Tübingen, 72770 Reutlingen, Germany
[4] Department of Human and Animal Cell Lines, DSMZ, German Collection of Microorganisms and Cell Cultures and German Biological Resource Center, 38124 Braunschweig, Germany
[5] CAAT-Europe, University of Konstanz, Konstanz, Germany

Running title: Human nociceptors to study functional neuropathies
Key words: Nociceptors; Peripheral Nervous System Diseases; Allodynia; Oxaliplatin; TRPV cation channels; Receptors, Purinergic P2X3

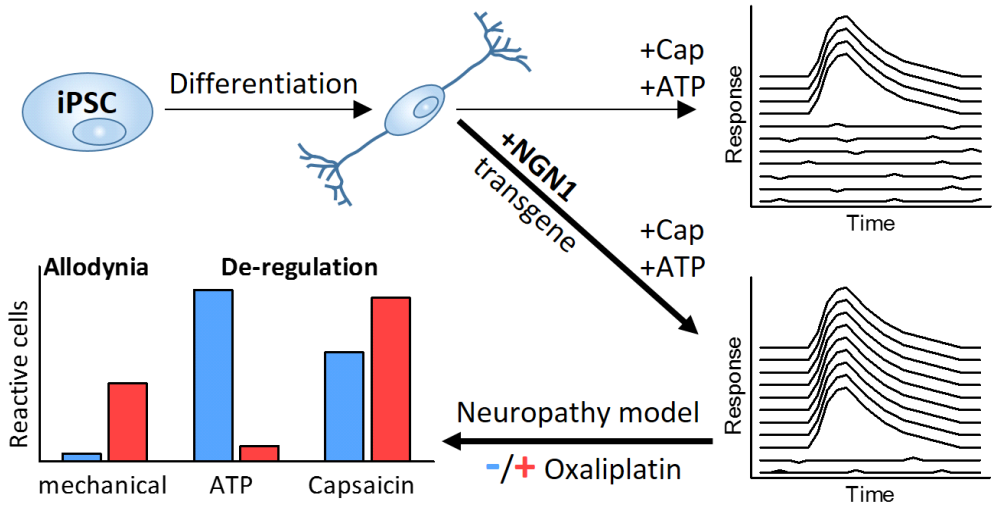

2.1.1 Abstract

In vitro models of the peripheral nervous system would benefit from further refinements to better support studies on neuropathies. In particular, the assessment of pain-related signals is still difficult in human cell cultures. Here, we harnessed induced pluripotent stem cells (iPSCs) to generate peripheral sensory neurons enriched in nociceptors. The objective was to generate a culture system with signaling endpoints suitable for pharmacological and toxicological studies. Neurons generated by conventional differentiation protocols expressed moderate levels of P2X3 purinergic receptors and only low levels of TRPV1 capsaicin receptors, when maturation time was kept to the upper practically-useful limit of 6 weeks. As alternative approach, we generated cells with an inducible *NGN1* transgene. Ectopic expression of this transcription factor during a defined time window of differentiation resulted in highly-enriched nociceptor cultures, as determined by functional (P2X3 and TRPV1 receptors) and immunocytochemical phenotyping, complemented by extensive transcriptome profiling. Single cell recordings of Ca^{2+}-indicator fluorescence from >9,000 cells were used to establish the "fraction of reactive cells" in a stimulated population as experimental endpoint, that appeared robust, transparent and quantifiable. To provide an example of application to biomedical studies, functional consequences of prolonged exposure to the chemotherapeutic drug oxaliplatin were examined at non-cytotoxic concentrations. We found (i) neuronal (allodynia-like) hypersensitivity to otherwise non-activating mechanical stimulation that could be blocked by modulators of voltage-gated sodium channels; (ii) hyper-responsiveness to TRPV1 receptor stimulation. These findings and several other measured functional alterations indicate that the model is suitable for pharmacological and toxicological studies related to peripheral neuropathies.

2.1.2 Introduction

In vitro models of the human peripheral nervous system (PNS) are still relatively scarce. They are required to study chemotherapy-induced peripheral neuropathy (CIPN) and other impairments of the PNS. Of particular interest are systems that allow the assessment of agents that functionally impair sensory neurons.

Cell-based model systems for the PNS are still mostly based on non-human cells, like rat dorsal root ganglion (DRG) neurons. Such DRG cultures have drawbacks concerning e.g., their comparability, and human-specific functions may only be modelled partially (Lehmann et al. 2020). In the past decade, stem cell technology has provided novel alternatives. The fundamental principles of generating peripheral neurons from human induced pluripotent stem cells (iPSCs) were described in 2012 by the Studer laboratory (Chambers et al. 2012). This protocol uses neuralization of iPSCs by dual SMAD inhibition. The fine-tuning of differentiation towards the sensory neuron fate is subsequently achieved by small molecule inhibitors combined with neurotrophins.

In vitro model systems for the PNS are indispensable for toxicity testing, as peripheral neurotoxicants are often not identified by models of the central nervous system (CNS) (Delp et al. 2018; Hoelting et al. 2016). The sensory neuronal subclass of nociceptors is of specific interest in CIPN research. Neuropathies involving this particular subpopulation (Basbaum et al. 2009; Boivie et al. 1989; Campbell and Meyer 2006) are amongst the side effects that most profoundly decrease the quality of life of chemotherapy-receiving patients (Shah et al. 2018; Staff et al. 2017).

Sensory neurons can be classified into nociceptors, mechanoceptors and proprioceptors. The first group expresses the nerve growth factor (NGF)-receptor TRKA (encoded by *NTRK1*) (Snider and McMahon 1998) during maturation, while the others depend on TRKB and TRKC tyrosine kinase signaling. While all peripheral neurons are derived from neural crest progenitors, the TRKA-expressing neurons develop from the subgroup of NGN1-positive neural crest cells (Ma et al. 1998; Ma et al. 1999). They can be further divided into nociceptor-subgroups: Peptidergic neurons release the neuropeptides substance P and calcitonin gene-related peptide and maintain TRKA expression. Non-peptidergic neurons lose expression of TRKA upon maturation, and express the RET neurotrophin receptor instead (Snider and McMahon 1998). Nociceptors can also be distinguished according to their expression of different cation channels like the transient receptor potential (TRP) channels or the purinergic receptor ion channels. Notable

members of the TRP family are TRPV1, TRPM8 and TRPA1 channels. The respective major functions are the sensing of heat, cold or electrophilic chemicals (Basbaum et al. 2009). Temperature-sensing TRP channels are polymodal and can respond to chemical agonists. A prominent example is the TRPV1 channel, which is activated by increased temperatures exceeding the threshold of ~43°C, but also by vanilloid compounds like capsaicin (Caterina et al. 1997). The purinoceptor P2X3 is the main ATP-activated pain-related channel on nociceptors. As TRPV1 and P2X3 are only found on nociceptors and not on other sensory neurons (e.g., stretch receptors), they can serve as characteristic functional biomarkers (Chen et al. 1995; Cook et al. 1997; Immke and Gavva 2006).

De-regulations of ligand-activated and voltage-gated ion channels on peripheral neurons are known to contribute to the dose-limiting side-effects induced by the chemotherapeutic drug oxaliplatin (Adelsberger et al. 2000; Calls et al. 2020). General neuronal hyperexcitability (Adelsberger et al. 2000; Lehky et al. 2004; Webster et al. 2005; Wilson et al. 2002), thermal hyperalgesia and mechanical allodynia (Adelsberger et al. 2000; Anand et al. 2010; Chen et al. 2015; Chukyo et al. 2018) are characteristic features of acute oxaliplatin-induced peripheral neuropathy (OXAIPN). While all platinum drugs lead to structural damage upon prolonged treatment, the acute form of OXAIPN occurs largely independent of neurodegeneration (Park et al. 2008).

The example of OXAIPN demonstrates the need for *in vitro* model systems that can identify functional impairments of the PNS. While assays to detect chemicals acting on neurite growth, neuroprogenitor migration or central neuronal signaling are well established (Delp et al. 2018; Hoelting et al. 2016; Klima et al. 2021a; Loser et al. 2021b; Loser et al. 2021c; Nyffeler et al. 2017; Stiegler et al. 2011; Wing et al. 2017), PNS systems optimized to detect functional impairments are still scarce, and data on the modulation of pain receptors are mostly not included (Boisvert et al. 2015).

Therefore, the aim of this study was to establish an *in vitro* system able to detect signaling alterations relevant for CIPN. A protocol to generate peripheral neurons with nociceptor features (PNN) from iPSCs was established. After an extensive phenotypic profiling, Ca^{2+}-imaging was chosen as a quantitative endpoint for the assessment of pain-receptor signaling. A case study of oxaliplatin treatment was performed to demonstrate the relevance of our novel PNS model, which offers pain-receptor related functional endpoints for CIPN research. Thus, our study explored whether complex functional impairments of nociceptors are reliably detectable and quantifiable *in vitro*.

2.1.3 Material and methods

Materials

Unless mentioned otherwise, all chemicals and cell culture reagents were from Merck (Darmstadt, Germany). All antibodies and PCR primers used are compiled in dedicated tables in the supplementary materials file. There, also an extensive chapter on supplementary methods is included.

Differentiation of sensory neurons from iPSC

We used the iPSC line Sigma iPSC0028 (Si28) and derived from this the transgenic iPSC line Si28-NGN1. Maintenance of the iPSCs was performed under xeno-free conditions (Chen et al. 2011) as detailed in the supplementary methods. The differentiation was performed according to Hoelting et al. (2015) (Hoelting et al. 2016; Klima et al. 2021a) with small modifications as shown in figure 2.1.S1 and described in Klima et al. (2021) (Hoelting et al. 2016; Klima et al. 2021a).
The detailed differentiation procedure is described in the supplementary methods (also see annex). In brief, iPSCs underwent neuralization induced by dual SMAD inhibition. Differentiation towards the sensory neuron fate was achieved by small molecule inhibition following the established literature [2]. After 9 days of differentiation (on DoD9'), immature peripheral neurons were frozen in 90% fetal bovine serum (FBS) (Thermo Fisher Scientific, Waltham, MA, USA) and 10% dimethyl sulfoxide (DMSO). Further maturation after thawing was driven by a growth factor cocktail. For the differentiation of PNN, doxycycline (2 µg/ml) exposure from DoD4'-9' and DoD1-14 was integrated in the standard small molecule differentiation protocol, as detailed in the results chapter.

PeriTox test

Immature peripheral neurons were thawed and used on DoD0 to assess the effects of test compounds on neurite area and cell viability (supplementary methods) as previously described (Delp et al. 2018; Hoelting et al. 2016; Klose et al. 2021; Krebs et al. 2020).

Generation of a gene-edited iPSC line

The human Si28 line was infected with the lentivirus described in figure 2.1.2A (also see supplementary methods). In brief, infected cells underwent hygromycin (Carl Roth, Karsruhe, Germany) selection followed by manual picking and expansion of the colonies. Stocks of the clones were cryopreserved in 90% FBS and 10% DMSO. Short tandem repeat (STR) DNA typing (described in detail in (Dirks and Drexler 2013)) was performed for cell line authentication. To evaluate the clone's NGN1 expression properties, iPSCs were seeded as single cells in E8 medium and exposed to doxycycline (2 µg/ml) for up to 5 days (Fig. 2.1.2B).

Assessment of gene and protein expression

Gene expression was investigated by quantitative reverse transcriptase PCR (RT-qPCR) using SsoFast™ EvaGreen® Supermix (Bio-Rad). Protein expression was assessed via immunofluorescence staining and microscopy. All samples were prepared, and analyzed exactly as described before (Dreser et al. 2020; Klima et al. 2021a), using primers and antibodies as detailed in supplementary methods.

Transcriptome data generation and analysis

Sample lysates were prepared as described (Klima et al. 2021a; Loser et al. 2021b). Measurements were performed at Bioclavis (BioSpyder Tech., Glasgow, UK) via the TempO-Seq targeted sequencing technology applied to the whole transcriptome set (House et al. 2017). For data processing, the R package DESeq2 (v1.32.0) was used for quality control, normalization and determination of differentially expressed genes (DEGs) (Love et al. 2014). A Benjamini-Hochberg-adjusted threshold of $P < 0.05$ and a fold change of 2 were used as filter for DEGs. Analysis of gene ontology (GO) term over-represenation was done with g:profiler software (Raudvere et al. 2019). All procedures are detailed in supplementary methods, and the data on numbers of reads for each gene analyzed, and the fold-changes for DEGs are provided in Supplement file1, organized as Excel workbook.

Electrophysiological data

For electrophysiological characterization of the PNN, manual patch-clamp recordings and multi-electrode array measurements were performed as described (Klima et al. 2021a; Loser et al. 2021c). Details are given in supplementary methods.

Measurement of changes in intracellular Ca^{2+} concentration $[Ca^{2+}]_i$

Sensory neurons were cultured in 96-well plates after thawing. Cells were loaded with the Ca^{2+}-indicator Fluo-4 (Thermo Fisher Scientific). Monitoring of $[Ca^{2+}]_i$ was performed using a VTI HCS microscope (Thermo Fisher Scientific) equipped with an automated pipettor and an incubation chamber providing an atmosphere with 5% CO_2 and 37°C. Cells were imaged for 45 s. Test compounds were automatically applied after baseline recording (10 s). The images were exported as *.avi video files and analysed with the CaFFEE software. Details are given in a dedicated technology paper (Karreman et al. 2020) and in supplementary methods.

Statistics

If not stated otherwise, experiments were performed on 3 or more independent cell preparations (here called biological replicates). In each cell preparation at least three different wells (here called technical replicates) were measured. Quantitative Ca^{2+}-imaging data were derived from time-dependent series of images by using the CaFFEE software (Karreman et al. 2020). The binary endpoint of reactive/non-reactive cells was defined primarily by a well-specific, noise level-based threshold of changes in fluorescence intensity: (mean(ΔF) + 3x SD(ΔF)), with an upper limit set to 18 (ΔF: fluorescent change by negative control stimulation). Information concerning descriptive statistics and experimental variability is included in the figure legends or the figures themselves. GraphPad Prism 5 software (Version 7.04, Graphpad Software, Inc, San Diego, USA) was used for significance testing and data display. Data were evaluated by ANOVA plus appropriate post-hoc testing method or by t-test for binary comparisons. *p*-values < 0.05 were regarded as statistically significant.

2.1.4 Results

Characterization of human sensory neurons generated from non-modified iPSCs

For the generation of sensory neuronal cultures, we optimized a previously published two-step differentiation protocol starting from iPSC (Hoelting et al. 2016). The time point of freezing of the cells was adapted (DoD9'), and the culture medium was supplemented with cytarabine from DoD3 until DoD14 to remove any mitotic, potentially non-neuronal cells (Fig. 2.1.S1A). This procedure yielded pure neuronal cultures that develop an extensive neurite network (Fig. 2.1.1A,B). The capacity of such cells to grow neurites within 24 h forms the basis for the established PeriTox test (Delp et al. 2018; Hoelting et al. 2016). This assay was used to verify that typical neurotoxicants exhibit a specific neurite-damaging effect. The pesticide rotenone, the gout medication colchicine and the three chemotherapeutics taxol, bortezomib and oxaliplatin all reduced the neurite area at concentrations that did not affect general neuronal viability (Fig. 2.1.1C, 4.1.S1C).
The sensory neuronal phenotype was confirmed by gene expression analysis. Markers like *PRPH*, *SCN9A* and *P2RX3* were expressed on DoD1 and further up-regulated over time. Indicators of the neural crest cell intermediary stage (*PAX3*, *TLX2*) were down-regulated (Fig. 2.1.1D). Markers for cortical neuron precursors (*PAX6*) or glial cells (*GFAP*) were absent. To investigate the functional expression of pain-related receptors, we used selective agonists of TRPV1 (capsaicin) and P2X3 (α,β-methylene ATP (α,β-meATP) (North 2003)). Under normal conditions, only 10% of the cells showed P2X3- and 1% TRPV1-signaling. This was not considerably changed by maturation of up to 40 days (Fig. 2.1.1E). By mimicking inflammatory conditions with increased NGF concentrations (Bonnington and McNaughton 2003; Chuang et al. 2001; D'Arco et al. 2007; Namer et al. 2015; Zhang et al. 2005) we obtained 60% of α,β-meATP-responsive cells. However, the capsaicin-responsive subpopulation did not exceed 5%. In summary, the optimized protocol generated largely pure, fully post-mitotic sensory neurons (Fig. 2.1. S1B), but the functional properties were not suitable for CIPN research related to altered pain sensation, e.g., through the TRPV1 receptor system.

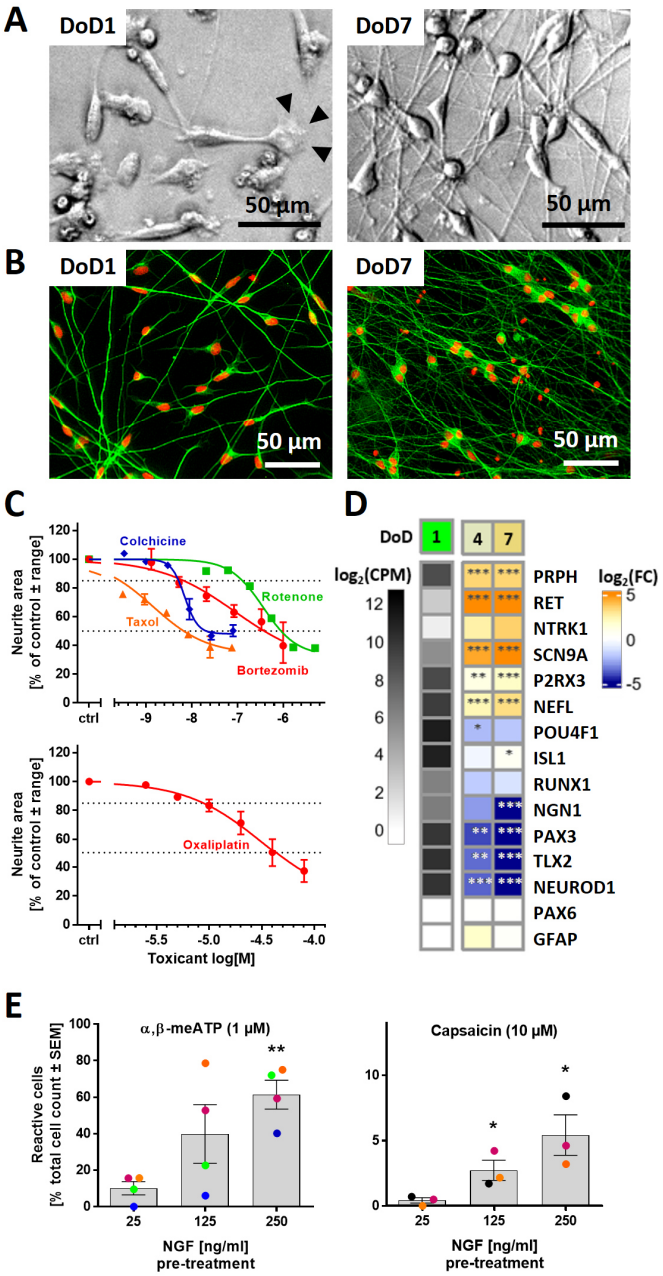

Figure 2.1.1: Human sensory neurons derived from iPSCs

Cells were pre-differentiated for 9 days and frozen (Fig. 2.1.S1A). Counting of peripheral neuronal age in days of differentiation (DoD) started after thawing and plating (= DoD0). **(A)** Phase-contrast images of DoD1/DoD7 neurons. Arrowheads indicate a growth cone. **(B)** DoD1/DoD7 cultures stained for the neuronal cytoskeletal marker β-III-tubulin (green); DNA is shown in red. **(C)** Neurons were used in the PeriTox test to assess the effects of toxicant exposure (24 h) on neurites. Data are given as mean ± range of 2-3 biological replicates. Viability was not significantly affected at the tested drug test concentrations (see Fig. 2.1.S1B). **(D)** Gene expression levels were determined by the TempO-Seq method. The left column shows the absolute expression levels of selected marker genes on DoD1 in counts of the corresponding gene per 1 million reads (CPM). The data for DoD4/DoD7 show the fold change (FC) of the expression levels *versus* DoD1. The color scale uses $\log_2$FC units (see supplementary files for complete data sets). **(E)** Mature neurons (DoD25-45) were used for Ca^{2+}-imaging. Cells reacting to the application of α,β-methylene ATP (α,β-meATP) and capsaicin were quantified. The effect of pre-treatment (48 h) with increased concentrations of nerve growth factor (NGF) on the percentage of reactive cells was assessed. Data displayed as bars are means ± SEM of 3-4 biological replicates. Color matching data points are derived from the same experiment. * $p < 0.05$, ** $p < 0.005$, when tested vs. control conditions (25 ng/ml NGF).

Generation of an iPSC line with inducible NGN1 expression

The standard differentiation protocols did not yield a sufficiently large nociceptor subpopulation to allow functional studies. Consequently, we investigated an alternative approach. NGN1 is a key transcription factor in the development of the here-desired neurons (Lallemend and Ernfors 2012; Ma et al. 1998; Ma et al. 1999). Therefore, we hypothesized that its time-controlled overexpression would improve differentiation success (Boisvert et al. 2015).

An iPSC line was generated, in which NGN1 expression can be controlled by adding doxycycline to the medium. After the NGN1 expression construct (Fig. 2.1.2A, 4.1.S2A) was stably inserted into the genome, the newly generated iPSC line Si28-NGN1 was authenticated by the established method of STR analysis (Dirks and Drexler 2013). On this basis, the Si28-NGN1 line and the commercially available Si28 line were declared identical (Fig. 2.1.S3). The pluripotency of the newly generated iPSC population was assessed by immunofluorescence imaging. The expression of several pluripotency markers (e.g., Nanog, OCT4) (Fig. 2.1.S2B-D) as well as the absence of the neuroectodermal markers PAX6 and SOX10 (data not shown) were similar to that of the pluripotent parent cell line. Further, the cells' NGN1 expression properties were verified (Fig. 2.1.2B). Gene expression of *NGN1* was found to be inducible by doxycycline (Fig. 2.1.2C). The functionality of the *NGN1* transgene was derived from the control of its downstream target *NTRK1*. Moreover, transgene expression for five days leads to the complete conversion of iPSCs into cells expressing the pan-neuronal marker βIII-tubulin (βIII-Tub) and exhibiting neuronal morphology. Furthermore, these cells expressed the PNS markers peripherin (PRPH), BRN3A and ISL1 (Fig. 2.1.2D, 4.1.S2E,F)). Such a staining pattern is typical for neurons that have exited the cell cycle (Ma et al. 1999). Taken together, these data confirm the successful generation of an iPSC line carrying an inducible *NGN1* transgene with the expected functionality of the gene product, NGN1.

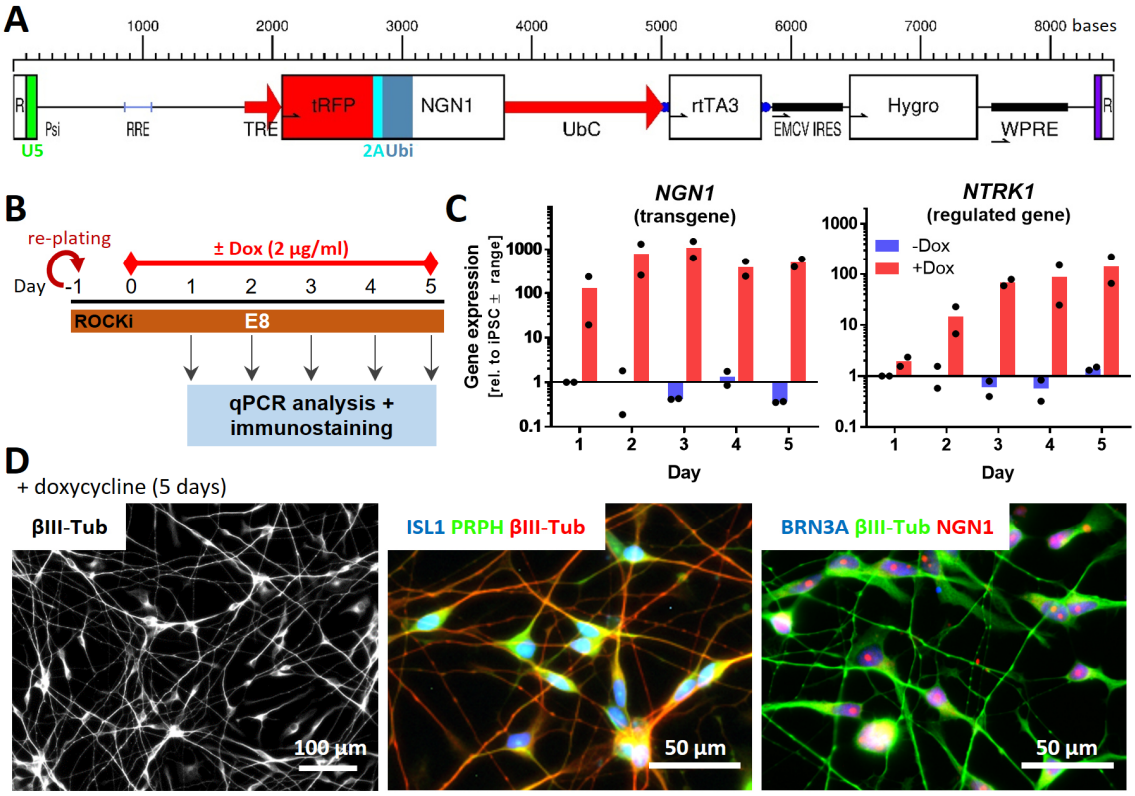

Figure 2.1.2: Generation of human iPSCs with inducible expression of ectopic NGN1

(A) Structure of the lentiviral construct used to generate a NGN1-overexpressing iPSC line. NGN1 is expressed as fusion protein with turbo red fluorescent protein (tRFP). tRFP and NGN1 are linked via a 2A region and ubiquitin (Ubi) to ensure the precise cleavage of NGN1 inside cells. Gene expression is controlled via the tetracycline-on system (TRE promotor). This system uses a reverse tetracycline-controlled transactivator (rtTA3) driven by the UbC promoter. R, repeat region of the HIV long terminal repeat (LTR) region; U5 (green), U5' region of the HIV LTR; Psi, packaging sequence; RRE, Rev response element; TRE, tetracycline response element; UbC, Ubiquitin C promotor; EMCV IRES, encephalomyocarditis virus internal ribosomal entry site; Hygro, hygromycin resistance; WPRE, woodchuck hepatitis virus post-translational regulatory element. **(B)** Experimental setup to assess the *NGN1* transgene expression. Cells were exposed for 5 days to doxycycline (0 or 2 µg/ml). **(C)** Gene expression of *NGN1* and its downstream-regulated gene *NTRK1* were monitored daily in control (blue) and doxycycline exposed cells. Gene expression was quantified by RT-qPCR. Data are given relative to iPSC (-Dox, day1). Data displayed as bars are means of two biological replicates (black dots). **(D)** Immunofluorescence images of cells treated with doxycycline for 5 days. Cells were labelled with antibodies against β-III tubulin (βIII-Tub), peripherin (PRPH) and the sensory neuronal transcription factors NGN1, ISL1 and BRN3A. Color code and scale bars are given in the images. More detail is given in figure 2.1.S2E,F.

Integration of NGN1 overexpression in the standard small molecule differentiation protocol

In a next step, it was tested, which time window of NGN1-overexpression was most suitable to improve the standard differentiation protocol. Three different doxycycline exposure schedules (S_1–S_3), integrated into the standard differentiation, were investigated (Fig. 2.1.3A). Gene expression of the sensory neuronal markers *NGN1*, *NTRK1*, *RUNX1*, *PRPH*, *POU4F1* (*BRN3A*) and *ISL1* was monitored daily until the day of freezing (Fig. 2.1.3B, 4.1.S4B). Early induction of *NGN1* expression on DoD2' in condition S_2 led to an earlier expression of *NGN1*, *NTRK1*, *PRPH* and *ISL1* compared to cells not exposed to doxycycline (S_1). However, up-regulation of *RUNX1* expression, a gene crucial for nociceptor specification (Chen C-L et al. 2006; Lallemend and Ernfors 2012), was poor, while the rate of cell death after thawing was increased (Fig. 2.1.3C). Differentiation condition S_3 resulted in the highest gene expression levels for *RUNX1*, and shifted *PRPH* and *NTRK1* expression to earlier time points. Immunofluorescence images on DoD3 showed that all three exposure schedules yielded peripheral neurons ($PRPH^+$ neurites). The sensory neuronal markers ISL1 and BRN3A were expressed to a large extent in conditions S_1 and S_3 (74-100% positive cells), but not in S_2 (Fig. 2.1.3C, 4.1.S4A,C,D), which was decisive to exclude S_2. Eight days after thawing uniformity of neuronal cultures was further assayed using tRFP fluorescence as an internal reporter of NGN1 expression (Fig. 2.1.3D). Quantification of red fluorescent cells showed S_3-derived cultures to be more uniform (96% tRFP-positive cells) than S_1 cultures (36% tRFP-positive cells) (Fig. 2.1.3E). Therefore, all future experiments were conducted using exposure schedule S_3, which yields neuronal cultures with the highest sensory neuron marker expression and uniformity.

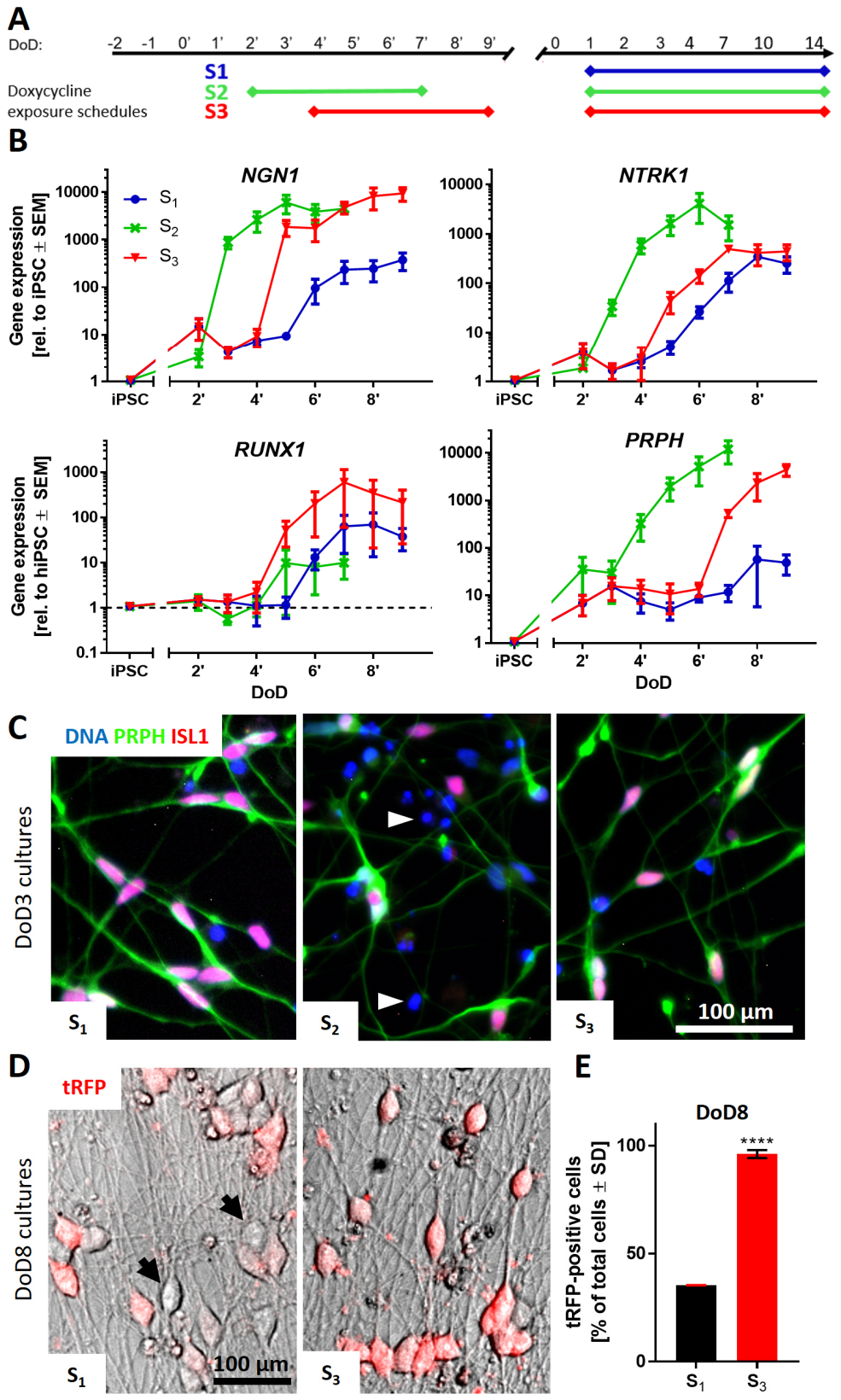

Figure 2.1.3: Integration of NGN1 overexpression in the standard small molecule differentiation protocol

(A) Schematic representation of three different doxycycline exposure schedules (S_1, S_2, S_3) incorporated in the standard differentiation protocol. Condition S_1 did not receive doxycycline treatment before freezing. Cells of condition S_2 were treated with doxycycline from DoD2' until DoD7' with subsequent freezing of the cells. Condition S_3 included doxycycline treatment from DoD4' until DoD9' with subsequent freezing. After thawing, all three conditions were exposed to doxycycline from DoD1 until DoD14. **(B)** Gene expression analysis of the nociceptor marker genes *NGN1*, *NTRK1*, *RUNX1* and the general sensory neuronal marker gene peripherin (*PRPH*) for all three exposure situations. Data are expressed relative to expression levels in iPSCs and given as means ± SEM of 3-4 biological replicates. **(C)** Immunofluorescence images of cultures (S_{1-3}) on DoD3 (after thawing). Cells were stained for peripherin (PRPH) and ISL1. Nuclei were stained with H33342 (blue). Details are displayed in figure 2.1.S4A. White arrowheads indicate exemplary dead cells. **(D)** Overlay of phase contrast and tRFP fluorescence images of condition S_1 and S_3 neuronal cultures on DoD8. Black arrows indicate exemplary tRFP-negative cells. **(E)** Quantification of tRFP positive cells in cultures of differentiation conditions S_1 and S_3 on DoD8. Data are shown as percentage of total cell count ± SD. DoD, day of differentiation; tRFP, turbo red fluorescent protein.

Transcriptomics-based characterization of mature iPSC-derived sensory neurons

We used time-dependent transcriptome profiling as broad and unbiased approach to describe the differentiation process of iPSC-derived sensory neurons. Transcript levels of about 19,000 genes were measured for 7 differentiation stages (Suppl. File2). A principal component analysis (PCA) was used as a first overview of the data structure. Independent biological replicates clustered closely together, and the first principle component coincided with increasing time of maturation (Fig. 2.1.4A). The absolute expression levels of the sensory neuron marker genes *ISL1* and *PRPH* were high (>1000 transcripts per 1 million reads) from DoD1 until DoD49. Nociceptor marker genes like *P2X3*, *RET* and *SCN9A* also reached high absolute levels (Suppl. File2). However, some essential genes (*NTRK1*, *SCN10A*, *TRPV1)* were not captured well by the transcriptome mapping approach. Consequently, their gene expression was investigated via RT-qPCR. The levels of *NGN1*, *RET*, *NTRK1*, *RUNX1* and *SCN10A* peaked at DoD3-7 and then declined until DoD21 (Fig. 2.1.4B). For *P2RX3*, *SCN9A*, *TRPM8* and *TRPV1* we found increased expression on DoD3-7, and thereafter largely stable levels until DoD21 (Fig. 2.1.4C).

The expression kinetics of these pre-selected transcripts are in good agreement with our objective of generating nociceptor-enriched sensory neuron cultures. For further transcriptome data mining, DEGs were determined for all sampling time points (Suppl. file2). For the 600 DEGs of DoD42 altogether 200 over-represented gene ontology (oGO) term groups were identified (Raudvere et al. 2019). The 50 oGOs with the lowest *p*-values mainly fell into the superordinate groups "synapse signaling", "neurotransmitters",

"receptors, channels, transporters" and "morphogenesis". They were also analyzed for the other time points (Fig. 2.1.S5A,B) and quantitative GO activation scores (Waldmann et al. 2014; Waldmann et al. 2017) were calculated for all time points (Fig. 2.1.4D, 4.1.5C). Activation scores for "synapse signaling" and "neurotransmitters" showed a continuous increase until DoD42 (Fig. 2.1.4E, upper graph). The activation scores of receptor/channel-related genes showed a plateau for DoD7-28 and then jumped to a higher level at late differentiation stages (DoD35-42) (Fig. 2.1.4E, lower graph). In summary, analysis of gene expression patterns over large biological categories confirmed that the here-established differentiation protocol yields peripheral neurons with nociceptor features (PNN). While most general neuronal markers were well established after 1-3 weeks of differentiation, genes linked to particular PNN functions continued to be up-regulated until at least DoD35-42.

Electrophysiological characterization of PNN

The basic functional characterization of the PNN also included a check for general neuronal electrophysiological features. Patch-clamp measurements provided evidence for all major classes of voltage-gated cation channels (K_V, Na_V and Ca_V) (Fig. 2.1.S7). All cells recorded showed that they could fire action potentials (Fig. 2.1.5A). Half of the cells showed a phasic firing pattern (Fig. 2.1.5B, left), while the other half displayed tonic firing behavior (Fig. 2.1.5B, right). This distribution is consistent with the current literature on the characterization of primary rat DRG neurons (Yu et al. 2014). After confirmation of these basic neuronal properties, we moved on to establish a neuronal signaling endpoint, more suitable for broader toxicological/pharmacological evaluation.

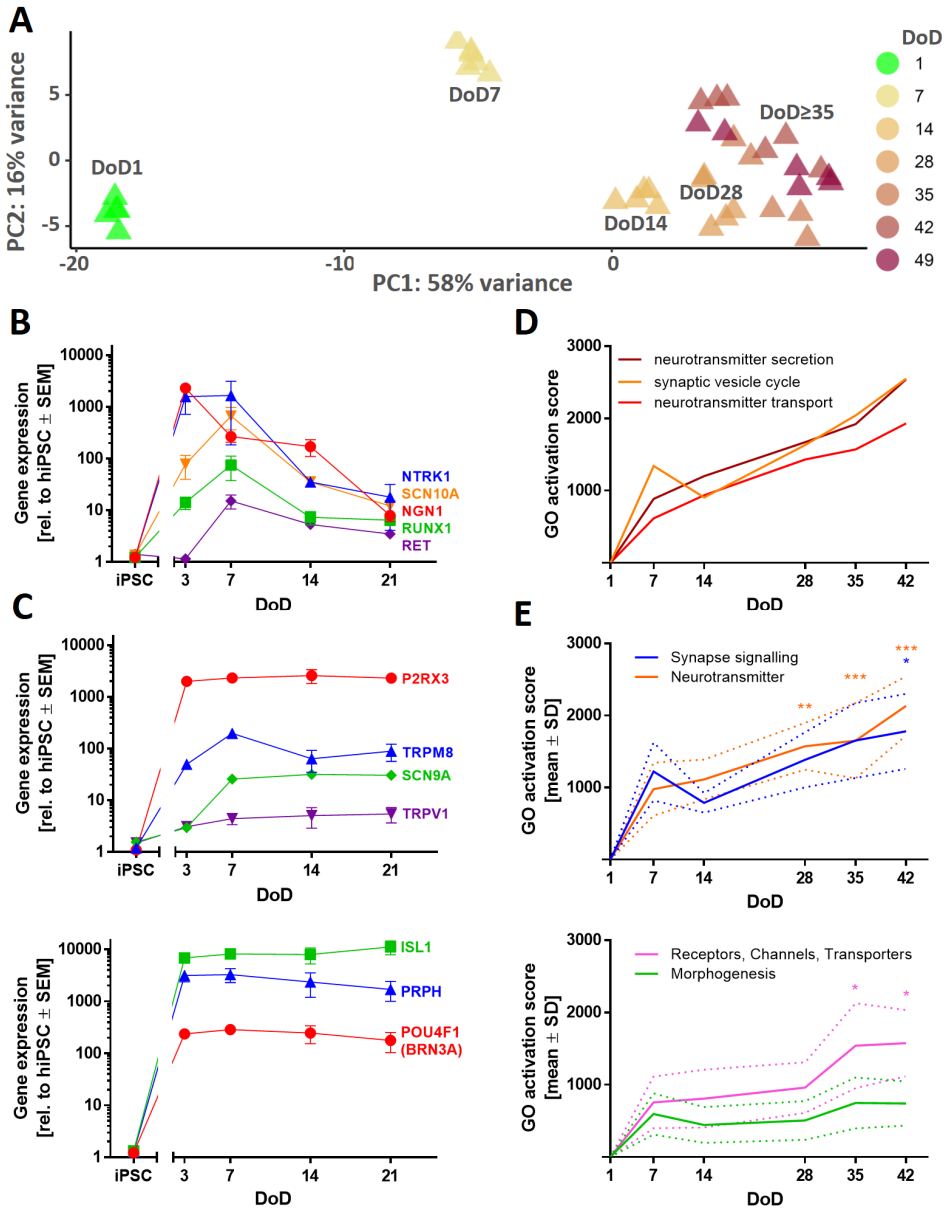

Figure 2.1.4: Time-dependent transcriptome profiling of iPSC-derived sensory neurons

(A) TempO-Seq whole transcriptome analysis (19,000 genes). For the top 500 variable genes of this data set (full data in Supplementary file1) a PCA was performed. In the two-dimensional PCA display, seven maturation stages of PNN are color-coded according to their DoD. Data points are derived from three independent differentiations. **(B,C)** Gene expression levels of sensory neuron and nociceptor marker genes were assessed via RT-qPCR. Data are means ± SEM, n = 3-4. Error bars smaller than the data point symbols are not shown. **(D)** Over-represented gene ontology (oGO) terms were determined for the significant DEGs on DoD42. Quantitative activation scores of the Top50 oGOs were calculated for all time points by "multiplying the percentage of genes within the GO that was found to be significantly regulated with the average fold change of these regulations" (Waldmann et al. 2014). Activation scores for the GO terms "neurotransmitter secretion", "synaptic vesicle cycle" and "neurotransmitter transport" are shown over time. **(E)** oGO terms were assigned to the superordinate groups "Synapse signaling", "Neurotransmitter", "Receptors, Channels, Transporters" and "Morphogenesis" (see Fig. 2.1.S5). Means of the activation scores of all oGOs belonging to one group are shown to visualize the development of these biological categories over time. The dotted lines indicate the upper and lower bounds of the SEM. Significance was tested against the respective mean activation scores on DoD7. * $p < 0.05$, ** $p < 0.001$, *** $p < 0.0001$.

Establishment of intracellular Ca^{2+}-measurement as test endpoint

We decided on the use of Ca^{2+}-imaging (Tsien and Tsien 1990) as signaling endpoint for our PNN. General proof-of-concept for the feasibility of this approach was obtained by recording strong signals triggered by increased K^+ concentrations in the medium or by opening of Na_V channels by veratridine (VTD) (Fig. 2.1.5C,D). As PNN are a mixed neuronal population, it was important to establish the Ca^{2+}-signaling endpoint on a single cell level. As practical approach to work with the multi-dimensional information provided by the recording of Ca^{2+} fluorescence time courses of thousands of cells, we decided to use a binary endpoint of "responsive" *versus* "non-responsive" cells. For this, we thoroughly investigated and defined suitable response thresholds (Fig. 2.1.S8). Based on the extensive evaluation (signal intensity changes (Δ) for >9200 cells), a robust algorithm was chosen to define responsive cells in Ca^{2+}-signaling experiments.

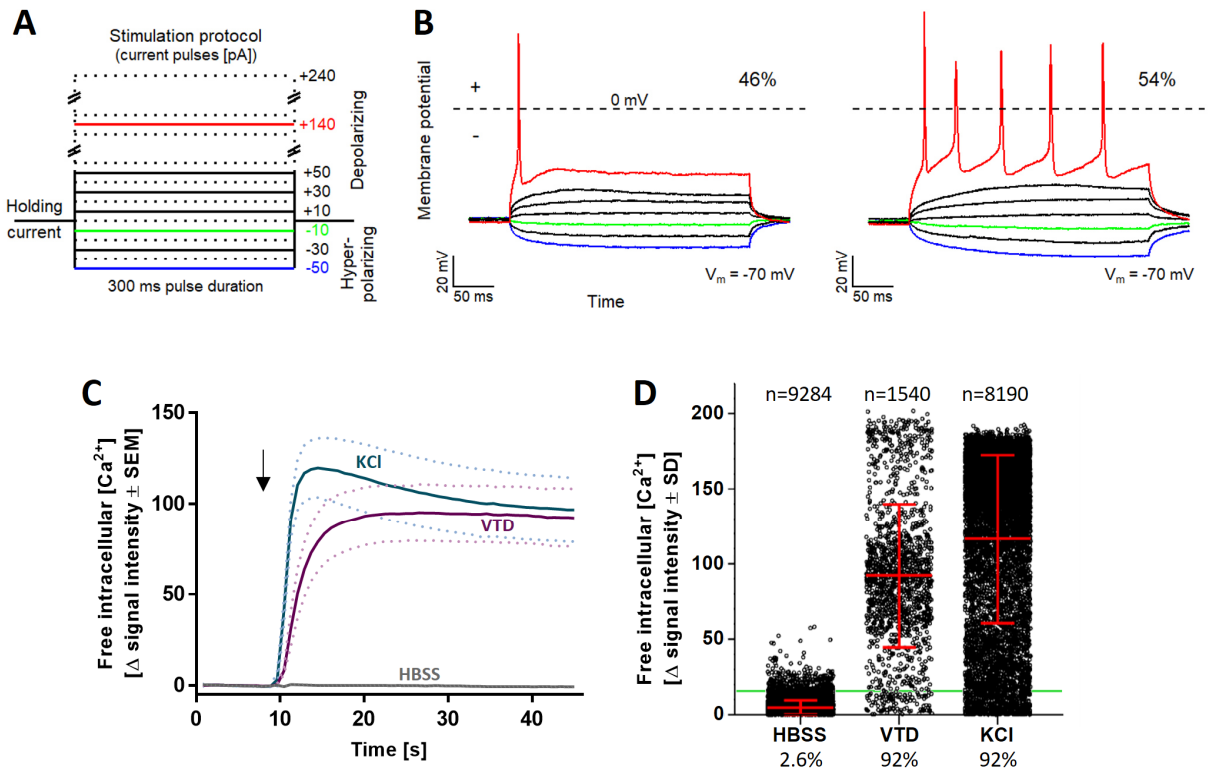

Figure 2.1.5: Characterization of neuronal excitability of PNN

PNN (DoD28-35) were used for current-clamp recordings and Ca^{2+}-imaging experiments. **(A)** Schematic representation of the stimulation protocol used for current-clamp recordings. Current pulses were applied with a pulse duration of 300 ms and a pulse frequency of 0.2 Hz, starting at -50 pA and increasing in steps of +10 pA. Example pulses are colored. **(B)** Current-clamp measurements of PNN (n=28). Cells exhibit phasic (46%) (B, left) or tonic (54%) (B, right) action potential firing behavior. **(C)** Representative traces of changes in Ca^{2+} indicator fluorescence (=Δ signal intensity) in response to the negative control HBSS (Hanks' balanced salt solution), the positive control KCl [50 mM] and the voltage-

gated sodium (Na_V) channel opener veratridine (VTD) [3 μM]. The arrow indicates the time point of stimulus addition. Data are shown as means of 4 biological replicates. The dotted lines indicate the upper and lower bounds of the SEM. **(D)** Quantification of the percentage of reactive cells according to their Δ signal intensity values upon HBSS, VTD or KCl addition. The green line indicates the noise boundary of the Δ signal intensity. Each dot represents the Δ signal intensity of an individual cell. The mean ± SD of all cells is shown graphically in red. The percentage of reactive cells is indicated below the diagram and the exact number of measured cells is given above. A total of more than 10,000 cells was individually measured in 14 experiments.

Functional characterization of PNN cultures regarding nociceptive features

A hallmark of nociceptive neurons is the expression of ion channels responsible for the sensation of pain. In this study, we focused on TRPV1 and P2X3. Immunofluorescence staining revealed the presence of both receptors in virtually all cells on DoD42 (Fig. 2.1.6A, 4.1.S9A,B). The specific agonist of P2X3 receptors α,β-meATP and the TRPV1-agonist capsaicin were used as tool compounds for functional characterization. The cultures did not react to the stimuli during the first 4 weeks after thawing. From then on, the percentage of reactive cells continuously increased until DoD42 (Fig. 2.1.S9C, left, right). For comparison, functional Na_V channels were found to be present from DoD7 on and maximum culture responsiveness towards the Na_V opener VTD was reached on DoD21 (Fig. 2.1.S9C, middle).

Responses induced by α,β-meATP were characterized by fast-inactivating inward currents typical for P2X3 receptors (Fig. 2.1.6B,C, left) (Bianchi et al. 1999; Koshimizu et al. 2000; North 2002). Capsaicin, in contrast, evoked sustained inward currents throughout the exposure period, as is typical for TRPV1 receptors (Fig. 2.1.6B,C, right) (Starkus et al. 2019; Ursu et al. 2010). The expression of functional TRPV1 receptors was further substantiated, as treatment with two other TRPV1-agonists, olvanil and piperine, induced Ca^{2+} influx in a subset of neurons (Fig. 2.1.S9G). Quantification of reactive cells revealed a concentration-dependency of both P2X3 and TRPV1 responses (Fig. 2.1.6E), which also makes this endpoint a useful model for pharmacological intervention studies in PNN. The reactivity of PNN towards nociceptive stimuli was clearly superior to the one observed in peripheral neurons differentiated conventionally (without transient NGN1 overexpression) (Fig. 2.1.6D, grey boxes).

As a next step, we performed double-stimulation studies to investigate the overlap of P2X3 and TRPV1 receptor-expressing cell populations (Fig. 2.1.S9D). PNN were treated with α,β-meATP followed by a capsaicin stimulus and vice versa. Independent of the

sequence, we found that 40% of the cells reacted to a P2X3 stimulus only, while about 10% reacted towards capsaicin only. One quarter of the whole population responded to both stimuli (Fig. 2.1.S9E). These sequential stimulation experiments also demonstrated that there was no cross-(de)sensitization of TRPV1 and ATP receptors, as has sometimes been claimed (Ambrosino et al. 2013; Jancsó et al. 1967; Jarvis 2010). This finding also significantly increased the throughput of this method, as double-stimulations can be used as the standard experimental design.

To ensure that the measured responses are P2X3- and TRPV1-specific, the cells were pre-incubated with the P2X3-selective antagonists AF-353 (Fig. 2.1.6E, left) or A-317491 (data not shown). A concentration-dependent decrease in Ca^{2+} influx was observed at ≥30 nM AF-353 and ≥2.5 µM A-317491, confirming P2X3 as the main P2X subtype expressed in PNN (Gever et al. 2010; Jarvis et al. 2002). To prove the specificity of TRPV1-responses the well-known antagonist capsazepine was used. We also tested SB-366791, which exhibits improved selectivity and potency (Gunthorpe et al. 2004; Varga et al. 2005). Both antagonists blunted the capsaicin responses. Selectivity of the receptor-antagonists A-317491 and capsazepine was confirmed by double-stimulation experiments demonstrating that only the respective target receptor was inhibited, but not the response of the other receptor (Fig. 2.1.S9F).

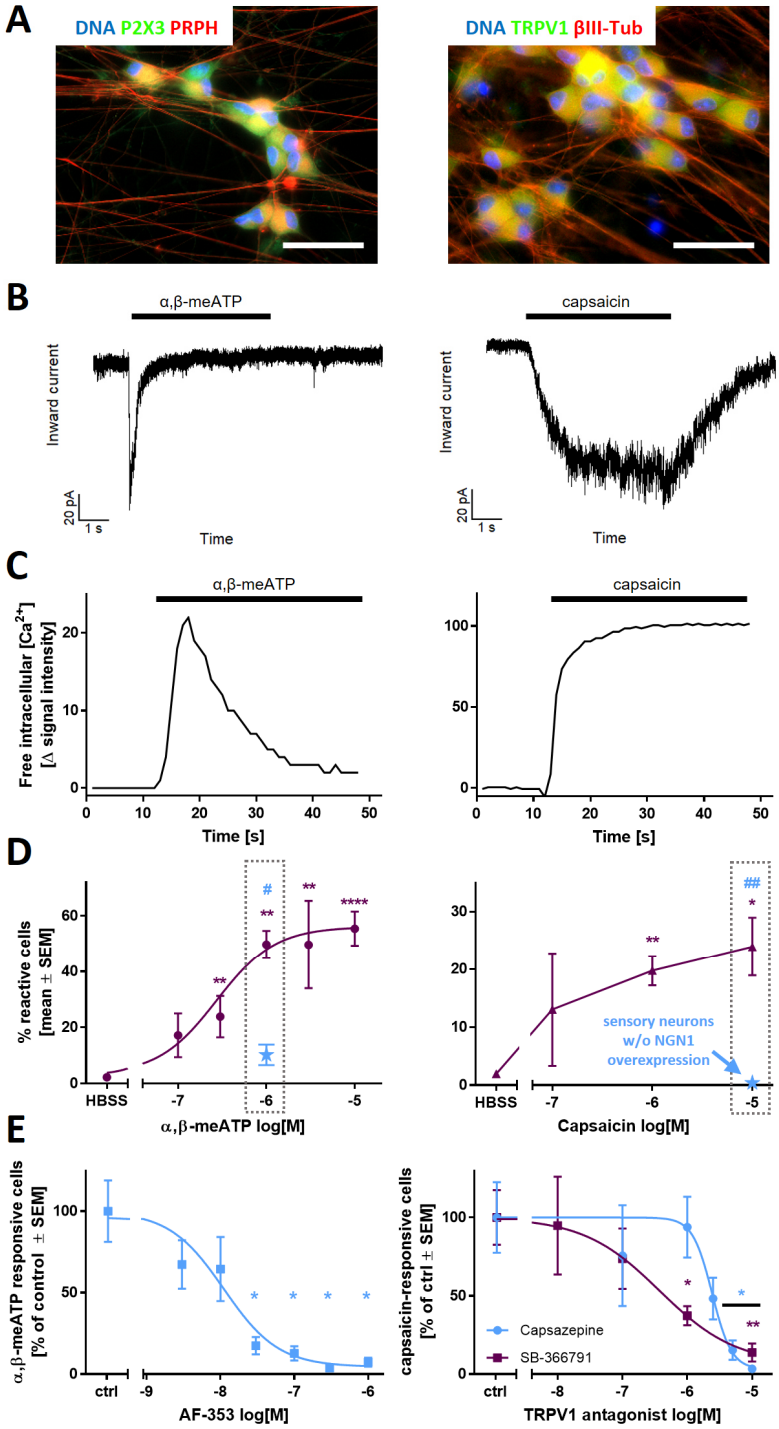

Figure 2.1.6: Functional characterization of the nociceptor-ion channels P2X3 and TRPV1 in PNN

Sensory neurons were differentiated for at least 37 days after thawing. **(A)** Representative immunofluorescence images of fixed cells stained for P2X3 and peripherin (PRPH) (left), as well as TRPV1 and βIII-tubulin (βIII-Tub) (right). Nuclei were stained using H33342 (DNA). Color code and scale bars are given in the images, and further details are shown in figure 2.1.S9A,B. **(B)** Representative voltage-clamp recordings of cells exposed to α,β-methylene ATP (α,β-meATP) [10 µM] (left) and capsaicin [1 µM] (right). The black bars indicate the time of compound exposure. **(C)** Representative traces of changes in intracellular Ca^{2+} concentration of single cells upon addition of α,β-meATP [1 µM] (left) and capsaicin [1 µM] (right). The black bars indicate the time of compound exposure. **(D)** Concentration-dependency of the percentage of reactive cells towards a stimulus of α,β-meATP (left) and capsaicin (right). The blue data point depicts the respective percentage of reactive cells in sensory neurons generated traditionally (without transient NGN1

overexpression). **(E)** Concentration-dependency of the P2X3-specific antagonist AF-353 (left) and the TRPV1-specific antagonists capsazepine (blue) and SB-366791 (purple) (right). All data are means ± SEM of at least 3 biological replicates. Significance was tested against control/HBSS (*) or against cells w/o NGN1 overexpression (#). */# $p < 0.05$, **/## $p < 0.005$.

Modeling CIPN-related alterations in pain receptor functions using PNN

Acute painful CIPN is often attributable to alterations in pain signaling, but not necessarily to morphological damage. We performed here an oxaliplatin case study to investigate the potential of PNN to model acute chemotherapy-related functional alterations *in vitro*. On the basis of the PeriTox test (DoD0 cells) (Hoelting et al. 2016), two oxaliplatin test concentrations were selected. This assay has been used broadly for identifying neurite-damaging agents (Delp et al. 2018; Krebs et al. 2020). Based on the test data (Fig. 2.1.S10A), we selected 5 µM (no effect) and 20 µM (moderately decreased neurite area, but no cell death) for further experiments.

In PNN, matured for several weeks, neither concentration affected the neurite integrity or viability (Fig. 2.1.S10B). Basic neuronal function (spontaneous firing) was also maintained (Fig. 2.1.S10C). Using Ca^{2+}-signaling as endpoint, we examined whether pain-related excitability was affected independent of morphological effects. First, we established a simple model of mechanical allodynia. Pre-treatment with 20 µM oxaliplatin (24 h) made PNN react to a mechanical stimulus (mild shear forces) with increased Ca^{2+} influx (Fig. 2.1.7A,B, Fig. 2.1.S11A,B). As Na_V channels have been implied in OXAIPN-mechanical allodynia (Deuis et al. 2013), we applied the inhibitors TTX and carbamazepine (Carb). They fully blocked Ca^{2+} signals following mechanical stress (Fig. 2.1.7B). This dampening effect was specific for the mechanical stress model, as the same inhibitors did not affect signaling triggered by direct TRPV1 activation (Fig. 2.1.S11D). P2X3 is not involved in this *in vitro* mechanical allodynia, as inhibition by A-317491 had no effect (Fig. 2.1.7B). We were interested in learning, whether the bare presence of oxaliplatin is sufficient to alter neuronal responsiveness (allodynia). The washout of oxaliplatin did not restore normal functions and a shortened pre-treatment time (1 h) did not lead to the same de-regulations as observed with 24 h incubation time (Fig. 2.1.7C,D). These data argue against a direct interaction of oxaliplatin with Na_V channels as a cause for the observed signaling changes.

As second approach to understand functional impairments triggered by oxaliplatin, we studied potentially modified receptor responses. Triggered by the pertinent literature (Anand et al. 2010; Calls et al. 2020) we focused on TRPV1. A significant hypersensitivity to capsaicin was observed at low oxaliplatin (5 µM) concentrations (Fig. 2.1.7E). The control stimulus (P2X3 receptors) was not affected at this concentration. However, the response of P2X3 receptors was found to be decreased at higher (20 µM) oxaliplatin pre-treatment (Fig. 2.1.7F). As the depression of P2X3 responses by oxaliplatin pre-treatment was quite pronounced, and some direct receptor inactivation by oxaliplatin may be conceived, we performed a series of experiments varying the presence of the chemotherapeutic drug during receptor stimulation. Only prolonged pre-treatment was effective, while direct presence of oxaliplatin was not required to attenuate P2X3 responses (Fig. 2.1.S11C).

In contrast to oxaliplatin, cisplatin treatment usually is not associated with acute pain effects (Staff et al. 2017). We investigated whether this was replicable in the *in vitro* model. In cisplatin pre-treated cells, we did neither observe mechanical allodynia-like signals nor TRPV1 hyper-responsiveness. However, a decrease in P2X3 responsiveness (Fig. 2.1.S11A,E) was observed as seen similarly for oxaliplatin.

In summary, these data suggest that CIPN-relevant alterations of ion channel functions can be observed and studied in PNN. As both hyper- and hypo-sensitivity to different stimuli can be simultaneously assessed in a concentration-dependent manner, the PNN-based test system allows for novel approaches to study CIPN *in vitro*.

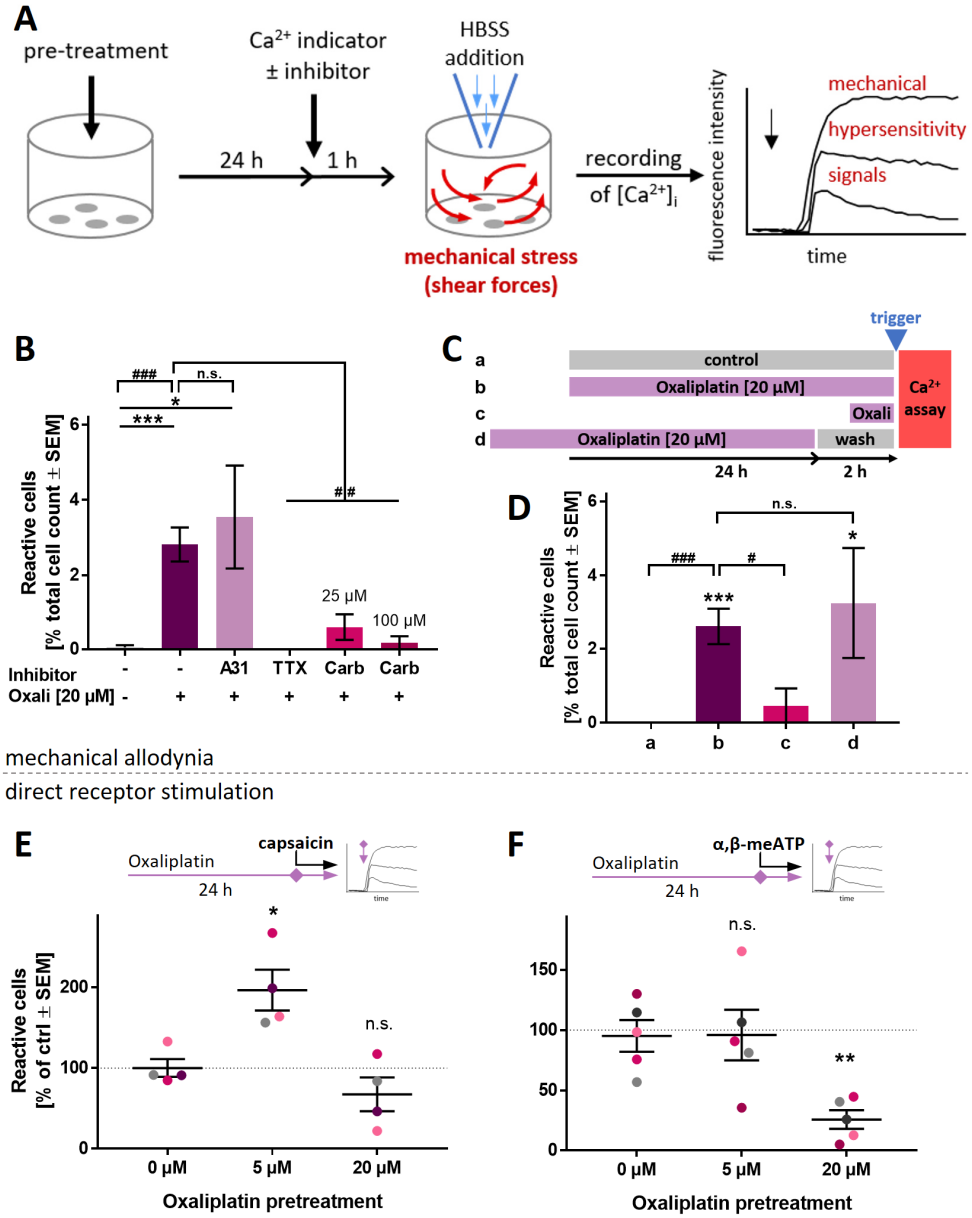

Figure 2.1.7: Functional impairment of PNN exposed to oxaliplatin

PNN (>DoD37) were used for Ca^{2+}-imaging experiments to assess oxaliplatin-induced functional impairments. **(A)** Schematic representation of the experimental setup to assess responses towards a mechanical stimulus. **(B)** PNN were pre-treated with oxaliplatin (Oxali) according to **(A)**. Cells received the P2X3 antagonist A-317491 (A31, 10 µM), or the Na_V channel inhibitors tetrodotoxin (TTX, 3 µM) or carbamazepine (Carb). The fractions of cells reacting with Ca^{2+}-influx ($\Delta F > 18$) were quantified. **(C)** Schematic representation of oxaliplatin exposure scenarios **a**-**d** before stimulation of cells by HBSS addition (see trigger mark). Some cells (**a**) did not receive oxaliplatin pre-treatment, while others (**b**) were pre-treated with oxaliplatin for 24 h prior to Ca^{2+} measurements. Condition **c** included pre-treatment with oxaliplatin for 1 h only. In scenario **d,** a 24 h oxaliplatin pre-treatment was ended 2 h before Ca^{2+}-measurement. **(D)** PNN were treated with oxaliplatin according to the scenarios **a**-**d**, and reactive cells were quantified. Data in B, D are means ± SEM, from 3-6 biological replicates. Significance was tested against condition **a** (*) or against condition **b** (#). */# $p < 0.05$, ***/### $p < 0.001$. **(E, F)** Effect of oxaliplatin pre-treatment (24 h) on **(E)** TRPV1 and **(F)** P2X3 PNN reactivity upon capsaicin or α,β-meATP stimulation (both 1 µM), respectively. Data points belonging to the same cell lot are color-matched. Means ± SEM are given. Significance was tested against the respective control (0 µM). * $p < 0.05$, ** $p < 0.005$, n.s. not significant.

2.1.5 Discussion

We present here a robust method to generate PNN. Moreover, the study provides a full characterization of a signaling endpoint that can be used to assess normal and disturbed neuronal signaling in such cultures. Finally, we demonstrate in an exemplary case study the applicability of PNN to assess pain-related altered neuronal excitability after exposure to a chemotherapeutic drug.

Altogether, this paper contains Ca^{2+}-signaling data for more than 60,000 individual neurons. The recording of intracellular Ca^{2+} concentrations over time provides a wealth of data (considering different curve shapes, peak heights, areas-under-the curve, relaxations times etc.). Extraction of robust information from such multidimensional data sets can be extremely difficult. Often it is not possible at all, unless the evaluation method is adapted and optimized from experiment to experiment. The latter procedure has a relatively large risk-of-bias. We explored here as alternative the use of a binary readout of "responsive" *versus* "non-responsive" cells. This allowed the clear and accessible display of the multidimensional data recorded by high-throughput imaging. With this test method in hand, we demonstrated, using the example of oxaliplatin, that drug-induced receptor hyper-sensitivity or mechanical allodynia can be assessed *in vitro*.

Until few years ago, the major models to study peripheral pain-related neuropathies were experimental animals and patients (Kanzawa-Lee et al. 2019; Lehmann et al. 2020). The few *in vitro* studies mainly focused on structural defects, and the main test systems for this were rodent neurons. Robust quantitative studies on nociceptor modulation are thus quite limited (Brüning et al. 2014). *In vivo* studies often assess behavioral outcome measures that are the result of a complex integration of peripheral, central, and glial cell type activities. In such situations, specific mechanisms or receptors are hard to assess. Within the published mechanistic studies, only a small fraction focused on functional neuronal properties (St Germain et al. 2020). Morphology-based test methods are more wide-spread and better-established, but they may miss signaling changes (Loser et al. 2021b). This is at present an important gap in CIPN-research, as it is known that chemotherapeutic drugs like oxaliplatin can alter neuronal excitability/function without structural damage (Park et al. 2008). Test systems based on nociceptor functions are therefore required in this area.

Since pluripotent stem cells have been established as readily-available resources, it became possible to generate complex human cell types not easily available from other

sources. Protocols to generate peripheral neurons from iPSCs have paved the way for new human-relevant test systems. *In vitro* test methods offer many advantages for the study of specific mechanistic and pharmacological aspects of peripheral neurotoxicity due to their relative "simplicity", and as environmental factors can be very tightly controlled. Indeed, iPSC-based *in vitro* test methods have been repeatedly used to measure the effects of chemotherapeutics on cellular viability or morphology (Delp et al. 2018; Hoelting et al. 2016; Morrison et al. 2016; Schinke et al. 2021; Wheeler et al. 2015; Wing et al. 2017). However, there is still a dearth of studies that employ human iPSC-derived nociceptor cultures to assess alterations of signaling endpoints. The cell system, together with the endpoints we characterized may help to fill this gap for toxicological or pharmacological studies.

Although we have several years of experience in the use of sensory neuronal cultures (Delp et al. 2018; Hoelting et al. 2016; Klima et al. 2021a; Klima et al. 2021b), it was not possible to significantly improve the nociceptor character of these cells by using modifications of conventional protocols (Chambers et al. 2012). Functional sensory neurons can indeed be obtained after differentiation times of > 60 days (Boisvert et al. 2015; Saito-Diaz et al. 2021). However, such time-demanding protocols severely limit the usefulness and robustness of the resulting cultures. Therefore, we harnessed here the nowadays widely used method of transcriptional programming (Boisvert et al. 2015; Desiderio et al. 2019; García-León et al. 2018; Hulme et al. 2020; Nickolls et al. 2020) to enhance the fate specification towards nociceptive neurons by transient NGN1 overexpression. The integration of this approach into the traditional small molecule differentiation protocol yielded PNN with a high abundance of P2X3 and TRPV1 receptors. It was interesting to note that gene expression patterns quickly resembled those of PNN, but the cells required considerably more time to acquire functional properties of nociceptors. For instance, high transcript levels for P2X3 were detected already on DoD1, while responses to P2X3 agonists were measured earliest from DoD28 onwards. This may be attributable to the continuing changes in several components of signaling pathways (Isensee et al. 2017). Our study therefore also demonstrates that the expression of receptor-encoding genes does not necessarily imply the functionality of these receptors.

We made here use of the fact that recording of Ca^{2+}-signaling on the level of single cells allows the assessment of the composition of functionally heterogeneous populations. This is important for nociceptors, which are known to be a phenotypically mixed population (e.g., TRPV1 expression is only found on half of the peptidergic nociceptors (Rostock et al.

2018)). Mixed populations also require large numbers of cells to be monitored to obtain robust results. In this sense, the endpoint presented here offers possibilities to re-evaluate other approaches that originally had to use < 20 individual cells for important statements (Anand et al. 2010).

2.1.6 Conclusion

The *in vitro* model of PNN opens new possibilities for the study of functional aspects of peripheral neuropathies. However, our study does not close all gaps. An important future goal is the further shortening of the culture time, and the generation of several, highly defined subpopulations of sensory neurons. For instance, nociceptors expressing TRPA1 (Calls et al. 2020), or other specific receptors and ion channels would be desirable. It should also not be forgotten that toxicity often is a network phenomenon that may involve interactions between several glial cells, nociceptors and central neurons (Carozzi et al. 2015; Wang et al. 2012). Next steps might therefore involve co-culturing of PNN with e.g., Schwann cells (Kraus et al. 2015). In the more distant future, it is likely that network recording tools, like multi-electrode arrays, will reach cellular resolution, and thus allow recording of single cell responses in mixed cultures.

2.1.7 Acknowledgements

This work was supported by CEFIC, the BMBF, EFSA, and the DK-EPA (MST-667-00205). It has received funding from European Union's Horizon 2020 research and innovation program under grant agreements No. 964537 (RISK-HUNT3R), No. 964518 (ToxFree) and No. 825759 (ENDpoiNTs). This work received financial support from the State Ministry of Baden-Wuerttemberg for Economic Affairs, Labour and Tourism.

2.1.8 Disclosure of potential conflicts of interests

The authors declare no conflict of interest.

2.1.9 Data availability statement

Raw data can be requested from the corresponding author.

2.1.10 Supplementary information

Supplementary Methods

Maintenance of induced pluripotent stem cells (iPSCs)

Maintenance of the iPSC lines Sigma iPSC0028 (Si28) (Merck, Darmstadt, Germany) and the in-house gene-edited iPSC line Si28-NGN1 was performed on human Laminin-521 (BioLamina, Sundbyger, Sweden) coating in essential 8 (E8) medium (Dulbecco's modified Eagle's medium/F12 [DMEM/F12] supplemented with 15 mM Hepes [Thermo Fisher Scientific, Waltham, MA, USA], 10 µg/ml holo-transferrin, 20 µg/ml insulin, 16 mg/ml L-ascorbic-acid, 0.7 mg/ml sodium selenite [all from Merck], 100 ng/ml bFGF [Thermo Fisher Scientific], 1.74 ng/ml TGFb [Bio-Techne, Minneapolis, MN, USA]) essentially as described (Chen et al. 2011). Passaging of the iPSCs was performed every 7 days. Cells were incubated with EDTA for 2 min (37°C, 5% CO_2) to detach the cells, so that clumps remain (no single cell suspension). iPSCs were washed off the plate with DMEM/F12. Cells were re-seeded in E8 medium on freshly coated plates in a final dilution of 1:40-60.

Differentiation of sensory neurons from iPSC

The iPSC line chosen has often been used for the generation of various cell types (Dreser et al. 2020; Fattorelli et al. 2021; García-León et al. 2020; Klima et al. 2021a; Nikasa et al. 2021; Shih et al. 2021; Terryn et al. 2018; Verheyen et al. 2015). The iPSCs were prepared for neural differentiation on day of differentiation minus 2 (DoD-2) by replating in a single cell suspension (90,000 cells/cm^2) onto Matrigel™ (Corning, Glendale, AZ, USA) coated 6-well plates in E8 medium supplemented with 10 µM Rock inhibitor (Y-27632 [Bio-Techne]).

On DoD0', E8 was replaced by neural differentiation medium KSR (knock out DMEM with 15% serum replacement, 1 x Glutamax, 1 x nonessential amino acids, and 50 µM β-mercaptoethanol [all from Thermo Fisher Scientific]) and the combination of five small molecule pathway inhibitors. From DoD0'-5', 17.5 ng/ml Noggin (Bio-Techne) and 10 µM SB-431642 (Bio-Techne) were added, and 1.5 µM CHIR99021 (Axon Medchem, Groningen, Netherlands), 5 µM SU5402 (Bio-Techne) and 5 µM DAPT (γ-Secretase inhibitor IX) (Merck) were added on DoD2'-9'. From DoD4' onwards, KSR medium was

gradually replaced by N2-S medium (DMEM/F12, 1 x GlutaMax [both from Thermo Fisher Scientific], 0.1 mg/ml apotransferrin, 1.55 mg/ml glucose, 25 µg/ml insulin, 20 nM progesterone, 100 µM putrescine and 30 nM selenium [all from Merck]) in 25% increments. On DoD9' the cells were cryopreserved in 90% fetal bovine serum (FBS) (Thermo Fisher Scientific) and 10% dimethyl sulfoxide (DMSO) (Merck).

After thawing of the pre-differentiated cells, sensory neuron precursors were cultured in 25% KSR and 75% N2-S supplemented with CHIR99021 (1.5 µM), SU5402 (5 µM) and DAPT (5 µM). Cells were seeded at a density of 100.000 cells/cm^2 on Matrigel™ coated plates. For further differentiation and maturation, half of the medium was changed on DoD1 and DoD2. With the fresh culture medium on DoD2, Matrigel was added to the cells at a final dilution of 1:80. On DoD3, medium was changed to N2-S medium supplemented with 12.5 ng/ml brain-derived neurotrophic factor, 25 ng/ml glia-derived neurotrophic factor and 25 ng/ml nerve growth factor (all from Bio-Techne) and 2 µM cytarabin (AraC; Merck). Half of the medium was changed on DoD4, 7 and 10 with further Matrigel addition on DoD10. On DoD14, medium was changed to maturation medium (N2-S supplemented with BDNF [12.5 ng/ml], GDNF and NGF [both 25 ng/ml]). Half medium exchanges are performed every three to four days. Matrigel is diluted in the culture medium at a final dilution of 1:80 every 10 days.

PeriTox test

Immature peripheral neurons were thawed and seeded at a density of 100,000 cells /cm^2 (Hoelting et al. 2016). Cells were left to attach for 1 h at 37°C, 5% CO_2 followed by treatment with the respective test compounds. Cells were exposed to the compounds for 24 h. One hour prior to analysis, peripheral neurons were stained with 1 µg/ml HOECHST-33342 (H-33342) and 1 µM calcein-AM (both from Merck). After incubation for 1 h at 37°C, 5% CO_2, image acquisition was performed automatically using an ArrayScan VTI HCS microscope (Thermo Fisher Scientific). Image analysis was performed as described previously (Stiegler et al. 2011). In brief, the calcein stain was used to identify the neuronal area and the somatic area, defined by the enlarged area of H-33342 stain, was subtracted resulting in the neurite area. The same images were used to derive data on cell viability. Each H-33342 stained cell was checked for a double stain with calcein-AM. Double-positive cells were classified as viable, cells that were only H-33342 positive as dead.

Lentiviral construct and the generation of a gene-edited iPSC line

The lentiviral sequence was designed to yield a fusion protein consisting of turboRFP (tRFP), the 2A sequence, ubiqitin (Ubi) and NGN1. This construct enables the exact generation of the NGN1 protein by cleavage. Equimolar amounts of tRFP and NGN1 are produced. The expression is driven by a synthetic promoter (Tet-responsive element [TRE]) that is dependant on the presence of Doxycycline (Dox). Furthermore, the lentivirus carries a hygromycin restistance gene allowing the selection for cells that incorporated the lentiviral DNA upon infection (Fig. 2.1.2A). The vector and the principle of the fusion construct was published earlier (Schildknecht et al. 2013).
The human Si28 line was infected with the described lentivirus. Infected cells underwent hygromycin (Carl Roth, Karsruhe, Germany) selection. After selection, the cells were cultured for 5 days in E8 medium without hygromycin. This was followed by manual picking and expansion of the colonies. Stocks of the clones were cryopreserved in 90% FBS and 10% DMSO. Short tandem repeat (STR) DNA typing (described in detail in (Dirks and Drexler 2013)) was performed for cell line authentication. Furthermore, bordering sequences of the inserted NGN1 expression virus were isolated by nested inverse PCR. Fragments were purified by gel isolation and sequenced. The construct was found to have integrated in an intron of the glutamate ionotropic receptor kainate type subunit 5 gene (GRIK5) on chromosome 19.
To evaluate the clone's NGN1 expression properties, iPSCs were seeded as single cells in E8 medium supplemented with 10 µM ROCKi, at a density of 10.000 cells/cm^2. After one day, medium was exchanged to E8 without ROCKi and cells were exposed to doxycycline (2 µg/ml) for up to 5 days (Fig. 2.1.2B).

Immunofluorescence staining and microscopy

Neurons, grown on glass coverslips coated with Matrigel™, were fixed with 4% paraformaldehyde at 4°C over night. All further steps were performed at room temperature. Paraformaldehyde was taken off and cells were washed (~1 min) with phosphate buffered saline (PBS) followed by permeabilization with 0.6% Triton X-100 in PBS for 7 min. Coverslips were washed (~1 min) with PBS and blocked for 1 h in PBS containing 5% FCS and 0.1% Triton X-100. Primary antibodies (see Tab. 4.1.S1) were diluted in fresh blocking solution and applied for 1 h. Residual free primary antibodies

are then washed off with PBS. Secondary antibodies and H-33342 are diluted in blocking solution and applied on the coverslips for 30 min. After washing with PBS, coverslips were placed upside-down on mounting medium on microscope slides.

RNA extraction, cDNA synthesis and reverse transcriptase qPCR

RNA was extracted with TRIzol (Thermo Fisher Scientific) according to the manufacturer's protocol. To produce cDNA, reverse transcription was performed with 1 µg RNA using iScript (Bio-Rad, Hercules CA, USA), following the manufacturer's protocol. SsoFast™ EvaGreen® Supermix (Bio-Rad) was used to quantify the cDNA. Determination of the threshold cycle (C_T) was done with the CFX data analysis software (Bio-Rad). Reference genes were used for normalization of the mRNA levels of the genes of interest which were then compared for different time points of differentiation according to the ΔΔ method (Livak and Schmittgen 2001). Primers used in this study are listed in detail in table 4.1.S2.

Transcriptome data generation and analysis

Sample lysates were prepared by medium removal, followed by a wash with 50 µl of phosphate buffered saline (PBS) (Thermo Fisher Scientific) and instant addition of 33 µl 1x Biospyder lysis buffer (BioSpyder Tech., Glasgow, UK). After incubation at RT for 10 minutes, the sample plates were stored at -80°C up to the time of dry ice shipping to Bioclavis (BioSpyder Tech., Glasgow, UK). The whole transcriptome was then measured via the TempO-Seq targeted sequencing technology (House et al. 2017). The set of genes analysed, and the read data are detailed in Supplement file2, organized as Excel workbook. Labelling and clear explanations are included.

Downstream data interpretation was performed using the R package DESeq2 (v1.32.0) for the differential gene expression (DGE) analysis (Love et al. 2014). The raw probe counts were normalized to total sample counts per million (CPM). No library size threshold was used; samples with replicate correlation (Pearson R) to group average below 0.8 were removed from the analysis. Prior to the DGE, the low-count genes (less than 3 samples above 5 CPM) were discarded. The Wald statistics test was used for significance evaluation of each differentiation stage against DoD1. Selection of the most significant differentially expressed genes (DEG) was done using a (Benjamini-Hochberg) p-adjusted maximum threshold of 0.05 and a $\log_2$(fold change) minimum threshold of 1.

Gene ontology (GO) terms were analysed for over-representation using g:profiler software (Raudvere et al. 2019), based on Fisher's *F* test. GO terms of the category biological process with a maximum size of 1000 genes were taken into account for further analysis. Quantitative activation scores were calculated according to Waldmann et al. (2014) by by "multiplying the percentage of genes within the GO that was found to be significantly regulated with the average fold change of these regulations" (Waldmann et al. 2014).

Manual patch-clamp recordings

Patch-clamp experiments were performed in the whole-cell mode (Hamill et al. 1981) using an EPC 10 USB patch-clamp amplifier and the PATCHMASTER software (version 2x91; HEKA Elektronik, Lambrecht, Germany). The extracellular solution contained (in mM): 140 NaCl, 4 KCl, 1 $MgCl_2$, 1.8 $CaCl_2$, 10 HEPES, and 10 D-glucose, pH 7.4. The intracellular solution contained (in mM): 107 K-gluconate, 10 KCl, 1 $MgCl_2$, 10 HEPES, 5 EGTA, and 4 Na_2ATP, pH 7.2. For the experiments in which the voltage-gated potassium ion channel currents were blocked, the following solutions were used: the extracellular solution contained (in mM): 140 NaCl, 10 tetraethylammonium chloride (TEA), 1 $MgCl_2$, 1.8 $CaCl_2$, 10 HEPES, and 10 D-glucose, pH 7.4. The intracellular solution contained (in mM): 117 CsCl, 10 TEA, 1 $MgCl_2$, 10 HEPES, 5 EGTA, and 4 Na_2ATP, pH 7.2. All substances were obtained from Carl Roth except K-gluconate, EGTA, Na_2ATP, TEA, and CsCl, which were from Sigma Aldrich.

The recordings were performed at room temperature and the cells were kept at a holding potential of -70 mV in all experiments. To investigate the action potential firing behavior, the cells were stimulated in current-clamp mode by hyper- and depolarizing current pulses from -50 pA to +240 pA in +10 pA steps with a pulse duration of 300 ms. In voltage-clamp mode, voltage-gated ion channels were stimulated by voltage pulses ranging from -70 mV to +60 mV in +10 mV steps with a pulse duration of 300 ms. For leak subtraction, the P/4 algorithm of the PATCHMASTER software was used in voltage-clamp mode. Both pulse protocols were executed at 0.2 Hz. For agonist tests with α,β-methylene ATP (α,β-meATP) and capsaicin in voltage-clamp mode, cells were exposed to these compounds for 5 s. Tetrodotoxin (TTX), α,β-meATP, and capsaicin were obtained from Tocris.

The data of the manual patch-clamp recordings were analyzed and visualized with scripts written in R (version 3.6.3) (R Core Team 2020). The following r packages were utilized

for data handling: cowplot (Wilke 2020), ephys2 (Danker 2018), ggplot2 (Wickham 2016), lemon (Edwards 2020).

Microelectrode array recordings

Sensory neurons were seeded at a density of 120.000 cells/7 µl drop on Matrigel™ coated 24-well CytoView multi-electrode array (MEA) plates with 16 electrodes per well (Axion Biosystems, Atlanta, USA). Neurons were left at 37°C, 5% CO_2 for 1 h to attach before the wells were filled with 500 µl DoD0 medium. Neurons were further differentiated and matured as described above. Measurement was performed on different days of differentiation for the same wells of a plate. After an equilibration time of 15 min, recordings with a Maestro Edge (Axion Biosystems) were started. Recordings were carried out for 15 min every hour for a total of 24 h to 38 h. In case of oxaliplatin treatment, the compound was applied in 50 µl of maturation medium. Control neurons were treated with 50 µl maturation medium alone. All recordings were captured using the Axion Integrated Studio Navigator (Axion Biosystems) with a recording chamber at 37°C and 5% CO_2. For raw data acquisition, signals from all electrodes were recorded simultaneously with a sampling frequency of 12.5 kHz/channel. The recorded raw files were converted offline from voltage traces into various time-dependent data sets, such as spiking frequency, etc. The threshold spike detector was set to 5.5x of the noise level (signal SD) on each electrode, using adaptive threshold crossing for spike detection (Klima et al. 2021a).

Measurement of changes in intracellular Ca^{2+}-concentration $[Ca^{2+}]_i$

Immature sensory neurons were seeded on DoD0 in 96-well plates at a density of 100.000 cells/cm^2. They were differentiated as described above for up to 49 days. One hour before the measurement, neurons were loaded with Fluo-4 Direct™ Calcium Assay Kit (Thermo Fisher Scientific) and H-33342 by exchanging half of the medium with the staining solution. Pre-incubation with e.g., receptor antagonists was done together with Fluo-4 loading. Test compounds were diluted in Hanks' Balanced Salt Solution (HBSS). Agonists and antagonists used in this study are listed in detail in table 4.1.S3.
Monitoring of $[Ca^{2+}]_i$ was performed using a VTI HCS microscope (Thermo Fisher Scientific) equipped with an automated pipettor and an incubation chamber. Neurons were kept at 37°C and 5% CO_2 during the experiments. Images were taken as fast as

possible for 45 s and test compounds were applied automatically 10 s after the first picture was taken. In a standard experiment with 4 stimuli applied to one well (e.g., negative control, P2X3 agonist, TRPV1 agonist, KCl), the cells were imaged 4 times for 45 s with one stimulus applied at a time. Subsequent stimuli applied to one well were separated by a minimum interval of 5 minutes.

The images were exported as .avi video files and analysed with the CaFFEE software (Karreman et al. 2020). In brief, the time point of peak fluorescence was identified. Fluorescence data for the ground state (F_0) and for the peak time point (F_1) were assessed automatically for all cells. The difference between the two fluorescence levels, $\Delta F=F_1-F_0$, was used for further data processing (Klima et al. 2021a).

Establishing a thresholding strategy to define reactive cells in Ca^{2+}-imaging experiments

Ca^{2+} imaging data from 10 different experiments were used to explore the performance and practical application of four different threshold setting approaches. The objective was to identify the best way of defining reactive cells (Fig. 2.1.S8A). Data were collected on the response to a negative control and a positive control (KCl). Only the data on Hanks' Balanced Salt Solution (HBSS, negative control) were used for thresholding. Two different methods were used:

Method **1** used a noise level-based cut off: The threshold (T) was defined at T=mean + (3 x SD). The mean fluorescence change triggered by HBSS (mean(ΔHBSS)) was considered as the noise level and 3 x SD(ΔHBSS) as the noise bandwidth. Three different approaches to determine a noise-level based cut off were tested. Method **1a** defined one general threshold that should be applicaple to all future experiments. For that purpose, >9000 HBSS Δ values of the whole test set (80 PNN cultures from 10 biological replicates) were combined. In this case, a threshold of T=18 was found. Method **1b** calculated a *well-specific* threshold: to each well (technical replicate), HBSS was applied in a first step and the resulting Δ values were used to define a specific threshold for further stimulus applications to this same well. Method **1c** resulted in an *experiment-specific* threshold with additional normalization by the KCl response (which may differ in absolute height between experiments): for each biological replicate the mean of "base" values of all HBSS measurements was calculated and substracted from the mean of all "top" values of all KCl measurements. The resulting number was defined as Δ_{max} and set to 100% change in signal intensity. All Δ values of this experiment were normalized to Δ_{max}. The normalized

data for HBSS was then further used for threshold calculation. All normalized HBSS Δ values of one experiment (8 technical replicates) were combined and the resulting threshold was then used for all measurements of this experiment.

Method **2** used a population-based cut off: In this approach T was defined at the 95% percentile of the ΔHBSS distribution. All HBSS Δ values of the test set were combined and the highest 5% of these Δ values were defined as "reactive". We defined the next lower integer Δ value as threshold (T) for reactivity. A threshold of T=13 resulted from this population-based cut off.

Reactive cells in response to HBSS, α,β-methylene ATP (1 µM) and capsaicin (1 µM) were quantified according to all 4 threshold setting approaches. Based on the comparison of the respective results, we chose, the well-specific method **1b** as standard thresholding approach for all further experiments. Additionally, we applied the rule that T=18 (method **1a**) was the maximum value acceptable for T.

Software used to transform images into accessible data

Most of the data was generated using the published program CaFFEE (Karreman et al. 2020). For the evaluation of the reactions of individual cells on different stimuli a special version of this program was developed. This special version, called MultiMovie, is capable of aligning the cells in up to five movies and follow their individual behaviour through all successive treatments (Fig. 2.1.S9D). This enabled us to assess cells that reacted only to some or to certain combinations of stimuli and capture these quantatively.

The accumulated amount of data of these programs exceeded the capacity of all our regularly used programs to visualize data. To accomplish this task, another program (BigData) was written, see figure 2.1.5D and 4.1.S8A,B.

Table 2.1.S1: Primary antibodies used in this study

Target	Isotype	Dilution	Supplier	Catalogue number
βIII-tubulin (pol.)	mouse IgG1	1:1000	BioLegend	921001
Peripherin	mouse IgG2a	1:200	Santa Cruz	sc-377093
Ki67 (PE)	mouse IgG1	1:500	BD Pharmingen	556027
ISL1	rabbit	1:200	Abcam	ab109517
BRN3A	rabbit	1:200	Merck Millipore	5945
P2X3	rabbit	1:200	Novus	NB100-1654
TRPV1	rabbit	1:200	Novus	NBP1-71774

NGN1	rabbit	1:100	Invitrogen	MA5-24912
Nanog	mouse IgG1	1:200	CellSignaling	9656 (Pluripotency Kit)
OCT4	rabbit	1:200		
SOX2	mouse IgG1	1:200		
Tra1-81	mouse IgM	1:500		
Tra1-60	mouse IgM	1:200		
SSEA4	mouse IgG3	1:500		
PAX6	rabbit	1:200	BioLegend	901308
SOX10	mouse IgG1	1:200	Abcam	ab181466

Table 2.1.S2: Primers used in this study

Target	Sequence (For)	Sequence (Rev)
POU4F1 (BRN3A)	CCCTGAGCACAAGTACCCGTC	CGGCTTGAAAGGATGGCTCTTGC
GAPDH	ATGGAGAAGGCTGGGGCTCA	AGTGATGGCATGGACTGTGGTCAT
ISL1	TTGGAATGGCATGCGGCATG	AGGCCACACAGCGGAAACAC
NANOG	GGTGAAGACCTGGTTCCAGAAC	CATCCCTGGTGGTAGGAAGAGTAAAG
NGN1	GACGACACCAAGCTCACCAA	AACAAGCGGCTCAGGTATCC
NGN2	AGGCCAAAGTCACAGCAACG	GGCTCCTCCTCCTCTTCTTC
OCT4	GCAAAGCAGAAACCCTCGTGC	ACACTCGGACCACATCCTTCTCG
P2RX3	TGACGCCACCTCAGGGCACC	AGGTCCGGAGCACAGAGCTG
PAX6	CCGCCTATGCCCAGCTTCAC	AAGTGGTGCCCGAGGTGCCC
PRPH	GAGAGCTGGAGCTGTTGGGC	AGGCGGGACAGAGTGGCATC
RET	GGTCTTTTGGTGTCCTGCTGTGG	GCATCAGGCGGTACATCTCCTC
RPL13A	GGTATGCTGCCCCACAAAACC	CTGTCACTGCCTGGTACTTCCA
RUNX1	ACCTCGAAGACATCGGCAGAAACTAG	GGAGTGGTTCAGGGAGGCAC
RUNX3	AGACCCCAATCCAAGGCACC	CCACGCTGAGGCTGCTGAT
SCN10A	GTGGGCCTGCATGGAAGTTG	GGGCCACCTGCAGGTTGTTC
SCN9A	TGCTCTCTGTCTGAGGTTGGG	GCCGGTGAACGGGAAAATGC
SOX10	CAGCAAAAGCAAGCCGCACG	CTTTCGTTCAGCAGCCTCCAGAG
TBP	GGGCACCACTCCACTGTATC	GCAGCAAACCGCTTGGGATTATATTCG
TRKA	GCTGTCAAGGCACTGAAGGAGG	CGGAGGAAGCGGTTGAGGTC
TRKB	ACAGATTTCTGCTCACTTCATGGGC	CCACAGCATAGACCGAGAGATGTTCC
TRKC	TCGCTGGATGCCTCCTGAAAG	CAATGACCTCCGTGTTTGAGAGTTGG
TRPM8	TGGGAGCCAGCAAGCTTCTG	CCGCCAGCTCCAGACAGTTG
TRPV1	AGAACGGAGCAGACGTCCAG	GTTGCCCACCGAGTCCCTGG

Table 2.1.S3: Agonists and antagonists used in Ca^{2+}-imaging experiments

Compound	Solvent	Concentration [µM]	Supplier	Catalogue number
α,β-methylene ATP	water	0.1, 0.3, 1, 3, 10	Cayman Chemical	10008956
A-317491	DMSO	0.1, 1, 2.5, 5, 10	Cayman Chemical	19256

AF-353	DMSO	0.003, 0.01, 0.03, 0.1, 0.3, 1	Cayman Chemical	23034
capsaicin	DMSO	0.1, 1, 10	Cayman Chemical	92350
capsazepine	DMSO	0.1, 1, 2.5, 5, 10	Cayman Chemical	10007518
carbamazepine	DMSO	25, 100	Merck	C4024
KCl	water	40,000	Merck	P9541
olvanil	DMSO	25	Cayman Chemical	90262
piperine	DMSO	100	Merck	P49007
SB-366791	DMSO	0.01, 0.1, 1, 10	Adipogen	AG-CR1-0034
tetrodotoxin	water	1	BioTechne	1078
veratridine	DMSO	3	alomone labs	V-110

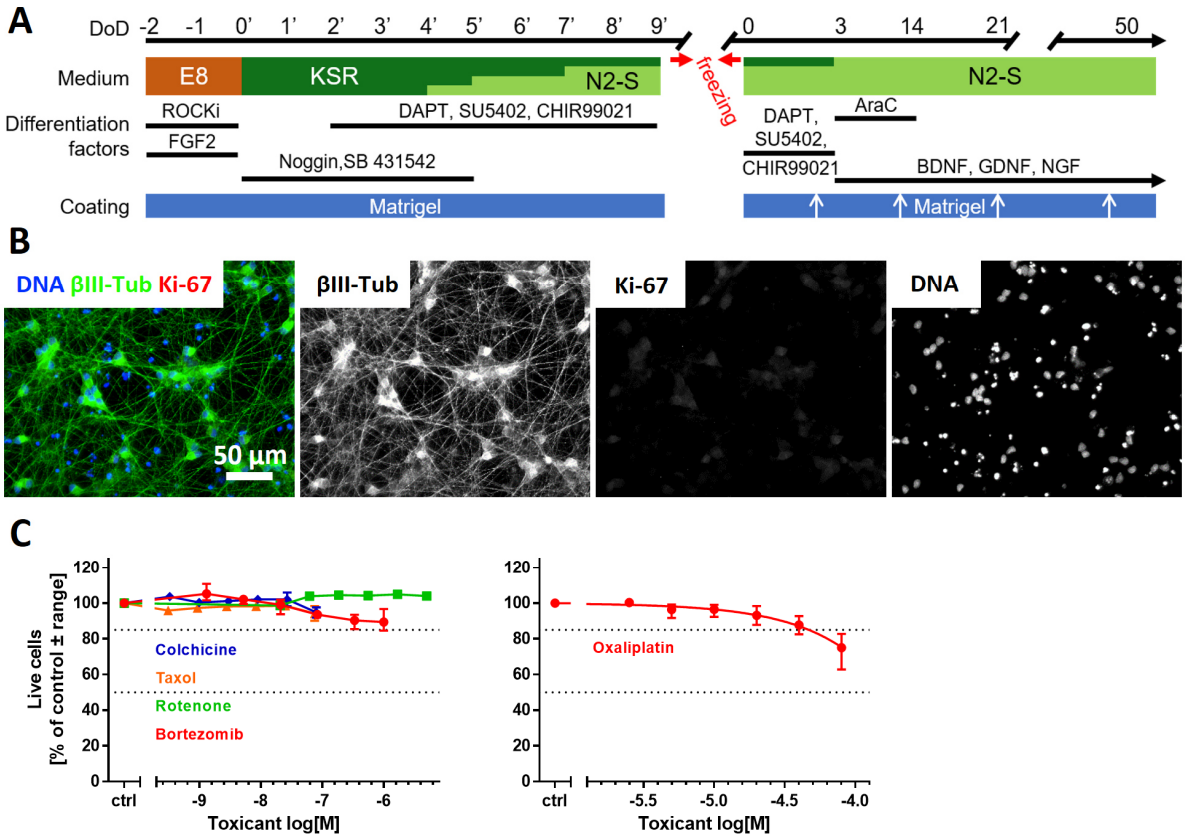

Figure 2.1.S1: Characterization of iPSC-derived sensory neurons

(A) Human sensory neurons were differentiated using the media, coating and supplements indicated. The first differentiation phase is shown left, after switching of E8 stem cell medium to differentiation media containing different ratios of knockout serum replacement (KSR) and N2-S media (with Noggin and the small molecule inhibitors SB431542, DAPT, CHIR99021 and SU5402 added). Note that the timing of this step is indicated by primed numbers. During the second phase (right), starting on DoD0, cells are matured for up to 50 days. The initial medium composition of 25% KSR and 75% N2-S is followed (DoD3) by 100% N2-S medium supplemented with brain-derived neurotrophic factor (BDNF), glia-derived neurotrophic factor (GDNF) and nerve growth factor (NGF). Cells were grown on Matrigel-coated plates, white arrows indicate the addition of liquid Matrigel to the culture medium every 10 days. AraC, cytarabine; FGF2, fibroblast growth factor 2; ROCKi, ROCK inhibitor **(B)** Fixed sensory neurons were immunostained for βIII-tubulin (βIII-Tub) and the proliferation marker Ki-67. The composite image is color coded and the single stain signals are given as b/w images. **(C)** The PeriTox test was performed on DoD0 using immature peripheral neurons to assess the effects of toxicant exposure (24 h) on the neurite area and on general viability. Concentration-response curves of the effects on cell survival are shown. Data are given as mean ± range of 2-3 biological replicates. Errorbars smaller than the data point symbols are not shown. Data on neurite area are displayed in figure 2.1.1D.

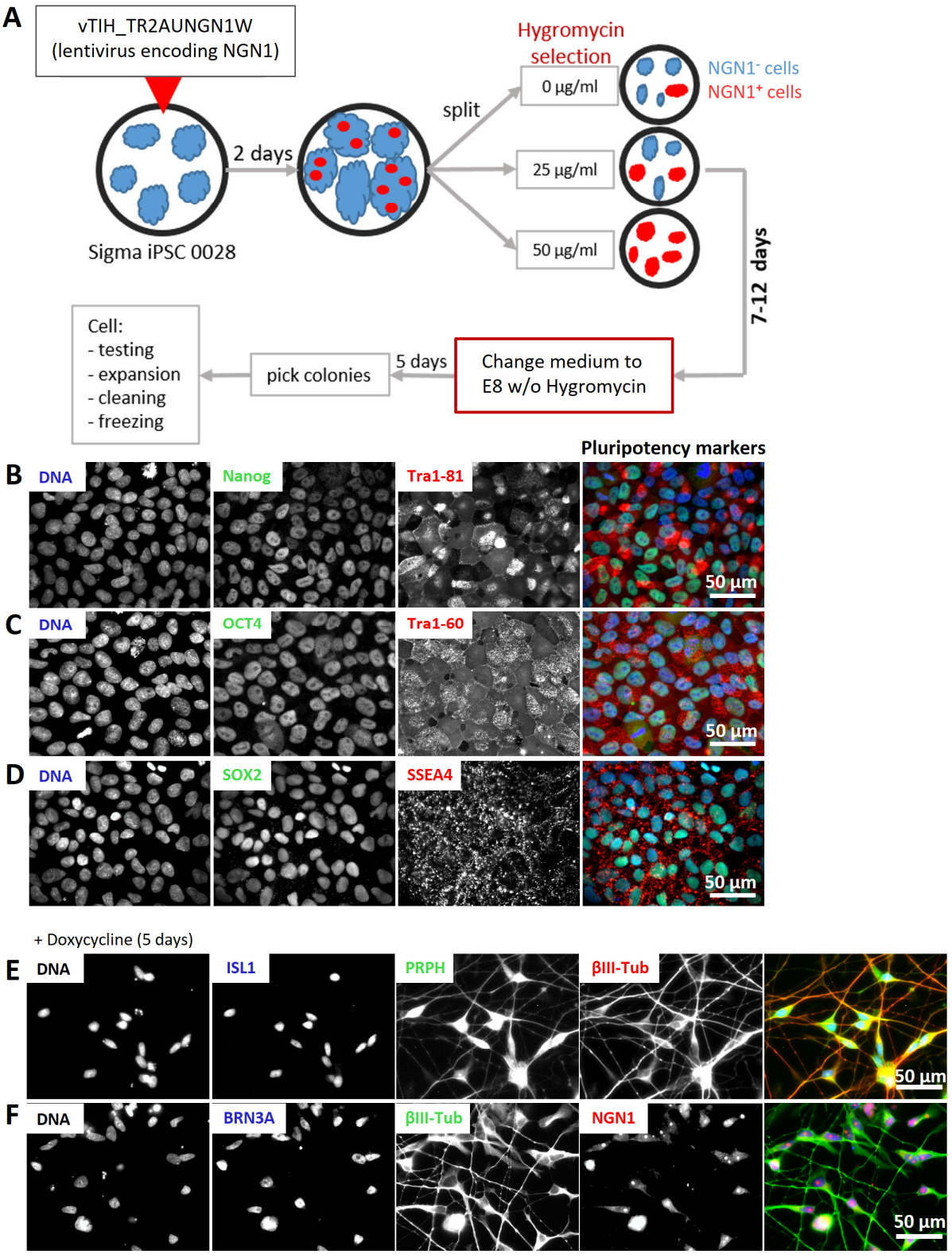

Figure 2.1.S2: Generation of the Si28-NGN1 iPSC line with inducible expression of NGN1

(A) Workflow for the generation of the iPSC-line Si28-NGN1 from the commercially available Si28 line. Si28 were infected with the lentivirus vTIH_TR2AUNGN1W, encoding NGN1. Cells were grown for two days, split and then cultured under different hygromycin selection conditions (0, 25 or 50 µg/ml) for 7-12 days. Afterwards, the medium was changed to E8 medium without (w/o) hygromycin for 5 days. Single colonies were picked, expanded and cleaned followed by testing (as depicted in Fig. 2.1.2B) of the clones. Si28-NGN1 iPSC stocks were frozen. **(B-**

D) Immunofluorescence images of iPSC cultures. Cells were stained for the pluripotency markers Nanog, Tra1-81 **(B)**, OCT4, Tra1-60 **(C)**, SOX2 and SSEA4 **(D)**. Nuclei were stained with H33342 (DNA). **(E,F)** Immunofluorescence images of cells treated with doxycycline for 5 days. Fixed cells were labelled with antibodies against the pan-neuronal marker β-III tubulin (βIII-Tub), the PNS specific intermediate filament peripherin (PRPH) and the sensory neuronal transcription factors NGN1, ISL1 and BRN3A (see also Fig. 2.1.2D). **(B-F)** Images of the single stainings are shown. The composite images of the stainings are color coded according to the detail images. Scale bars are given in the images.

STR analysis of Sigma iPSC0028

STR loci	Data-sheet (Sigma/ Merck)		wt (our data)		NGN1 (our data)	
TH01	9	9.3	9	9.3	9.3	9.3
D5S818	12	13	12	13	12	13
D13S137	8	12	8	12	8	12
D7S820	8	11	8	11	8	11
D16S539	11	12	11	12	11	12
SCF1P0	10	12	10	12	10	12
AMEL	X	X	X	X	X	X
vWA	16	16	16	16	16	16
TPOX	8	9	8	9	8	9
D3			15	16	15	16
D21			28	30	28	30
D18			13	16	13	16
PentaE			7	10	7	10
Penta D			8	11	8	11
D8			10	14	10	14
FGA			22	25	22	25
D19			13	13	13	13
D2			17	20	17	20

Figure 2.1.S3: STR typing of the iPSC lines Si28 and Si28-NGN1

Short tandem repeat (STR) analysis was used to authenticate the newly generated iPSC line Si28-NGN1. The STR profile for Si28 provided by the vendor is given in green columns. A larger set of STR loci was investigated for Si28 (as used in our laboratory) and Si28-NGN1 iPSC. For each STR locus, the number of repeats is given for both alleles (two sub-columns per sample).

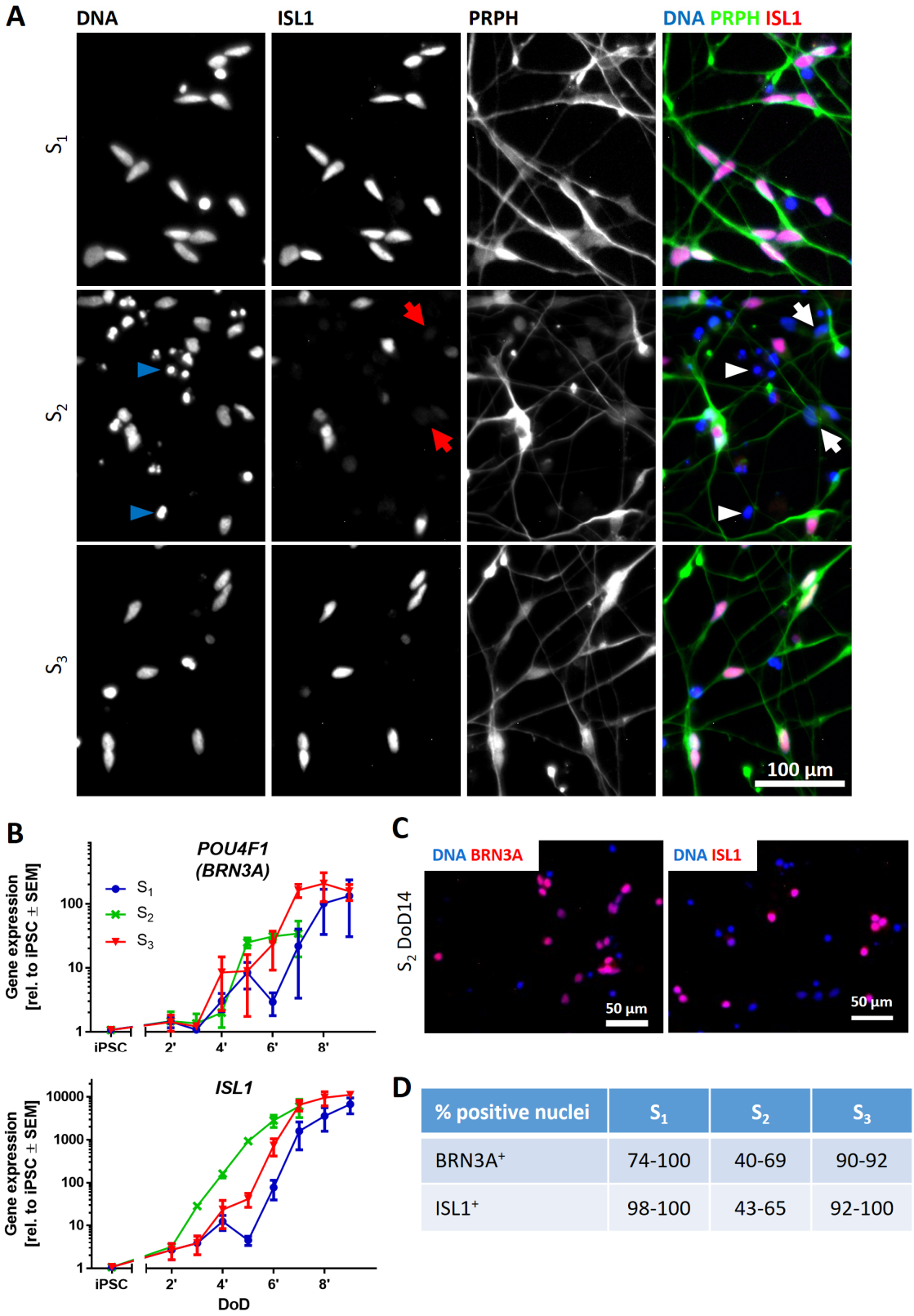

% positive nuclei	S_1	S_2	S_3
BRN3A⁺	74-100	40-69	90-92
ISL1⁺	98-100	43-65	92-100

Figure 2.1.S4: Characterization of neurons resulting from different doxycycline exposure scenarios integrated in the standard differentiation protocol

(A) Immunofluorescence images of cells differentiated according to doxycycline exposure scenarios S_1-S_3 on DoD3 (after thawing). Fixed cells were labelled with antibodies against PRPH (green) and ISL1 (red). Nuclei were stained with

H33342 (blue). Single staining images of the composite images shown in Fig. 2.1.3C are given. The composite images are color coded and the scale bar is given in the image. Arrowheads depict exemplary dead cells, arrows point out exemplary ISL1-negative nuclei. **(B)** Gene expression analysis of the sensory neuron marker genes *POU4F1* (*BRN3A*) and *ISL1*. Data are expressed relative to expression levels in iPSCs and given as means ± SEM of 3-4 biological replicates. **(C)** Immunofluorescence images of cells differentiated according to S_2. Cells were fixed on DoD14 and labelled with antibodies against BRN3A or ISL1 (red). Nuclei were stained with H33342 (blue). Scale bars are given in the images. **(D)** Quantification of ISL1-positive and BRN3A-positive nuclei in DoD14 cultures differentiated according to the three doxycycline exposure conditions described in Fig. 2.1.3A. The range of the percentage of positive nuclei is given.

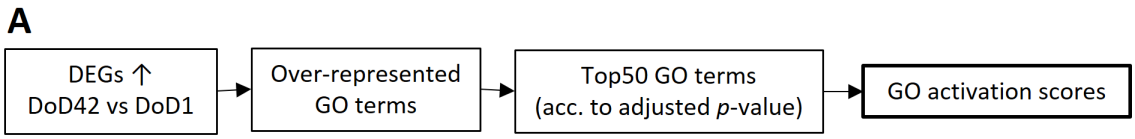

B

	GO term	DoD 7	14	28	35	42
1	synaptic signaling	x	x	x	x	x
2	chemical synaptic transmission	x	x	x	x	x
3	anterograde trans-synaptic signaling	x	x	x	x	x
4	trans-synaptic signaling	x	x	x	x	x
5	learning or memory	x	x	x	x	x
6	cognition	x	x	x	x	x
7	regulation of trans-synaptic signaling	x	x	x	x	x
8	modulation of chemical synaptic transmission	x	x	x	x	x
9	neurotransmitter secretion	x	x	x	x	x
10	signal release from synapse	x	x	x	x	x
11	neurotransmitter transport	x	x	x	x	x
12	regulation of cation channel activity	x	x	x	x	x
13	synaptic transmission, glutamatergic	x	x	x	x	x
14	regulation of neurotransmitter levels	x	x	x	x	x
15	synaptic vesicle cycle	x	x	x	x	x
16	synaptic vesicle exocytosis	x	x	x	x	x
17	vesicle-mediated transport in synapse	x	x	x	x	x
18	regulation of synaptic transmission, glutamatergic	x	x	x	x	x
19	regulation of transmembrane transporter activity	x	x	x	x	x
20	regulation of signaling receptor activity	x	x	x	x	x
21	neuron projection morphogenesis	x	x	x	x	x
22	regulation of ion transmembrane transporter activity	x	x	x	x	x
23	regulation of vesicle-mediated transport	x	x	x	x	x
24	plasma membrane bounded cell projection morphogenesis	x	x	x	x	x
25	cell projection morphogenesis	x	x	x	x	x
26	regulation of regulated secretory pathway	x	x	x	x	x
27	neuron cell-cell adhesion	x	x	x	x	x
28	regulation of intracellular protein transport			x	x	x
29	regulation of transporter activity	x	x	x	x	x
30	positive regulation of intracellular protein transport			x	x	x
31	dendrite morphogenesis	x		x	x	x
32	cellular component morphogenesis	x	x	x	x	x
33	cell morphogenesis involved in neuron differentiation	x	x	x	x	x
34	cell part morphogenesis	x	x	x	x	x
35	regulation of anatomical structure size	x	x		x	x
36	postsynapse organization	x	x	x	x	x
37	regulation of cellular component size	x	x	x	x	x
38	regulation of synaptic vesicle exocytosis	x	x	x	x	x
39	synapse organization	x	x	x	x	x
40	regulation of exocytosis	x	x	x	x	x
41	positive regulation of synaptic transmission	x	x	x	x	x
42	regulation of neurotransmitter secretion	x	x	x	x	x
43	regulation of cation transmembrane transport	x	x	x	x	x
44	neuron projection organization	x	x	x	x	x
45	regulation of neurotransmitter receptor activity	x	x	x	x	x
46	positive regulation of kinase activity	x	x	x	x	x
47	synapse assembly	x	x	x	x	x
48	regulation of intracellular transport	x	x	x	x	x
49	dendritic spine organization	x	x	x	x	x
50	positive regulation of intracellular transport			x	x	x

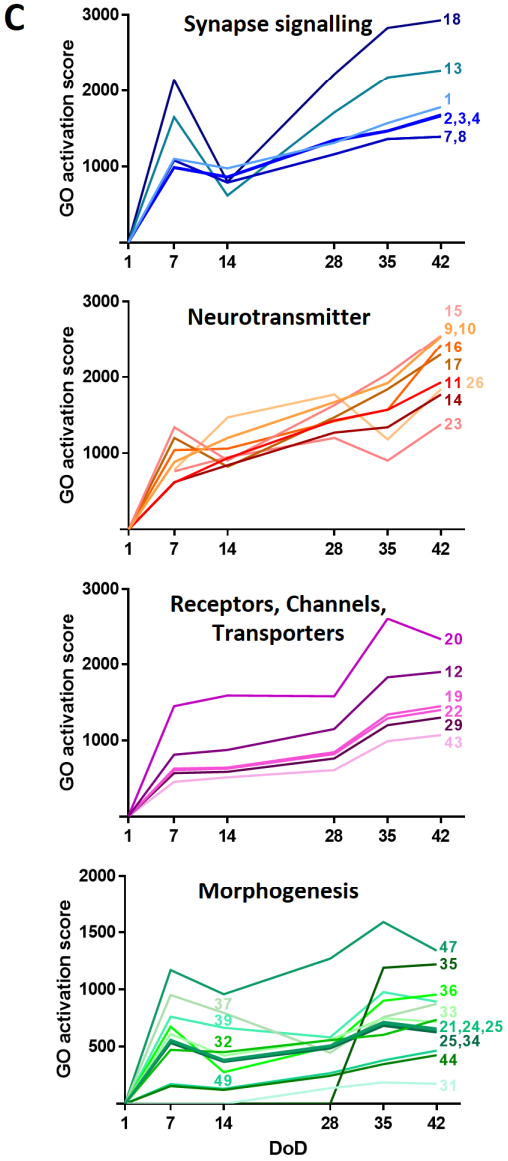

Figure 2.1.S5: Unbiased, transcriptomics-based approach to explore the differentiation of PNN

Transcriptome data were obtained by the TempO-Seq approach for 19,000 genes and DoD1, 7, 14, 28, 35, 42. **(A)** First, DEGs were determined for DoD42 cells (vs. DoD1). All upregulated DEGS with a fold change > 2 and an adjusted *p*-value ≤ 0.05 were used for over-representation analysis of gene ontology (GO) terms (Raudvere et al. 2019). GO terms of the category biological process with a maximum size of 1,000 genes were taken into account for the analysis. The Top50 GO terms with the lowest adjusted *p*-value were used for calculation of quantitative activation scores (Waldmann et al. 2014). **(B)** The Top50 GO terms are listed according to their adjusted *p*-value (1 = lowest *p*-value). The table gives information about the over-representation of the respective GO terms on the investigated days of differentiation (x = over-represented). The GO terms are colored according to their assigned superordinate group: "synapse signaling" (blue), "neurotransmitter" (orange), "receptors, channels, transporters" (pink) and "morphogenesis" (green). **(C)** Quantitative activation scores for each of the Top50 GO terms are shown over time. Numbers on the right refer to the list numbers **(B)** of the respective GOs depicted in the graphs. Summary data, e.g., combined scores for the four superordinate processes color-coded here, are displayed in figure 2.1.4.

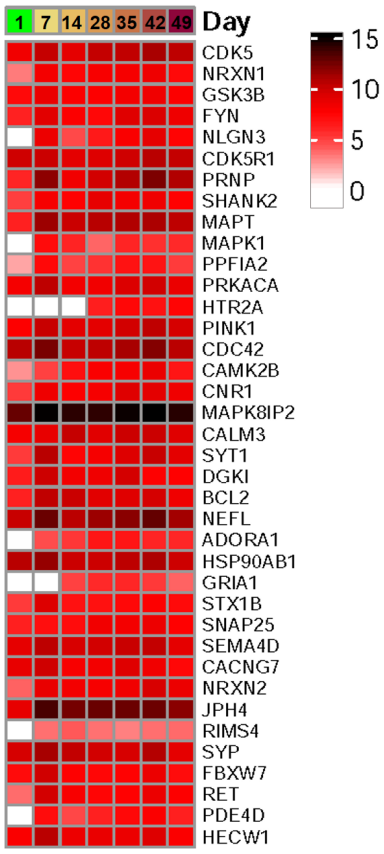

Figure 2.1.S6: Driver genes of the oGO terms.

Among the DEGs determined for DoD42 *versus* DoD1, 200 GO terms were found to be over-represented. We were interested, which genes were drivers of these GOs. The number of GO terms, in which each gene occurs, was quantified. The genes found in more than 15% of the oGO terms were further analyzed for their absolute transcript levels to confirm that the oGOs were driven by reasonably expressed genes. The heatmap shows the absolute expression levels of the GO driver genes for all timepoints examined. Data are given as counts per million (CPM) on a $\log_2$ scale. The complete set of raw data is found in supplementary file2.

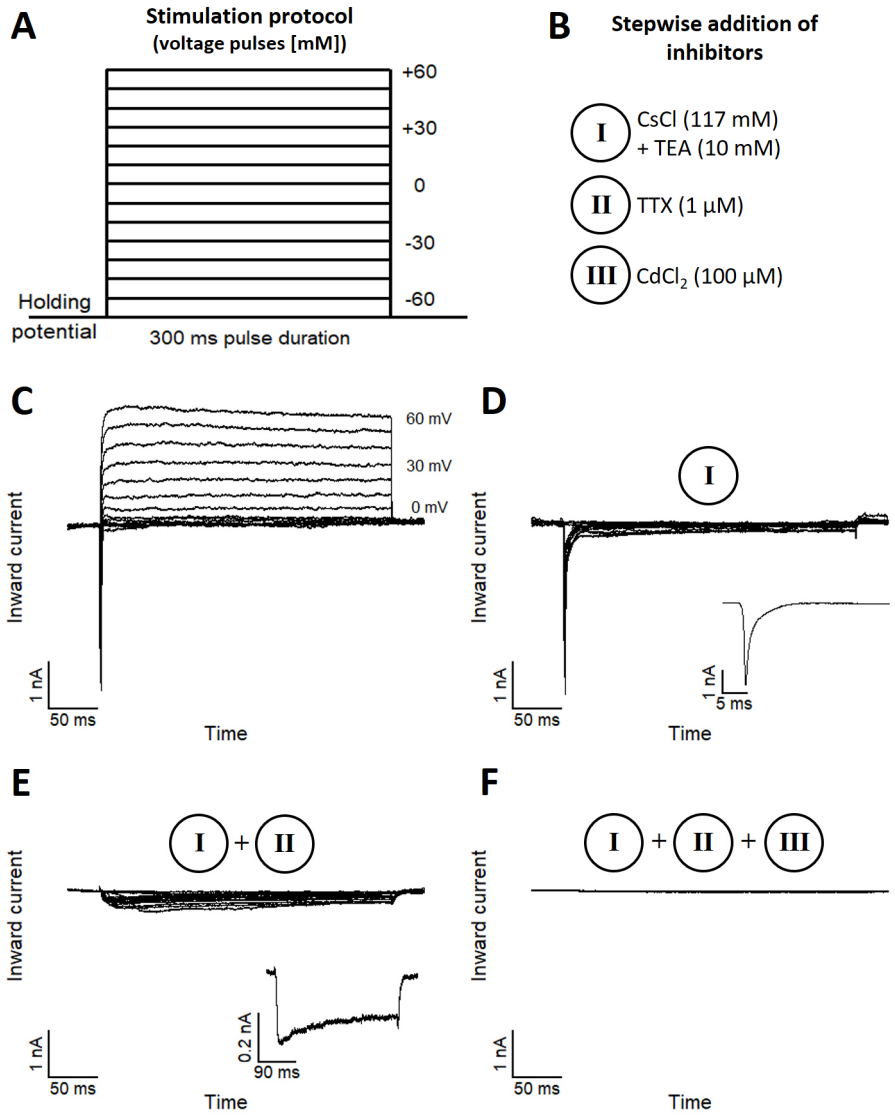

Figure 2.1.S7: Expression of functional voltage-gated ion channels.

PNN used on DoD25-35 for voltage-clamp experiments to investigate the expression of voltage-gated ion channels by a step-wise blocking approach. **(A)** Schematic representation of the stimulation protocol used for voltage-clamp recordings. Voltage pulses were applied with a pulse duration of 300 ms and a pulse frequency of 0.2 Hz, starting at -70 mV and increasing in steps of +10 mV. **(B)** Overview of the step-wise blocking approach to differentially assess major cation channel classes. Inhibitors used for the step-wise blocking approach: (I) K_V channel currents were blocked by tetraethylammonium (TEA) combined with the intracellular replacement of K^+ ions by Cs^+. (II) Block of Na_V channel currents was achieved by tetrodotoxin (TTX). (III) Ca_V channel currents were blocked by $CdCl_2$. **(C)** Representative current responses of a cell in normal recording buffer without any inhibitors added. **(D)** Recording of Na_V currents (with small contribution of Ca_V channels) after the block of K_V channel currents. Inset shows a single trace of a remaining Na_V current at a -30 mV pulse. **(E)** Conditions as in **(D)**, but additional block of Na_V channel currents. Inset shows a single trace of a Ca_V channel current (at V=0 mV) with characteristic, slow inactivation kinetics. **(F)** Condition as in **(E)**, but additional block of Ca_V channel currents, resulting in a complete block of all current responses at all voltage pulses.

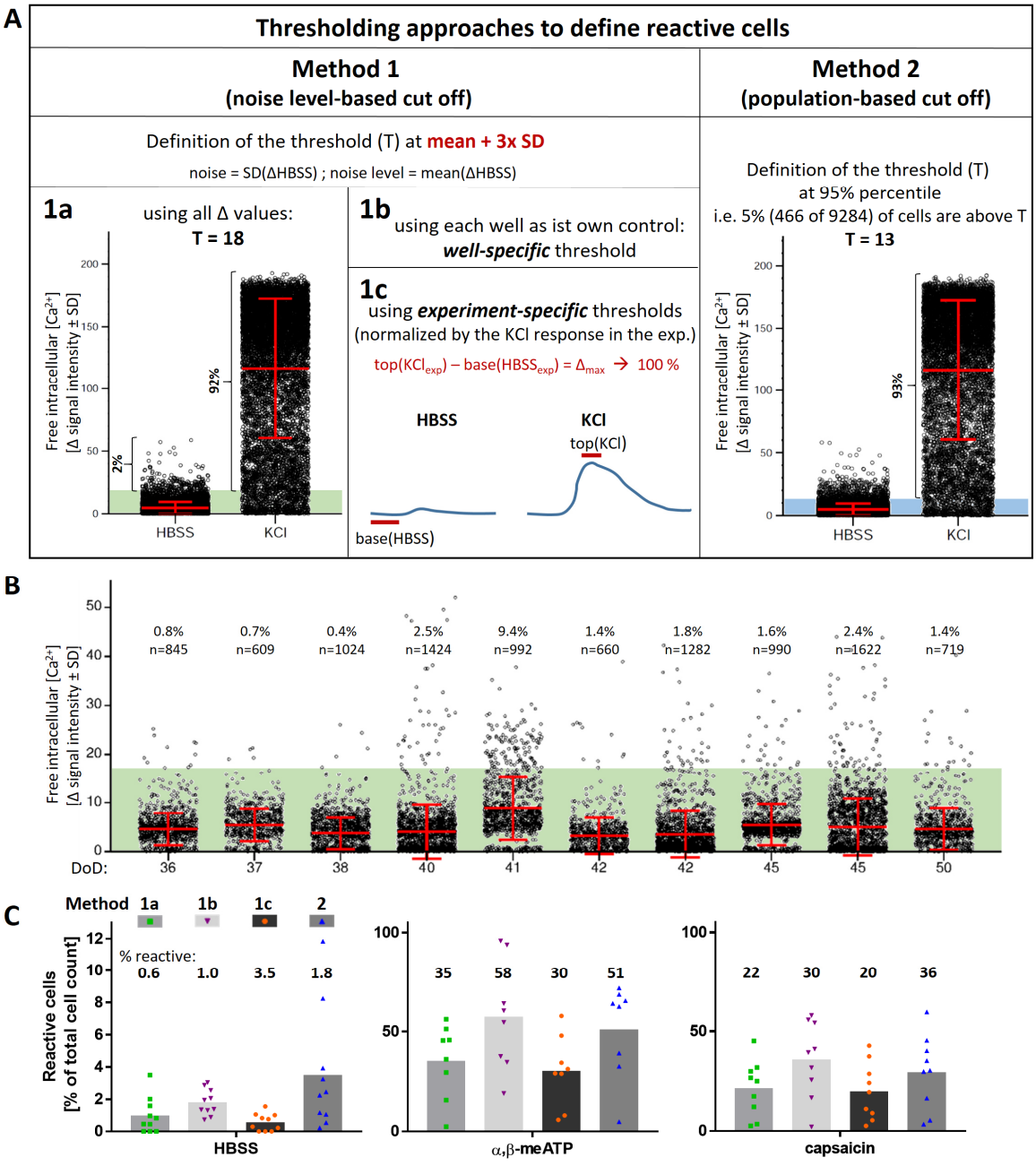

Figure 2.1.S8: Thresholding approaches for Ca²⁺-imaging evaluation to define reactive cells

(A) Summary and illustration of the approaches as described in the supplementary methods that were investigated for threshold setting. Thresholding was always based on the response to the negative control (Hanks' Balanced Salt Solution (HBSS)). The green area in **1a** covers all cells with ΔHBSS<18, while the blue area in **2** covers all cells with ΔHBSS<13. (B) The application of method 1a (T=18) on the HBSS Δ values of the single biological replicates of the test set is exemplified. The percentage of reactive cells is given. The number of all cells measured in each experiment is also indicated. Each dot represents a single cell measured. The means ± SD are indicated graphically in red for each experiment. The green area covers all cells defined as "non-reactive". DoD: day of differentiation (C) Evaluation of reactive cells according to all 4 threshold setting methods using all technical replicates available for each of the 10 biological replicates (also including wells that were not part of the test set): Quantification of reactive cells in response to HBSS, α,β-methylene ATP (1 µM) and capsaicin (1 µM) is shown as mean (grey bars) in % of the total cell number. Each data point represents one replicate (each with several hundred cells). The well-specific method **1b** was chosen as standard thresholding approach for all experiments with an upper threshold limit of T=18 (method **1a**).

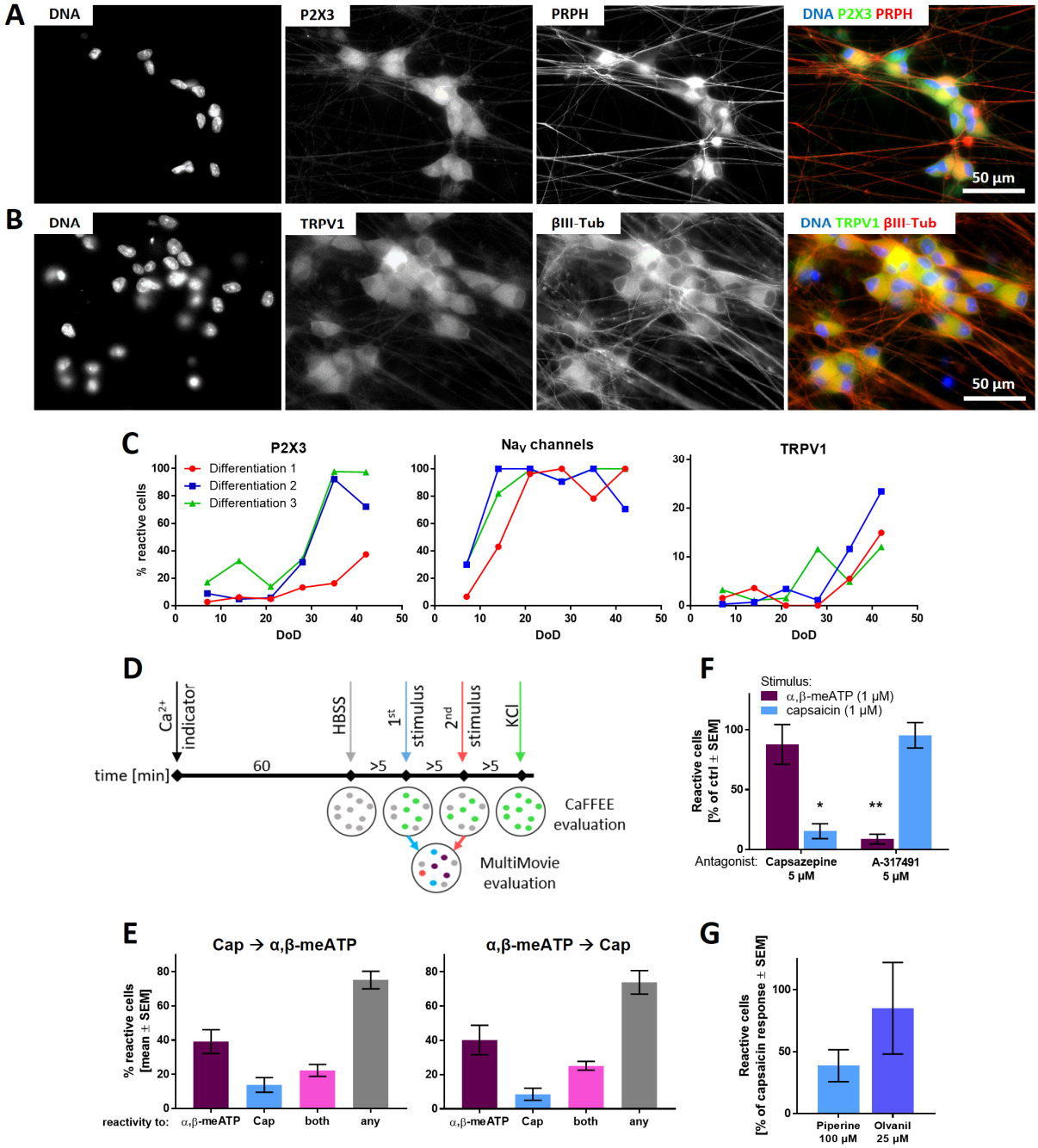

Figure 2.1.S9: Characterization of sensory neurons and their use in Ca^{2+}-imaging experiments.

(A,B) Immunofluorescence images of cells stained for P2X3 and peripherin (PRPH) **(A)**, or TRPV1 and βIII-tubulin (βIII-Tub) **(B)**. Single staining images of the composite images shown in Fig. 2.1.6A are given and the composite image is color-coded. **(C)** Weekly Ca^{2+}-measurements monitored the development of three independently differentiated cultures from DoD7-42. Responses towards the specific agonists of P2X3 (α,β-meATP, 1 µM) and TRPV1 (capsaicin, 1 µM), and towards a Na_V channel modulator (veratridine, 3 µM) were quantified. **(D)** Sequence of a typical Ca^{2+} imaging experiment conducted in one well. Four different stimuli were applied to the same well with >5 min intervals inbetween. Each measurement can be evaluated for itself using the CaFFEE program. Combination of several measurements for evaluation in the MultiMovie program allows determination of possible polymodality. **(E)** Characterization of cells regarding P2X3- and TRPV1-polymodality using the MutliMovie program. Additionally, the influence of the sequence of applied stimuli was investigated. **(F)** The specificity of the TRPV1-antagonist capsazepine and the P2X3-antagonist A-317491 was investigated with α,β-meATP as the first, and capsaicin as the second stimulus. Data are normalized to the

respective stimulus response of cells not pre-incubated with an inhibitor and given as means ± SEM. Significance was tested for treatments ± antagonist. * $p < 0.05$, ** $p < 0.005$ **(G)** Response of sensory neuronal cultures towards the TRPV1 agonists piperine [and olvanil. Data are normalized by the culture response to capsaicin (=100%) and given as means ± SEM.

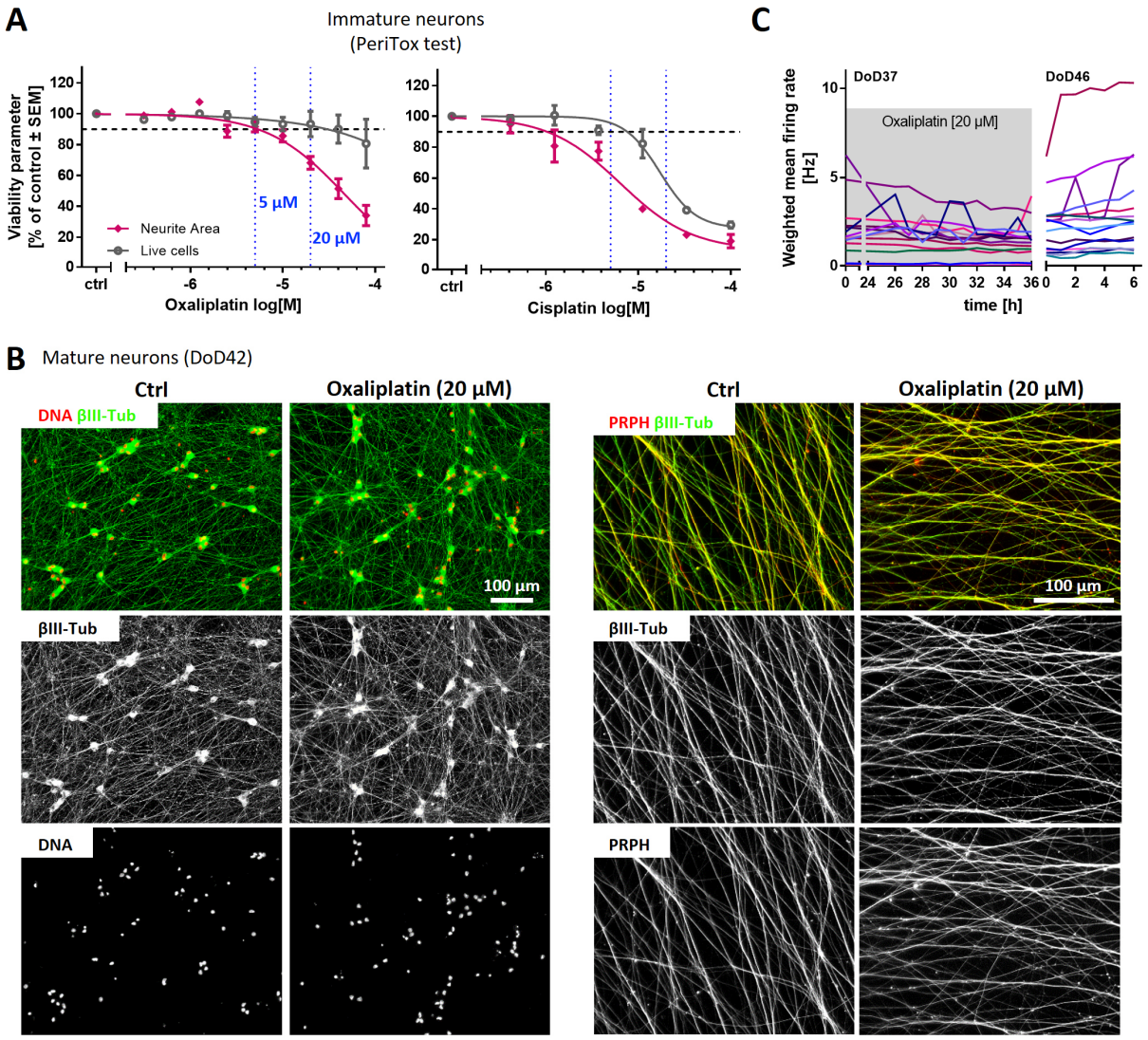

Figure 2.1.S10: Effects of platinum compounds on viability parameters.

(A) The PeriTox test was used to assess concentration-dependent effects on neurite growth (pink) and cell survival (grey) of oxaliplatin (left) and cisplatin (right). Horizontal, dashed line: 'no effect' cut-off (90%) for live cells. Vertical, dotted lines: concentrations (5 µM, 20 µM) used in Ca^{2+} imaging experiments. **(B)** PNN on DoD42 were either exposed to oxaliplatin for 24 h before fixation or not (Ctrl). PNN imaged at low magnification (left) after staining for βIII-tubulin (βIII-Tub) and DNA did not reveal significant impairments of either viability or neurite structure. The representative image data were confirmed by qualitative high content imaging of the neurite area. Images on the right focus on neurites at higher magnification. Microtubules (βIII-Tub) and intermediate filaments (PRPH) were stained to visualize potential damage to neurites. Blinded observers were not able to distinguish Ctrl PNN from oxaliplatin-treated PNN. Composite images are color coded and the single stains are shown in b/w. **(C)** PNN were cultured on multi-electrode array (MEA)

plates. On DoD37, oxaliplatin was added for 36 h. Right after oxaliplatin addition and during the last 12 h of the treatment (hourly), the mean firing rate was recorded. Data are given as the 15 min averaged weighted mean firing rates. The grey box indicates oxaliplatin treatment. Presence of oxaliplatin for 24 h did not alter the mean firing rate. After 36 h, oxaliplartin was washed-out. On DoD46, integrity was assessed visually amd firing signals were recorded for 6 h, demonstrating PNN viability.

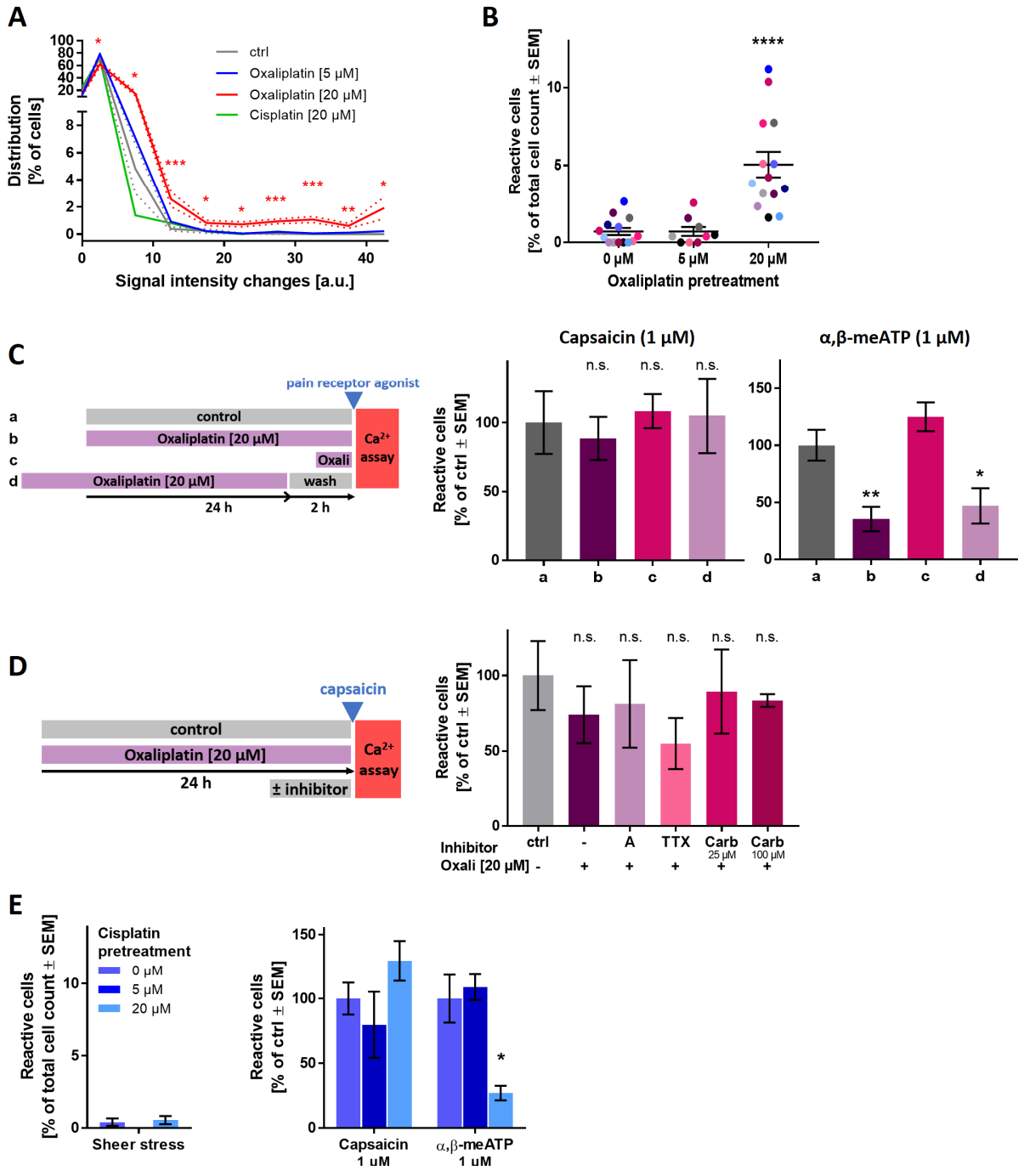

Figure 2.1.S11: Functional changes in mature PNN exposed to platinum compounds
(A) PNN were pre-treated with oxaliplatin or cisplatin for 24 h and their response to mechanical stress was assessed (see figure 2.1.7A). For each signal intensity change value (in arbitrary units, a.u.), the number of cells responding accordingly was determined. This was normalized to the total number of cells. This way, signal intensity change distribution curves (=relative frequencies of $[Ca^{2+}]_i$ changes) were obtained for all conditions. This revealed a significant subpopulation of oxaliplatin pre-treated PNN exhibiting increases in the $[Ca^{2+}]_i$ change. The data from these curves formed the rationale for us to choose the general threshold of T=18 for the quantifications shown in figures 4.1.7B and 4.1.S11B. **(B)** PNN were pre-treated with oxaliplatin for 24 h and their response to mechanical stress was assessed. Each dot represents one biological replicate. Experiments are represented by matching colors. **(C)** The influence of different oxaliplatin exposure schedules (**a**-**d**) on the responsiveness towards capsaicin (left) or α,β-meATP (right) was investigated. **(D)** Cells were pre-treated with oxaliplatin for 24 h. A-317491 (A, 10 µM), TTX (3 µM) or carbamazepine (Carb) were added to the PNN 1 h before stimulation. Then, the response towards capsaicin (1 µM) application was assessed. **(E)** PNN were pre-treated with cisplatin for 24 h. Responses towards mechanical stress (left), capsaicin and α,β-meATP (right) were assessed. **(A-E)** Data are means ± SEM. Significance was tested against the respective control. * $p < 0.05$, ** $p < 0.005$, *** $p > 0.0005$.

Appendix to supplementary information

DB-ALM Protocol:

Differentiation of human iPSC-derived immature dorsal root ganglia-like cells and their use in the PeriTox-test to test neurotoxicants

DB-ALM Protocol

EURL ECVAM DATABASE SERVICE ON ALTERNATIVE METHODS TO ANIMAL EXPERIMENTATION

Part A. Protocol Introduction

Protocol Name: Differentiation of human iPSC-derived immature dorsal root ganglia-like cells and their use in the PeriTox-test to test neurotoxicants

Abstract: This protocol provides information about the differentiation of human induced pluripotent stem cells into immature human dorsal root ganglia-like cells. These cells provide the basis for the PeriTox-test, which allows the identification of specific (peripheral) neurotoxicants.

Résumé

The current protocol describes the differentiation of human induced pluripotent stem cells (hiPSCs) to immature human dorsal root ganglia-like (iDRG) cells performed according to a previously published protocol (Chambers, Qi et al. 2012) with modifications like the introduction of a freeze-and-thaw step.

These iDRG neurons provide the basis for the PeriTox-test. Besides cytotoxicity, the PeriTox-test allows the identification of neurotoxicants, as it includes the functional endpoint of neurite growth inhibition. The test includes single dose treatment of the cells for 24 hours and a direct image-based readout via Cellomics Array Scan VTI HCS high content reader. Treatment of the cells is only possible in concentration ranges where no precipitation of the compound is visually observed.

Experimental Description

Biological Endpoint and Endpoint Measurement:

The PeriTox-test enables the assessment of peripheral neurotoxicity using human iPSC-derived immature human dorsal root ganglia-like cells. Neurite outgrowth as a functional endpoint as well as cytotoxicity are investigated via high content imaging.

Endpoint Value:

Concentration-response-curve (including EC_{10}, EC_{25}, EC_{50}, NOEL…)

Experimental System:

The human iPSC line Sigma iPSC0028 (EPITHELIAL-1) (derived from adult human epithelial cells by OSKM retrovirus reprogramming, purchased from Sigma-Aldrich (Cat# IPSC0028)) is used to generate immature human dorsal root ganglia (iDRG) neurons.

Sigma iPSC0028-derived iDRG neurons are further used for the PeriTox-test.

Discussion

Work requires S1 cell culture laboratories (genetically modified cells).

The current protocol describes the differentiation of human induced pluripotent stem cells (hiPSC) to immature dorsal root ganglia-like (iDRG) cells performed according to a previously published protocol (Chambers, Qi et al. 2012) with modifications like the introduction of a freeze-and-thaw step. The hiPSC line Sigma iPSC0028 is used for the iDRG cell differentiation in this protocol. The Sigma iPSC0028 line is maintained feeder-free on Laminin-521 in E8 medium and during the first two days of differentiation the cells are maintained E8 medium.

In the PeriTox-test human iPSC-derived immature dorsal root ganglia-like cells are used. No specific ethical approval is required.

The duration of the PeriTox-test is 25 h including 24 h of toxicant exposure.

For the performance of the PeriTox-test special equipment like a high content imaging microscope (e.g., Cellomics ArrayScanVTI, Thermo Fisher) equipped with a 10x lens is needed for image acquisition.

To prevent negative edge effects, the edge wells of a 96-well plate are filled with water and only the inner 60 wells are used for testing.

Compounds that reveal autofluorescence can interfere with the detection of calcein-AM or H-33342 in the microscope read-out. In this case, images are blurry and cells cannot be detected by the software. The PeriTox-test can not be used to assess neurite growth and viability endpoints for such compounds.

Training of operators of approximately 4 weeks is needed. During the differentiation, medium change should be performed as fast as possible to keep cells as short as possible at room temperature. From day of differentiation 7’ on, medium should be added carefully and slowly so that cells are not washed away from the plate as the cells detach easier the more dense the culture is. Thawing of the cells has to be performed as fast as possible so that cells are no longer exposed to high DMSO concentrations than necessary.

The PeriTox-test is a high-throughput assay. Reproducible and robust results are gained with three technical replicates. With this assay neurite specific compound effects can be identified. The comparison to results of a complementary assay using central neurons, e.g., the NeuriTox test (Krug et al. 2013), gives insight about the peripheral specificity of an effect.

Status

In Development:

The general method is published in (Hoelting et al. 2016).

The exact feeder-free protocol for maintenance of iPSC and their differentiation to iDRG neurons as described here, is not published yet, however, the basic procedure highly comparable to the previously published protocol.

Known Laboratory Use:

University of Konstanz (used by different operators in this laboratory)

Participation in Evaluation Study:

The test system was not tested in different laboratories yet. But intra-laboratory testing revealed a high robustness across different operators and assay runs.

Different classes of chemotherapeutics, which are known to cause peripheral neuropathies, were identified in the PeriTox test whereas testing on human central neurons missed these compounds. This demonstrates the relevance of this test system for safety testing of drugs.

Participation in Validation Study:

No

Regulatory Accepted:

No

Proprietary and/or Confidentiality Issues

The distribution of the protocol or any protocol components is not limited.

Health and Safety Issues

General precautions:

No general precautions.

MSDS Information:

In addition to the safety measures regarding the compounds in use, there are no safety measures needed for the performance of this method

Abbreviations and Definitions

FGF: fibroblast growth factor

DAPT: γ-Secretase Inhibitor IX

DMEM: Dulbecco's minimum essential medium

DMSO: dimethylsulfoxide

E8: Essential 8

FBS: fetal bovine serum

FITC: fluorescein isothiocyanate

HSA: human serum albumine

iDRG: immature dorsal root ganglia-like

iPSC: induced pluripotent stem cell

KSR: knockout serum replacement

MEM NEAA: minimum essential medium non-essential amino acids

PBS: phosphate-buffered saline

RT: room temperature

Last Update: 04.01.2021

Part B. Technical Description

Procedure Details, Latest Version: 04/01/2021

Protocol Name: PeriTox-test to test neurotoxicants on human iPSC-derived immature dorsal root ganglia-like cells

Final modified protocol

Contact person
Marcel Leist, University of Konstanz, Universitätsstraße 10, 78464 Konstanz

+49 7531 885038

Marcel.Leist@uni-konstanz.de

Contact person
Anna-Katharina Holzer, University of Konstanz, Universitätsstraße 10, 78464 Konstanz

+49 7531 885331

Anna-Katharina.Holzer@uni-konstanz.de

Materials and Preparations

Cell or Experimental system

The human iPSC line Sigma iPSC0028 (derived from adult human epithelial cells by OSKM retrovirus reprogramming, purchased from Sigma-Aldrich (Cat# IPSC0028)) is used to generate immature human dorsal root ganglia (iDRG) neurons.

Sigma iPSC0028 -derived iDRG neurons are further used for the PeriTox-test.

Equipment

Fixed Equipment

Cellomics Array Scan VTI HCS high content reader (Thermo Fisher)

Centrifuge
Freezer (-20°C and -80°C)
Fridge (4°C)

Humidified incubator (37°C, 5% CO_2 in air)

Ice machine

Laminar flow hood for sterile atmosphere

Light microscope

liquid nitrogen storage

Mr.Frosty™ freezing container (Thermo Fisher)

Multichannel pipettes

Micropipettes

Neubauer counting chamber

Water bath

Consumables

Gloves

Sterile cryovials

Sterile eppendorf tubes (1.5 ml)

Sterile plastic tubes (15 ml, 50 ml)

Sterile single wrapped pipettes

Sterile 6-well plates (Falcon)

Sterile 96-well plates (Falcon)

Sterile 6 cm cell culture dishes (Sarstedt)

Sterile 0.22 mm bottle-top vacuum filter system (Corning)

Sterile 500 ml storage bottle (Corning)

Media, reagents, sera, others

Material	Supplier	Catalogue Number
0.5M EDTA UltraPure pH 8.0	Invitrogen	15575
2-mercaptoethanol	Gibco	31350
Accutase	PAA	L11-007
Apotransferin	Sigma	T-2036
Basic fibroblast growth factor (bFGF)	Invitrogen	13256029
Calcein-AM	Sigma	17783
CHIR99021	Axon Medchem	1386
Dulbecco's minimum essential medium (DMEM) F12	Invitrogen	21331
DMEM/F12, 15 mM HEPES	Gibco	11330
DMEM / GlutaMax	Gibco	31966-047
Dimethyl sulfoxide (DMSO)	Sigma	D2650
Fetal bovine serum (FBS)	PAA	A15-101

Glucose	Sigma	G7201
GlutaMax®	Invitrogen	35050-061
Hoechst H-33342	Sigma	14533-100MG
Holo-Transferrin	Sigma	T0665
Human Serum Albumin	Sigma	A6608
Insulin	Sigma	I9278
Knock out DMEM	Gibco	10829
Knockout serum replacement (KSR)	Gibco	10208
L-Ascorbic Acid	Sigma	A8960
Laminin-521	BioLamina	LN521-25
Matrigel	Corning	354234
Minimum essential medium non-essential amino acids (MEM NEAA)	Invitrogen	11140
Narciclasine	Sigma	N9789
Sodium chloride (NaCl)	Roth	3957.1
Noggin	R&D	719-NG
Phosphate buffered saline (PBS) (-Ca^{2+}, -Mg^{2+})	Gibco	14190-169
Phosphate buffered saline (PBS) (+Ca^{2+}, +Mg^{2+})	Gibco	14040-091
Progesterone	Sigma	P-7556
Putrescine	Sigma	P-5780
Recombinant human FGF	PeproTech	100-18B
ROCK inhibitor Y-27632	Tocris	1254
TGF-beta inhibitor SB 43154	Tocris	1614
Sodium Selenite	Sigma	S-5261
SU5402	Tocris	3300
TGF-β1	R&D	240-B/CF
Trypan blue stain (0.4%)	Gibco	15250061
γ-Secretase Inhibitor IX (DAPT)	Merck	565784

Preparations

Media and Endpoint Assay Solutions

- 250X-media

Components	**Volume required per 100 ml**
DMEM/F12, 15 mM Hepes	99.515 ml
L-Ascorbic Acid	1.6 g
Sodium selenite (0.7 mg/ml) stock solution	0.485 ml

  Sterile filter and prepare aliquots (2 ml). Freeze at -20°C.

- Holo-Transferrin (1000x)

Dissolve 10 mg in 1 ml PBS and store aliquots at -20°C. The solution is stable for at least 3 months under these conditions

- 0.05% HSA-Solution
  Add 50 µl of a 10% HSA stock solution (in PBS; A6608-100mg) to 10 ml PBS
- Recombinant human FGF Aliquots (1000x)
  Dissolve 1 mg FGF in 10 ml of 0.05% HSA in PBS. Prepare aliquots and store at -80°C for a maximum of 3 months.
- TGF-β1 Aliquots (1000x)
  Prepare a solution of 0.05% HSA, 4 mM HCl in PBS (add 3.5 µl of 25% (8M) HCl to 7 ml 0.05% HSA-solution). Dissolve 10 µg TGF-β1 in 5.75 ml of the prepared solution. Aliquot and store at -80°C for a maximum of 3 months.
- SB 43154 Aliquots
  Add 2404 µl ethanol (100%) to 10 mg of SB 43154 to a final concentration of 10 mM. Aliquot SB 43154 solution in 200 µl aliquots and store at -80°C for a maximum of 1 month.
- Noggin Aliquots
  Add 2 ml 0.1% (m/v) BSA in PBS to 500 µg of noggin to a final concentration of 250 µg/ml. Aliquot noggin solution in 25 µl aliquots and store at -80°C for a maximum of 3 months.
- CHIR 99021 Aliquots
  Add 3.58 ml DMSO to 5 mg of CHIR 99021 to a final concentration of 3 mM. Aliquot CHIR 99021 solution in 120 µl aliquots and store at -20°C.
- Rock inhibitor Y-27632 Aliquots
  Add 15.185 ml sterile water to 50 mg of Y-27632 dihydrochloride to a final concentration of 10 mM. Aliquot Y-27632 solution in 500 µl aliquots and store at -20°C for a maximum of 1 month.
- γ-Secretase Inhibitor IX (DAPT) Aliquots
  Thaw InSolution γ-Secretase Inhibitor IX, which is a 25 mM solution of γ-Secretase Inhibitor IX in DMSO. Aliquot γ-Secretase Inhibitor IX in 40 µl aliquots and store at -20°C. This solution is stable for at least 3 months under these conditions.
- SU5402
  Add 336 µl DMSO to 1mg of SU5402 to a final concentration of 10 mM. Aliquot SU5402 solution in 50 µl aliquots and store at -20°C for a maximum of 1 month.
- Putrescine Aliquots

Add 31.04 ml of sterile water to 5 g of Putrescine dihydrochloride to a final concentration of 1 M. Aliquot putrescine in 300 µl aliquots and store at -80°C. This solution is stable for at least 3 months.

- Sodium Selenite Aliquots

  E8 stock solution:

  Dissolve 0.7 mg sodium selenite in 1 ml destilled water. Sterile filter the solution and freeze aliquots at -20°C.

  N2-S stock solution:

  Add 5.78 ml sterile water to 100 mg of sodium selenite to a concentration of 100 mM for the master solution. Either freeze the master solution or dilute master solution 1:200 in sterile water to obtain a final stock concentration of 500 µM. Aliquot the selenium stock solution in 500 µl aliquots and store at -80°C.

- Progesterone Aliquots

  Add 12.08 ml sterile water to 100 mg of progesterone-water soluble powder (contains 76 mg progesterone per 1 g powder, Lot # 048K1642) to a progesterone concentration of 2 mM for the master solution. Either freeze the master solution or dilute master solution 1:20 in sterile water to obtain a final stock concentration of 100 µM. Aliquot the progesterone stock solution in 500 µl aliquots and store at -80°C.

- Calcein-AM Aliquots

  Add 251 µl DMSO to 1 mg of Calcein-AM to a final concentration of 4 mM. Aliquot Calcein-AM solution in 10 µl aliquots and store at -20°C. This solution is stable for at least 1 month under these conditions.

- H-33342 Aliquots

  Add 5 ml sterile water to 5 mg of H-33342 to a final concentration of 1 mg/ml. Aliquot H-33342 solution in 500 µl aliquots and store at +4°C. This solution is stable for at least 6 months under these conditions.

- Accutase Aliquots

  Thaw out Accutase bottle, prepare 10 ml aliquots and store at -20°C. The aliquots are stable for at least 1 month under these conditions.

- Matrigel Aliquots

  Thaw out Matrigel by placing Matrigel bottle on ice until Matrigel becomes liquid. Aliquot Matrigel in 330 µl and 1 ml aliquots and store at -20°C. The aliquots are stable for at least 2 months under these conditions

- KnockOut serum replacement Aliquots

  Thaw out KnockOut serum replacement bottle, prepare 50 ml aliquots and store at -20°C. The aliquots are stable for at least 3 months under these conditions

- Preparation of EDTA dissociation solution

Dissolve 0.45 g NaCl in 250 ml PBS (-Ca^{2+}, -Mg^{2+}). Add 250 µl of 0.5M EDTA UltraPure pH 8.0. Sterile filter and store at 4°C.

- Preparation of full E8 medium (E8)

  Mix all the components in the table below in a bottle and sterilize it by filtering through a 0.22 µm filter bottle.Label the bottle with content and date keep, it at 4°C for two weeks. Medium should not be re-warmed, it is imperative to only warm up the medium amount to be used immediatly and not keeping it for more than 2 weeks after the preparation day.

Components of medium	**Volume required per 100 ml**
DMEM/F12, 15 mM Hepes	99.1 ml
250X-media	0.4 ml
Insulin	0.2 ml
Holo-Transferrin	0.1 ml
Recombinant human FGF	0.1 ml
TGF-β1	0.1 ml

- Preparation of N2-S medium (N2-S)

  The stock solutions of the supplements putrescine (1 M), selenium (500 µM) and progesterone (100 µM) are prepared and aliquoted upon first use and stored at -80°C. Thawed aliquots can be stored at 4°C for up to two weeks. Weigh apotransferin and glucose into a plastic bottle and dissolve in DMEM/F12 medium. Add all medium components and sterilize by filtering through a 0.22 µm filter bottle. Wrap the bottle in aluminium foil, label with content and date keep it at 4°C for two weeks. Medium should not be re-warmed, it is imperative to only warm up the medium amount to be used immediatly and not keeping it for more than 2 weeks after the preparation day.

Components of medium	**Volume required per 100 ml**
DMEM/F12	98.6 ml
Apotransferin	10 mg
Glucose	155 mg
Insulin	400 µl
Putrescine (1 M)	10 µl
Selenium (500 µM)	6 µl
Progesterone (100 µM)	20 µl
GlutaMax®	1.0 ml

- Preparation of Knockout serum replacement (KSR) medium

  Mix all the components in the table below in a bottle and sterilize it by filtering through a 0.22 µm filter bottle. Wrap the bottle in aluminium foil, label with content and date. Keep it at 4°C. Medium should not be re-warmed, it is imperative to only warm up the

medium amount to be used immediately and not keeping it for more than 2 weeks after the preparation day.

Components of medium	Volume required per 100ml
Knock out DMEM	83 ml
Knock out serum replacement	15 ml
GlutaMax®	1 ml
MEM NEAA	1 ml
2-mercaptoethanol	100 µl

- Wash medium

  25% KSR medium and 75% N2-S medium. Medium should not be re-warmed, it is imperative to only prepare and warm up the medium amount to be used immediately.
- Freezing medium

  Add 10% DMSO to fetal bovine serum (FBS) and sterilize by filtering through a 0.22 µm filter. Medium can be used for up to 1 week when stored at 4°C.
- Staining solution

  calcein-AM (11 µM), Hoechst-33342 (11 µg/ml) in PBS. Use within 2 days and avoid light exposure.

Test Compounds

- Test and control compounds are stored according to the manufacturer's instructions (e.g., 4°C, room temperature, -20°C), compound aliquots at -80°C.
- Stock solutions should be dissolved in sterile water or DMSO, if possible 1000x more concentrated than the working solution. The used DMSO is stored in a lightproof, air-tight bottle at room temperature.
- Final DMSO concentration on the cells is 0.1% (v/v)
- After dissolving the compounds which are delivered in a solid/powder form, all compound solutions are aliquoted into volumes sufficient for one experiment (i.e. one biological replicate). In this way repeated freezing and thawing which can damage the compound's stability and efficiency can be avoided.
- For conducting an experiment, a compound aliquot is thawed and diluted with *day 0* culture medium with supplements in a separate deepwell-plate.
- All compound dilutions in the deepwell-plate contain 0.4% (v/v) DMSO, so that a final concentration of 0.1% (v/v) DMSO is reached on the cells when 25 µl of test or control compound solution is added to the cells (75 µl of day 0 medium with supplements, without DMSO). The highest compound concentration is diluted with medium 1:250 without DMSO as 0.4% (v/v) is already reached with the DMSO the compound is solved in. The serial dilution (normally 1:3) is

done with *day 0* culture medium (75% N2-S, 25% KSR supplemented with CHIR99021 (1.5 µM), SU5402 (5 µM) and DAPT (5 µM)) supplemented with 0.4% (v/v) DMSO.
- The compound dilutions (25 µl each) are added to the cells (75 µl) using a multichannel pipette, 6 filter tips at a time

Positive control(s)

- As positive control, Narciclasine is used in a final concentration of 50 nM.
- Therefore, the Narciclasine preparation follows the same indications as for the test compound: stock solution in DMSO (50 µM) and dilution in day 0 culture medium (75% N2-S, 25% KSR supplemented with CHIR99021 (1.5 µM), SU5402 (5 µM) and DAPT (5 µM)) to a concentration of 200 nM in the deepwell-plate. These controls should have the same amount of solvent as the test compounds
- 25 µl of the compound dilution are added to the cells (75 µl).

Negative control(s)

- As negative control, *day 0* culture medium supplemented with 0.1% (v/v) DMSO is used.
- Therefore, *day 0* culture medium supplemented with 0.4% (v/v) DMSO is prepared in the deepwell-plate
- 25 µl of the DMSO dilution are added to the cells (75 µl)

Method

Experimental System Procurement

The human iPSC line Sigma iPSC0028 (EPITHELIAL-1) is purchased from Sigma-Aldrich (Cat# IPSC0028).

Routine Procedures

Maintenance of Sigma iPSC0028

Day -3: Thawing of Sigma iPSC0028 cells (6 cm dish)

(1) Prepare one Laminin-521-coated 6 cm dish:
    a. 4 ml of coating solution are needed per 6 cm dish, solution should cover the dish
    b. Dilute Laminin-521 in PBS ($+Mg^{2+}$, $+Ca^{2+}$) 1:40

c. Add 4 ml coating solution to the dish, distribute equally and incubate at 37°C for 2 h or at 4°C over night

(2) Pre-warm 10 ml DMEM/F12 and 4 ml E8 medium at 37°C

(3) Thaw 1 vial of frozen Sigma iPSC0028 iPS cells in the waterbath (37°C) until a raisin sized frozen part is still left

(4) Transfer the cell suspension immediately into a 15 ml plastic tube with 10 ml of prewarmed DMEM/F12

(5) Rinse the cryovial with 1 ml DMEM/F12 and combine with other cell suspension

(6) Spin 3 min at 500 x g

(7) Discard supernatant and resuspend the cell pellet in 4 ml E8 medium sothat cell clumps (not single cells!) are floating in the medium

(8) Aspirate the coating solution from one 6 cm dish and add the cell clump solution to the dish. Distribute the clups equally by shaking the dish slowly.

Day 0: Splitting of Sigma iPSC0028 (6 cm dish) (repeat every 7 days / when cells get >70% confluent)

(1) Prepare one Laminin-521-coated 6 cm dish:

- 4 ml of coating solution are needed per 6 cm dish, solution should cover the dish
- Dilute Laminin-521 in PBS ($+Mg^{2+}$, $+Ca^{2+}$) 1:40
- Add 4 ml coating solution to the dish, distribute equally and incubate at 37°C for 2 h or at 4°C over night

(2) Pre-warm 7 ml EDTA dissociation solution, 10 ml DMEM/F12 medium and 4 ml E8 medium at 37°C

(3) Aspirate medium from the Sigma iPSC0028 cells

(4) Wash the cells twice with 2 ml EDTA dissociation solution and aspirate immediately.

(5) Add 1 ml EDTA dissociation solution and incubate for 2 min in the incubator (37°C / 5% CO2)

- Meanwhile aspirate coating solution from prepared 6 cm dishand add 4 ml E8 (pre-warmed)

(6) Aspirate EDTA dissociation solution carefully from the cells. Add 2 ml pre-warmed DMEM/F12 to the cells) and pipet 4 - 5 x up and down with a sterile 2 ml plastic pipette. The cells should stay in clumps.

(7) Transfer the cells into a 15 ml plastic tube.

(8) Rinse the Sigma iPSC0028 dish with 8 ml DMEM/F12 medium and transfer to the medium into the same 15 ml plastic tube.Distribute 0.25 ml of the Sigma iPSC0028 cell suspension per per prepared 6 cm dish

Differentiation of Sigma iPSC0028 cells into immature dorsal root ganglia-like cells

Day -2:

(1) Prepare DMEM/F12 medium, E8 medium and EDTA dissociation solution and prewarm.

(2) Prepare Matrigel coated plate(s)

a. Matrigel has to cover the plate bottom (therefore 1 ml suspension for one well of a 6-well plate is required)

b. Add cold DMEM/F12 to frozen Matrigel pellet and resolve it so that it is diluted 1:40

c. Add solution to the plate(s) and incubate for 1.5 h at RT or 30 min at 37°C

d. After the incubation time, remove Matrigel solution (you can leave DMEM/F12 on the plate(s) as long as you need to prepare your cells)

(3) Wash Sigma iPSC0028 cells twice gently with 2 ml EDTA dissociation solution

(4) After discarding the EDTA add 1 ml of prewarmed EDTA dissociation solution and incubate 4 min at 37°C.

(5) Add 1 ml of DMEM/F12 medium and detach Sigma iPSC0028 cells from the plate by pipetting with a P1000. Cells should not be clumped, single cell suspension should be ensured by pipetting gently up and down

(6) Collect the cell suspension in a 50 ml plastic tube

(7) Spin 3 min at 500 x g

(8) Remove supernatant

(9) Resuspend pellet in 10 ml DMEM/F12

(10) Spin again 3 min at 500 x g

(11) Remove supernatant

(12) Resuspend cells in 1 ml E8 containing 10 µM ROCK inhibitor

(13) count cells in a Neubauer chamber using Trypan blue

(14) plate 90 000 cells/cm² on Matrigel coated plate(s) in E8 medium containing 10 µM ROCK inhibitor (for 6 well plate use 1.5 ml medium per well)

Day -1:

(15) Change medium to fresh prewarmed E8 medium containing 10 µM ROCK inhibitor

Day 0':

(16) Cells should have 90% confluency today

(17) Change Medium to prewarmed KSR supplemented with Noggin (17.5 ng/ml) and the special TGF-beta inhibitor SB 431542 (10 µM)

Day 1'-8':

Day	Medium		Supplements				
	KSR	N2-S	Noggin (17.5 ng/ml)	SB431542 (10 µM)	CHIR99021 (1.5 µM)	SU5402 (5 µM)	DAPT (5 µM)
1'	x		x	x			
2'	x		x	x	x	x	x
3'	x		x	x	x	x	x
4'	x (75%)	x (25 %)	x	x	x	x	x
5'	x (50%)	x (50%)			x	x	x
6'	x (50%)	x (50%)			x	x	x
7'	x (25%)	x (75%)			x	x	x
8'	x (25%)	x (75%)			x	x	x

Day 9': (Freezing of cells)

(18) Prepare freezing medium and wash medium

(19) Discard the cell supernatant, add 500 µl Accutase per each of the 6 wells and incubate 25 min at 37°C

(20) Add 1 ml wash medium to each well of the 6 well-plate and detach cells from the plate by pipetting with a P1000 (ensure a single cell suspension by pipetting gently up and down). Transfer the cell suspension to a 50 ml plastic tube.

(21) Wash the whole 6 well plate with 1 ml wash medium in total and pool remaining cells in the 50 ml tube

(22) Spin the tube 3 min at 500 x g

(23) Discard supernatant and resuspend the cell pellet in 10 ml of wash medium

(24) Take 10 µl of the cell suspension for counting the cells in a Neubauer chamber using Trypan blue
(25) While counting the cells, spin the remaining cell suspension 3 min at 500 x g
(26) Discard supernatant and incubate the cell pellet on ice for 3 min

From now on all steps are performed on ice

(27) Resuspend the cell pellet in freeze medium in a concentration of 8 x 10^6 cells per ml
(28) Distribute 1 ml of cell suspension per cryovial and put them in a Mr. Frosty freezing container and store them overnight at -80°C
(29) After 24 h store the vials in a cardboard storage box and transfer to liquid nitrogen

Test material exposure procedures

Thawing of dorsal root ganglia-like cells

Day 0:

(1) Prepare wash medium and prewarm
(2) Prepare Matrigel coated plate(s)
    - Matrigel has to cover the plate bottom (therefore 50 µl suspension for one well of a 96-well plate for PeriTox is required)
    - Add cold DMEM/F12 to frozen Matrigel pellet and resolve it so that it is diluted 1:40
    - Add solution to plate(s) and incubate for 1.5 h at RT or 30 min at 37°C
    - After incubation time, remove Matrigel solution (you can leave DMEM/F12 on the plate(s) as long as you need to prepare your cells)
(3) For two 96 well plates thaw one vial of Day 9' cells in the waterbath until a raisin sized frozen part is still left
(4) Transfer the cell suspension immediately into a 15 ml plastic tube with 10 ml of prewarmed wash medium
(5) Rinse the cryovial with 1 ml wash medium and combine with other cell suspension
(6) Spin 3 min at 500 x g
(7) Discard supernatant and resuspend the cell pellet in 1 ml wash medium supplemented with CHIR99021 (1.5 µM), SU5402 (5 µM) and DAPT (5 µM)
(8) count cells in a Neubauer chamber using Trypan blue

(9) plate 100 000 cells/cm² on Matrigel coated plate(s) in wash medium containing CHIR99021 (1.5 µM), SU5402 (5 µM) and DAPT (5 µM) with a Multipette at speed "3" (for PeriTox use 75 µl medium/well)

PeriTox assay

Day 0:

(1) One hour after seeding add 25 µl of prewarmed wash medium supplemented with CHIR99021 (1.5 µM), SU5402 (5 µM) and DAPT (5 µM) containing the test compounds to each well.

Day 1:

(2) 23 h after adding the test compounds, stain cells by adding 10 µl of staining solution to the cells (100 µl medium per well) and incubate 1 h at 37°C.
(3) Read the fluorescence signal using an ArrayScan VTI HCS microscope (Cellomics) to measure cell viability and neurite growth.

Typical plate layout:

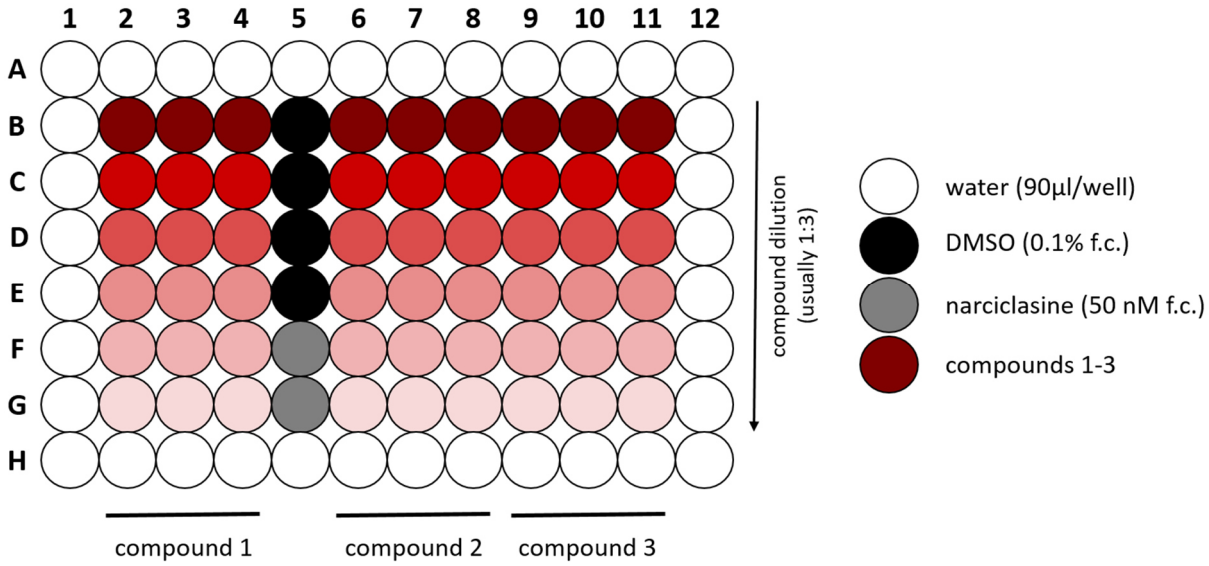

Figure 2.1.A1. Each data point (= one biological replicate) includes usually 3 technical replicates measured on the same plate (see plate layout). For data analysis, at least 3 biological replicates are required.

Endpoint Measurement

Cells are stained with calcein-AM to mark viable cells. Co-staining with Hoechst H-33342 allows the identification of any cell.

Cells are stained for 60 min at 37°C and 5% CO2 in the incubator.

The cell staining is imaged in a Cellomics Array Scan VTI HCS reader, using the proper channels for each staining filter. Exposure times are set manually.

To measure the neurite area, the software acquires the Hoechst to identify the cells as objects (via identification of the nuclei), and the calcein-AM in a different channel to measure neurite area. Double positive cells are counted as viable.

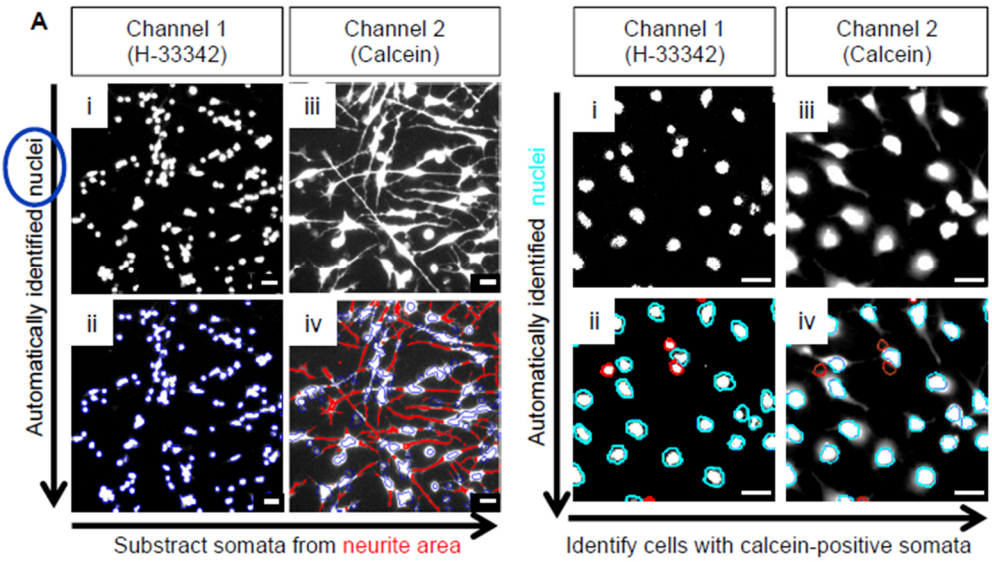

Figure 2.1.A2. Basic principle of the imaging algorithm used for neurite area and viability quantification. (**Left side neurite area**): Untreated hESC-derived iDRG are stained withH-33342 and calcein. The nuclei are detected by their H-33342 staining in channel 1 (i); they are automatically identified and marked (indicated by a blue circle) (ii). All viablecells are stained by calcein, which is detected in channel 2 (iii). The algorithmautomatically expands the nuclear outline to define a "virtual soma area". All calcein-positivepixels outside the virtual soma area are defined as neurite area (shown in red)and they are automatically quantified (iv). (**Right side - viability**) Cells of the examplepictures were treated for 24 h with 50 nM epothilone A. (i) H-33342 staining; (ii) automatic identification of cell nuclei, displayed with a color-coded outline of their shape(cyan for normal nuclei, red for objects that are not normal nuclei (e.g., apoptotic nuclei or fragments)). (iii) Live cell labelling by calcein. (iv) The algorithm quantifies thecalcein intensity in the cells' "virtual soma areas" (cyan circled). Cells with calcein staining below athreshold value are classified by the program as not viable (red circles). (from (Hoelting et al. 2016))

Acceptance criteria

A rough qualitative evaluation considers the following endpoints on day 1:

Control cells are attached to the plate and neurites are visible under the microscope in phase-contrast.

For toxicity testing:

Positive control narciclasine:

Neurite area ≤ 75% of DMSO control

Viability ≥ 90% of DMSO control (or not significantly changed)

Negative control DMSO:

Neurite area ≥ 150.000

Data Analysis

The data are analyzed and represented with GraphPad Prism.

For the concentration curve, a nonlinear regression fit is calculated. The fitting method is least squares. If a non-linear curve fit is not possible, a linear curve fit is performed. The curve deriving from the fit is a 4-parameter log function. To calculate the EC50 value, this log-function is solved for y=50% of the total scale, not for 50% of the min-max scale (see example below). Treated concentrations are analyzed for deviation from control. Statistics applied are one-way ANOVA (and nonparametric) with Dunnett's post-test.

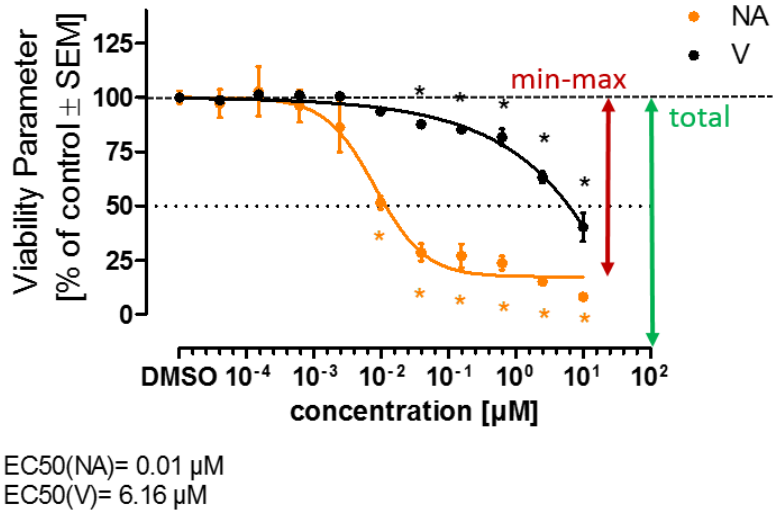

Figure 2.1.A3. Example graph showing the standard representation of neurite area and viability data as % of control using GraphPad Prism. The min-max scale as well as the total scale are depicted in this graph for better understanding of the EC50 calculation. Statistics applied are one-way ANOVA with Dunnett's post-test, statistically significant data points are highlighted by '*'.

Prediction Model

Two different prediction models are used:

1. prediction model for screening:

hit = decrease/increase in neurite area while viability is not changed

(compare to narciclasine positive control:

Neurite area ≤ 75% of DMSO control

Viability ≥ 90% of DMSO control)

2. prediction model for compound hazard evaluation:

hit confirmation testing;

EC_{25} Viability (V) / Neurite Area (NA) ≥ 3 → specifically neurotoxic

A prediction model for the PeriTox test has been developed that allows the classification of toxicants as either specifically neurotoxic, unspecifically cytotoxic or inactive. Specifically neurotoxic compounds decrease the neurite area at concentrations that do not affect the viability of the cells. Unspecifically cytotoxic compounds decrease the neurite area and the viability in the same concentration range to a similar extent. Inactive compounds have no effect on the cells.

The prediction model for the PeriTox test was designed in Hoelting et al. (2016), follwing these steps: (a) use of the "ratio" of EC_{50} (viability)/EC_{50} (neurite area) as the primary endpoint; (b) measurement of this value for "unspecific toxicants" (average ratio: 1.37±0.39); (c) definition of a "noise band" (4xSD from the average of the ratios of these compounds); and (d) definition of compounds with a ratio outside the noise band (EC_{50} ratio of >3) as "neurite specific."

The US national toxicology program (NTP) assembled a screening library, which consists of different substance classes such as organophosphates, organochlorines, drug-like compounds, pesticides and polycyclic aromatic hydrocarbons (PAHs). This screening library was screened with the PeriTox test and the high level of confirmation (88%) in the hit-confirmation phase indicates that the PeriTox test is technically robust (Delp et al. 2018).

Due to concerns about the relevance of the EC_{50} value for risk assessment, the prediction model was adjusted using BMC_{25} values to make predictions based on the onset of toxicity. This adapted model proved useful and meaningful in subsequent screening projects (Klose et al. 2021; Krebs et al. 2020; Masjosthusmann et al. 2020).

2.2 Specific attenuation of purinergic signaling during bortezomib-induced peripheral neuropathy

bioRxiv (2022) doi: 10.1101/2022.02.17.479688

Anna-Katharina Holzer[1,2], Ilinca Suciu[1], Thomas Goj[1], Christiaan Karreman[1], Marcel Leist[1,3]

[1] In vitro Toxicology and Biomedicine, Dept inaugurated by the Doerenkamp-Zbinden foundation, University of Konstanz, 78457 Konstanz, Germany

[2] Graduate school Biological Sciences (GBS)

[3] CAAT-Europe, University of Konstanz, Konstanz, Germany

Running title: Inhibition of P2X3 in peripheral neuropathies

Key words: Nociceptors; Peripheral Nervous System Diseases; Bortezomib; proteasom inhibitors; Receptors, Purinergic P2X3

2.2.1 Abstract

Human peripheral neuropathies are poorly-understood, and the availability of experimental models limits further research. The PeriTox test uses immature dorsal root ganglia (DRG)-like neurons, derived from induced pluripotent stem cells (iPSC), to assess cell death and neurite damage. Here, we explored the suitability of matured peripheral neuron cultures for detection of sub-cytotoxic endpoints, such as altered responses of pain-related P2X receptors. A 2-step differentiation protocol, involving transient expression of ectopic neurogenin-1 (NGN1), allowed for the generation of homogeneous cultures of sensory neurons. After > 38 days-of-differentiation, they showed a robust response (Ca^{2+}-signalling) to the P2X3 ligand α,β-methylene ATP. The clinical proteasome inhibitor bortezomib abolished the P2X3 signal at ≥ 5 nM, while 50-200 nM were required in the PeriTox test to identify neurite damage and cell death. A 24 h treatment with low nM concentrations of bortezomib led to moderate increases in resting cell intracellular [Ca^{2+}], but signalling through transient receptor potential-V1 (TRPV1) receptors or depolarization-triggered Ca^{2+}-influx remained unaffected. We interpret the specific attenuation of purinergic signalling as functional cell stress response. A reorganization of tubulin to dense structures around the cell somata confirmed a mild, non-cytotoxic stress triggered by low concentrations of bortezomib. The proteasome inhibitors carfilzomib, delanzomib, epoxomycin and MG-132 showed similar stress responses. Thus, the model presented here may be used for profiling of new proteasome inhibitors as to their side effect (neuropathy) potential, or for pharmacological studies on the attenuation of their neurotoxicity. P2X3 signalling proved useful as endpoint to assess potential neurotoxicants in peripheral neurons.

2.2.2 Introduction

Models of the human peripheral nervous system are required to better understand why proteasome inhibitors (PIs) cause neuropathies. These drugs target a ubiquitous cellular function (protein degradation via the ubiquitin-proteasome system) and are used clinically to treat multiple myeloma (Kane et al. 2003; Richardson et al. 2003). Adverse effects related to sensory neurons and nociceptors are frequent. Clinical and pathological findings include neurite damage (Csizmadia et al. 2008; Meregalli et al. 2014; Poruchynsky et al. 2008; Staff et al. 2013; Zheng et al. 2012). However, they are also associated with several neurofunctional defects, including an altered pain regulation (Argyriou et al. 2014; Carozzi et al. 2013). Cell culture models for functional impariments are still very scarce.

The first proteasome inhibitor that entered clinics is bortezomib (BTZ). The boronic acid peptide reversibly blocks the chymotrypsin-like protease of the 20S proteasome (Adams et al. 1999), and it is known to induce severe adverse events in the majority of patients. Peripheral neuropathy is one of the most significant BTZ-related toxicities and affects up to 64% of patients (Jagannath et al. 2004; Richardson et al. 2009; San Miguel et al. 2008; Velasco et al. 2010). BTZ-induced peripheral neuropathy (BIPN) affects long sensory neurons and the associated pain leads to therapy modification in up to 30% of the patients (Richardson et al. 2006; Richardson et al. 2009; San Miguel et al. 2008; Velasco et al. 2010). Examples for second generation PIs are delanzomib (DLZ), also belonging to the class of peptide boronic acids, and carfilzomib (CFZ), which is epoxyketone-based. Both PIs exhibit improved neurotoxic profiles, but peripheral neuropathies are still commonly experienced (Kortuem and Stewart 2013; Schlafer et al. 2017; Siegel 2013; Siegel et al. 2013; Vogl et al. 2017; Yong et al. 2018).

Several ion channel classes (e.g., purinergic (P2X) and transient receptor potential (TRP)) interact to regulate sensory neurons. Purinergic signaling is triggered by the binding of ATP, causing ion channels to open. Subsequent influx of cations, such as Ca^{2+} or Na^{+}, leads to depolarization of the cell membrane and the generation of action potentials. In particular, the signaling via the purinoceptor P2X3 plays a role in pain perception and neuropathic pain (Bleehen and Keele 1977; Honore et al. 2002; Jarvis et al. 2002). P2X3, which is specifically located on the nociceptive neurons of the sensory nervous system (Chen et al. 1995; Cook et al. 1997), contributes to the sensation of many types of pain: (i) injury-induced mechanical allodynia and thermal hyperalgesia, (ii) inflammation-induced thermal hyperalgesia, and (iii) chemical (formalin)-induced pain behaviour (Honore et al. 2002; Jarvis et al. 2002; Souslova et al. 2000). A highly complex involvement of P2X3 ion channels in pain perception is

suggested by differential effects of antagonists in various pain models (Honore et al. 2002; Jarvis et al. 2002).

The study of the initial mechanisms and steps leading to BIPN requires human-relevant experimental models of the peripheral nervous system. Some test methods are based on human peripheral neurons derived from induced pluripotent stem cells (iPSCs). They have been mostly used to investigate drug effects on neurite morphology or cell viability (Hoelting et al. 2016; Schinke et al. 2021; Wang et al. 2021; Wing et al. 2017). Such endpoints correlate with events during full-blown BIPN, such as loss of intra-epidermal nerve fibers and alterations in cytoskeletal structure and impairment of axonal transport (Csizmadia et al. 2008; Meregalli et al. 2014; Poruchynsky et al. 2008; Staff et al. 2013; Zheng et al. 2012). Early effects of BTZ are less characterized , but they include aggresome formation (perinuclear accumulation of protein aggregates) (Csizmadia et al. 2008) and a reorganization of the cytoskeleton in the cell somata (Staff et al. 2013). Alterations in sensory signaling may also occur at initial stages. Despite the obvious link between neuropathic pain and abnormalities in nociceptor ion channels, only few studies focused on BTZ-induced impairments of ion channels and signaling (Li et al. 2018; Tomita et al. 2019; Trevisan et al. 2013). It is not clear whether such findings from rodent models can be related to clinical situations, as sensory neurons of humans and other model organisms differ (Chen et al. 2008; Davidson et al. 2014; La Roche et al. 2013; Serrano et al. 2012). The use of human cell-based models of neuronal function may bridge this species-extrapolation gap, and provide new clues on the mechanisms underlying the initial development of peripheral neuropathies in humans.

Taking a step into this direction, we established here human iPSC-derived sensory neurons suitable for the study of altered ion channel function. We asked how well human iPSC lines differentiated towards peripheral neurons and we explored, whether transient expression of an NGN1-transgene improved the expression of functional P2X3 receptors. The usefulness of iPSC-derived sensory neuron cultures to assess PI-induced early alterations in signaling and morphology was then investigated. We focused on purinergic signaling as a sensitive endpoint affected by PIs *in vitro*. In parallel, microtubule arrangement in cell somata was studied as an indicator of initial morphological stress responses. Our study used a panel of five PIs to study multiple functional adaptations and to identify readouts of cell changes occuring well before signs of general cytotoxicity or a general breakdown of membrane signaling.

2.2.3 Results

Human iPSC-derived peripheral neurons for toxicity testing

Three different iPSC lines were differentiated towards peripheral neurons. The objective was to test the general applicability and robustness of a previously established two-step protocol (Hoelting et al. 2016; Klima et al. 2021a). Neuronal precursors were generated and cryopreserved from the iPSC lines SBAD2, Si28 and mciPSC. After thawing and further differentiation, all cells exhibited similar neuronal morphology, neurite growth, and expression of peripheral neuron marker proteins, such as the transcription factors BRN3A and Islet-1 (ISL1), as well as the intermediate filament peripherin (PRPH). Data are displayed here for SBAD2- and Si28-derived neurons, while the process for mciPSC has been documented earlier (Hoelting et al. 2016) (Fig. 2.2.1A, 4.2.S1). Whole transcriptome analysis of three early differentiation stages (DoD1, 4 and 7 after thawing) revealed a development of both, SBAD2- and Si28-derived neurons that was highly conserved between replicates, batches and cell lines (Fig. 2.2.1B,C). Moreover, the pattern was similar to other pluripotent stem cell lines described earlier (Hoelting et al. 2016). The 50 most-regulated genes were selected and clustered: (i) the genes that were up-regulated during differentiation comprised the peripheral markers *PRPH*, *SCN9A* and *RET*, (ii) the genes that were down-regulated included markers for neural crest cells (*PAX3, TLX2*) (Fig. 1B). In a principal component analysis (PCA) of the 500 most variable genes, samples of the same differentiation stage clustered closely together irrespective of their iPSC line origin (Fig. 2.2.1C). These results confirmed that the protocol originally developed for embryonic stem cells can be broadly applied to generate peripheral neurons. In order to test, whether also functional properties were similar, we investigated toxicant-sensitivity. The PeriTox test, a well established screening assay (Delp et al. 2018; Klose et al. 2021; Masjosthusmann et al. 2020), was used to assess effects on the neurite area and the cell viability of immature neurons on DoD0. Peripheral neurons of all three iPSC line-origins were equally sensitive to a diverse set of peripheral neurotoxicants (taxol, bortezomib, colchicine and acrylamide) (Fig. 2.2.1D). The importance of functional testing became evident, when so-called peripheral neurons were obtained from a commercial supplier. These cells reacted to colchicine and acrylamide, but they were insensitive to taxol and bortezomib (Fig. 2.2.S2). Thus, these cells showed a neuronal response, as described earlier for central neurons (Hoelting et al. 2016). The missing of specific peripheral toxicants (taxol, bortezomib) would make such cells unsuitable for many toxicological applications. Taken together, the two-step differentiation protocol evaluated here was found to work for a variety of iPSC lines. The high reproducibility

of the peripheral neuron differentiation represents an important basis for the reliable identification of neurotoxicants in the PeriTox test. The transcriptome data obtained here provide evidence that the differentiation towards peripheral neurons continues for at least 7 days after thawing and would allow for an extension of the test period or a shift of the test window towards a more mature state.

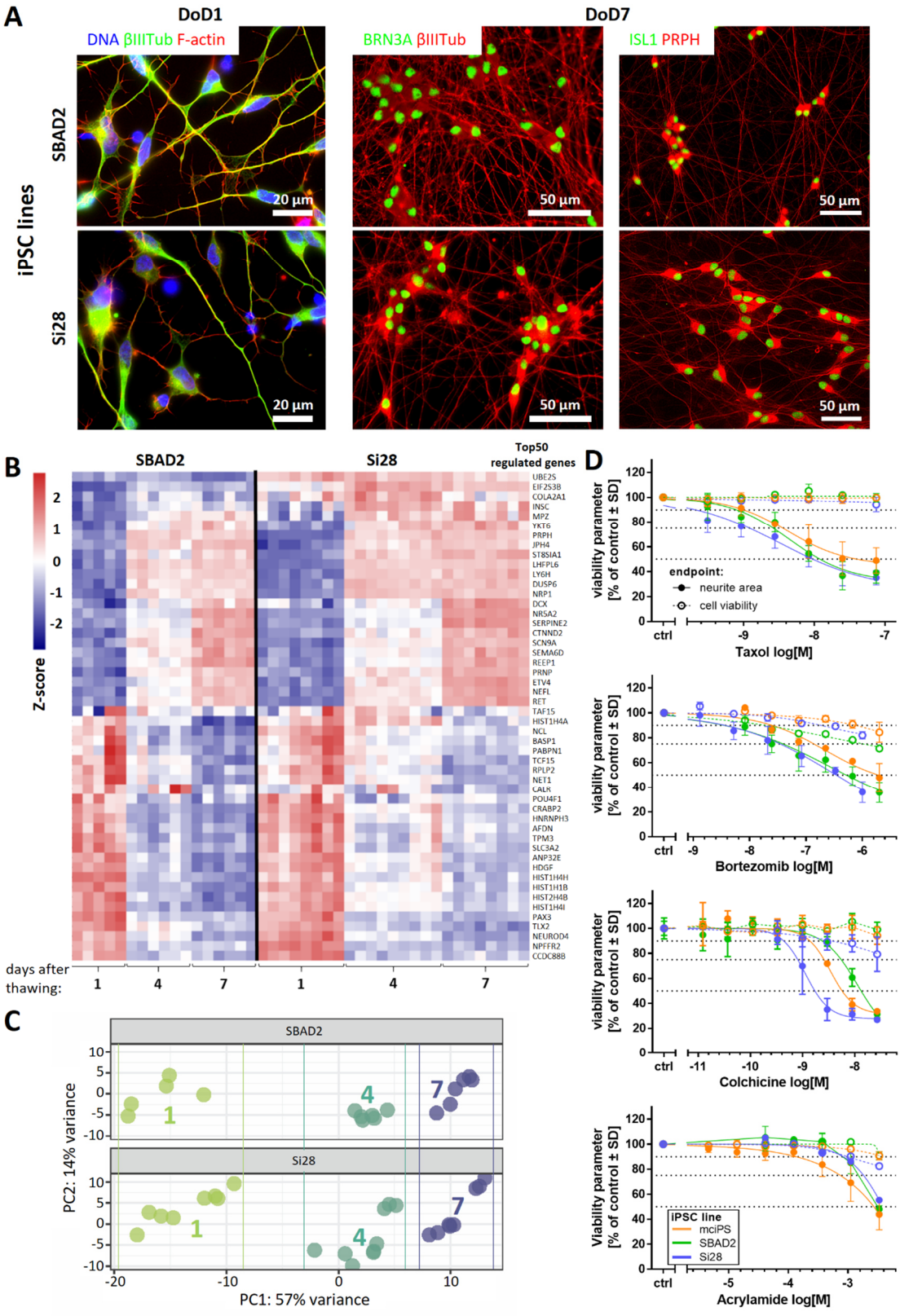

Figure 2.2.1: Reproducible generation of peripheral neurons from different iPSC lines and their use in the PeriTox test.

(A) Peripheral neurons derived from the iPSC lines SBAD2 and Si28 were fixed and stained on DoD1 (left) for the neuronal cytoskeletal marker βIII-tubulin (βIIITub, green) and F-actin (red); and on DoD7 (middle, right) for the sensory neuronal transcription factors BRN3A or ISL1 (green) and the cytoskeletal proteins βIIITub or peripherin (PRPH) (red). Color code and scale bars are given in the images, details are shown in figure 2.2.S1. DoDx: day of differentiation, counting from thawing of frozen neural precursors on DoD0. **(B,C)** Whole transcriptome analysis (19,000 genes) was performed for early differentiation states (DoD1, 4 and 7) of SBAD2- and Si28-derived neurons. Data are from three independent differentiations (full data in Supplementary file1). **(B)** The heatmap depicts the row-wise Z-scores of the top 50 regulated genes (exhibiting the highest variance across all samples). The upper group, defined by the clustering algorithm, mainly consists of genes up-regulated (red) during differentation and the lower group mainly consists of genes down-regulated (blue). **(C)** For the top 500 variable genes of this data set, a PCA was performed. In the two-dimensional PCA display, three differentiation stages are color-coded according to their DoD. Data points and heatmap columns correspond to all technical replicates measured in the 3 experiments per cell line. **(D)** Peripheral neurons derived from the iPSC lines mciPS (orange), SBAD2 (green) and Si28 (blue) were used in the PeriTox test. The (peripheral) neurotoxicants taxol, bortezomib, colchicine and acrylamide were used as positive controls. Effects on the neurite area (solid symbols and lines) and the cell viability (open symbols, dashed lines) are shown. Data are means ± SD of 3 biological replicates.

Need for novel test strategies to further improve sensitivity

Although the PeriTox test has been used successfully to screen for environmental chemicals, an increased sensitivity is desirable for pre-clinical testing of drugs. To refine the standard PeriTox test, scenarios of prolonged exposure to toxicants at different time points of differentiation were investigated (Fig. 2.2.2A, 4.2.S3A). First, a prolonged toxicant exposure time (48 h and 72 h, DoD0-2 and DoD0-3, respectively) was explored. The sensitivity of neurites to acrylamide, colchicine and taxol did not change significantly. However, the rate of cell death increased with prolonged incubation time (Fig. 2.2.S3B-D). For bortezomib, the neurite area was affected more with longer exposure times. However, this effect was attributable to the concomitant decrease in cell viability (Fig. 2.2.2B, 4.2.S3E). Taken together, these findings meant, that the assay became less specific for neurite toxicants. The prediction model for the standard PeriTox test (Hoelting et al. 2016; Masjosthusmann et al. 2020) requires the specific toxicants to affect neurites at concentrations three times lower than cell viability. This requirement was not met in the prolonged assay (Fig. 2.2.2C,D).

Next, we explored, whether shifting the time window of exposure to a later time point (DoD4-7) would result in more potent neurite toxicity. This was not the case (Fig.

2.2.2B,D, 4.2.S4A,B). Moreover, any specificity for neurite effects (relative to general cell death) was lost. Altogether, these results suggest that polonged toxicant exposure is not a suitable measure to improve the PeriTox test. We concluded that other approaches and new functional endpoints are required for a more sensitive assay for compounds that may trigger peripheral neuropathies.

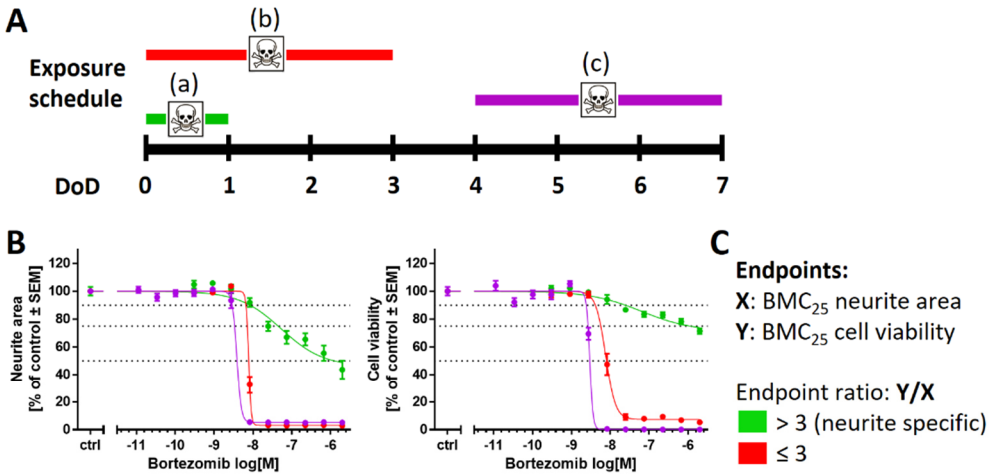

D

Endpoint		Neurite Area (BMC_{25})			Cell viability (BMC_{25})			Ratio		
Compound	Exposure	a	b	c	a	b	c	a	b	c
Colchicine [nM]		1.7	3	8.6	>80	4.3	6.3	*>47*	*1.4*	*0.7*
Acrylamide [mM]		0.7	0.6	1.3	4.6	1.3	1.2	*7*	*2.2*	*0.9*
Taxol [nM]		2	14	500	>75	10	66	*>38*	*0.7*	*0.07*
Bortezomib [nM]		34	7.2	3.8	>2000	5.2	2.7	*>59*	*0.7*	*0.7*

Figure 2.2.2: Variation of the exposure schedule to assess compound toxicity

(A) Schematic representation of the applied exposure schedules with a 24 h treatment starting on DoD0 (a, standard PeriTox test, green), immediate 72 h treatment (b, DoD0-3, red) and delayed 72 h treatment (c, DoD4-7, purple). DoDx: day of differentiation, counting from thawing of frozen neural precursors on DoD0. **(B)** SBAD2-derived peripheral neurons were exposed to bortezomib according to the three exposure schedules. Effects on the neurite area and the cell viability were assessed. Data are means ± SEM of 3 independent experiments. **(C)** Prediction model for the classification of compound-induced effects: The concentrations relating to the benchmark response level of 25% decrease of a test endpoint (BMC_{25}) was calculated for both endpoints, neurite area (X) and cell viability (Y). A ratio of Y/X > 3 is classified as a "neurite-specific" compound effect (green); Y/X ≤ 3 marks effects that are "not neurite-specific", such effects were classified as "cytotoxic" (red). **(D)** BMC_{25} values were calculated for both test endpoints in all three exposure scenarios. Effects induced by colchicine, acrylamide, taxol and bortezomib were classified according to the prediction model. Respective concentration-response curves are given in figure 2.2.S4.

Purinergic signaling as a functional feature of iPSC-derived sensory neurons

One of the most important functional changes during peripheral neuropathy is altered pain perception. This suggests that assessment of pain-related neuronal signals might be a suitable endpoint for peripheral neurotoxicity testing *in vitro*. To explore this possibility, we set out to generate cultures of peripheral neurons that allowed the quantification of nociceptor function.

Our preliminary experiments showed that peripheral neurons could be cultured and further matured for at least 2 months. However, we did not succeed in obtaining robust nociceptor responses suitable for drug screening. For this reason, we introduced an inducible NGN1 transgene into the iPSC line Si28 to generate Si28-NGN1 cells. This strategy has been described earlier to enhance nociceptor differentiation (Boisvert et al. 2015), and we found indeed that our 2-step protocol, enhanced by induction of NGN1 for a defined time period, led to an improved differentiation. The neurons generated by this protocol (Fig. 2.2.3A) were found to be post-mitotic already on DoD1 after thawing (Fig. 2.2.3B, 4.2.S5A,B). They could be cultured for at least 42 days as stable neuronal network suitable for single cell observations (Fig. 2.2.3C, 4.2.S5C). To characterize the Si28-NGN1-derived neurons, we tested them for the expression of the nociceptor-specific receptors P2X3 and TRPV1. Immunostaining showed that most cells (>80%) were P2X3 and peripherin double-positive (Fig. 2.2.3D, 4.2.S5D). Moreover, we used differentiated neurons in Ca^{2+}-imaging experiments: Cells were generated from the iPSC lines SBAD2 and Si28 as well as Si28-NGN1 and used after at least 38 days of differentiation. Only <15% of neurons fom standard iPSCs responded to the P2X3-specific agonist α,β-methylene ATP (α,β-meATP). More than 80% of the neurons generated from Si28-NGN1 revealed increased $[Ca^{2+}]_i$ upon application of an α,β-meATP stimulus (Fig. 2.2.3E). The transient signal in continued presence of the ligand was typical for self-inactivating P2X3 ion channels (Fig. 2.2.3F). The application of the TRPV1-specific agonist capsaicin hardly stimulated neurons from SBAD2 or Si28. About 40% of all neurons in cultures from Si28-NGN1 showed a clear response. This was specifically blocked by a TRPV1 antagonist (Fig. 2.2.S6). The sub-population responding to ATP (a general agonist for all P2X receptors) was of similar size to the P2X3-responsive neuronal sub-population. Moreover, the strong efficacy of a P2X3-specific antagonist to block ATP responses suggested that most functional P2X receptors were P2X3 (Fig. 2.2.3E,F).

For experimental logistics, it is important to know how long cells need to be differentiated to reach good functionality. Therefore, neurons were tested after increasing differentiation times: at DoD7, already >90% of neurons showed a Ca^{2+}-response upon depolarization (KCl), but no

response to P2X3 stimulation. The latter response started to increase at DoD20-30, and reached its saturation level at >DoD35 (Fig. 2.2.3F).

Taken together, the overexpression of NGN1 during early differentiation steps allowed the generation of peripheral neurons with enhanced nociceptor features (PNN). PNN were found suitable to quantitatively evaluate functional P2X3 responses of single cells in Ca^{2+}-imaging experiments. Next, a full transcriptomic characterization of this promising drug discovery model was performed.

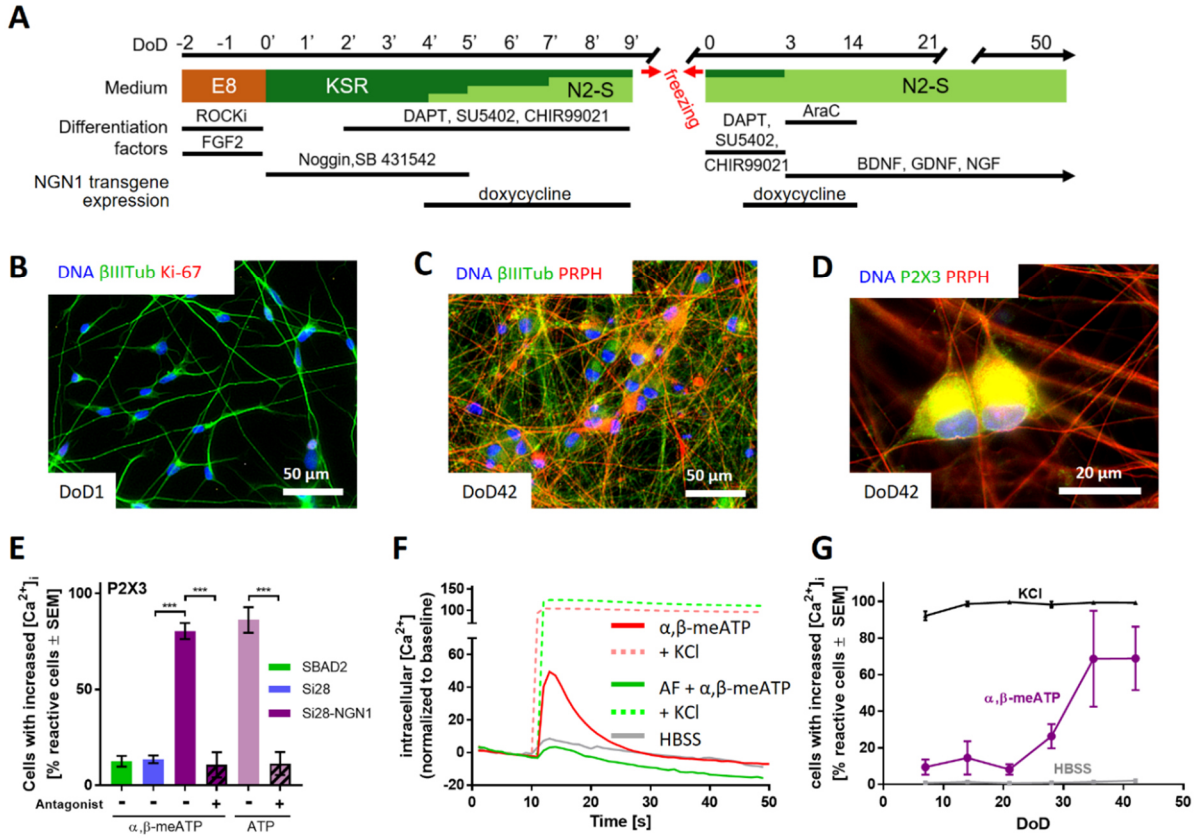

Figure 2.2.3: Sensory neurons exhibiting functional P2X3 receptor signaling

(A) Schematic representation of the differentiation protocol for the generation of functional sensory neurons from the genetically modified iPSC line Si28-NGN1. During the standard differentiation procedure, transient NGN1-transgene expression was induced from DoD4' until DoD9' and from DoD1 until DoD14 by addition of doxycycline. DoDx': day of differentiation, counting from pluripotent state (DoD0'); DoDx: day of differentiation, counting from thawing of frozen neural precursors on DoD0. Other factors added (e.g., ROCKi) are detailed in the methods. **(B-D)** Representative immunofluorescence images of cells fixed on DoD1 and stained for βIII-tubulin (βIIITub) and the proliferation marker Ki-67 **(B)**; or on DoD42 and stained for peripherin (PRPH) and βIIITub **(C)** or P2X3 **(D)**. Nuclei were stained using H33342 (DNA). Color code and scale bars are given in the images. Details are shown in figure 2.2.S5. **(E)** Peripheral neurons derived from the iPSC lines SBAD2 (green), Si28 (blue) and Si28-NGN1 (purple) were differentiated for >38 days and used for Ca^{2+}-imaging experiments. The P2X3-specific agonist α,β-methylene ATP (α,β-meATP) was used to determine the expression of functional P2X3 receptors. ATP was used as a general agonist for purinergic receptors. AF-

353, a P2X3-specific antagonist, was used to confirm exclusive P2X3 expression. **(F)** Exemplary traces (red) of changes in intracellular [Ca^{2+}] upon α,β-meATP (1 μM) application (solid lines). After the primary stimulus, KCl (dashed lines) was added. Some cells were pre-treated with AF-353 (0.1 μM) (green). The grey line depicts changes upon application of the negative control (HBSS, grey). **(G)** Time-dependency of the expression of functional P2X3 receptors. Sensory neurons were tested weekly for their potential to respond to HBSS, α,β-meATP and general membrane depolarization induced by KCl. **(E,G)** Data are means ± SEM of 3 independent biological replicates. *** $p < 0.0001$.

Transcriptomics profile of Si28-NGN1-derived sensory neurons

The expression levels of about 19,000 genes were determined for 6 differentiation stages of sensory neurons generated from Si28-NGN1 cells (Suppl. File2). A principle component analysis (PCA) of the whole set of genes provided a first overview on the dynamics of gene expression, and showed a continuous progression of cell differentiation until DoD42. Furthermore, the PCA demonstrated the good reproducibility of the differentiation protocol, as three independent differentiations clustered closely together (Fig. 2.2.S7A). Transcriptome changes continued until late differentiation stages (DoD35-42) as shown by the up-regulated gene expression of, e.g., plexin C1 (*PLXNC1*), which is involved in axon guidance, and the serotonin receptor 2A (*HTR2A*) (Usoskin et al. 2015; van Steenwinckel et al. 2009), and the down-regulation of growth cone-related genes, such as *ROBO2*, and the netrin receptor *UNC5B* (Mondal et al. 2020; Zhang et al. 2010) (Fig. 2.2.S7B).

To generate a condensed overview of the expression profile for Si28-NGN1-derived PNN, a small panel of 122 genes characteristic for neural cell types and signaling pathways was assembled (Fig. 2.2.4). Most pan-neuronal markers included in this panel were found to be expressed already on DoD1 and remained highly expressed over 6 weeks (e.g., neurofilaments (*NEFL/M/H*), acetylcholine esterase (*ACHE*) and microtubule associated protein tau (*MAPT*)). The sensory neuronal marker genes *ISL1*, *POU4F1* (BRN3A) and *PRPH*, the nociceptor markers *SCN9A* and *RET*, as well as various pre- and post-synaptic markers showed high expression levels throughout the monitored time of differentiation. Neural crest-specific genes (i.e. those related to PNN precursors), such as *PAX3* and *MSX1*, were down-regulated over time. These data confirm that the newly established differentiation protocol yields peripheral neurons with many features expected from nociceptors. Relatively few indications for other cell types were found, as only a subset of potentially glial genes was expressed, and there was little evidence for non-neural cell types.

Especially the pattern of receptor subtypes was highly distinct, as indicated here by three examples.: (i) Amongst dopamine receptors,the D2 subtype (*DRD2, DRD4*), which is known to be expressed in dorsal root ganglia (DRG) neurons (Almanza et al. 2019) was dominant, whereas *DRD3* and *DRD5* transcripts were absent; (ii) Genes encoding the metabotropic glutamate receptors 2 and 3 (*GRM2/3*), both expressed in human DRG neurons (Carlton et al. 2001; Sheahan et al. 2018), were found to be expressed, but not *GRM1*; (iii) Among the P2X receptors, only the nociceptor-characteristic P2X3 transcripts were measured at all differentiation stages.

In a last step, we picked a limited set (n=17) of highly expressed genes (Fig. 2.2.4A). We felt that these genes could be suitable for differentiation control by PCR for further use of the cultures or for inter-laboratory method transfer. A brief overview of the broad biological functions covered was assembled (Fig. 2.2.4B). In this context, it was interesting to see that *RBFOX3* mRNA levels were relatively low. This gene codes for the pan-neuronal marker NeuN that is very frequently used for immunostaining of CNS neurons by the community (Duan et al. 2016; Jeon et al. 2012; Sanchez-Ramos et al. 2000). The low gene expression in PNN was consistent with our finding that these cells very poorly stain for NeuN (not shown), compared to all our other central neuronal cultures (Klima et al. 2021a; Scholz et al. 2011; Smirnova et al. 2016).

The transcriptome analysis confirmed that even after more than 30 days of PNN cultivation, the differentiation processes are not fully completed. Ongoing alterations at the level of gene expression may explain why P2X3 responses of PNN are observed only at ≥DoD28 (Fig. 2.2.3G). For documentation of late transcriptome changes, we compiled exemplary genes that are clearly (> 4-fold) and significantly regulated at late time points (DoD35-42) relative to DoD7 (Fig. 2.2.S7B). These observations supported our decision to use PNN for further functional studies at late stages of differentiation, i.e. at >DoD35, to ensure the best possible maturation.

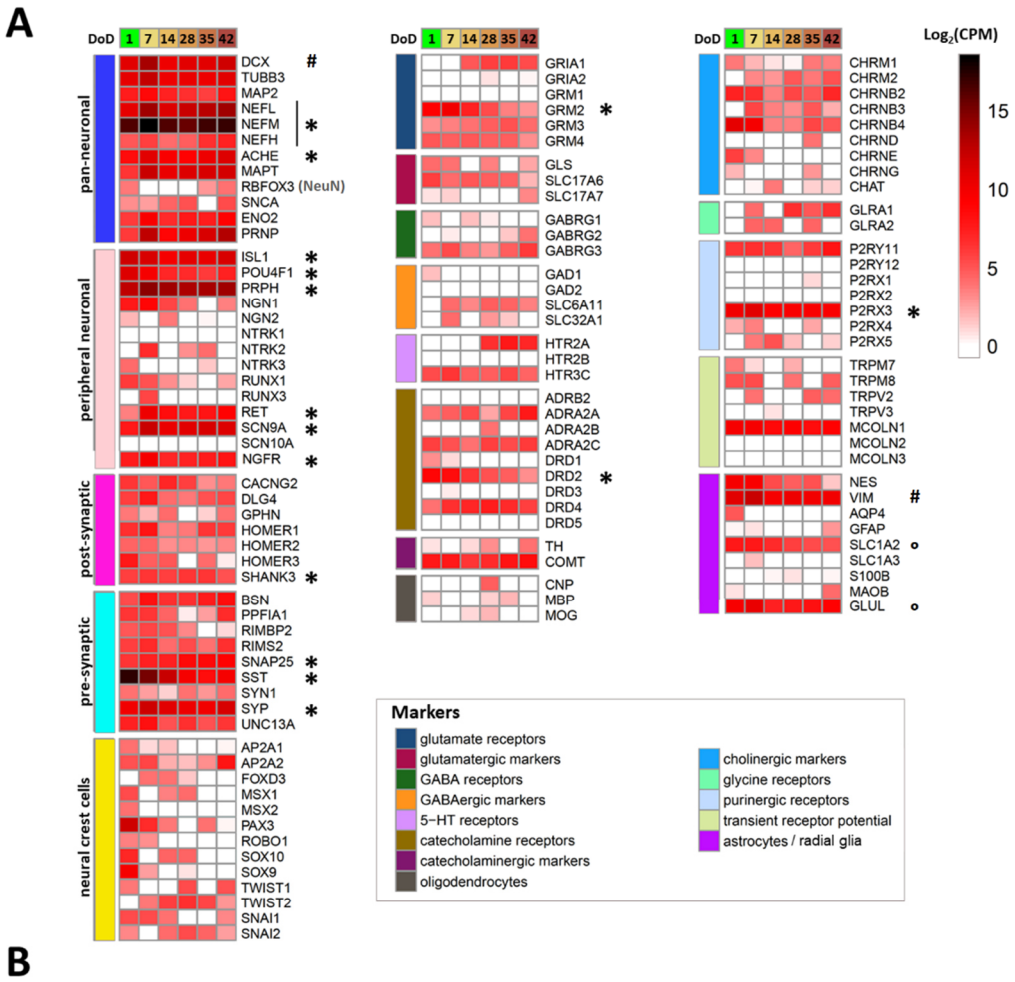

B

Gene	Full name	Comment
NEFL/M/H	Neurofilament ligh/medium/heavy chain	Intermediatefilaments; maintaining axonal calibre; particularly in long neurites
ISL1	ISLET1	Transcriptional activator, expressed in all peripheral neurons
POU4F1	BRN3A	Transcription factor, expressed in somatosensory neurons
PRPH	Peripherin	Intermediate filament protein of peripheral neurons
RET	RET receptor tyrosine kinase	Receptor for neurotrophins (e.g., GDNF), maker for nonpeptidergic nociceptors
SCN9A	Sodium voltage-gated channel alpha subunit 9	Voltage-gated sodium channel; role in nociception
NGFR	Nerve growth factor receptor	Receptor for neurotrophins (e.g., NGF), marker for nociceptors
SHANK3	SH and multiple ankyrin repeat domains 3	Major postsynaptic density scaffold protein
SST	Somatostatin	Neuromodulatory peptide, expressed in DRG neurons
SYP / SNAP25	Synaptophysin / Synaptosome associated protein 25	Membrane protein of synaptic vesicles; synapse markers
GRM2	Glutamate metabotropic receptor 2	Major metabotropic glutamate receptor in sensory neurons
DRD2	Dopamine receptor D2	Pain regulation in DRG neurons
ACHE	Acetylcholinesterase	Hydrolysis of the neurotransmitter acetylcholine, e.g., from motor neurons
P2RX3	Purinergic receptor P2X3	ATP-responsive ion channel required for normal perception of pain

Figure 2.2.4: Transcriptome profiling of Si28-NGN1-derived sensory neurons

Neurons were pre-differentiated to immature sensory neurons and frozen. **(A)** After thawing, gene expression levels were determined for 6 differentiation stages (on day of differentiation (DoD) 1, 7, 14, 28, 35 and 42) by the TempO-Seq method. The heatmap visualizes the normalized counts for each gene (rows) and the DoD (columns). The neuronal overview panel of 122 genes is clustered by gene groups (e.g. neuronal and glial subtypes, receptor and ion channel classes). The gene groups are indicated by color bars (left). The absolute expression levels are given in counts of the corresponding gene per 1 million reads (CPM). The color scale uses $\log_2$(CPM) units (see supplementary files for complete data sets) and ranges from white (no expression) to dark red (high expression). Data are derived from 3

independent differentiations. A subset of genes that that may be used for routine culture controls is highlighted (*). High expression levels of VIM and DCX (#) indicate a still relatively "young" state of the cells that may be even further matured. SLC1A2 and GLUL (°) are often considered glial markers, but the absence of GFAP, AQP, S100B and MBP indicate that the cultures do not contain classical astrocytes or Schwann cells. **(B)** Overview of highly expressed differentiation markers highlighted in **(A)** (*), with their full names and a brief explanation of their biological functions.

Purinergic signaling as test endpoint to assess peripheral neurotoxicity

To explore the usefulness of Ca^{2+}-imaging as a readout for disturbed pain signaling, we first investigated two clinically used proteasome inhibitors (PIs) known to cause peripheral neuropathy: bortezomib and carfilzomib. Pre-screening of the compounds in the PeriTox test indicated a cytotoxicity threshold of 200 nM for bortezomib and 66 nM for carfilzomib (Fig. 2.2.5A, left, middle). PNN were exposed on DoD≥38 to sub-cytotoxic concentrations (5 and 20 nM) for 24 h. After this "drug treatment", we tested whether the neurons were still able to show purinergic signaling. Bortezomib concentrations of 5 nM and higher resulted in a complete shut-down of P2X3 signaling, as indicated by Ca^{2+}-imaging experiments (Fig. 2.2.5B, left, 4.2.S8B). Carfilzomib induced a similar non-responsiveness at ≥20 nM (Fig. 2.2.5B, middle). In order to make sure that neurons were not made generally non-responsive by a cytotoxic response missed in the PeriTox test, they were exposed to a membrane depolarizing KCl stimulus after the α,β-meATP stimulation. The cells still showed Ca^{2+}-flux at PI drug concentrations that had blunted P2X3 signaling (Fig. 2.2.S9A). Thus, neurons were still able to respond by Ca^{2+}-signaling, and we suggest that PI treatment specifically impairs purinergic signaling. As further control, we investigated signaling through pain-related TRPV1 receptors. PI-treated neurons did not differ from control cells in this response (Fig. 2.2.S9B). These results further confirm that the attenuation of P2X3 signaling was not attributable to generally decreased cell viability, or an overall loss of signaling functions.

On closer inspection, we observed that pre-treatment with bortezomib or carfilzomib led to a mild deregulation of $[Ca^{2+}]_i$ in the unstimulated state (Fig. 2.2.5C, 4.2.S8A). This may explain an unresponsiveness of P2X3, possibly as counter-regulation or tachyphylaxis mechanism.

To address the question of whether also a non-PI peripheral neurotoxicant would attenuate P2X3 signaling, we repeated several of the above experiments with taxol. The chemotherapeutic drug group of taxanes (including taxol) alters microtubule dynamics, but does not affect the proteasome function. Exposure to taxol in the PeriTox test showed no effect on cell viability at concentrations up to 75 nM, but neurites were strongly

affected at concentrations ≥1 nM (Fig. 2.2.5A, right). We chose pre-treatment conditions of 15 and 60 nM to test for functional impairments of P2X3 or TRPV1 receptors and of depolarization induced Ca^{2+}-influx. None of the endpoints was affected (Fig. 2.2.5B, right, Fig. 2.2.S9). These findings suggest that impaired P2X3 signaling is a sensitive and specific endpoint for early PI-induced functional impairments.

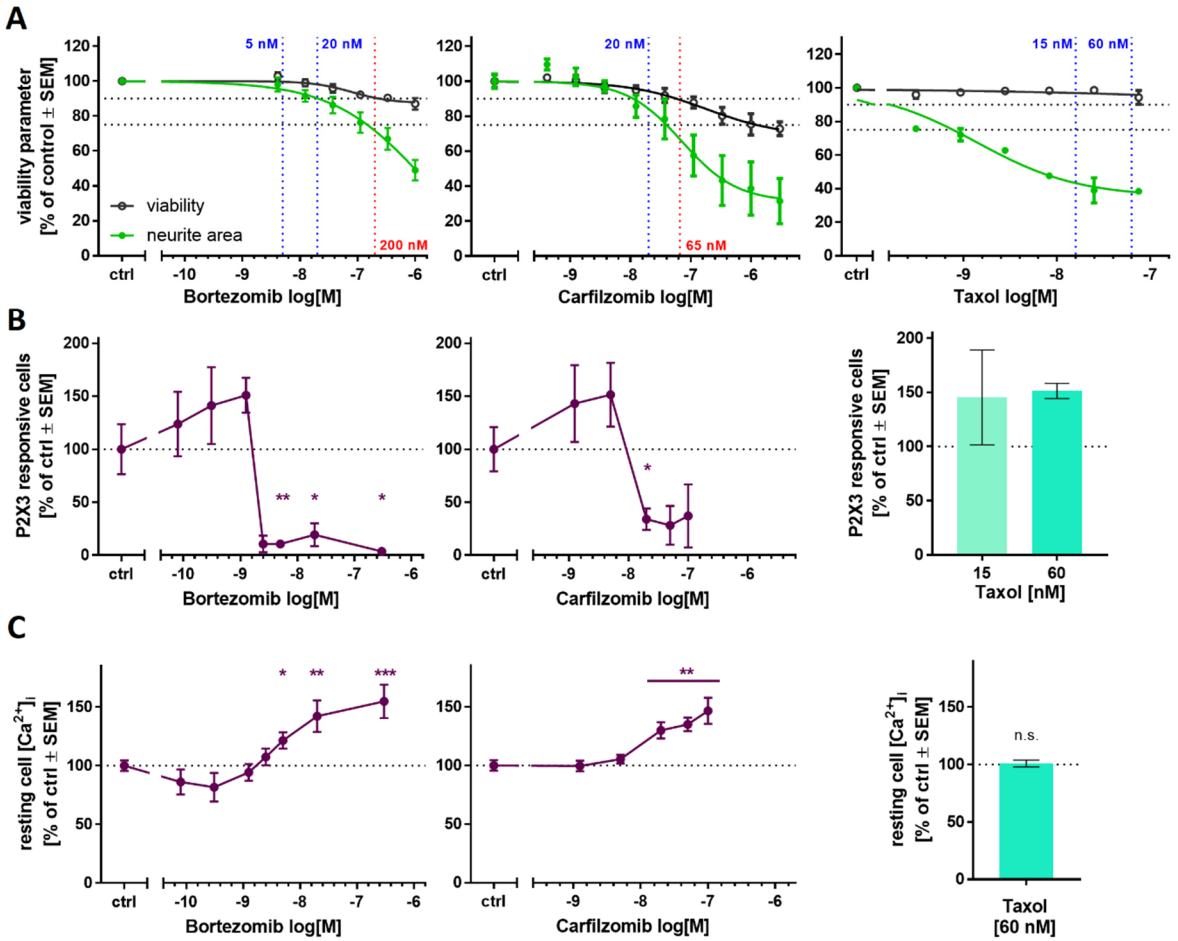

Figure 2.2.5: Ca^{2+} signaling as sensitive functional endpoint to assess proteasome inhibitor toxicity

The compounds bortezomib (left), carfilzomib (middle) and taxol (right) were investigated regarding their effects on different test endpoints. **(A)** The PeriTox test was used to assess their effects on neurite area and viability. Horizontal dashed lines at 90% and 75% indicate the cytotoxicity threshold the neurite effect threshold, respectively. Vertical dashed lines indicate the lowest cytotoxicity-inducing concentration (red) and the concentrations further used for Ca^{2+}-imaging experiments (blue). **(B,C)** Sensory neurons (>DoD38) were pre-treated with the test compounds for 24 h, before Ca^{2+}-imaging experiments were performed. **(B)** The number of cells responsive towards stimulation with the P2X3-specific agonist α,β-methylene ATP was assessed. **(C)** Baseline fluorescence, indicating the resting cell intracellular $[Ca^{2+}]_i$ was quantified for whole sensory neuron cultures. Exemplary single cell fluorescence traces are shown in figure 2.2.S8. **(A-C)** Data are given as % of untreated control cells and are means ± SEM of at least 3 biological replicates. * $p < 0.05$, ** $p < 0.001$, *** $p < 0.0001$.

PI-associated reorganization of the microtubule structure in cell somata

We used several structural endpoints to potentially identify additional features of mild cell stress that would parallel impaired P2X3 signaling in the low nM range. We hypothesized that such findings would give additional evidence for early non-cytotoxic changes that preceede full-blown neuropathies. Staining of PNN for the cytoskeletal protein βIII-tubulin confirmed that the neurite network was fully intact (no neurite fragmentation or blebbing). However, we observed a conspicuous ring-like tubublin accumulation in the periphery of cell somata of bortezomib- and carfilzomib treated cells (Fig. 2.2.6A, 4.2.S10). To follow up on this, cells exhibiting such a circular tubulin structure were quantified. Distinctive microtubule reorganization occurred in >80% of the cells pre-treated with PI concentrations that also resulted in the attenuation of P2X3 signaling (Fig. 2.2.6B). Further experiments showed that the accumulation in ring structures was a tubulin-specific phenomenon, as such structures were not found in stainings of the same cells for the cytoskeletal intermediate filament peripherin (Fig. 2.2.S10). However, also peripherin showed a mild reorganization phenotype: While its structure in neurites was not altered, PI-treated cells showed some peripherin clustering in the somata. This was mainly seen in cytosolic areas (outside the nucleus, but not ring-shaped under the plasma membrane). For comparison, PNN were also treated with taxol (60 nM). A small number of cells presented with tubulin accumulations (Fig. 2.2.6B). Closer examination revealed that these structures were more diffuse than the very sharp rings triggered by PIs (Fig. 2.2.6A, 4.2.S10). Thus, sharp tubulin-rings correlated with P2X3 impairment. These findings are in good agreement with observations in primary dorsal root ganglia that accumulation of cytoskeletal proteins in the cell somata is specific for early PI-induced neuronal stress (Alé et al. 2015; Staff et al. 2013).

While we studied the accumulation of cytoskeletal elements in somata, we wondered whether PNN nuclei were also affected by PIs. The neurons were examined in more detail for signs of condensed or fragmented chromatin, indicative for apoptotic cells. No changes in the size of neuronal nuclei or the intensity of the DNA stain were observed. However, the nuclei had an altered (more bean-shaped) morphology (Fig. 2.2.S11). This may be a consequence of protein accumulations in the cytosol exerting “pressure” on the normally more rounded nuclei.

Taken together, these data show that P2X3 impairment was accompanied by a structural change, i.e., cytoskeletal protein accumulation in somata. This occurred at concentrations that did not alter any other endpoint investigated in this study. In the next step, we investigated whether our findings applied to PIs in general.

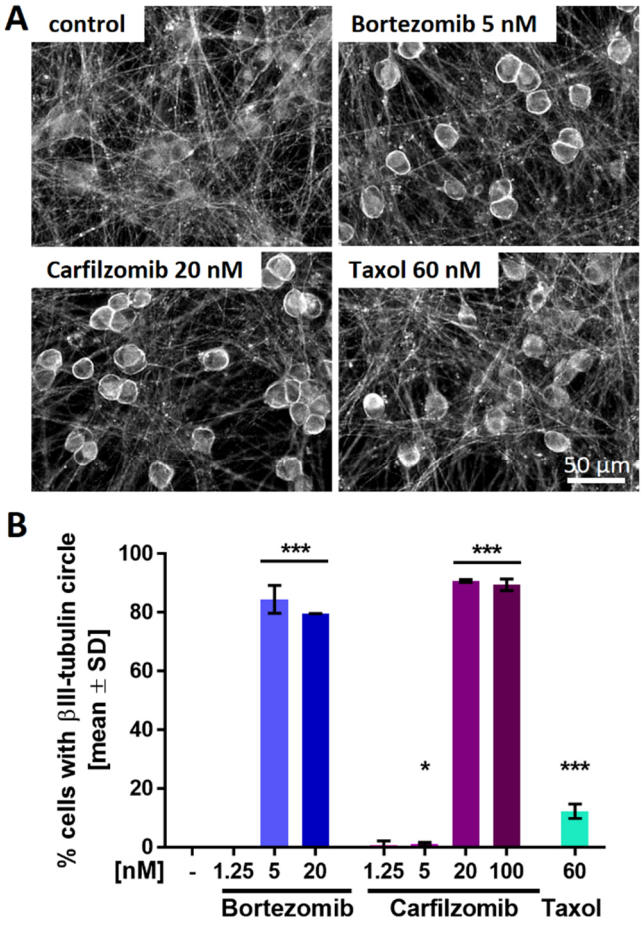

Figure 2.2.6: Proteasome inhibitor-induced reorganization of the microtubule structure in neuronal somata

Sensory neurons were differentiated for at least 38 days after thawing and exposed to bortezomib, carfilzomib or taxol for 24 h before fixation. **(A)** Representative immuno-fluorescence images of cells stained for βIII-tubulin. Scale bar is given in the images, and further details are shown in figure 2.2.S11. **(B)** Cells exhibiting intense, circular βIII-tubulin staining around the cell somata (covering at least 50% of a full circle) were quantified. Data are given as % of the total cell count (number of viable cell nuclei) and are means ± SD of 2-3 biological replicates. * $p < 0.05$, *** $p < 0.0001$

Blunted P2X3 signaling and tubulin re-organization as PI class-effects

To explore whether impairment of P2X3 signaling in PNN and somatic tubulin accumulation are class-effects of PIs, we examined three additional compounds: (i) delanzomib, a peptide boronic acid like bortezomib that has been tested in clinical trials; (ii) epoxomicin, an epoxyketone like carfilzomib; and (iii) the peptide aldehyde MG-132. Delanzomib neither affected the viability nor the neurite growth in the PeriTox at test concentrations up to 10 µM (Fig. 2.2.7A). Pre-treatment of PNN (>DoD38) with concentrations as low as 5 nM lead to the attenuation of Ca^{2+}-signaling upon P2X3 stimulation (Fig. 2.2.7B), while TRPV1 signaling was not impaired (Fig. 2.2.S9B). As previously observed with bortezomib, a slight increase in resting cell $[Ca^{2+}]_i$ was detected at delanzomib concentrations associated with inhibition of P2X3 signaling (Fig. 2.2.7C). Thus, delanzomib, which inhibits the proteasome with a similar K_i as bortezomib (Berkers et al. 2012), also showed here similar *in vitro* effects as the PIs studied earlier.

Pre-screening of the experimental PIs epoxomicin and MG-132 in the PeriTox test revealed high cytotoxicity thresholds of ≥1,000 nM (Fig. 2.2.7D). For both compounds, test concentrations were chosen that did not alter any PeriTox test endpoint (100 nM epoxomicin and 300 nM MG-132). Pre-treatment of PNN to such conditions resulted in a complete blunting of P2X3 responses, accompanied by elevated $[Ca^{2+}]_i$ in resting cells (Fig. 2.2.7E,F). For all three PIs, we found that the neurite network remained intact upon exposure to P2X3-attenuating concentrations. As expected, we found that inhibition of the P2X3 responses again correlated with the emergence of sharp annular βIII-tubulin accumulations in the cell somata (Fig. 2.2.7G, 4.2.S12A,B). These results suggest that attenuation of P2X3 signaling and βIII-tubulin reorganization are indeed class-effects of PIs.

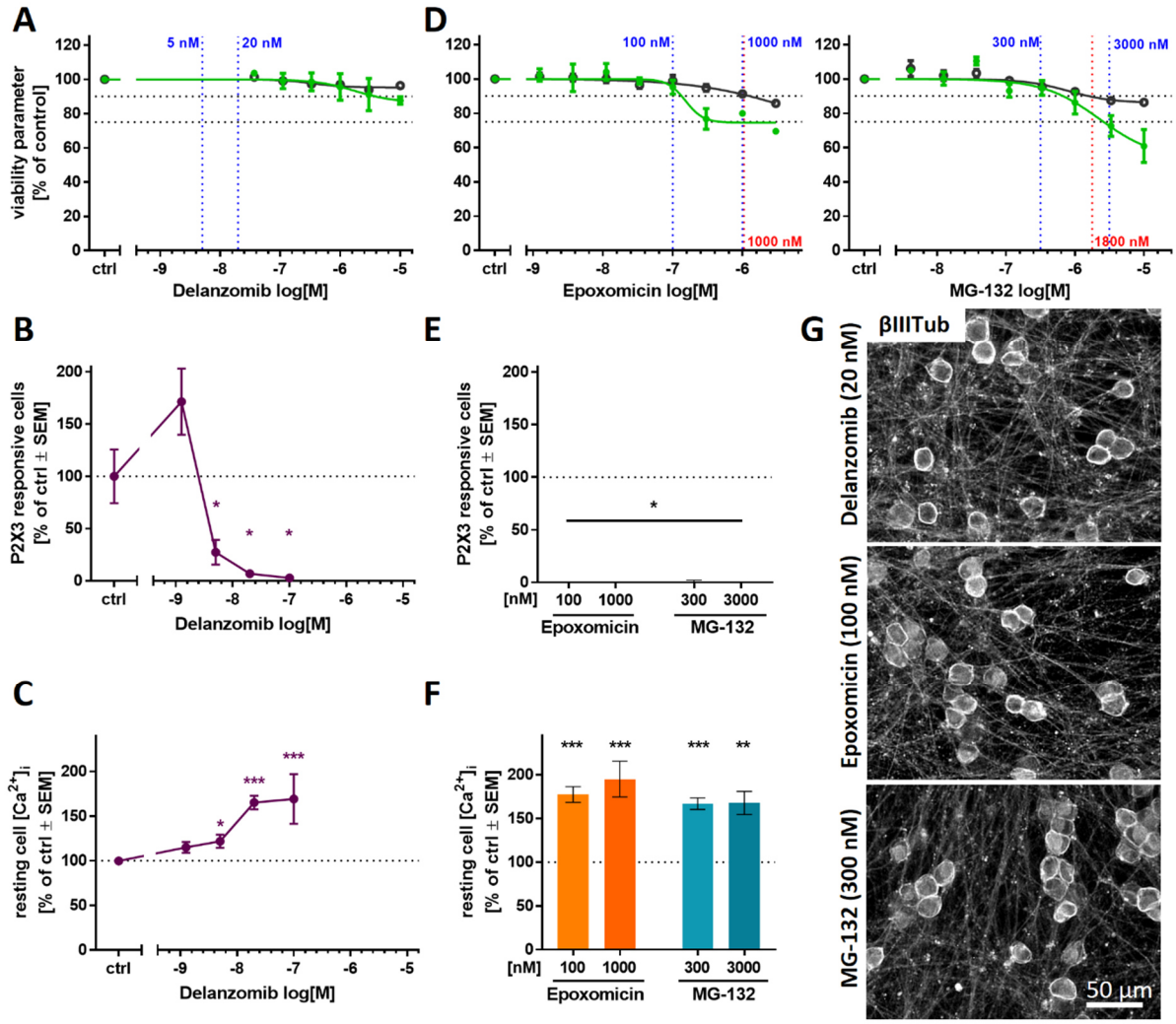

Figure 7: Attenuation of P2X3-signaling and microtubule reorganization as potential PI class-effects

The PIs delanzomib **(A-C,G)**, epoxomicin and MG-132 **(D-E,G)** representing different PI classes were investigated regarding their effects on various test endpoints. **(A,D)** The compounds' effects on neurite area and viability were assessed in the standard PeriTox test. Horizontal dashed lines at 90% and 75% indicate the cytotoxicity threshold the

neurite effect threshold, respectively. Vertical dashed lines indicate the lowest cytotoxicity-inducing concentration (red) and concentrations further used for Ca^{2+}-imaging experiments (blue). **(B,C,E,F)** Sensory neurons (>DoD38) were pre-treated with the test compounds for 24 h before Ca^{2+}-imaging experiments were performed. **(B,E)** The number of cells responding to stimulation with the P2X3-specific agonist α,β-methylene ATP (1 µM) was assessed. **(C,F)** Baseline fluorescence, indicating the resting cell intracellular $[Ca^{2+}]_i$ was quantified for whole sensory neuron cultures. **(A-F)** Data are given as % of untreated control cells and are means ± SEM of at least 3 biological replicates. * $p < 0.05$, ** $p < 0.001$, *** $p < 0.0001$. **(G)** After differentiation of >38 days, sensory neurons were exposed to the PIs for 24 h, fixed and stained for βIII-tubulin. Representative immunofluorescence images are shown. The scale bar is given in the images. Further details and quantification of cells with circular βIII-tubulin staining are given in figure 2.2.S12.

2.2.4 Discussion and conclusion

We have developed and documented here a robust differentiation protocol that yields human PNN useful to address various biomedical questions. The cultures generated in this way have many characteristics of nociceptors, and they can be used reproducibly after 6 weeks of differentiation (without cell detachment, with no signs of de-differentiation, and completely without any overgrowth by non-wanted cells) for single cell Ca^{2+}-imaging of P2X3 receptors. The cells maintain their original network of individual somata, connected by long neurites. This is noteworthy, as many other culture protocols designed to yield peripheral neurons tend to generate cells that cluster together over time, and that make imaging of $[Ca^{2+}]_i$ in individual cells nearly impossible. These PNN allowed us to study very early adverse effects of PIs at clinically-relevant low nM concentrations (Papandreou et al. 2004; Reece et al. 2011). All five compounds investigated behaved similarly in that they induced a pronounced down-regulation of P2X3 responses and a clustering of tubulin to ring-like structures around the somata, at concentrations that were non-cytotoxic and that did not damage any of the neurite network features.

The PeriTox test is a well established *in vitro* screening assay using human iPSC-derived peripheral neurons to identify peripheral neurotoxicants (Hoelting et al. 2016). It has been successfully used to identify environmental neurotoxicants by assessing their effects on the neurite structures (Delp et al. 2018; Klose et al. 2021; Masjosthusmann et al. 2020). However, for pre-clinical drug testing, an increased sensitivity in detecting the potential neurotoxicity of chemotherapeutics is desirable. To achieve this, we pursued different strategies:

First, we explored whether longer exposure times would decrease the toxicity threshold concentrations (Flury 1921; Haber 1924; Macko et al. 2021). We found that prolonged exposure to toxicants increased the sensitivity for cytotoxicity, but the specificity for neurite effects was

lost. This is in good agreement with the fact that in many neuronal cultures neurite damage is followed by general cell death or apoptosis, if given sufficient incubation time (Berliocchi et al. 2005; Herkenham et al. 1991; Volbracht et al. 1999). The sequence of neurite damage triggering cell death may be particularly pronounced in still differentiating iPSC-derived neurons, while *in vivo* matured neurons that are functionally integrated in regulatory circuits are known to separate the neurite pruning program from downstream death of the somata (Geden and Deshmukh 2016; Geden et al. 2019).

As second approach, we explored whether functional changes in sensory receptors would allow for more sensitive readouts. Indeed, signaling through P2X3 receptors proved to be highly sensitive to proteasome inhibitors. The measurement of such responses required a new culture setup, using cells differentiated for ≥5 weeks. The detection of PI-induced effects by the new approach at ≥10-fold higher sensitivity than in the PeriTox test suggests that alterations at the functional level of signaling may often precede structural impairments.

Further examinations of timing aspects appear highly relevant. It would be interesting to learn whether P2X3 signaling remains a specifically altered endpoint upon prolonged exposure (48-72 h) to low nM concentrations, or whether specificity is lost, as already observed in the extended PeriTox test. Also repeated exposure scenarios are of interest, as they might model a possible accumulation of PIs in the DRG (Carozzi et al. 2012; Papandreou et al. 2004).

Although we used the pronounced regulation of P2X3 here mainly as indicator of dysregulation, we wondered whether this may also play a pathophysiological role. Indeed, P2X3 is part of several complex pain regulation circuits. E.g., the acid sensing ion channel ASIC3, which is also involved in pain signaling, can lead to inhibition of P2X3 responses (Deval et al. 2008; Stephan et al. 2018). Since bortezomib induces aerobic glycolysis and thus extracellular acidification, the above process may play a role in tissue (Ludman and Melemedjian 2019). Whether an interaction of P2X3 and ASIC3 is relevant in PNN needs to be clarified. Our results further show that P2X3 responses and intracellular baseline Ca^{2+} levels are de-regulated at identical toxicant concentrations. Thus, blunted P2X3 responses could be caused by or function as indicator of Ca^{2+} de-regulation (Cook et al. 1998; Ishchenko et al. 2017).

Coinciding with the functional effect of P2X3 attenuation, we detected a somatic accumulation of tubulin in PI-treated PNN. Our conclusion that tubulin accumulation is a PI class effect is further supported by a study on the PI lactacystin (not used here), which elicited the same pattern of tubulin re-organization into sharp rings (Staff et al. 2013). Furthermore, somatic accumulation of cytoskeletal proteins upon PI treatment was reported also in mouse *in vivo*

studies, suggesting that tubulin re-organization observed *in vitro* also occurs in animals (Alé et al. 2015). It will be interesting to study a potential association of tubulin accumulation and changes in axonal transport. Since Ca^{2+} is also known to be a regulator of the cytoskeleton (Mattson 1992), de-regulation of $[Ca^{2+}]_i$ may be a common cause of P2X3 signaling impairments and morphological changes observed in PI-treated PNN.

When taxol was compared here to the class of PIs, we neither observed P2X3 inactivation, nor tubulin rings. Thus, different initial processes may be involved in the development of taxol peripheral neuropathies. Future experiments should test more classes of neuropathy-inducing cytostatics, such as platinum compounds or vinca alkaloids.

Overall, this study demonstrates the feasibility of developing target cell-specific test methods that are based on human cells. Using neuronal cultures other than peripheral neurons for research on chemotherapy-induced peripheral neuropathy can miss functional effects only detectable in the relevant target cells (Hoelting et al. 2016; Wing et al. 2017). Moreover, the use of high toxicant concentrations and of blunt endpoints (such as cell death) may make it very difficult to identify compounds that would attenuate the toxicity. We suggest that insights on specifically-impaired processes are important for the development of pharmacological countermeasures for peripheral neuropathies.

2.2.5 Materials and methods

Differentiation of human iPSCs to peripheral neurons

We used the human iPSC lines mciPS (model no. SC301A-1; System Biosciences, Palo Alto, CA, USA), SBAD2 (Snijders et al. 2021), Sigma iPSC0028 (Si28) (EPITHELIAL-1, #IPSC0028, Merck, Darmstadt, Germany) and the transgenic iPSC line Si28-NGN1. IPSC cultures were maintained under xeno-free conditions (see supplementary methods) (Chen et al. 2011).

The differentiation procedure for all iPSC lines is detailed in the supplementary methods (see also table S1). In brief, iPSCs were neuralized by dual SMAD inhibition followed by direction of the differentiation towards the sensory neuron fate using small molecule inhibitors (Chambers et al. 2012). After 9-12 days of differentiation, immature peripheral neurons were frozen in 90% fetal bovine serum (FBS) (Thermo Fisher Scientific, Waltham, MA, USA) and 10% dimethyl sulfoxide (DMSO; Merck, Darmstadt, Germany). After thawing, further maturation was driven by the growth factors glia-derived

neurotrophic factor (GDNF, 25 ng/ml), brain-derived neurotrophic factor (BDNF, 12.5 ng/ml) and nerve growth factor (NGF, 25 ng/ml) (all from Bio-Techne, Minneapolis, MN, USA). For the differentiation of peripheral neurons with nociceptor features, doxycycline (2 µg/ml) exposure from DoD4'-9' and DoD1-14 was integrated in the basis small molecule differentiation protocol, starting from Si28-NGN1 iPSC.
Peri.4U cells were provided by Axiogenesis (Cologne, Germany) and maintained according to the manufacturer's protocol.

Generation of the gene-edited iPSC line Si28-NGN1

Analogous to Boisvert et al. (Boisvert et al. 2015), an iPSC line with inducible NGN1-overexpression was created. A lentiviral sequence was designed to express the human NGN1 gene under control of a Tet-responsive element (TRE), which is dependant on the presence of Doxycycline (Dox). The expression of NGN1 was linked to the expression of turboRFP to monitor the induction. For selection, a hygromycin restistance gene was included. The vector and the principle of the fusion construct was published earlier (Schildknecht et al. 2013). The cell line was authenticated by short tandem repeat DNA typing and pluripotency was confirmed (data not shown) (Dirks and Drexler 2013).

Toxicity testing by assessment of neurite area and cell viability

Immature peripheral neurons were thawed and seeded at a density of 100,000 cells /cm^2. For initial toxicity assessment, cells were left to attach for 1 h at 37°C, 5% CO_2 followed by treatment with the test compounds. Cells were exposed to the compounds for 24 h, 48 h and 72 h and readout was performed on DoD1, 2 and 3, respectively.

For delayed toxicity assessment, cells were cultured until DoD4. On DoD4, test compounds were added to the cells together by performing a half medium exchange. Readout was performed after 72 h (on DoD7).

For the readout, neurons were stained with 1 µg/ml HOECHST-33342 (H-33342) and 1 µM calcein-AM (both from Merck, Darmstadt, Germany) one hour prior to the imaging. After incubation for 1 h at 37°C, 5% CO_2, images were acquired automatically using an ArrayScan VTI HCS microscope (Thermo Fisher Scientific, Waltham, MA, USA). Images were analysed for neurite area and cell viability as previsouly described (Stiegler et al. 2011).

Immunofluorescence staining

Protein expression was assessed qualitatively via immunofluorescence staining and microscopy. All samples were prepared, and analyzed exactly as described before (Dreser et al. 2020; Klima et al. 2021a), using antibodies as detailed in supplementary methods.

The quantification of somata with βIII-tubulin circles was performed manually by independent observers. Criteria for the quantification were sharply defined, intense, and circular βIII-tubulin staining with presumably sub-membraneous location covering at least 50% of a full circle.

To quantify the nuclear area, images of H-33342 stainings were converted into binary images and the area of randomly chosen H-33342-objects was measured using the Fiji software.

Transcriptome data generation and analysis

Sample lysates were prepared by medium removal, followed by a wash with 50 µl of phosphate buffered saline (PBS) (Thermo Fisher Scientific, Waltham, MA, USA) and instant addition of 33 µl 1x Biospyder lysis buffer (BioSpyder Tech., Glasgow, UK) (Klima et al. 2021a; Loser et al. 2021b). After incubation at RT for 10 minutes, the sample plates were stored at -80°C up to the time of dry ice shipping to Bioclavis (BioSpyder Tech., Glasgow, UK). Measurement of the whole transcriptome set was performed via the TempO-Seq targeted sequencing technology (House et al. 2017). The gene set analyzed, and the read data are detailed in supplementary file 2 (organized as Excel workbook). For data processing, the R package DESeq2 (v1.32.0) was used for quality control and normalization (Love et al. 2014). Further details on data analysis are given in the supplementary methods.

Measurement of changes in intracellular Ca^{2+} concentration $[Ca^{2+}]_i$

Sensory neurons were cultured in 96-well plates for at least 35 days after thawing. One day before Ca^{2+}-imaging experiments were performed, cells were optionally pre-treated with the test compounds. One hour before the experiment, cells were loaded with the Ca^{2+}-indicator Fluo-4 (Thermo Fisher Scientific, Waltham, MA, USA). Pre-treatment with antagonists was performed together with Fluo-4 loading. Monitoring of $[Ca^{2+}]_i$ was performed using an ArrayScan VTI HCS microscope equipped with an automated pipettor and an incubation chamber providing an atmosphere with 5% CO_2 and 37°C. Cells were imaged as fast as possible for 45 s. Test compounds were automatically applied after

baseline recording (10 s). In a standard experiment with 4 stimuli applied to one well (e.g., negative control, P2X3 agonist, TRPV1 agonist, KCl), the cells were imaged 4 times for 45 s with one stimulus applied at a time.

The images were exported as *.avi video files and analysed with the CaFFEE software (Karreman et al. 2020). In brief, the time point of peak fluorescence was identified. Fluorescence data for the ground state (F_0) and for the peak time point (F_1) were assessed automatically for all cells. The difference between the two fluorescence levels, $\Delta F=F_1-F_0$, was used for further data processing (Klima et al. 2021a). The noise level-based threshold (mean(ΔF) + 3x SD(ΔF)) of each well was determined by the application of a negative control stimulus (Hanks' Balanced Salt Solution (HBSS)), with an upper threshold-limit set to ΔF=18. According to this threshold, cells were defined as reactive ($\Delta F_{stimulus}$>threshold) or non-reactive ($\Delta F_{stimulus}$ ≤threshold).

Statistics

If not stated otherwise, experiments were performed on 3 or more independent cell preparations (here called biological replicates). In each cell preparation at least three different wells (here called technical replicates) were measured.

Information concerning descriptive statistics and experimental variability is included in the figure legends or the figures themselves. GraphPad Prism 7 software (Version 7.04, Graphpad Software, Inc, San Diego, USA) was used for significance testing and data display. Data were evaluated by ANOVA plus appropriate post-hoc testing method or by t-test for binary comparisons. *p*-values < 0.05 were regarded as statistically significant.

2.2.6 Acknowledgements

This work was supported by CEFIC, the BMBF, EFSA, and the DK-EPA (MST-667-00205). It has received funding from the European Union's Horizon 2020 research and innovation program under grant agreements No. 681002 (EU-ToxRisk), No. 964537 (RISK-HUNT3R), No. 964518 (ToxFree) and No. 825759 (ENDpoiNTs). We are grateful to M. Kapitza for invaluable experimental support.

2.2.7 Disclosure of Potential Conflicts of Interest

The authors declare no conflict of interest.

2.2.8 Supplementary information

Supplementary Methods

Maintenance of induced pluripotent stem cells (iPSCs)

Maintenance of all iPSC lines used in this study was performed on human Laminin-521 (BioLamina, Sundbyger, Sweden) coating in essential 8 (E8) medium (Dulbecco's modified Eagle's medium/F12 [DMEM/F12] supplemented with 15 mM Hepes [Thermo Fisher Scientific, Waltham, MA, USA], 10 µg/ml holo-transferrin, 20 µg/ml insulin, 16 mg/ml L-ascorbic-acid, 0.7 mg/ml sodium selenite [all from Merck, Darmstadt, Germany], 100 ng/ml bFGF [Thermo Fisher Scientific, Waltham, MA, USA], 1.74 ng/ml TGFb [Bio-Techne, Minneapolis, MN, USA]) essentially as described (Chen et al. 2011). Passaging of the iPSCs was performed every 7 days. Cells were incubated with EDTA (Thermo Fisher Scientific, Waltham, MA, USA) for 2 min (37°C, 5% CO_2) to detach the cells, so that clumps remain (no single cell suspension). IPSCs were washed off the plate with DMEM/F12. Cells were re-seeded in E8 medium on freshly coated plates in a final dilution of 1:40-60.

Differentiation of sensory neurons from iPSC

The iPSCs were prepared for neural differentiation on day of differentiation minus 2 (DoD-2) by replating in a single cell suspension (90,000 cells/cm^2) onto Matrigel™ (Corning, Glendale, AZ, USA) coated 6-well plates in E8 medium supplemented with 10 µM Rock inhibitor (Y-27632 [Bio-Techne, Minneapolis, MN, USA]).
On DoD0', E8 was replaced by neural differentiation medium KSR (knock out DMEM with 15% serum replacement, 1 x Glutamax, 1 x nonessential amino acids, and 50 µM β-mercaptoethanol [all from Thermo Fisher Scientific, Waltham, MA, USA]) and the combination of five small molecule pathway inhibitors as described in detail in table S1. From DoD0'-5', Noggin and SB-431642 (both from Bio-Techne, Minneapolis, MN, USA) (± dorsomorphine hydrochloride [Dorso; Merck, Darmstadt, Germany]) were added, and CHIR99021 (Axon Medchem, Groningen, Netherlands), SU5402 (Bio-Techne,

Minneapolis, MN, USA) and DAPT (γ-Secretase inhibitor IX; Merck, Darmstadt, Germany) were added on DoD2'-9'. From DoD4' onwards, KSR medium was gradually replaced by N2-S medium (DMEM/F12, 1 x GlutaMax [both from Thermo Fisher Scientific, Waltham, MA, USA], 0.1 mg/ml apotransferrin, 1.55 mg/ml glucose, 25 µg/ml insulin, 20 nM progesterone, 100 µM putrescine and 30 nM selenium [all from Merck, Darmstadt, Germany]) in 25% increments. On DoD9' or DoD12' (depending on the iPSC line used, see table S1), the cells were cryopreserved in 90% fetal bovine serum (FBS) (Thermo Fisher Scientific, Waltham, MA, USA) and 10% dimethyl sulfoxide (DMSO; Merck, Darmstadt, Germany).

After thawing of the pre-differentiated cells, sensory neuron precursors were cultured in 25% KSR and 75% N2-S supplemented with CHIR99021 (1.5 µM), SU5402 (5 µM) and DAPT (5 µM). Cells were seeded at a density of 100,000 cells/cm² on Matrigel™ coated plates. For further differentiation and maturation, half of the medium was changed on DoD1 and DoD2. With the fresh culture medium on DoD2, Matrigel was added to the cells at a final dilution of 1:80. On DoD3, medium was changed to N2-S medium supplemented with 12.5 ng/ml brain-derived neurotrophic factor (BDNF), 25 ng/ml glia-derived neurotrophic factor (GDNF) and 25 ng/ml nerve growth factor (NGF) (all from Bio-Techne, Minneapolis, MN, USA) and 2 µM cytarabin (AraC; Merck, Darmstadt, Germany). Half of the medium was changed on DoD4, 7 and 10 with further Matrigel addition on DoD10. On DoD14, medium was changed to maturation medium (N2-S supplemented with BDNF [12.5 ng/ml], GDNF and NGF [both 25 ng/ml]). Half medium exchanges were performed every three to four days. Matrigel was diluted in the culture medium at a final dilution of 1:80 every 10 days.

Assessment of neurite area and cell viability

Cells stained with calcein-AM and HOECHST-33342 (H-33342) (both from Merck, Darmstadt, Germany) were imaged automatically using an ArrayScan VTI HCS microscope (Thermo Fisher Scientific, Waltham, MA, USA). Images were analysed for neurite area and cell viability by an automated algorithm. H-33342 staining was used to identify the cell nuclei. The nuclear area was enlarged to define the somatic area, which was then substracted from the calcein stain. The remaining calcein-positive pixels were quantified to derive the neurite area. Data on cell viability was derived from the same images by checking each H-33342 stained object (cell) for a double stain with calcein. Double-positive cells were classified as viable, calcein-negative cells as dead (Stiegler et al. 2011).

Immunofluorescence staining and microscopy

Neurons, grown on glass coverslips coated with Matrigel™, were fixed with 4% paraformaldehyde at 4°C over night. All further steps were performed at room temperature. Paraformaldehyde was taken off and cells were washed (~1 min) with phosphate buffered saline (PBS) followed by permeabilization with 0.6% Triton X-100 in PBS for 7 min. Coverslips were washed (~1 min) with PBS and blocked for 1 h in PBS containing 5% FCS and 0.1% Triton X-100. Primary antibodies (see Tab. S2) were diluted in fresh blocking solution and applied for 1 h. Residual free primary antibodies are then washed off with PBS. Secondary antibodies and H-33342 are diluted in blocking solution and applied on the coverslips for 30 min. After washing with PBS, coverslips were placed upside-down on mounting medium on microscope slides.

Transcriptome data analysis

For data processing, the R package DESeq2 (v1.32.0) was used for quality control, normalization and differential gene expression (DGE) analysis (Love et al. 2014). The raw probe counts were normalized to total sample counts per million (CPM). No library size threshold was used; samples with replicate correlation (Pearson R) to group average below 0.8 were removed from the analysis. Prior to the DGE, the low-count genes (less than 3 samples above 5 CPM) were discarded. The Wald statistics test was used for significance evaluation of each differentiation stage against DoD1 or DoD7. Selection of the most significant differentially expressed genes (DEG) was done using a (Benjamini-Hochberg) p-adjusted maximum threshold of 0.05 and a $\log_2$(fold change) minimum threshold of 1.

Table 2.2.S1: Schedule for differentiation media and supplementing factors

X: applies for all iPSC lines

X: applies for mc-iPSC

X: applies for SBAD2

X: applies for Si28-NGN1

DoD	Medium		Supplements						
	KSR	N2S	Noggin (17.5 ng/ml)	SB431542 (10 µM)	Dorso (600 nM)	CHIR99021 (1.5 µM)	SU5402 (5 µM)	DAPT (5 µM)	Dox (2 ng/ml)
0'	X		X	X	X				
1'	X		X	X	X				
2'	X		X	X	X	X	X	X	
3'	X		X	X	X	X	X	X	
4'	X (75%)	X (25%)	X	X	X	X	X	X	X
5'	X (50%)	X (50%)				X	X	X	X
6'	X (50%)	X (50%)				X	X	X	X
7'	X (25%)	X (75%)				X	X	X	X
8'	X (25%)	X (75%)				X	X	X	X
9'	X (25%)	X (75%)				X	X	X	
10'	X (25%)	X (75%)				X	X	X	
11'	X (25%)	X (75%)				X	X	X	

Table 2.2.S2: Primary antibodies used in this study

Target	Isotype	Dilution	Supplier	Catalogue number
βIII-tubulin (pol.)	mouse IgG1	1:1000	BioLegend	921001
Peripherin	mouse IgG2a	1:200	Santa Cruz	sc-377093
Ki67 (PE)	mouse IgG1	1:500	BD Pharmingen	556027
ISL1	rabbit	1:200	Abcam	ab109517
BRN3A	rabbit	1:200	Merck Millipore	5945
P2X3	rabbit	1:200	Novus	NB100-1654
F-actin	Phalloidin-555	1:500	Molecular Probes	8953S

Table 2.2.S3: Agonists and antagonists used in Ca^{2+}-imaging experiments

Compound	Solvent	Concentration [µM]	Supplier	Catalogue number
α,β-methylene ATP	water	1	Cayman Chemical	10008956
AF-353	DMSO	0.1	Cayman Chemical	23034
capsaicin	DMSO	1	Cayman Chemical	92350
capsazepine	DMSO	10	Cayman Chemical	10007518
KCl	water	40,000	Merck	P9541

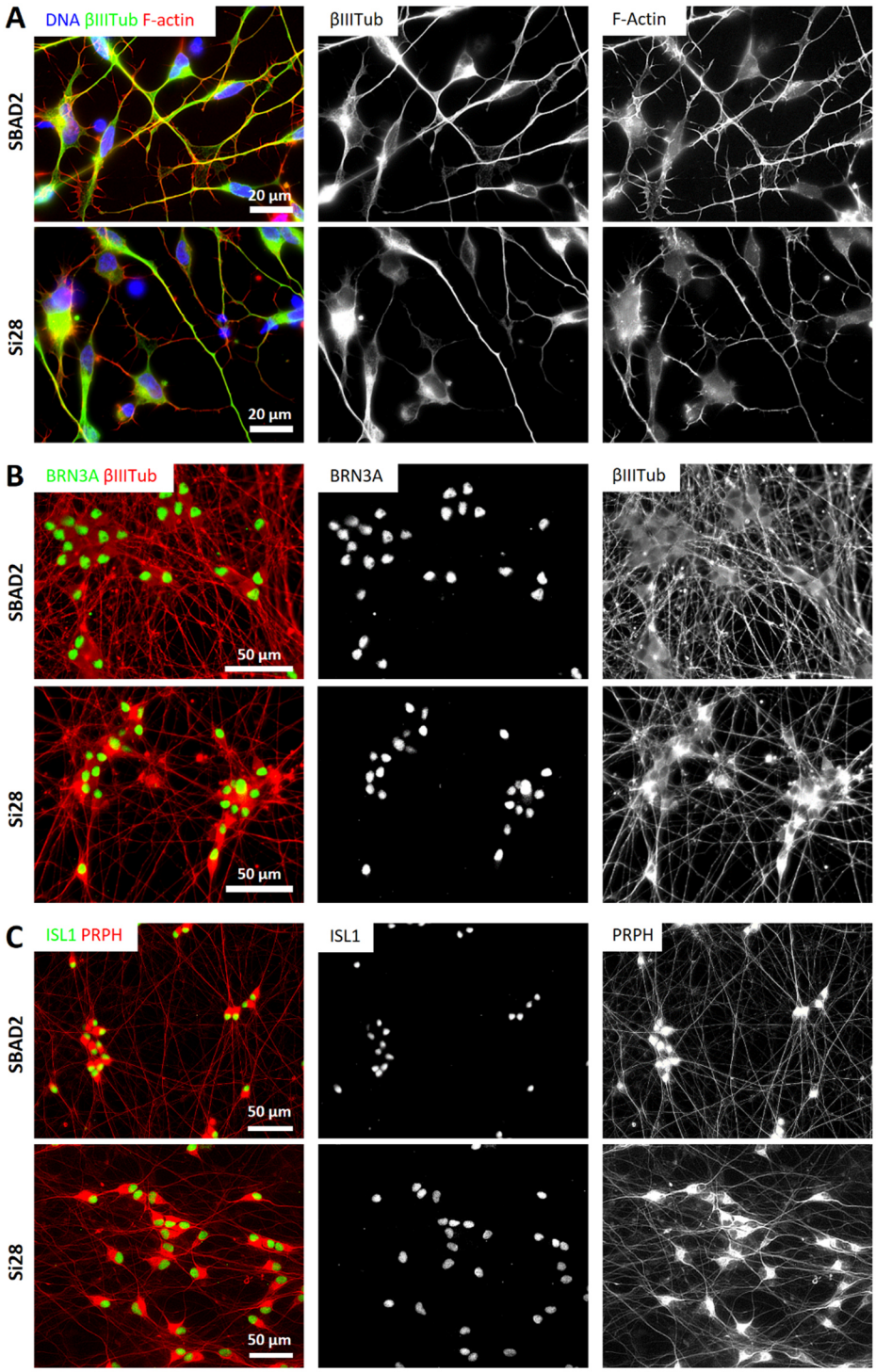

Figure 2.2.S1: Characterization of iPSC-derived early-stage sensory neurons

Neurons were differentiated from the iPSC-lines SBAD2 and Si28 according to the standard protocol . **(A)** Cells were fixed on DoD1 after thawing and stained for the pan-neuronal marker βIII-tubulin (βIIITub), and for F-actin. Growth cones with filopodia are evident on the growing neurites. **(B,C)** Cells were fixed on DoD7 and stained for βIIITub and the peripheral neuron transcription factors BRN3A **(B)** or Islet-1 and the intermediate filament peripherin (PRPH) **(C)**. Images of different fluorescent channels are shown to visualize the staining by individual antibodies. The composite images of the stainings are color coded according to the detail images (also see figure 2.2.1A). Scale bars are given in the images. All images are representative of typical cultures, but structures have not been quantified.

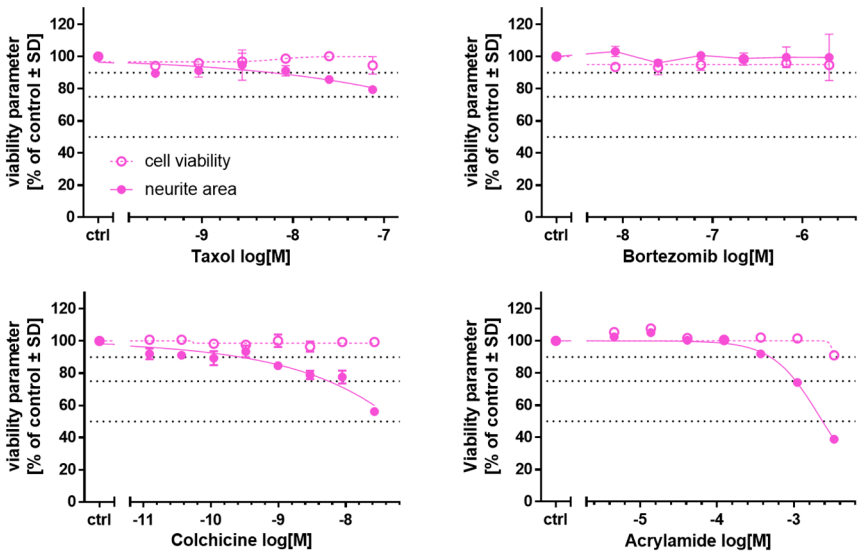

Figure 2.2.S2: Exploration of toxicant responses (in the PeriTox test) of neurons generated and offered by a commercial source.

The Peri.4U cell preparation, which had been generated to provide a commercial source of peripheral neurons, was used in the PeriTox test. Cells were exposed to the positive control compounds taxol, bortezomib, colchicine and acrylamide, which are known for their (peripheral) neurotoxic potential. Effects on neurite area (solid symbols and lines) and viability (open symbols, dashed lines) are shown. Data are means ± SD of 2 biological replicates.

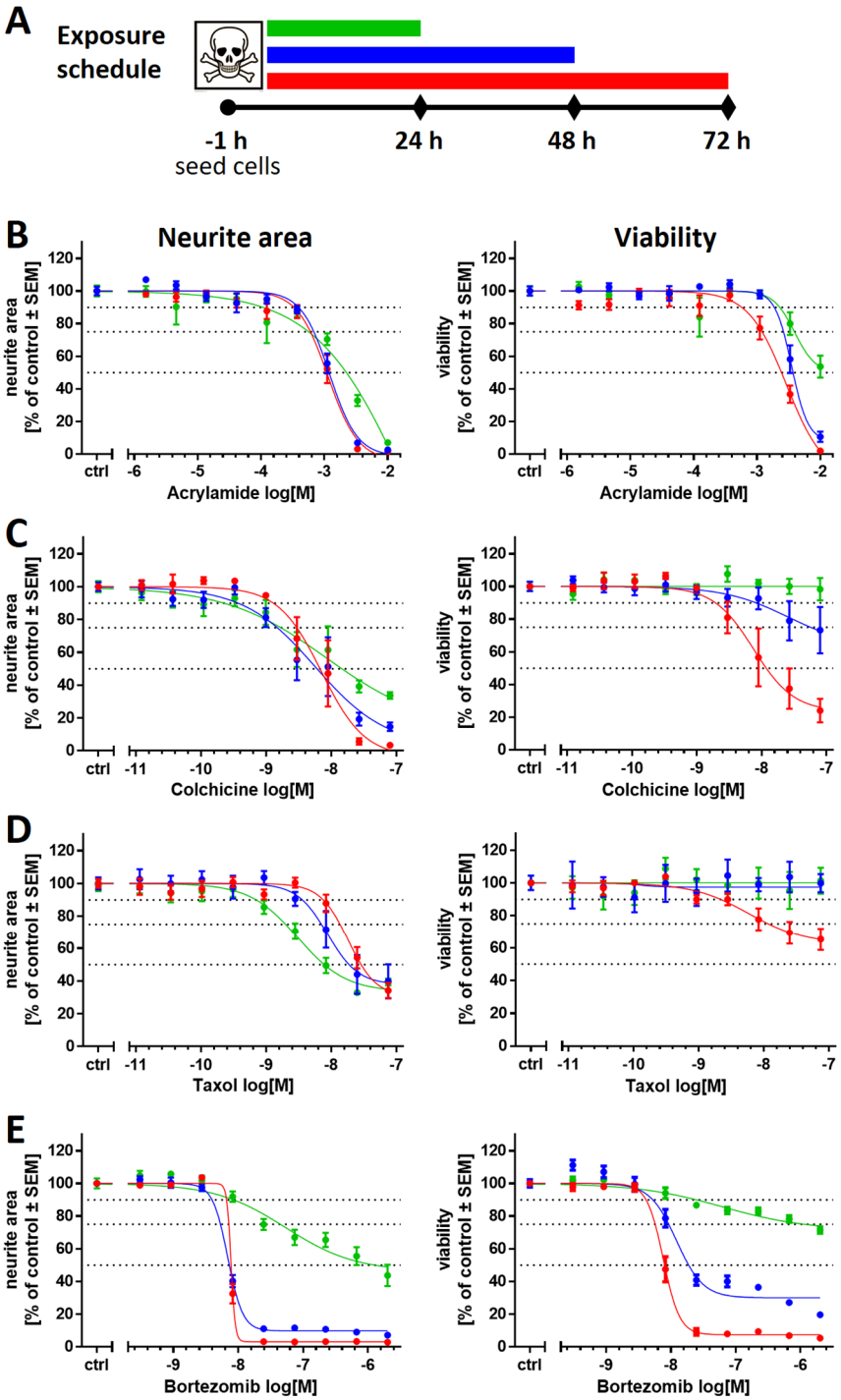

Figure 2.2.S3: Time-dependency of compound effects assessed in the extended PeriTox test

Compound-induced effects on the neurite area and cell viability were assessed in the extended PeriTox test. **(A)** Exposure schedules for the extended PeriTox test are depicted. One hour after plating of the peripheral neuron precursors, cells were exposed to the test compounds for 24 h (green), 48 h (blue) and 72 h (red). **(B-E)** Effects on neurite area (left) and viability (right) are shown for all three exposure times for the positive controls acrylamide **(B)**, colchicine **(C)**, taxol **(D)**, and bortezomib **(E)**. Data sets are colour coded to the respective exposure schedule in **(A)**. Data are means ± SEM of 2-3 biological replicates.

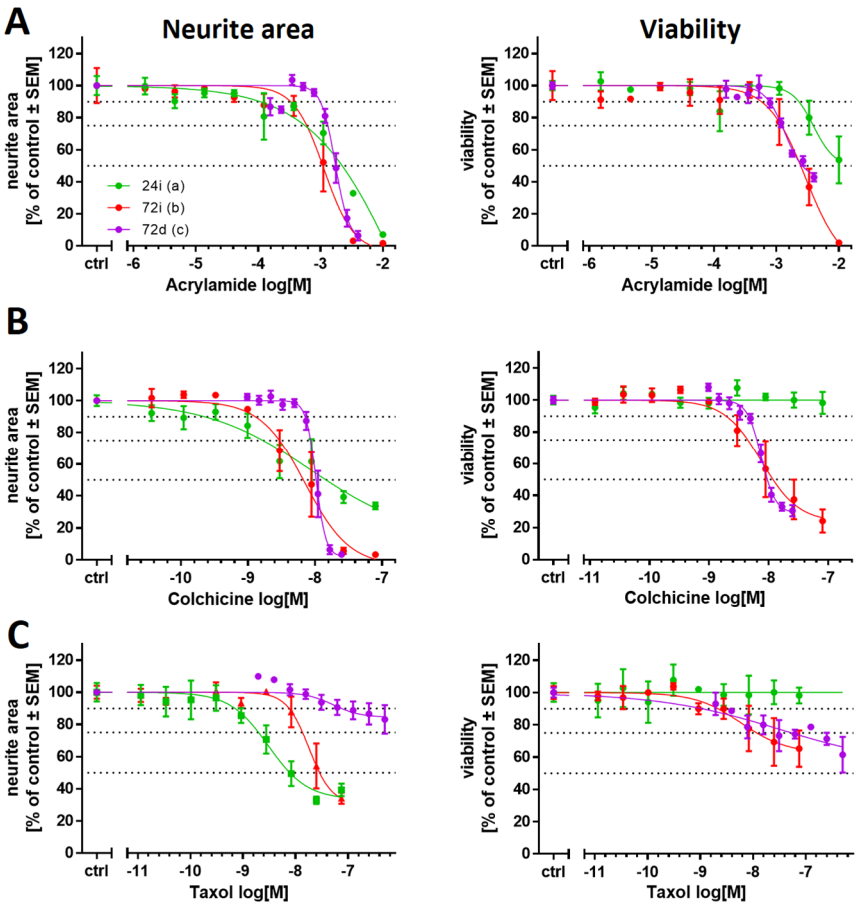

Figure 2.2.S4: Variation of exposure time point and duration to assess compound toxicity

The positive control compounds acrylamide **(A)**, colchicine **(B)** and taxol **(C)** were tested regarding their effects on immature peripheral neurons. Cells were exposed to the test compounds according to the exposure scenarios depicted in figure 2.2.2A: (a) immediately after thawing (1 h) for 24 h (green, 24i) and (b) 72 h (red, 72i), or (c) at a delayed time point, starting on DoD4, for 72h (purple, 72d). Compound effects on neurite area (left) and viability (right) are shown. Data are means ± SEM of 3 independent experiments.

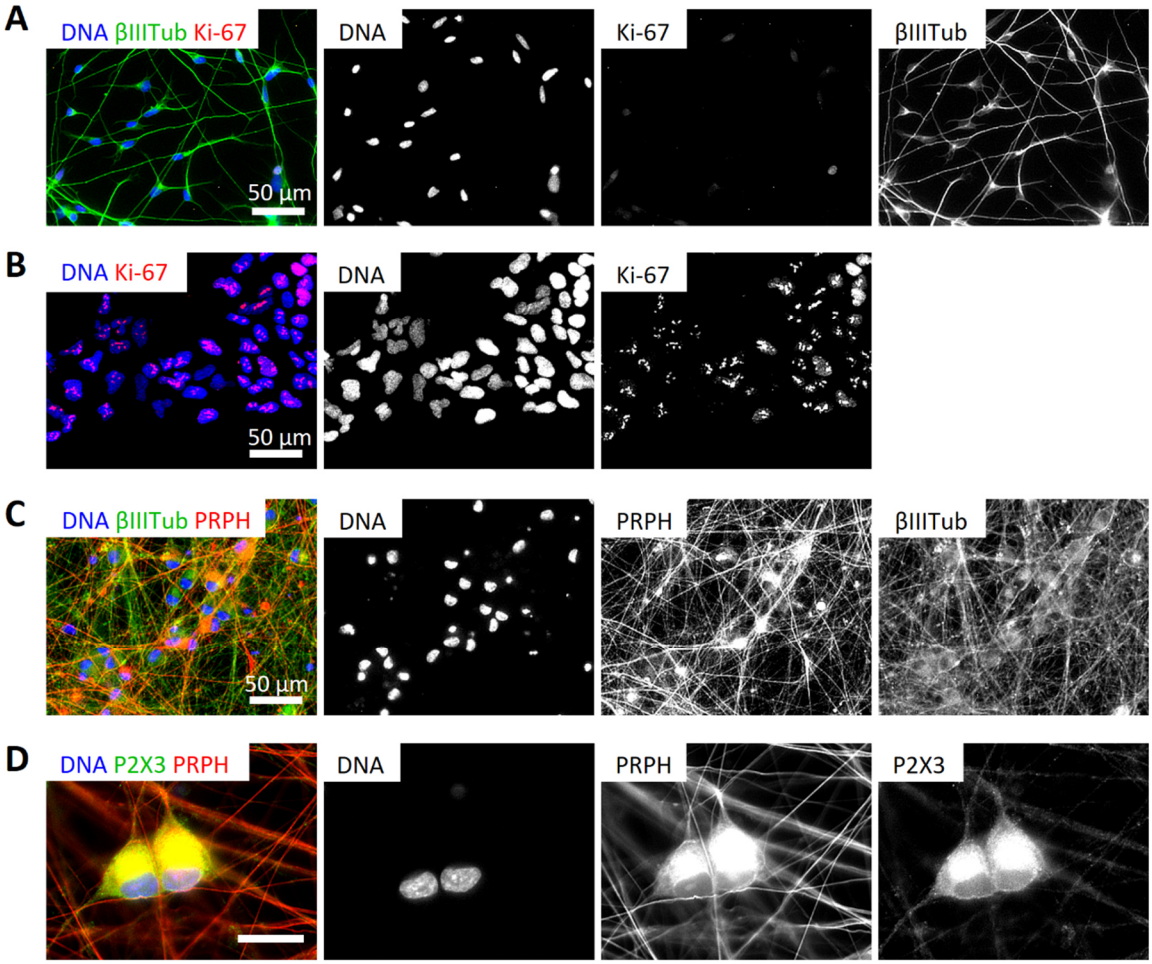

Figure 2.2.S5: Characterization of peripheral neurons derived by NGN1-overexpression

(A) Peripheral neurons differentiated from Si28-NGN1 iPSCs were fixed on DoD1 and stained for βIII-tubulin (βIIITub) and the proliferation marker Ki-67. **(B)** As a positive control for proliferating cells, neuroepithelial precursor cells (Dreser et al. 2020) were fixed and stained for Ki-67, exhibiting the characteristic pattern of Ki-67-staining in the nucleus, thus verifying the functioning of the Ki-67-antibody. **(C,D)** Neurons were differentiated for 42 days after thawing and fixed. Immunofluorescence images show an extensive neurite network, stained positive for βIIITub and peripherin (PRPH) **(C)**, and the expression of P2X3 receptors in PRPH-positive cells **(D)**. Images of the single stainings are shown. The composite images of the stainings are color coded according to the detail images (**(A,C,D)** see also figure 2.2.3B). Scale bars are given in the images.

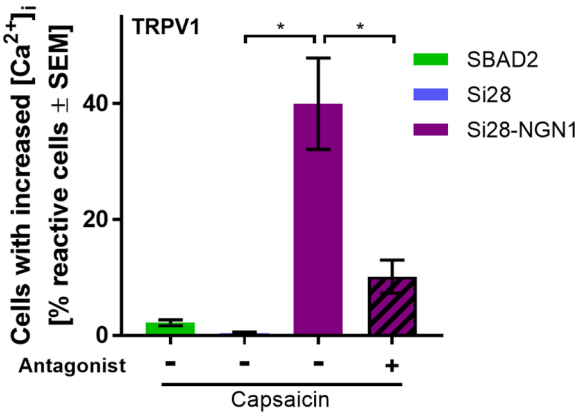

Figure 2.2.S6: Expression of functional TRPV1 channels

Peripheral neurons derived from the iPSC lines SBAD2 (green), Si28 (blue) and Si28-NGN1 (purple) were differentiated for >38 days and used for Ca^{2+}-imaging experiments. The TRPV1-specific agonist capsaicin [1 µM] was used to determine the expression of functional TRPV1 receptors. To confirm signaling through TRPV1, cells were pre-treated (1 h) with capsazepine, an antagonist of TRPV1, before stimulation with capsaicin. Data are means ± SEM of at least 3 biological replicates

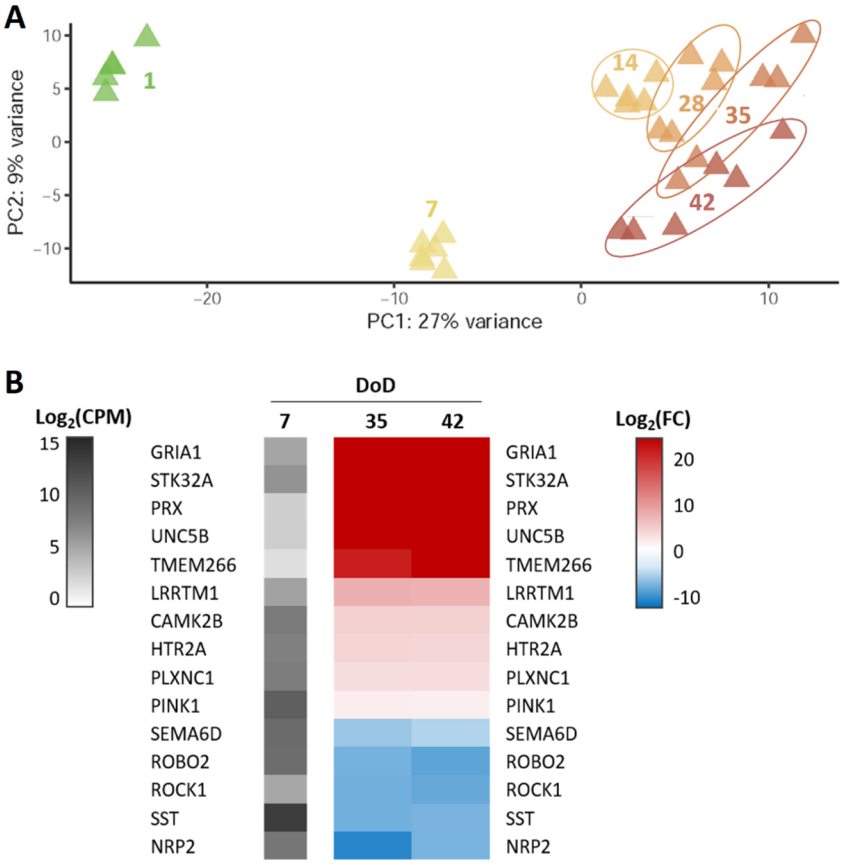

Figure 2.2.S7: Time-dependent transcriptome profiling of PNN

(A) PNN were grown from DoD1 - DoD42 and mRNA of different maturation stages was used for whole transcriptome analysis by TempO-Seq (full data in Supplementary file1, complementary data in figure 2.2.4). A PCA was performed for all of the >19,000 measured genes. In the two-dimensional PCA display, six maturation stages (day of differentiation (DoD) 1, 7, 14, 28, 35 and 42) of PNN are color-coded according to their DoD. Data points are derived from three independent differentiations, and all individual samples analyzed are depicted. **(B)** To gain insight into gene expression changes that occur during late differentiation, DoD35 and DoD42 samples were analyzed for differentially expressed genes (DEGs) *versus* DoD7. Examples of significant DEGs (adjusted *p*-value ≤ 0.05) with a fold change (FC) >4 were assembled. The left column shows the absolute expression levels of selected significant DEGs on DoD7 in counts of the corresponding gene per 1 million reads (CPM). The data for DoD35/DoD42 show the fold change (FC) of the expression levels *versus* DoD7. The color scales use $\log_2$ units (see supplementary files for complete data sets).

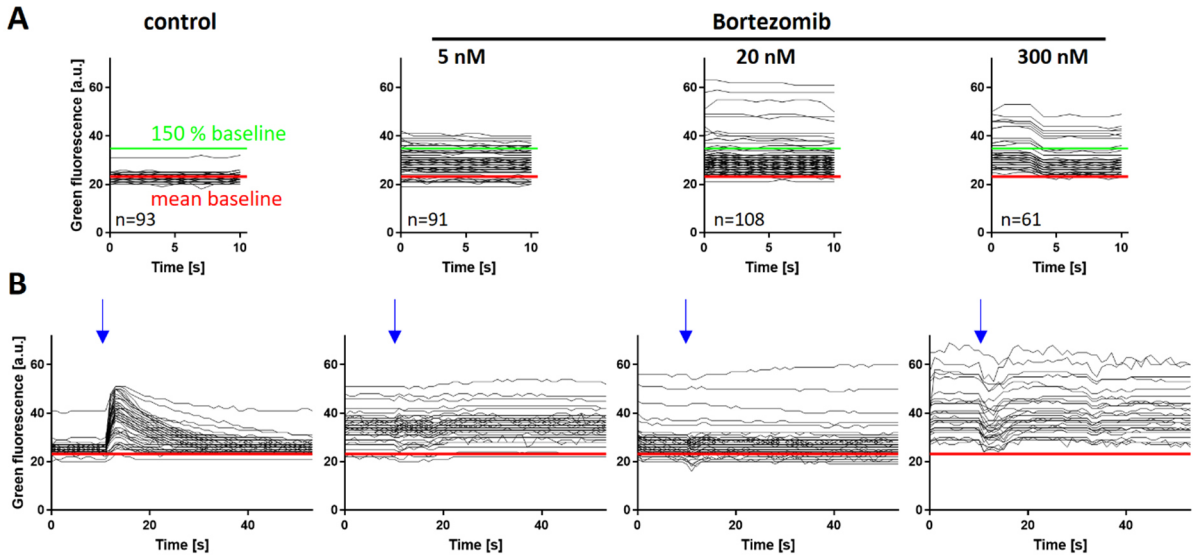

Figure 2.2.S8: $[Ca^{2+}]_i$-dependent fluorescence signals of single cells

Sensory neurons (>DoD38) were cultured under control conditions or exposed to bortezomib for 24 h, before Ca^{2+}-imaging was performed. Ca^{2+}-measurements depicted in **(A)** and **(B)** were executed with the same cells. **(A)** Baseline fluorescence of single sensory neurons recorded during the first 10 seconds of a Ca^{2+}-measurement, immediately before the first stimulus application. Fluorescence traces of one whole neuronal culture per pre-treatment condition with 61-108 single cells each are shown. Red horizontal lines indicate the mean baseline fluorescence of control cells. Green lines indicate the threshold of 150% control baseline fluorescence used for quantification of cells with increased resting cell $[Ca^{2+}]_i$. **(B)** Time-dependent fluorescence traces of single cells during experiments using the P2X3-specific agonist α,β-methylene ATP (addition to the cells is indicated by blue arrows). For clarity, only 50% of the cells depicted in **(A)** are shown (randomly chosen by software). Red horizontal lines correspond to the mean baseline fluorescence of control cells determined in **(A)**.

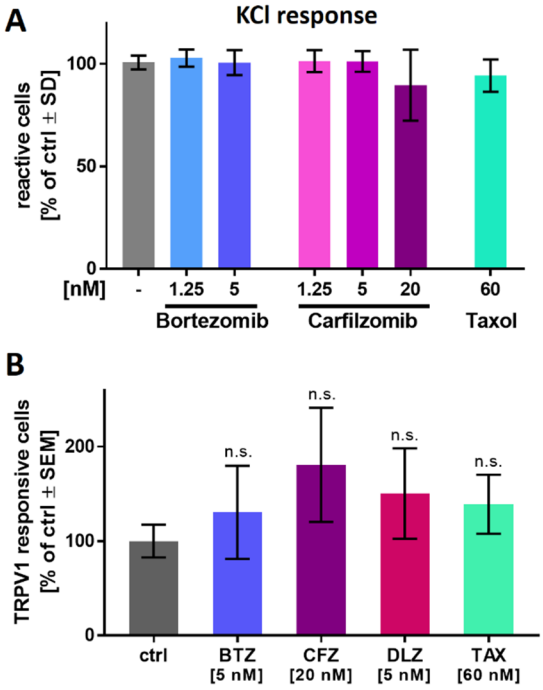

Figure 2.2.S9: Membrane depolarization and TRPV1 responses are unaltered upon toxicant exposure

Sensory neurons were differentiated for >38 days and used for Ca^{2+}-imaging experiments. Cells were pre-treated with the proteasome inhibitors bortezomib (BTZ), carfilzomib (CZF) and delanzomib (DLZ), or taxol for 24 h, before Ca^{2+}-measurements were performed. **(A)** Sensory neurons, which were first exposed to a P2X3-specific stimulus (see figure 2.2.5B,C), were subsequently subjected to an increased concentration of KCl [50 mM], which induces membrane depolarization in functional neuronal cells. Responsive cells were quantified. **(B)** Cells were stimulated with capsaicin [1 µM] and the number of responsive cells was assessed. Data are given as % of untreated control cells and are means ± SEM of at least 3 independent experiments. n.s., not significant

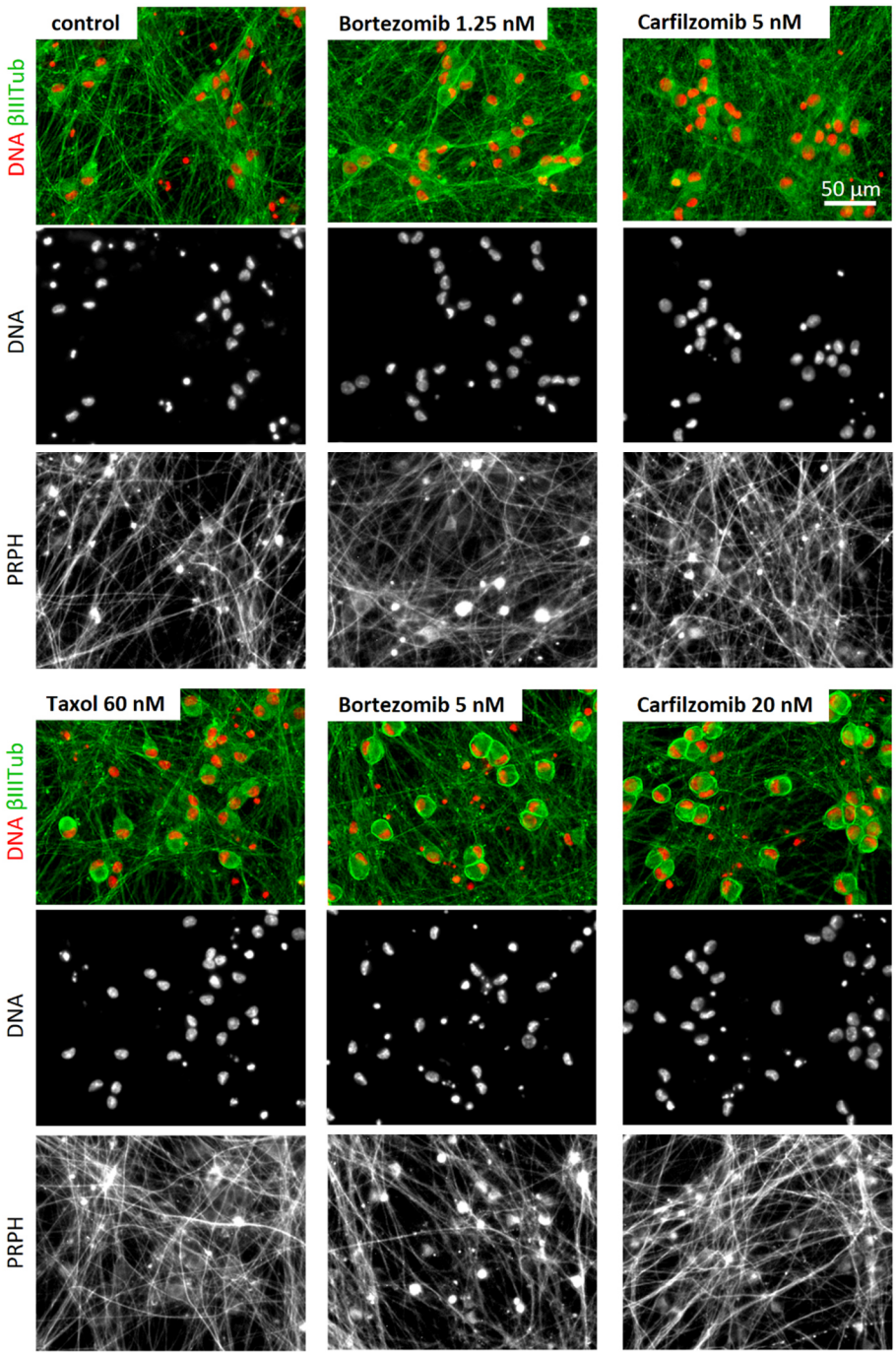

Figure 2.2.S10: Reorganization of the cytoskeletal structure upon PI exposure

Sensory neurons were differentiated for at least 38 days after thawing and exposed to bortezomib, carfilzomib or taxol for 24 h before fixation. Representative immunofluorescence images are shown (see also figure 2.2.6A). Composite images show stainings of nuclei (DNA, red) and βIII-tubulin (βIIITub, green), revealing aberrant staining for βIIITub at high concentrations of bortezomib or carfilzomib. Single staining images shown for (i) the nuclei (DNA) and (ii) the corresponding peripherin (PRPH) staining (for clarity not included in the composite images). Peripherin staining of PI-treated cells did not exhibit βIIITub-like reorganization to rings, but rather a clustering in the soma (outside the nucleus). The scale bar is given in the images.

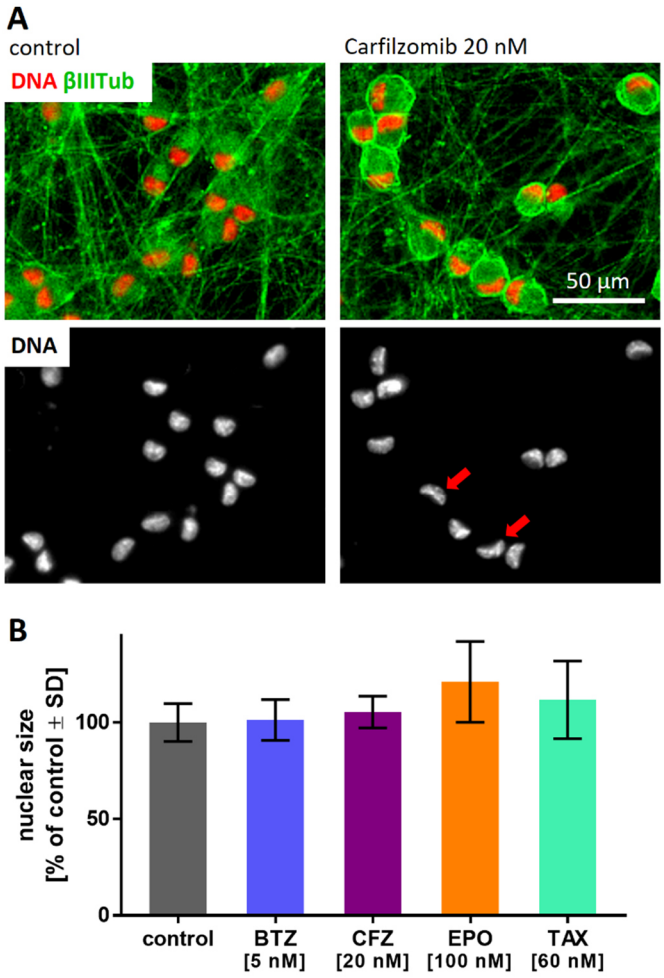

Figure 2.2.S11: Quantifiaction of the nuclear area as cell viability indicator

(A) Sensory neurons were fixed on DoD42 upon exposure to control condition (left) or carfilzomib (20 nM, 24 h) (right). Immunofluorescence images of cells stained for βIII-tubulin (βIIITub) and DNA (using H33342) are shown. DNA staining revealed a deformation of the nuclei in carfilzomib-treated cells, red arrows indicate example nuclei in the single staining image. Images are color coded and the scale bar is given in the images. **(B)** Quantification of the nuclear area of cells cultured under control condition or exposed to bortezomib (BTZ), carfilzomib (CFZ), epoxomicin (EPO) or taxol (TAX) for 24 h at the indicated concentrations. Data are means ± SD of 25 randomly chosen nuclei per condition.

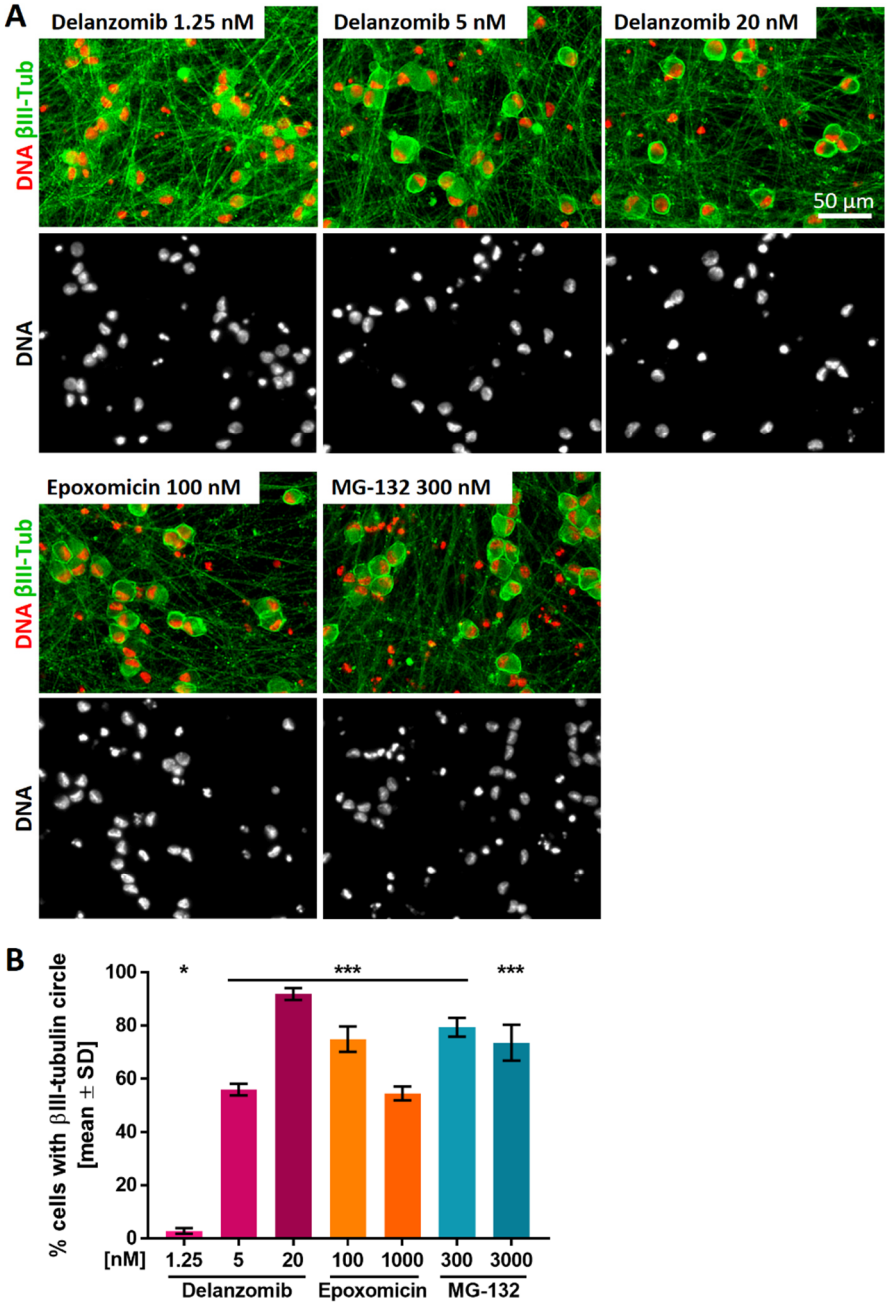

Figure 2.2.S12: Reorganization of the microtubule structure as a general PI effect

Sensory neurons (>DoD38) were exposed to the PIs delanzomib, epoxomicin or MG-132 for 24 h before fixation. Representative immunofluorescence images show stainings of nuclei (DNA, red) and βIII-tubulin (βIIITub, green) (see also figure 2.2.7G). Composite images are colour coded and single staining images are shown for cell nuclei (DNA). The scale bar is given in the pictures. **(B)** Quantification of cells exhibiting intense, circular βIII-tubulin staining around the cell somata (covering at least 50% of a full circle). Data are given as % of the total cell count (number of viable cell nuclei) and are means ± SD of 2-3 biological replicates. * $p < 0.05$, *** $p < 0.0001$

2.3 CaFFEE: a program for evaluating time courses of Ca^{2+} dependent signal changes of complex cells loaded with fluorescent indicator dyes

published in *ALTEX* 37, 332–336 (2020)

Christiaan Karreman[1], Anna-Katharina Holzer[1], Stefanie Klima[1,2], Marcel Leist[1,3]

[1] In vitro Toxicology and Biomedicine, Dept inaugurated by the Doerenkamp-Zbinden foundation, University of Konstanz, 78457 Konstanz, Germany

[2] Graduate school Biological Sciences (GBS)

[3] Cooperative doctorate college InViTe, University of Konstanz, Konstanz, Germany

[4] CAAT-Europe, University of Konstanz, Konstanz, Germany

Key words: Ca^{2+} imaging, automatization, laboratory software, big data, stem cell

2.3.1 Abstract

Quantification of changes in intracellular free Ca^{2+} concentrations ($[Ca^{2+}]$) are fundamental to the understanding of the physiology of single cells in response to both environmental and endogenous stimuli. We present here software that is freely available, easy to use and allowing especially the evaluation of $[Ca^{2+}]_i$ signals in complex and mixed cultured. The program CaFFEE (Calcium Fluorescent Flash Evaluating Engine) enables the user to evaluate the response of hundreds of cells to treatments that influence $[Ca^{2+}]_i$. CaFFEE processes large quantities of image data, automatically identifies individual cells in mixed, heterogeneous populations, and evaluates their fluorescence signal. All data are exported in spreadsheet format and data on thousands of cells may be batch processed. Moreover, the program optimizes the visual representation of time-lapse image data for user-guided data exploration (setting of parameters for semi-automated data processing). The software, freely downloaded, allows the standardized and transparent processing of imaging data independent of the platform that generated the data.

2.3.2 Image-based $[Ca^{2+}]_i$ quantification

As Ca^{2+} signaling is involved in muscle contraction, blood clotting, hormone regulation and nerve conduction, and many other processes, the intracellular concentration of Ca^{2+} ($[Ca^{2+}]_i$) is tightly regulated. *Vice versa*, disturbed $[Ca^{2+}]_i$ regulation is a good indicator of toxicity (Bano et al. 2017; Leist and Nicotera 1998; Orrenius et al. 2003).

There are different ways to measure $[Ca^{2+}]_i$ (Bassett and Monteith 2017; Brini et al. 1999; Hayashi and Miyata 1994; June and Moore 2004; Ma et al. 2017; Ronzhina et al. 2013; Simpson 2006; Tsien 1992). One of them is imaging of cells loaded with calcium indicators. For this purpose, fluorescent dyes (e.g., Fura-2, Indo-1 or Fluo-4) that change their fluorescence properties in response to Ca^{2+} binding are commonly used. Depending on the indicator, Ca^{2+} concentrations are assessed either by changes in fluorescence intensity or a shift of emission/excitation wavelengths. There are different ways to monitor these changes, like the use of fluorimeters (for suspended cells), FACS analysis (for individual cells), whole well fluorescence detection (e.g., using FLIPR instruments) or imaging by fluorescence microscopy. In the latter case, signals may be captured on a standard microscope (upright or inverted), by confocal microscopy or by high content imaging. In all these cases, 2D images (sometimes as stacks into the third dimension) are obtained before and after a stimulus or as a continuous sequence of frames in a time series (time-lapse imaging).

To gain quantitative information from these images one can compare the changes in overall brightness or the changes in brightness of the single pixels that make up an individual cell. For this purpose, the regions of interest (ROI), i.e., the pixel areas to be quantified, need to be defined either manually or by automatic definition. Automatic definition means that cells are identified automatically based on additional staining or structural features. CaFFEE uses a nuclear stain to identify the cells, and it then uses this information to define each cell as an ROI. Subsequently, the average fluorescent intensity of these pixels is measured over a series of pictures. Thus, time-dependent fluorescent values are obtained for every single cell. This information is converted to curves from which different parameters can be derived (Fig 2.3.1). Furthermore, it is also possible to define subcellular structures (e.g., nuclei) that can be evaluated for $[Ca^{2+}]_i$-responses.

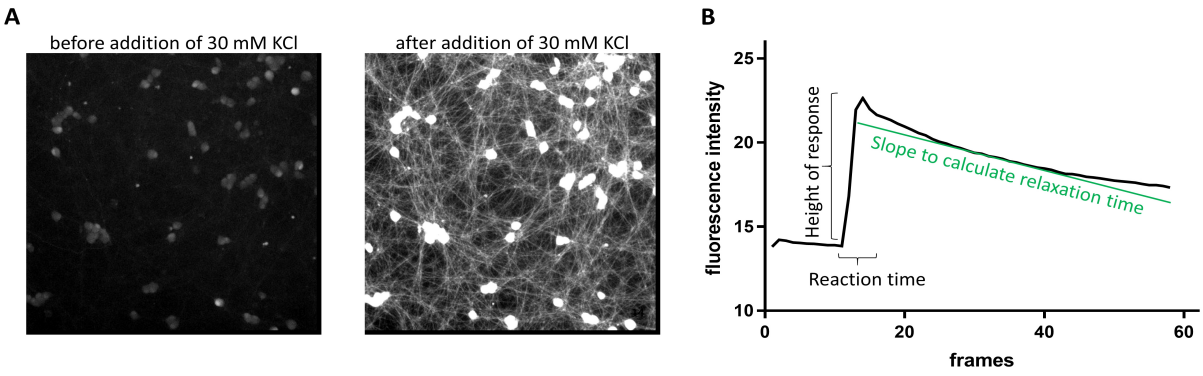

Figure 2.3.1: Examples of typical graphs and images from CaFFEE

(A) Automatically taken images from a time series before and after the addition of 30 mM KCl (trigger of Ca^{2+} increase). **(B)** Typical shape of the behaviour of intracellular Ca^{2+} after addition of 30 mM KCl. Various parameters (height of response, reaction time and slope for the calculation of the relaxation time) calculated by CaFFEE are indicated.

2.3.3 Special requirements for stem cell-derived neuronal cultures

In neuronal cultures, the identification of different cell structures allows the differentiation between the cell body (soma) and the neurites. The changes in $[Ca^{2+}]_i$ might differ between these two parts of the neuron. Challenges in stem cell-derived neuronal cultures are: (i) dead cells and (ii) the heterogeneity of the cell population. The cultures may include, for example, partially differentiated neurons or glial cells. Moreover, the neurons differ in their receptor number, size, thickness and shape. Once every single cell is identified, the program allows exclusion of specific cells from the analysis, depending on their size or response characteristics.

2.3.4 Challenges and problems

Many programs are available to analyze $[Ca^{2+}]_i$ imaging experiments. Some have a much higher level of sophistication and a broader panel of available tools than CaFFEE. However, independent of the software used, background correction and adaptation of image dynamics are problems that cannot be solved perfectly in a fully automated way. CaFFEE offers the user visual tools to manually optimize images. The optimized settings are then used on the entire time series batch. When the cell population is heterogeneous, it is also challenging to identify the active cells and analyze only their response characteristics. This becomes particularly challenging if large numbers of cells are to be analyzed in parallel.

2.3.5 Main features of CaFFEE

Here, we describe the CaFFEE (Calcium Fluorescent Flash Evaluating Engine) program, which can solve several of these problems. It evaluates time series images (in an uncompressed file format .avi [Audio Video Interleave]) that describe the $[Ca^{2+}]_i$ of neurons under various conditions. The program comprises the four distinct functions detailed below.

Function 1: Image processing

By using the image processing module, the different channels (typically green for Ca^{2+}-fluorescence and blue for nuclei) can be optimized individually. The general background can be forced to zero and the highest brightness to full white, thereby giving the remaining levels of gray the full dynamic range (0-255 for normal monitors). The representation of the pictures does not have to be a linear transformation of the original pictures. Different non-linear monotonous transformations are offered in CaFFEE. Image optimization can be done separately for the two channels, and the information (image sequence) can later again be combined. This feature enables the user to generate a multi-colour image sequence from optimized sequences of the individual channels. In short, image sequences processed by CaFFEE provide information with more contrast and a better signal to noise ratio. The enhanced quality of the resulting image sequence will not influence the later evaluation of the brightness / intensity response characteristics, as these calculations will always be performed on the original set of images.

Function 2: Visualization of averaged responses

Another feature of CaFFEE is a visual, spatially resolved depiction of differences in $[Ca^{2+}]_i$ in one picture. In short: an artificial picture is created that shows the differences in fluorescence before and after stimulation pixel by pixel. A typical experiment has a period during which baseline images are recorded. Then, at a specified timepoint, a stimulant is added and the response of the selected cells is recorded. In simple terms, there is a "before" and an "after" period in most experimental setups. CaFFEE averages the signals of "before" frames and compares these with the signals of the averaged "after" frames. The resulting differences are then depicted in one picture, showing the differences in the fluorescence for each pixel in a false color representation or as a 3-dimensional picture.

Function 3: Evaluation of time series images

The central function of CaFFEE is the evaluation of the $[Ca^{2+}]_i$ fluorescence signal, or any other time dependent fluorescence signal for defined ROI, usually corresponding to cell bodies. Here, images are transformed to numbers and curves, which may be graphically displayed and exported. CaFFEE uses the fluorescence signal of the nuclei to determine their number and to calculate their position. With the resulting data, it then checks whether these areas are consecutively represented in every image in the series. For those nuclei that are present in every frame, the fluorescence of the same area in the Ca-specific channel is measured before (F_0) and after stimulation (F) as the average brightness/pixel.

These data are used to determine parameters like maximum delta (the increase of fluorescence signal over baseline ($F-F_0$) "Delta" (Fig. 2.3.2A)), the relative increase of signal ($(F-F_0)/F_0$ "Delta/F0" (Fig. 2.3.2A)) and the fold increase of signal ((F/F_0) "F1/F0" (Fig. 2.3.2A)). The measurements are typically fitted to sigmoid or double sigmoid curves. The user can look at every cell trace individually to observe its behavior or can sort by the various parameters and know which cell is responsible. All data shown on the screen are interactive and will show all data that belong together with just one click. The raw data and the calculated summary data are easily exported to an Excel file.

A

#	Base	EC50	Top	Delta	Delta/F0	F1/F0
478	72	14	138	66	0.92	1.92
479	42	14	44	2	0.05	1.05
450	47	14	50	3	0.06	1.06
451	46	14	61	15	0.33	1.33

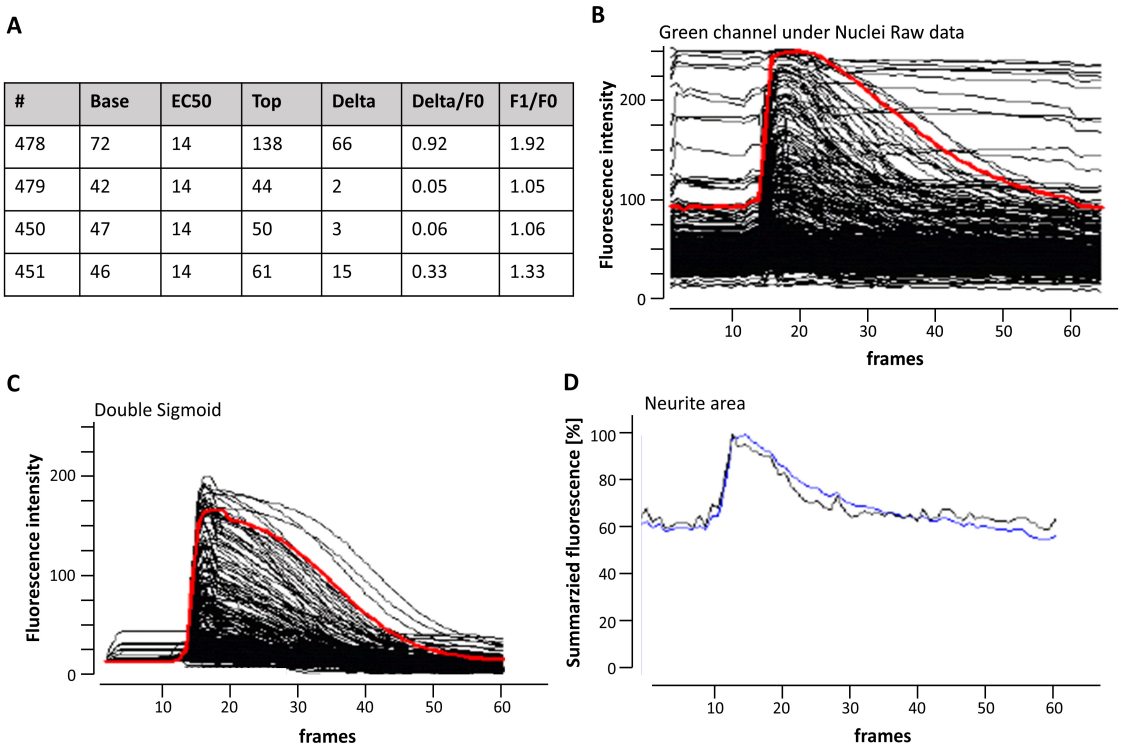

Figure 2.3.2: Different analysis outputs provided by CaFFEE
(A) Table showing the calculated values of the single cells. Each *bona fide* cell is assigned a unique number („#"). Data for four examplary cells are shown. The value of fluorescence intensity is given for the baseline (F_0) „Base" and for the peak (F) „Top". From these values, the maxium difference „Delta" ($F- F_0$), the relative increase of signal "Delta/F0" ($F-F_0/F_0$) and the fold increase of signal "F1/F0" (F/F_0) are calculated. CaFFEE automatically calculates the frame at which the curves deviate from the baseline. It interprets this as the timepoint when the addition of the stimulus occured „EC50". **(B)** Graphical representation of the raw data showing the fluorescence intensity of hundreds of single cells. **(C)** Mathematical approximation of the corresponding raw data (baseline correction and curve fitting). **(D)** Graph of total fluorescence intensity of the whole frame sequence (black) compared to total fluorescence intensity of the identified cells (blue). The matching curves show that the behavior of the fluorescence of the images is completely explained by that of the identified cells, indicating no major disturbances (pipetting artefacts, etc.) play a role in this experiment.

Function 4: Batch processing of data

Often, a whole set of experiments (e.g., controls, different treatments and various concentration of the stimulant) will be performed, each resulting in a separate .avi file. If these files are all placed in the same subdirectory (folder), CaFFEE can be used to evaluate all of these files in one single pass. The result will be an Excel workbook with one sheet for every .avi file containing all the data for that file and an extra "summary" sheet on which the relevant data of the different experiments are summarized in a single table. The batch feature makes the analysis of large experiments with high numbers of biological and technical replicates, as they are common in toxicological studies, very fast and efficient.

2.3.6 Experimental preconditions

To analyze the time lapse sequence, CaFFEE uses two fluorescence channels. The nuclei are visualized by staining with H-33342 (or DAPI), and the $[Ca^{2+}]_i$ is detected by staining with Fluo-4-AM (or any single wavelength indicator showing similar fluorescence properties). They are visualized in blue and green, respectively. The present version of CaFFEE expects these two channels to be used. It is not possible to swap channels in the program or to leave one out. Each time lapse sequence must be in an .avi file format with a frame size of 512 x 512 pixels or smaller. Larger frame sizes will not be shown in full size, and cannot be analyzed. The magnification (10 x or 20 x in our system) chosen for the microscope does not influence the analysis. If the output is to be subsequently exported directly to Microsoft Excel, this program must be installed on the computer in order to use this feature.

For defining a baseline (F_0), it is necessary to record some images before addition of the stimulus. CaFFEE automatically calculates the baseline from all images that are recorded before the stimulus is added. Notably, CaFFEE does not automatically recognize the addition of a stimulus, nor can this information be entered. The program uses the part of the curve with the highest slope as indicator that stimulation has occured and gives out the corresponding frame.

It is important to realize that CaFFEE uses frames as units on the x-axis instead of time. Thereby CaFFEE is independent of the original time frame of the image series. With knowledge of the experimental protocol, the x-axis can be converted later using the Excel data matrix. No fixed number of images is necessary for the analysis, but the precision of the analysis increases with the number of images available. These simplified features make it unnecessary to enter other experimental data in CaFFEE, which often is a source of errors.

2.3.7 Example

Practical examples often help to illustrate program features. Here we present an experiment based on neurons derived from stem cells (Hoelting et al. 2016) where we assessed their response to 30 mM KCl. We used an automated microscope system (Cellomics, VTI ArrayScan, Thermo Fisher) with an incubation chamber set to maintain 5% CO_2 and 37°C. Images were taken for 45 s at maximum speed, which results in a rate of approx. one image per second. It is important to be aware of such recording characteristics and inter-image time intervals, as CaFFEE always labels the x-axis in units of frames instead of real time. In our experiment, 30 mM KCl was administered by an automated pipettor after 10 s (=10 frames). Pictures were taken over the remaining time of 30 s. First, CaFFEE was used to optimize the contrast of the images in the image sequence (.avi file). Second, nuclear size and intensity were used to define *bona fide* nuclei. Size exclusion was used to exclude shrunken (dead) nuclei or fragments. The settings were translated by CaFFEE into a color-coded picture, where blue nuclei are *bona fide* nuclei, yellow ones are excluded on account of their size and red ones on account of their intensity. Sliders for the different parameters allow quick manual, visually controlled optimization of the settings.

Next, pressing the “Evaluation” button started the fully automated evaluation process by which CaFFEE identified all cells based on their nuclear position and provided fluorescence data (F_0, F) for every single cell for every frame. Such data are presented as (A) a table in spread sheet format, (B) a graph for intensity of every identified cell without baseline correction of every frame, (C) a mathematical approximation for every identified cell of every frame, and (D) a graph of total fluorescence intensity of the whole picture compared to total fluorescence intensity of the cells (Fig. 2.3.2). The raw and the calculated data were exported to Excel for further quantitative analysis. For more detailed instructions on the various described steps, see the handbook and the program (http://invitrotox.uni-konstanz.de/CaFFEE, which are both freely available for download.

2.3.8 Outlook

The program is under dynamic development. New features are planned, e.g., defining neurites, or setting the stimulation trigger time. All new versions will be placed on the website above.

3 Concluding discussion and perspectives

Peripheral neurons are constantly in direct contact with the environment, making them exceptionally vulnerable to potential toxicants such as medical agents. Drug toxicity is the main reason for the development of peripheral neuropathies with sensory, often painful symptoms. Therefore, it would be beneficial to identify such undesirable side effects early during drug development by improved risk assessment. However, risk assessment can only be advanced by (i) using robust human-relevant test methods and (ii) gaining a better understanding of the underlying disease mechanisms. In this thesis, cultures of iPSC-derived human peripheral neurons were used for toxicity testing to take an important step in this direction. Signaling features such as receptor and ion channel function were examined for their usefulness as test endpoints to detect functional alterations upon drug treatment. Exposure of peripheral neurons with nociceptor features (PNN) to chemotherapeutic agents that induce peripheral neuropathy *in vivo* confirmed that functional impairments might precede structural alterations, demonstrating the relevance of such signaling endpoints for *in vitro* toxicity testing.

3.1 *In vitro* cultures of human peripheral neurons

For pharmacological and toxicological studies on drug safety, it is of great interest to establish robust and well-characterized *in vitro* systems of the specific cell types affected *in vivo* (Delp et al. 2018; Schmidt et al. 2017). In the manuscripts 1 and 2 of this work, the reproducibility of the here-used differentiation protocol for the generation of peripheral neurons, and its transferability to various iPSC lines was demonstrated. In addition, the principle of transcriptional programming was exploited to enhance the fate specification towards the sensory subtype of nociceptive neurons by transient overexpression of NGN1.

3.1.1 General applicability and robustness of a previously established differentiation protocol

Various differentiation principles can be followed to generate peripheral neurons from human iPSCs (Alshawaf et al. 2018; Chambers et al. 2012; Guimarães et al. 2018). A widely

applied approach is the two-dimensional small molecule inhibitor-based differentiation of human iPSCs starting with the induction of neuroectoderm formation by dual SMAD inhibition followed by the differentiation direction to the peripheral neuronal fate. For neuron maturation, three growth factors are supplied, which are the brain-derived neurotrophic factor (BDNF), the glia-derived neurotrophic factor (GDNF), and the nerve growth factor (NGF) (Cao et al. 2016; Chambers et al. 2012; Hoelting et al. 2016; Klima et al. 2021a; Klima et al. 2021b; Schinke et al. 2021; Schwartzentruber et al. 2018; Young et al. 2014). All peripheral neurons used in this thesis were generated according to this differentiation principle. An important feature of the here-used protocol is the division of the differentiation into a pre-differentiation and a maturation part (Hoelting et al. 2016). Thus, large quantities of peripheral neuron precursors can be generated within ten days of differentiation, frozen as aliquots and stored in liquid nitrogen so that they are readily available for experiments.

In this work, several iPSC lines were subjected to this differentiation strategy, and only minor changes in differentiation time or inhibitor concentration were required to successfully generate immature peripheral neurons. Whole transcriptome analysis confirmed a robust differentiation procedure. Gene expression patterns were found to be conserved between technical replicates, independent differentiations and different iPSC lines, even after extensive maturation times of 40 days. Such high reproducibility is an important requirement for iPSC-derived neuronal cultures used for toxicity testing to ensure the comparability of results (Schmidt et al. 2017). Therefore, another interesting and crucial step to prove the robustness of the method would be to transfer the differentiation procedure to other laboratories (Bal-Price et al. 2018). The detailed standard operating procedure included in manuscript 1 describes all handling steps and provides a sound basis for a successful method transfer (Krebs et al. 2020).

3.1.2 Enhancing the nociceptor character of iPSC-derived sensory neuronal cultures

Gene expression analysis of early peripheral neurons generated according to the standard differentiation protocol confirmed the expression of nociceptor-characteristic genes, such as *RUNX1* and *NTRK1*, but also of mechanoceptor- and proprioceptor-markers (e.g., *RUNX3* and *NTRK2*). Together with the poor response of matured neurons to pain receptor-activating stimuli, this suggested that the conventional differentiation protocol

yielded sensory neurons, however, composed of various subtypes. This considerably limited the usefulness of these neuronal cultures for the study of functional features that are involved in pain signaling.

However, a major aim of this thesis was the establishment of an *in vitro* system capable of modeling aspects of chemotherapy-induced peripheral neuropathy (CIPN), which is often associated with painful symptoms. Thus, an enhanced nociceptor character of the iPSC-derived peripheral neuron cultures was envisaged. One approach that was followed to increase the culture responsiveness was the sensitization of the neurons with increased NGF concentrations, which is, for example, known to induce membrane integration as well as *de novo* synthesis of TRPV1 (Ji et al. 2002; Zhang et al. 2005). Mimicking inflammatory conditions *in vitro* in this way indeed led to an increase in the responsiveness of the neuronal cultures to P2X3- and TRPV1-specific agonists. However, it was anticipated that this strategy would not be useful for further application in experiments investigating CIPN-induced functional de-regulations, as inflammation is also a predictor for CIPN development (Kleckner et al. 2021).

Moreover, TRPV1-responses were only detected in about 5% of the sensitized cells. Yet, TRPV1 is one of the major pain receptors in nociceptive neurons *in vivo*, expressed in about 20-40% of mouse sensory neurons, and tending to be even more abundant in humans (Orozco et al. 2001; Rostock et al. 2018; Zwick et al. 2002). Therefore, in order to generate functional nociceptor cultures that better reflect the *in vivo* situation, we aimed to further increase the proportion of TRPV1-responsive cells by other means. This would also be a prerequisite to allow a reliable assessment of the modulation of TRPV1 function upon exposure to toxicants.

To obtain nociceptor cultures that allow for functional studies on pain receptors, the widely used method of transcriptional programming, which has already been shown to improve neuronal fate specification, was applied next (Boisvert et al. 2015; Desiderio et al. 2019; Hulme et al. 2020; Nickolls et al. 2020; Schrenk-Siemens et al. 2015). Controlled transient overexpression of the transcription factor NGN1, which is essentially expressed during the development of nociceptors, was integrated into the standard small molecule differentiation procedure (Ma et al. 1998; Ma et al. 1999). This new differentiation approach led to a significant increase in neurons expressing functional P2X3 and TRPV1 receptors compared to the conventional differentiation procedure. Interestingly, *P2RX3*

and *TRPV1* gene expression levels were comparable in immature neurons differentiated with and without NGN1 overexpression. Hence, it would be of great interest to compare the transcriptome of matured neurons of both differentiation conditions. Differentially expressed genes could allow conclusions to be drawn about factors necessary for pain receptor function. Such findings could be used to further accelerate maturation into functional neurons.

3.1.3 Maturation time is essential for the development of nociceptor functionality

Characterization of iPSC-derived peripheral neurons revealed that pain receptor-encoding genes were expressed in neurons as early as DoD1, independent of the differentiation procedure used. Moreover, from DoD7 onward, general Ca^{2+}-signaling was observed upon membrane depolarization by KCl or opening of Na_V channels. However, maturation of at least four weeks was shown to be indispensable for the development of receptor functionality, as functional responses of pain receptors were detected at the earliest from DoD28.

Time-dependent transcriptome analysis revealed that the iPSC-derived sensory neurons are in continuous development until at least DoD35 after thawing. Significant changes in gene expression detected at late differentiation stages (DoD35-42) were primarily related to functional neuronal properties, such as neurotransmitters and synaptic signaling. Therefore, these changes were presumed to be most likely responsible for the late onset of pain receptor function. As expression patterns of sensory neuron markers are known to change in rats until at least postnatal week 6, and the timing of neural development *in vitro* was shown to be similar to the *in vivo* situation, it is not surprising that human iPSC-derived sensory neurons are not fully developed after 5-6 weeks *in vitro* (Isensee et al. 2017; Toma et al. 2016). The weak expression of NeuN, an indicator of mature neurons, in PNN underscored a general issue of iPSC-derived cells, most of which still exhibit a rather fetal phenotype (Pamies et al. 2018). However, the present study has confirmed that transcriptional programming is a valuable tool to guide and accelerate the development of iPSC-derived cells, so that functional neuronal cultures can still be generated in a feasible time frame (Boisvert et al. 2015). In the future, neuronal maturation may be further accelerated by co-culturing PNN with glia cells (Burke et al. 2020; Mudge 1984). Moreover, improved nociceptor functionality and maturation could be achieved using a three-dimensional (3D) culture (Leeuw et al. 2021; Zhang et al. 2016).

Preliminary experiments investigating such a 3D culture approach already showed that iPSC-derived peripheral neurons could form spheroids that also exhibit self-organization properties evolving into polarized organoids similar to dorsal root ganglia (data not shown) (Zerboni and Arvin 2015).

3.2 Morphology-based assessment of neurotoxicity using human iPSC-derived immature peripheral neurons

The majority of chemicals on the market have never been tested for their toxic potential, and the toxicological data available for the relatively few compounds that have been tested are derived mainly from animal models (Hartung and Leist 2008). These days, however, large quantities of chemicals have to be tested to meet regulatory requirements. This urges for the development of fast, efficient, and predictive test methods as alternatives to laborious animal experiments (Bal-Price et al. 2010). Test methods based on human peripheral neurons are relatively scarce, and often neurons of the central nervous system are used to test for peripheral neurotoxicants (Wheeler et al. 2015). However, differences between cortical and peripheral neurons are not negligible, and it has already been shown that the two types of neurons have different sensitivity to certain groups of substances (Adelsberger et al. 2000; Hoelting et al. 2016; Wing et al. 2017). Therefore, it is necessary to use cells corresponding to the cell type affected *in vivo* to ensure appropriate and specific toxicity evaluation.

3.2.1 The PeriTox test

One of the few test methods using human peripheral neurons for toxicity testing is the PeriTox test (Hoelting et al. 2016). It is a well-established screening assay, which assesses compound-induced adverse effects on the neurite area and cell viability of human immature peripheral neurons (Delp et al. 2018; Masjosthusmann et al. 2020). The PeriTox test was initially established on human embryonic stem cell (ESC)-derived peripheral neurons. However, to avoid the ethical issues associated with the use of ESCs, the use of iPSC-derived peripheral neurons was envisaged. To date, peripheral neurons derived from five different iPSC lines were successfully applied in the PeriTox test, of which three were used in manuscript 2 of this thesis. In the PeriTox test, all iPSC-derived as well as

ESC-derived peripheral neurons, differentiated according to the here-used standard protocol exhibited similar sensitivity to known peripheral neurotoxicants, such as acrylamide (Hoelting et al. 2016). Moreover, the results obtained with the PeriTox test were highly reproducible between different operators and over time, with at least five independent operators over the past six years contributing to the PeriTox test data presented in this work. Such inter-cell line and intra-laboratory reproducibility indicates a high robustness of the PeriTox test. However, the ultimate proof of robustness would be a transfer of the test method between different laboratories (Bal-Price et al. 2018; OECD 2018). Nevertheless, a previous evaluation against test method performance criteria showed that the PeriTox test has a high level of readiness, making it suitable for initial prioritization of compounds (Bal-Price et al. 2018).

3.2.2 The influence of exposure duration and timing on sensitivity to toxicants

The PeriTox test can be used for high-throughput screening approaches to identify environmental toxicants and exhibits an increased sensitivity to known peripheral neurotoxicants compared to other test methods that use neurons of the central nervous system (Delp et al. 2018; Hoelting et al. 2016; Masjosthusmann et al. 2020; Wheeler et al. 2015). However, for use in pre-clinical drug testing, it is desirable to refine the PeriTox test for higher sensitivity. For that purpose, we investigated in manuscript 2 whether toxicity threshold concentrations would change with prolonged exposure times (Flury 1921; Haber 1924; Macko et al. 2021). The sensitivity for cytotoxicity was found to increase with longer exposure times. Yet, the specificity of the neurite effects was lost as they could no longer be separated from the effects of general cytotoxicity. These observations are undesirable for refining the test method but are well consistent with the fact that neurite damage is often followed by cell death or apoptosis given a sufficiently long exposure time (Berliocchi et al. 2005; Herkenham et al. 1991; Volbracht et al. 1999). However, induction of cell death by neurite damage may be particularly relevant in immature cells such as the iPSC-derived, still-developing neurons used in the PeriTox test. In neurons integrated into a functional network *in vivo*, maturation-associated signals constrain the apoptotic machinery, thus, increasing the threshold of apoptosis induction (Kole et al. 2013). The mechanism of axon pruning, i.e. the local degeneration of axons without affecting the somata, which is distinct from apoptosis, plays a predominant role in mature neurons (Geden and Deshmukh 2016; Geden et al. 2019). Therefore, the effects

observed in the extended PeriTox test approach most likely do not reflect the actual situation in peripheral nervous system toxicity occurring *in vivo* mainly in adults.

In a next approach, the toxicant exposure was shifted to a later time point of differentiation, DoD4, to study the effects on more mature neurons. However, the effects of a 72-hour exposure starting on DoD4 did not differ from treatment initiation on DoD0. Considering the findings from the PNN transcriptome analysis revealing continuous development until at least DoD35-42 after thawing, it is not surprising that the effects of toxicant exposure initiated on DoD0 and DoD4 did not differ, as both differentiation stages are very immature. Thus, for studies on mature neurons, it is important to move experimental investigations to DoD35 and later to allow for advanced maturation status of the cells (Schinke et al. 2021). As the neurites of peripheral neurons continue to grow and the network becomes more cluttered over time, a quantitative assessment of the effects on neurite area becomes increasingly less informative. Consequently, new endpoints and analytical methods need to be established for toxicological studies in mature peripheral neurons.

3.3 Ca^{2+}-signaling as an endpoint to assess neuronal function

Neuronal function can be assessed using various methods such as the patch-clamp technique, multi-electrode arrays, or Ca^{2+}-imaging experiments. However, not every readout is suitable for implementation in a toxicological test method. For reasons of reproducibility, the method should allow for a certain degree of automation to minimize deviations, and have a reasonable throughput. Ca^{2+}-imaging was chosen as functional readout to assess pain receptor signaling because it allows examination of not only entire cell cultures but also numerous individual cells simultaneously. Cells were loaded with a fluorescent calcium indicator and subjected to high content imaging to monitor the intracellular Ca^{2+}-concentration ($[Ca^{2+}]_i$). Time-lapse imaging was performed to allow the evaluation of changes in $[Ca^{2+}]_i$ following (pain) stimulus application.

Ca^{2+}-imaging experiments are often used to examine stimulus-induced responses of whole cell cultures based on the overall fluorescence of a culture well (Lilja and Forsby 2004; Loser et al. 2021a; Loser et al. 2021b; Loser et al. 2021c; Stacey et al. 2018). This

approach is especially useful in highly uniform cultures of cell lines, such as the Lund Human Mesencephalic (LUHMES) cells (Loser et al. 2021a; Loser et al. 2021b; Loser et al. 2021c). However, neuronal populations often consist of different subtypes with distinct receptor expression profiles *in vivo*. As PNN cultures reflect the natural diversity of nociceptive neurons, it was of great importance to establish a strategy for the evaluation of Ca^{2+}-signaling responses on the single-cell level.

3.3.1 CaFFEE – a dedicated software for the analysis of Ca^{2+}-imaging experiments

To obtain quantitative information from Ca^{2+}-imaging experiments, large amounts of imaging data had to be processed and analyzed with respect to individual cells. The CaFFEE software, presented in manuscript 3 of this thesis, was developed to meet this challenge. With respect to the present work, one of the most important features of this program is the manual setting of parameters that define a region of interest, i.e. an object to be analyzed. Filtering by size and fluorescence intensity allows the exclusion of dead cells that would otherwise be counted as non-reactive cells if included in the analysis, thus distorting the evaluation, e.g., with regard to the proportion of reactive cells. This feature might also be useful for future experiments using co-culture systems, for example composed of neurons and glia, to enable differential evaluation of the two cell types according to the size of their nuclei. In addition, it allows the use of different magnification settings for imaging, which is important because higher magnifications may be beneficial for detecting smaller changes in $[Ca^{2+}]_i$. The manual setting of object-defining parameters makes CaFFEE a highly flexible tool for the evaluation of Ca^{2+}-imaging experiments.

Since CaFFEE is an in-house software, it can be further developed and tailored to specific research questions. An advanced version of CaFFEE, the MultiMovie program, was created during the course of this work to allow more detailed characterization of cell cultures providing insights into the receptor expression profiles of individual cells. MultiMovie, as the name implies, combines multiple (up to five) time-lapse videos recorded on the exact same cells, but using different stimuli in each experiment. The MultiMovie program allowed confirmation of the similarity between the *in vitro* PNN cultures used here and *ex vivo* characterized human dorsal root ganglia by quantifying P2X3-, TRPV1-, or double-responsive cells representing the nociceptor subclasses of peptidergic and non-peptidergic neurons (Rostock et al. 2018).

3.3.2 Providing robust and accessible information on Ca^{2+}-signaling responses

For each individual experiment, CaFFEE provides the user with data on numerous measurement parameters for hundreds of single cells. These include information about the Ca^{2+}-indicator fluorescence intensity at different times of the experiment, as well as kinetic information on the increase and decline of $[Ca^{2+}]_i$. Such multidimensional data sets open up a wide range of possible features to be studied. However, the extreme example of multi-electrode array data containing information on hundreds of features highlights the need to focus on specific endpoints or patterns to convey clear messages (Gramowski et al. 2006; Scelfo et al. 2012). To allow for clear and accessible data presentation, a binary endpoint of "responsive" *versus* "non-responsive" cells was established based on the changes in $[Ca^{2+}]_i$ upon stimulus application. A defined thresholding strategy should enable the standardized and unbiased identification of reactive cells. Investigations on ten independent cell preparations including more than 9,000 individual cells, revealed a slight general variability in the noise level, i.e. the increase in Ca^{2+}-indicator fluorescence upon application of a negative control stimulus. This might be attributable to technical issues, such as an unstable light source, but also to a general shift in baseline excitability during development of the neurons (Balmer et al. 2014). To overcome such generally encountered problems, a dynamic yet defined thresholding approach based on the individual culture's noise levels was found to be preferable to a fixed threshold.

The assessment of the "fraction of responsive cells" based on single cell data allowed investigation of alterations in cell culture responses even when only a small subpopulation expressed the particular ion channel of interest. In manuscript 1, this binary readout enabled the comprehensive study of more than 60,000 individual cells, and still provided an accessible way to communicate the resulting complex data. Moreover, previous studies using single-cell readouts drew conclusions from less than 100 cells examined (Anand et al. 2010; Xiong et al. 2021). In contrast, each experiment in the studies presented here included several hundreds or even thousands of cells lending more validity to the data obtained.

A change in the number of cells responding to a specific stimulus is perhaps the most obvious reason for, e.g., altered pain perception. However, it should be noted that there are many other parameters that can lead to neuronal dysfunction if altered. Ion channel kinetics play an important role in maintaining proper neuronal function. For example, a

slowdown of the inactivation kinetics of ion channels leads to a prolongation of ion influx, thus, contributing to neuronal hyperexcitation and hypersensitivity (Adelsberger et al. 2000; Narahashi 1996). Moreover, an increase in ion channel membrane integration may also result in increased ion influx (Zhang et al. 2005). CaFFEE provides all quantitative data required to study such impairments, which are not necessarily associated with an altered number of responsive cells. A curve fit is calculated for every single cell based on its fluorescence intensity trace. The respective Hill slopes describing the kinetics of the changes in $[Ca^{2+}]_i$ can provide information on the opening and closing kinetics of ion channels. Therefore, future Ca^{2+}-imaging studies could also investigate additional endpoints in order to identify sensitive criteria that, alone or in combination, improve the detection of neuronal dysfunction.

3.4 The relevance of PNN as an *in vitro* model for CIPN

The successful generation of PNN offered a test system of high biological plausibility for studies of chemotherapy-induced peripheral neuropathy (CIPN). The combination of PNN with the test endpoint of Ca^{2+}-imaging was intended to allow the investigation of functional alterations induced by the exposure to chemotherapeutic agents. Studies on such functional impairments of receptors and ion channels are relatively rare, especially those using human sensory neurons (Stacey et al. 2018; Xiong et al. 2021). However, they are of great importance, as CIPN is not necessarily linked to structural damage but also to altered neuronal excitability (Park et al. 2008). Morphology-based test methods might therefore miss important functional changes (Loser et al. 2021b). Providing a new human cell-based *in vitro* platform to study CIPN could thus allow for a better understanding of the underlying mechanisms and an improved risk assessment of future drug candidates. In order to explore the suitability of this new platform for studying CIPN *in vitro*, case studies were performed with chemotherapeutic agents known to induce CIPN *in vivo*.

3.4.1 Platinum compounds and altered neuronal function

Platinum derivatives such as oxaliplatin, cisplatin, and carboplatin are important chemotherapeutic agents used to treat cancer of the colon, head, lung, and testes (Ewertz et al. 2015). However, they are frequently associated with the development of persisting

CIPN, which is linked to structural damage of sensory neurons most likely induced by platinum accumulation in the dorsal root ganglia (Cavaletti et al. 1992; Gregg et al. 1992; Miltenburg and Boogerd 2014). Oxaliplatin is known to additionally induce an acute form of CIPN in more than 80% of the patients (Ewertz et al. 2015). Acute oxaliplatin-induced peripheral neuropathy (OXAIPN) is marked by functional, but not structural impairments, and manifests as thermal hyperalgesia, mechanical allodynia, and general neuronal hyperexcitability (Adelsberger et al. 2000; Anand et al. 2010; Chen et al. 2015; Chukyo et al. 2018; Ferrier et al. 2013; Lehky et al. 2004; Ling et al. 2007; Webster et al. 2005; Wilson et al. 2002). As acute OXAIPN occurs within hours after a single treatment, we anticipated that oxaliplatin would be a useful tool to examine the suitability of PNN as a CIPN model (Ewertz et al. 2015).

Thermal hyperalgesia in vitro

Indeed, hyper-responsiveness of oxaliplatin-treated cells to stimulation with capsaicin, a compound agonist of the heat-sensing TRPV1 receptor, was found. This was interpreted as an *in vitro* indicator of the thermal hyperalgesia observed *in vivo*. It should be noted, that TRPV1 responses were increased at an oxaliplatin concentration of 5 µM, which is in good agreement with the blood concentration of patients receiving oxaliplatin infusion (3.6 µM) (Ehrsson et al. 2002). Since TRPV1 is known to exhibit enhanced responsiveness to activating stimuli in acidic environments, the cytosolic acidification detected in oxaliplatin- but not cisplatin-treated cells may provide a mechanistic explanation for the acute hyper-responsiveness observed in PNN (Riva et al. 2018; Tominaga et al. 1998). Further studies on this hypothesis may help to understand the unusual acute symptoms induced by oxaliplatin and to develop a new generation of platinum-based drugs that do not cause, e.g., such pH modulation.

Mechanical hyperalgesia in vitro

The addition of a liquid (e.g., a negative control buffer) to the cell culture well during Ca^{2+}-imaging experiments produces mild shear forces that act on the cells, but do not usually elicit cell responses. Strikingly, oxaliplatin-treated PNN exhibited a significant increase in the percentage of cells responding with elevated $[Ca^{2+}]_i$ to such shear forces, reflecting mechanical allodynia-like behaviour *in vitro*. Inhibition of different types of ion channels revealed that Na_V channels might play a role in the observed response to mechanical stimuli. Yet, whether a specific type of Na_V channel accounts for this mechanical

hypersensitivity remains unknown. However, this would be an interesting question to address with regard to the development of targeted treatments for CIPN. Since Na_V channels play an important role in general neuronal signaling, targeted interference with a single responsible subtype would be advantageous over complete inhibition of Na_V channel function in the treatment of CIPN. A promising candidate may be the subtype $Na_V1.6$ known to regulate the excitability of mechanosensitive sensory neurons, which was previously shown to contribute to mechanical allodynia induced by the chemotherapeutic agent vincristine (Chen et al. 2020; Deuis et al. 2013; Israel et al. 2019). Moreover, the increased expression of $Na_V1.6$ detected in the dorsal root ganglia of rats with oxaliplatin-induced neuropathic pain encourages further research on the involvement of this channel subtype in mechanical allodynia and general CIPN (Li et al. 2019).

Oxaliplatin versus cisplatin

Oxaliplatin and cisplatin exhibit the highest neurotoxic potential among the platinum chemotherapeutic agents (Kanat et al. 2017). However, cisplatin is not known to induce acute CIPN symptoms (Staff et al. 2017). Therefore, a direct comparison of the effects of both compounds on PNN function was an obvious next step to explore the usefulness of PNN as a platform to study CIPN and the underlying mechanisms. Since responses to capsaicin and shear forces were not altered in cisplatin-treated cells, this confirmed that PNN are not generally impaired in function by compound treatment, but are able to model particular effects of different chemotherapeutic agents.

3.4.2 Proteasome inhibitors and early CIPN indicators

Proteasome inhibitors (PIs) are a powerful tool in treating multiple myeloma, however, their use is frequently accompanied by CIPN development (Jagannath et al. 2004; Kane et al. 2003; Richardson et al. 2003; Richardson et al. 2006). The development of new proteasome inhibitors with an improved profile of side effects is therefore of great interest, and an advanced strategy to accelerate pre-clinical testing of such new drug candidates would be beneficial. To date, studies of bortezomib-induced CIPN have been mostly based on animal models or cell lines (Velasco et al. 2019). The only recent study using human iPSC-derived peripheral neurons, albeit at an early stage of maturation, examined bortezomib-induced proteomic changes (Hrstka et al. 2021). In this study,

treatment with 100 nM bortezomib resulted in significant changes in microtubule dynamics-associated proteins, which is in good agreement with the impairment of neurite growth observed at 34 nM in the PeriTox test. However, in manuscript 2 of this dissertation, it could be shown that matured human peripheral neurons exhibit an increased sensitivity towards bortezomib treatment. In PNN, distinct impairments were detected at concentrations as low as 5 nM, which corresponds to the IC_{50} value determined for the inhibition of the proteasomal subunits β1 and β5, as well as for the induction of cytotoxicity in multiple myeloma cell lines (Berkers et al. 2012; Piva et al. 2008).

While the integrity of the neurite network remained unchanged, a distinct pattern of tubulin reorganization was observed in the somata of PNN exposed to low nanomolar bortezomib concentrations. Such cytoskeletal reorganization has previously been linked to impaired axonal transport, which is presumably a key mechanism in the development of CIPN (Alé et al. 2015; Nicolini et al. 2015; Staff et al. 2013). Moreover, these changes were detected exclusively in PI-treated neurons but not when exposed to platinum compounds or taxol, suggesting that this distinct cytoskeletal reorganization is a PI-specific phenomenon.

Another pivotal factor in abnormal nociception is disturbed Ca^{2+} homeostasis (Velasco et al. 2019). Previous approaches decreasing cytosolic Ca^{2+} levels have been shown to alleviate neuropathic symptoms, even in CIPN models of vincristine and taxol neuropathy (Coderre and Melzack 1992; Siau and Bennett 2006; White and Cousins 1998). This suggests that increased intracellular Ca^{2+} levels, which have also been observed in proteasome inhibitor-treated PNN, may contribute to CIPN development. Thus, the cytoskeletal structure and intracellular Ca^{2+} concentration that can be studied in PNN *in vitro* represent two endpoints that are very sensitive to PI-induced impairments and are highly relevant to CIPN research.

Concomitantly, a complete blunting of functional P2X3 receptor signaling was detected. This impairment of receptor function was specific to P2X3, while TRPV1 signaling and general membrane depolarization were not affected. Since P2X3 signaling was also found to be affected upon treatment with platinum compounds in manuscript 1, this may be an interesting novel candidate to pursue as a sensitive indicator of disturbed neuronal function. However, further research on the integration of P2X3 into general pain signaling

networks is needed to understand better the implications of attenuated P2X3 signaling (Stephan et al. 2018).

Impairments of tubulin organization, $[Ca^{2+}]_i$, and P2X3 signaling were observed with all proteasome inhibitors tested. Alterations always occurred in all three endpoints simultaneously, never individually, suggesting a possible common upstream dysregulation. Since Ca^{2+} is an important second messenger involved in the regulation of neuronal signaling, but also of the cytoskeleton, the observed altered intracellular Ca^{2+} levels could be causative for concurrent impairments of the two other endpoints (Mattson 1992). Future studies should address this potentially causal relationship, and could further investigate whether influx of extracellular Ca^{2+}, endoplasmatic reticulum stress, or mitochondrial dysfunction might account for the observed changes in $[Ca^{2+}]_i$ (Chine et al. 2019; Tomita et al. 2019; Yousuf et al. 2020).

3.5 Available neurotoxicity assays using human iPSC-derived peripheral neurons

In 2016, the PeriTox test, which was the first test method for neurotoxicity assessment using human iPSC-derived peripheral neurons, was published (Hoelting et al. 2016). Since 2017, the use of this specific neuronal cell type for CIPN research has increased, in part due to the availability of commercial human iPSC-derived peripheral neurons, i.e., the Peri.4U neurons (Rana et al. 2017; Schinke et al. 2021; Snyder et al. 2018; Wang et al. 2021; Wing et al. 2017; Xiong et al. 2021). Yet, the development of human cell-based peripheral neurotoxicity assays has been slow and lacking in diversity. So far, all these assays have been based on measuring the same endpoints, namely cell viability and neurite morphology, however, the results vary widely (see table 3.1). Bortezomib can be mentioned as an example of the sometimes extreme variability of the different test methods. In three studies, effects of bortezomib were noted at low nanomolar concentrations, whereas in two other studies effects were detected only at 100 µM or not at all. Moreover, the endpoint of neurite morphology is redundant to the cell viability readout in most test methods discussed here, as both often decline at similar rates.

The PeriTox test is the only test method that was able to distinguish between specific neurite effects and general cytotoxicity induction for all chemotherapeutic agents tested. Additionally, the PeriTox test features a defined prediction model, which also allows an unbiased classification of the test substances into neurite-specific, cytotoxic, or no-effect compounds based on their effects on both endpoints (Hoelting et al. 2016; Masjosthusmann et al. 2020). Other published assays usually lack such prediction models, making them more suitable for exploratory studies than large-scale screening approaches.

Table 3.1: Compilation of IC_{25} values of the respective most sensitive endpoint determined for exemplary chemotherapeutic agents in studies using human iPSC-derived peripheral neurons

Study	*Endpoint*	*Bortezomib [nM]*	*Cisplatin [µM]*	*Taxol [nM]*	*Oxaliplatin [µM]*
Schinke et al. 2021	viability (24 h)	5	3	20	
Rana et al. 2017 *(IC_{50})*	neurites (24 h)	>100,000	>100	<1	74
Snyder et al. 2018	neurites (24 h)	100,000	>10	1,000	>50
Wing et al. 2017	neurites (72 h)	1	2	8	
Wang et al. 2021	neurites (24 h)	10	0.1		
Xiong et al. 2021	neurites (72 h)			100	
PeriTox test	**neurites (24 h)**	**34**	**5**	**2**	**15**
PNN	**function (24 h)**	**2.5**	**20**	**≥60**	**5**

As discussed earlier, neurotoxic effects do not necessarily manifest in morphologic changes, underscoring the need for the implementation of new test endpoints to ensure comprehensive risk assessment. Only the most recently published studies on human iPSC-derived peripheral neurons used for toxicity testing take a step in this direction (Wang et al. 2021; Xiong et al. 2021). The study of Wang et al. examined effects on gene expression of nociceptor-characteristic ion channels and neurotransmitter release in addition to neurite morphology and cell viability. Xiong et al. additionally studied changes in mitochondrial membrane potential and glutamate-induced Ca^{2+}-signaling. The data suggest that these additional endpoints may be useful for gaining new mechanistic insights. However, due to the small number of compounds and the limited range of concentrations tested, it is difficult to evaluate whether these additional endpoints would also add value to pre-clinical risk assessment. Subjecting these new endpoints to a larger number of test compounds will be necessary to determine their utility for toxicant

screening purposes. The generation of concentration-response curves for known CIPN-inducing agents will further be essential to evaluate the sensitivity of these new endpoints.

Although it has recently been possible to generate sensory neurons with functional nociceptor signaling properties, this progress has not yet been used to gain insight into toxicant-induced pain signaling perturbations (Schinke et al. 2021; Xiong et al. 2021). This gap is now being filled with the novel system of PNN, which has proven to be a useful tool for modeling CIPN-related functional alterations at non-cytotoxic concentrations. Testing of various concentrations of proteasome inhibitors revealed an increased sensitivity of PNN compared to PeriTox test results. However, the performance of PNN has to be further validated using a more comprehensive set of test compounds that also include negative controls and unspecific toxicants. This would also enable the establishment of a prediction model representing the missing building block to complete a functional PNN-based *in vitro* test method. Until then, PNN may still provide valuable mechanistic insights as they present the first platform to study pain CIPN-relevant functional impairments in human peripheral neurons.

This thesis, and specifically the comparison of available assays for assessing peripheral neurotoxicity *in vitro* presented here, has also demonstrated that the PeriTox test and the biological system of PNN, with the various endpoints they provide, complement each other in identifying adverse effects. Thus, a standard combination of these two platforms in a peripheral neurotoxicity test battery may provide a powerful and sensitive tool for risk assessment in the future.

3.6 Perspectives for the use of human iPSC-derived peripheral neurons in CIPN research

Most of the current knowledge on chemotherapeutic agents and their side effects is derived from studies based on experimental animals. These animals have been used not only to evaluate behavioural changes, but often simply to isolate nerves for functional studies *in vitro* (Alé et al. 2015; Chen et al. 2020; Deuis et al. 2013; Israel et al. 2019; Staff et al. 2013). The novel biological system of human iPSC-derived PNN presented in this thesis proved useful for modeling CIPN-relevant functional impairments *in vitro*. Thus, in the future, PNN may provide a superior alternative to animal-based experimental models, such as isolated rodent neurons, and may reduce the number of animals used for toxicity testing. PNN represent a new *in vitro* platform to study peripheral neurotoxicity with increased relevance to human pathology, particularly concerning mechanistic studies. Research on CIPN mechanisms may be advanced by such *in vitro* models as they greatly facilitate the generation of specific receptor knock-outs, for example, using the CRISPR-Cas9 technology (Harjuhaahto et al. 2020). Moreover, *in vitro* systems offer the possibility to precisely control the experimental environment, e.g., the pH value. Hence, the use of PNN may accelerate the acquisition of new knowledge about CIPN under well-controlled experimental conditions while reducing the number of experimental animals needed.

The use of *in vitro* test methods for toxicity testing may significantly increase the throughput of pre-clinical risk assessment compared to the exclusive testing in *in vivo* models (Fig. 3.1). This is particularly important in the early stages when large substance libraries are tested for their (neuro)toxic potential. PNN provide various test endpoints that can be assessed simultaneously to detect peripheral neurotoxicity with high sensitivity. However, the generation of PNN as well as the analytical method of Ca^{2+}-imaging are relatively time-consuming and labor-intensive compared to high-throughput test methods, such as the PeriTox test. Therefore, using these two assays in a sequential testing strategy would be beneficial, starting with screening a wide concentration range in the PeriTox test to define appropriate concentrations for targeted follow-up experiments in matured PNN. Yet, the PeriTox test should not be used as a selection criterion, in this case, to reduce the number of compounds to be followed up in PNN. Results derived from the PeriTox test should instead be complemented by functional

testing in PNN, as signaling alterations can indeed occur at concentrations that do not alter morphology and *vice versa*.

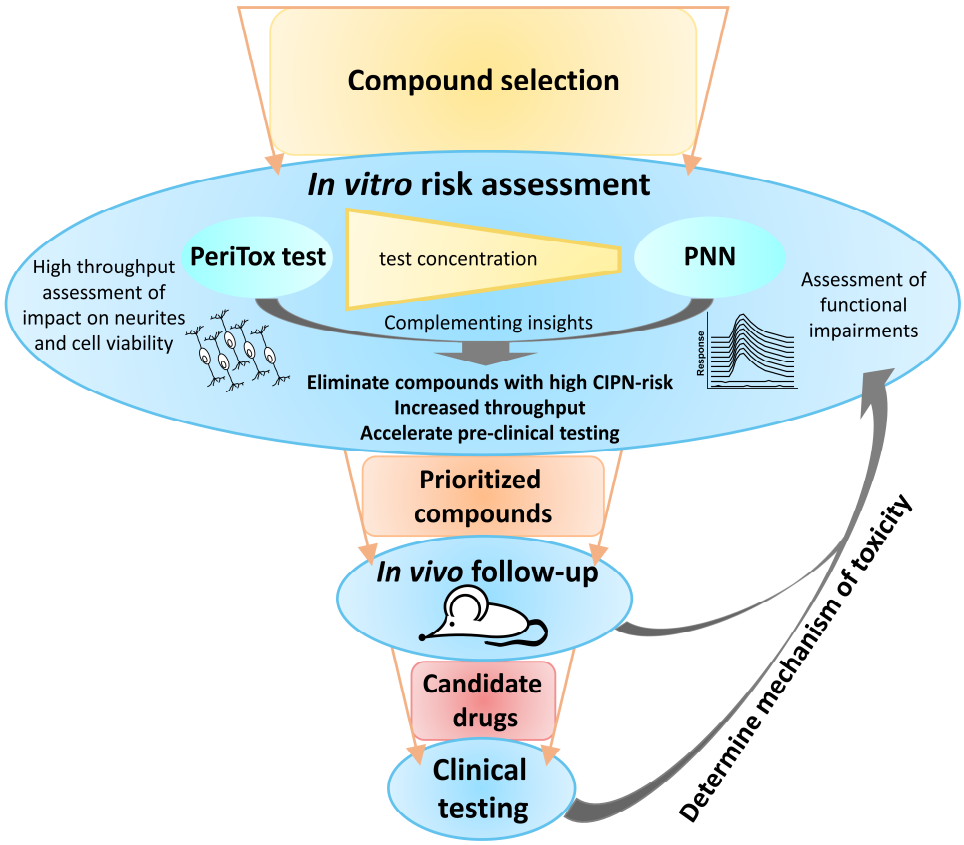

Figure 3.1: Proposed model for integrating *in vitro* approaches into pre-clinical assessment of peripheral neurotoxicity during drug development.

This thesis presents a new platform for studying peripheral neurotoxicity *in vitro,* enabling the investigation of toxicant-induced impairments in pain signaling. Beyond its future application in toxicological and mechanistic studies, this platform also provides numerous avenues for future advancements. These may include the establishment of additional functional endpoints, such as signaling via other sensory receptors or neurotransmitter release, to cover as many pain-related functions as possible. Moreover, it should be considered that not only nociceptive neurons, but also glial cells and central neurons are involved in pain signaling *in vivo*. Adding complexity to the *in vitro* cell culture, e.g., by co-culturing PNN with Schwann cells, may further increase the relevance for CIPN research. However, such developments will also pose new analytical challenges that will require further refinement of the CaFFEE software to meet the emerging demands. Finally, the newly gained expertise will highly facilitate the further development and application of this advanced platform for assessing peripheral neurotoxicity *in vitro*.

4 Author contributions

Manuscript 1: Generation of human nociceptor-enriched sensory neurons for the study of pain-related dysfunctions

The experiments for this manuscript were conceived and designed in collaboration with Christiaan Karreman and Marcel Leist. Most of the laboratory work was performed by me. Harald Wohlfarth and Lara-Seline Furmanowsky contributed to the characterization of the peripheral neurons. Christiaan Karreman was involved in the generation of the lentiviral construct and the evaluation of Ca^{2+}-imaging data. He further provided software to handle various challenges in data analysis and representation. Ilinca Suciu and I analyzed the transcriptome data. Electrophysiological recordings were performed by Dominik Loser and Emilio Pardo González. Cell line authentication was performed by Wilhelm G Dirks. The manuscript was written by Marcel Leist and me.

Manuscript 2: Specific attenuation of purinergic signaling during bortezomib-induced peripheral neuropathy

For this manuscript, Marcel Leist and I were responsible for the concept and design of the experiments. I performed the main experimental work. Thomas Goj worked on refining the PeriTox test. Analysis of the transcriptomics data was performed by Ilinca Suciu. Christiaan Karreman was involved in the generation of the gene-edited iPSC line and the evaluation of Ca^{2+}-imaging data. The manuscript was written by Marcel Leist and me.

Manuscript 3: CaFFEE: a program for evaluating time courses of Ca^{2+} dependent signal changes of complex cells loaded with fluorescent indicator dyes

The CaFFEE software was developed by Christiaan Karreman. Stefanie Klima and I were involved in testing and improving the applicability of the program using Ca^{2+}-imaging data derived from different neuronal cultures. The manuscript was written by Christiaan Karreman, Stefanie Klima and Marcel Leist.

5 Bibliography

Adams J, Palombella VJ, Sausville EA, Johnson J, Destree A, Lazarus DD, Maas J, Pien CS, Prakash S, Elliott PJ (1999) Proteasome inhibitors: a novel class of potent and effective antitumor agents *Cancer Res* 59, 2615–2622.

Adelsberger H, Quasthoff S, Grosskreutz J, Lepier A, Eckel F, Lersch C (2000) The chemotherapeutic oxaliplatin alters voltage-gated Na+ channel kinetics on rat sensory neurons *Eur J Pharmacol* 406, 25–32.

Albany C, Dockter T, Wolfe E, Le-Rademacher J, Wagner-Johnston N, Einhorn L, Lafky JM, Smith E, Pachman D, Staff N, Ma C, Loprinzi CL, Costello BA (2021) Cisplatin-associated neuropathy characteristics compared with those associated with other neurotoxic chemotherapy agents (Alliance A151724) *Support Care Cancer* 29, 833–840.

Alé A, Bruna J, Herrando M, Navarro X, Udina E (2015) Toxic effects of bortezomib on primary sensory neurons and Schwann cells of adult mice *Neurotox Res* 27, 430–440.

Alé A, Bruna J, Navarro X, Udina E (2014) Neurotoxicity induced by antineoplastic proteasome inhibitors *Neurotoxicology* 43, 28–35.

Almanza A, Segura-Chama P, León-Olea M, Luis E, Garduño-Gutiérrez R, Mercado-Reyes J, Simón-Arceo K, Coffeen U, Hernández-Cruz A, Pellicer F, Mercado F (2019) Cellular Mechanism for Specific Mechanical Antinociception by D2-like Receptor at the Spinal Cord Level *Neuroscience* 417, 81–94.

Alshawaf AJ, Viventi S, Qiu W, D'Abaco G, Nayagam B, Erlichster M, Chana G, Everall I, Ivanusic J, Skafidas E, Dottori M (2018) Phenotypic and Functional Characterization of Peripheral Sensory Neurons derived from Human Embryonic Stem Cells *Sci Rep* 8, 603.

Ambrosino P, Soldovieri MV, Russo C, Taglialatela M (2013) Activation and desensitization of TRPV1 channels in sensory neurons by the PPARα agonist palmitoylethanolamide *Br J Pharmacol* 168, 1430–1444.

Anand U, Otto WR, Anand P (2010) Sensitization of capsaicin and icilin responses in oxaliplatin treated adult rat DRG neurons *Mol Pain* 6, 82.

Argyriou AA, Cavaletti G, Bruna J, Kyritsis AP, Kalofonos HP (2014) Bortezomib-induced peripheral neurotoxicity: an update *Arch Toxicol* 88, 1669–1679.

Argyriou AA, Park SB, Islam B, Tamburin S, Velasco R, Alberti P, Bruna J, Psimaras D, Cavaletti G, Cornblath DR (2019) Neurophysiological, nerve imaging and other techniques to assess chemotherapy-induced peripheral neurotoxicity in the clinical and research settings *J Neurol Neurosurg Psychiatry* 90, 1361–1369.

Balmer NV, Klima S, Rempel E, Ivanova VN, Kolde R, Weng MK, Meganathan K, Henry M, Sachinidis A, Berthold MR, Hengstler JG, Rahnenführer J, Waldmann T, Leist M (2014) From transient transcriptome responses to disturbed neurodevelopment: role of histone acetylation and methylation as epigenetic switch between reversible and irreversible drug effects *Arch Toxicol* 88, 1451–1468.

Bal-Price A, Hogberg HT, Crofton KM, Daneshian M, FitzGerald RE, Fritsche E, Heinonen T, Hougaard Bennekou S, Klima S, Piersma AH, Sachana M, Shafer TJ, Terron A, Monnet-Tschudi F, Viviani B, Waldmann T, Westerink RHS, Wilks MF, Witters H, Zurich M-G, Leist

M (2018) Recommendation on test readiness criteria for new approach methods in toxicology: Exemplified for developmental neurotoxicity *ALTEX* 35, 306–352.

Bal-Price AK, Hogberg HT, Buzanska L, Coecke S (2010) Relevance of in vitro neurotoxicity testing for regulatory requirements: challenges to be considered *Neurotoxicol Teratol* 32, 36–41.

Bandell M, Story GM, Hwang SW, Viswanath V, Eid SR, Petrus MJ, Earley TJ, Patapoutian A (2004) Noxious Cold Ion Channel TRPA1 Is Activated by Pungent Compounds and Bradykinin *Neuron* 41, 849–857.

Bano D, Jewell SA, Nicotera P (2017) Calcium signaling then and now, via Stockholm *Biochem Biophys Res Commun* 482, 384–387.

Basbaum AI, Bautista DM, Scherrer G, Julius D (2009) Cellular and molecular mechanisms of pain *Cell* 139, 267–284.

Bassett JJ, Monteith GR (2017) Genetically Encoded Calcium Indicators as Probes to Assess the Role of Calcium Channels in Disease and for High-Throughput Drug Discovery *Adv Pharmacol* 79, 141–171.

Bautista DM, Jordt S-E, Nikai T, Tsuruda PR, Read AJ, Poblete J, Yamoah EN, Basbaum AI, Julius D (2006) TRPA1 mediates the inflammatory actions of environmental irritants and proalgesic agents *Cell* 124, 1269–1282.

Bautista DM, Siemens J, Glazer JM, Tsuruda PR, Basbaum AI, Stucky CL, Jordt S-E, Julius D (2007) The menthol receptor TRPM8 is the principal detector of environmental cold *Nature* 448, 204–208.

Berkers CR, Leestemaker Y, Schuurman KG, Ruggeri B, Jones-Bolin S, Williams M, Ovaa H (2012) Probing the specificity and activity profiles of the proteasome inhibitors bortezomib and delanzomib *Mol Pharm* 9, 1126–1135.

Berliocchi L, Fava E, Leist M, Horvat V, Dinsdale D, Read D, Nicotera P (2005) Botulinum neurotoxin C initiates two different programs for neurite degeneration and neuronal apoptosis *J Cell Biol* 168, 607–618.

Bhatt S, Diaz R, Trainor PA (2013) Signals and switches in Mammalian neural crest cell differentiation *Cold Spring Harb Perspect Biol* 5, a008326.

Bianchi BR, Lynch KJ, Touma E, Niforatos W, Burgard EC, Alexander KM, Park HS, Yu H, Metzger R, Kowaluk E, Jarvis MF, van Biesen T (1999) Pharmacological characterization of recombinant human and rat P2X receptor subtypes *Eur J Pharmacol* 376, 127–138.

Bischoff A (1967) The ultrastructure of tri-ortho-cresyl phosphate-poisoning. I. Studies on myelin and axonal alterations in the sciatic nerve *Acta Neuropathol* 9, 159–174.

Bleehen T, Keele CA (1977) Observations on the algogenic actions of adenosine compounds on the human blister base preparation *Pain* 3, 367–377.

Bodin P, Burnstock G (2001) Evidence that release of adenosine triphosphate from endothelial cells during increased shear stress is vesicular *J Cardiovasc Pharmacol* 38, 900–908.

Boehmerle W, Huehnchen P, Peruzzaro S, Balkaya M, Endres M (2014) Electrophysiological, behavioral and histological characterization of paclitaxel, cisplatin, vincristine and bortezomib-induced neuropathy in C57Bl/6 mice *Sci Rep* 4, 6370.

Boisvert EM, Engle SJ, Hallowell SE, Liu P, Wang Z-W, Li X-J (2015) The Specification and Maturation of Nociceptive Neurons from Human Embryonic Stem Cells *Sci Rep* 5, 16821.

Boivie J, Leijon G, Johansson I (1989) Central post-stroke pain — a study of the mechanisms through analyses of the sensory abnormalities *Pain* 37, 173–185.

Bonnington JK, McNaughton PA (2003) Signalling pathways involved in the sensitisation of mouse nociceptive neurones by nerve growth factor *J Physiol* 551, 433–446.

Brini M, Pinton P, Pozzan T, Rizzuto R (1999) Targeted recombinant aequorins: Tools for monitoring [Ca2+] in the various compartments of a living cell *Microsc Res Tech* 46, 380–389.

Brouwers EEM, Huitema ADR, Boogerd W, Beijnen JH, Schellens JHM (2009) Persistent neuropathy after treatment with cisplatin and oxaliplatin *Acta Oncol* 48, 832–841.

Brüll M, Spreng A-S, Gutbier S, Loser D, Krebs A, Reich M, Kraushaar U, Britschgi M, Patsch C, Leist M (2020) Incorporation of stem cell-derived astrocytes into neuronal organoids to allow neuro-glial interactions in toxicological studies *ALTEX* 37, 409–428.

Bruna J, Alberti P, Calls-Cobos A, Caillaud M, Damaj MI, Navarro X (2020) Methods for in vivo studies in rodents of chemotherapy induced peripheral neuropathy *Exp Neurol* 325, 113154.

Brüning T, Bartsch R, Bolt HM, Desel H, Drexler H, Gundert-Remy U, Hartwig A, Jäckh R, Leibold E, Pallapies D, Rettenmeier AW, Schlüter G, Stropp G, Sucker K, Triebig G, Westphal G, van Thriel C (2014) Sensory irritation as a basis for setting occupational exposure limits *Arch Toxicol* 88, 1855–1879.

Burke EE, Chenoweth JG, Shin JH, Collado-Torres L, Kim S-K, Micali N, Wang Y, Colantuoni C, Straub RE, Hoeppner DJ, Chen H-Y, Sellers A, Shibbani K, Hamersky GR, Diaz Bustamante M, Phan BN, Ulrich WS, Valencia C, Jaishankar A, Price AJ, Rajpurohit A, Semick SA, Bürli RW, Barrow JC, Hiler DJ, Page SC, Martinowich K, Hyde TM, Kleinman JE, Berman KF, Apud JA, Cross AJ, Brandon NJ, Weinberger DR, Maher BJ, McKay RDG, Jaffe AE (2020) Dissecting transcriptomic signatures of neuronal differentiation and maturation using iPSCs *Nat Commun* 11, 462.

Calls A, Carozzi V, Navarro X, Monza L, Bruna J (2020) Pathogenesis of platinum-induced peripheral neurotoxicity: Insights from preclinical studies *Exp Neurol* 325, 113141.

Campbell JN, Meyer RA (2006) Mechanisms of neuropathic pain *Neuron* 52, 77–92.

Canta A, Pozzi E, Carozzi VA (2015) Mitochondrial Dysfunction in Chemotherapy-Induced Peripheral Neuropathy (CIPN) *Toxics* 3, 198–223.

Cao L, McDonnell A, Nitzsche A, Alexandrou A, Saintot P-P, Loucif AJC, Brown AR, Young G, Mis M, Randall A, Waxman SG, Stanley P, Kirby S, Tarabar S, Gutteridge A, Butt R, McKernan RM, Whiting P, Ali Z, Bilsland J, Stevens EB (2016) Pharmacological reversal of a pain phenotype in iPSC-derived sensory neurons and patients with inherited erythromelalgia *Sci Transl Med* 8, 335ra56.

Carlton S, Hargett G, Coggeshall R (2001) Localization of metabotropic glutamate receptors 2/3 on primary afferent axons in the rat *Neuroscience* 105, 957–969.

Carozzi VA, Canta A, Chiorazzi A (2015) Chemotherapy-induced peripheral neuropathy: What do we know about mechanisms? *Neurosci Lett* 596, 90–107.

Carozzi VA, Renn C, Peter R, Gallop D, Marmiroli P, Cavaletti G, Dorsey S (2012) Abstract 934: Electrophysiological, behavioural and molecular characterization of the neuropathic pain in bortezomib-induced peripheral neuropathy *Experimental and Molecular Therapeutics.* Proceedings: AACR 103rd Annual Meeting 2012-- Mar 31-Apr 4, 2012; Chicago, IL American Association for Cancer Research, 934.

Carozzi VA, Renn CL, Bardini M, Fazio G, Chiorazzi A, Meregalli C, Oggioni N, Shanks K, Quartu M, Serra MP, Sala B, Cavaletti G, Dorsey SG (2013) Bortezomib-induced painful peripheral neuropathy: an electrophysiological, behavioral, morphological and mechanistic study in the mouse *PLoS One* 8, e72995.

Casey EB, Jellife AM, Le Quesne PM, Millett YL (1973) Vincristine neuropathy. Clinical and electrophysiological observations *Brain* 96, 69–86.

Catala M, Kubis N (2013) Gross anatomy and development of the peripheral nervous system *Handb Clin Neurol* 115, 29–41.

Caterina MJ, Leffler A, Malmberg AB, Martin WJ, Trafton J, Petersen-Zeitz KR, Koltzenburg M, Basbaum AI, Julius D (2000) Impaired nociception and pain sensation in mice lacking the capsaicin receptor *Science* 288, 306–313.

Caterina MJ, Schumacher MA, Tominaga M, Rosen TA, Levine JD, Julius D (1997) The capsaicin receptor: a heat-activated ion channel in the pain pathway *Nature* 389, 816–824.

Cavaletti G, Frigeni B, Lanzani F, Mattavelli L, Susani E, Alberti P, Cortinovis D, Bidoli P (2010) Chemotherapy-Induced Peripheral Neurotoxicity assessment: a critical revision of the currently available tools *Eur J Cancer* 46, 479–494.

Cavaletti G, Tredici G, Marmiroli P, Petruccioli MG, Barajon I, Fabbrica D (1992) Morphometric study of the sensory neuron and peripheral nerve changes induced by chronic cisplatin (DDP) administration in rats *Acta Neuropathol* 84, 364–371.

Chambers SM, Qi Y, Mica Y, Lee G, Zhang X-J, Niu L, Bilsland J, Cao L, Stevens E, Whiting P, Shi S-H, Studer L (2012) Combined small-molecule inhibition accelerates developmental timing and converts human pluripotent stem cells into nociceptors *Nat Biotechnol* 30, 715–720.

Chen AI, Nooij JC de, Jessell TM (2006) Graded activity of transcription factor Runx3 specifies the laminar termination pattern of sensory axons in the developing spinal cord *Neuron* 49, 395–408.

Chen CC, Akopian AN, Sivilotti L, Colquhoun D, Burnstock G, Wood JN (1995) A P2X purinoceptor expressed by a subset of sensory neurons *Nature* 377, 428–431.

Chen C-L, Broom DC, Liu Y, Nooij JC de, Li Z, Cen C, Samad OA, Jessell TM, Woolf CJ, Ma Q (2006) Runx1 determines nociceptive sensory neuron phenotype and is required for thermal and neuropathic pain *Neuron* 49, 365–377.

Chen G, Gulbranson DR, Hou Z, Bolin JM, Ruotti V, Probasco MD, Smuga-Otto K, Howden SE, Diol NR, Propson NE, Wagner R, Lee GO, Antosiewicz-Bourget J, Teng JMC, Thomson JA (2011) Chemically defined conditions for human iPSC derivation and culture *Nat Methods* 8, 424–429.

Chen J, Zhang X-F, Kort ME, Huth JR, Sun C, Miesbauer LJ, Cassar SC, Neelands T, Scott VE, Moreland RB, Reilly RM, Hajduk PJ, Kym PR, Hutchins CW, Faltynek CR (2008) Molecular determinants of species-specific activation or blockade of TRPA1 channels *J Neurosci* 28, 5063–5071.

Chen K, Zhang Z-F, Liao M-F, Yao W-L, Wang J, Wang X-R (2015) Blocking PAR2 attenuates oxaliplatin-induced neuropathic pain via TRPV1 and releases of substance P and CGRP in superficial dorsal horn of spinal cord *J Neurol Sci* 352, 62–67.

Chen L, Huang J, Benson C, Lankford KL, Zhao P, Carrara J, Tan AM, Kocsis JD, Waxman SG, Dib-Hajj SD (2020) Sodium channel Nav1.6 in sensory neurons contributes to vincristine-induced allodynia *Brain* 143, 2421–2436.

Chine VB, Au NPB, Ma CHE (2019) Therapeutic benefits of maintaining mitochondrial integrity and calcium homeostasis by forced expression of Hsp27 in chemotherapy-induced peripheral neuropathy *Neurobiol Dis* 130, 104492.

Choi J-S, Dib-Hajj SD, Waxman SG (2006) Inherited erythermalgia: limb pain from an S4 charge-neutral Na channelopathy *Neurology* 67, 1563–1567.

Chuang HH, Prescott ED, Kong H, Shields S, Jordt SE, Basbaum AI, Chao MV, Julius D (2001) Bradykinin and nerve growth factor release the capsaicin receptor from PtdIns(4,5)P2-mediated inhibition *Nature* 411, 957–962.

Chukyo A, Chiba T, Kambe T, Yamamoto K, Kawakami K, Taguchi K, Abe K (2018) Oxaliplatin-induced changes in expression of transient receptor potential channels in the dorsal root ganglion as a neuropathic mechanism for cold hypersensitivity *Neuropeptides* 67, 95–101.

Coderre TJ, Melzack R (1992) The role of NMDA receptor-operated calcium channels in persistent nociception after formalin-induced tissue injury *J Neurosci* 12, 3671–3675.

Colburn RW, Lubin ML, Stone DJ, Wang Y, Lawrence D, D'Andrea MR, Brandt MR, Liu Y, Flores CM, Qin N (2007) Attenuated cold sensitivity in TRPM8 null mice *Neuron* 54, 379–386.

Cook SP, McCleskey EW (2002) Cell damage excites nociceptors through release of cytosolic ATP *Pain* 95, 41–47.

Cook SP, Rodland KD, McCleskey EW (1998) A Memory for Extracellular Ca 2+ by Speeding Recovery of P2X Receptors from Desensitization *J Neurosci* 18, 9238–9244.

Cook SP, Vulchanova L, Hargreaves KM, Elde R, McCleskey EW (1997) Distinct ATP receptors on pain-sensing and stretch-sensing neurons *Nature* 387, 505–508.

Coutaux A, Adam F, Willer J-C, Le Bars D (2005) Hyperalgesia and allodynia: peripheral mechanisms *Joint Bone Spine* 72, 359–371.

Craiu A, Gaczynska M, Akopian T, Gramm CF, Fenteany G, Goldberg AL, Rock KL (1997) Lactacystin and clasto-lactacystin beta-lactone modify multiple proteasome beta-subunits and inhibit intracellular protein degradation and major histocompatibility complex class I antigen presentation *J Biol Chem* 272, 13437–13445.

Croft PB, Wilkinson M (1965) The incidence of carcinomatous neuromyopathy in patients with various types of carcinoma *Brain* 88, 427–434.

Csizmadia V, Raczynski A, Csizmadia E, Fedyk ER, Rottman J, Alden CL (2008) Effect of an experimental proteasome inhibitor on the cytoskeleton, cytosolic protein turnover, and induction in the neuronal cells in vitro *Neurotoxicology* 29, 232–243.

Danker T (2018) tdanker/ephys2: Read, analyze and plot HEKA Patchmaster files. R package version 0.12.0. https://rdrr.io/github/tdanker/ephys2/.

D'Arco M, Giniatullin R, Simonetti M, Fabbro A, Nair A, Nistri A, Fabbretti E (2007) Neutralization of nerve growth factor induces plasticity of ATP-sensitive P2X3 receptors of nociceptive trigeminal ganglion neurons *J Neurosci* 27, 8190–8201.

Davidson S, Copits BA, Zhang J, Page G, Ghetti A, Gereau RW (2014) Human sensory neurons: Membrane properties and sensitization by inflammatory mediators *Pain* 155, 1861–1870.

Davis JB, Gray J, Gunthorpe MJ, Hatcher JP, Davey PT, Overend P, Harries MH, Latcham J, Clapham C, Atkinson K, Hughes SA, Rance K, Grau E, Harper AJ, Pugh PL, Rogers DC, Bingham S, Randall A, Sheardown SA (2000) Vanilloid receptor-1 is essential for inflammatory thermal hyperalgesia *Nature* 405, 183–187.

Delp J, Gutbier S, Klima S, Hoelting L, Pinto-Gil K, Hsieh J-H, Aichem M, Klein K, Schreiber F, Tice RR, Pastor M, Behl M, Leist M (2018) A high-throughput approach to identify specific neurotoxicants/ developmental toxicants in human neuronal cell function assays *ALTEX* 35, 235–253.

Desiderio S, Vermeiren S, van Campenhout C, Kricha S, Malki E, Richts S, Fletcher EV, Vanwelden T, Schmidt BZ, Henningfeld KA, Pieler T, Woods CG, Nagy V, Verfaillie C, Bellefroid EJ (2019) Prdm12 Directs Nociceptive Sensory Neuron Development by Regulating the Expression of the NGF Receptor TrkA *Cell Rep* 26, 3522-3536.e5.

Deuis JR, Zimmermann K, Romanovsky AA, Possani LD, Cabot PJ, Lewis RJ, Vetter I (2013) An animal model of oxaliplatin-induced cold allodynia reveals a crucial role for Nav1.6 in peripheral pain pathways *Pain* 154, 1749–1757.

Deval E, Noël J, Lay N, Alloui A, Diochot S, Friend V, Jodar M, Lazdunski M, Lingueglia E (2008) ASIC3, a sensor of acidic and primary inflammatory pain *EMBO J* 27, 3047–3055.

Dhaka A, Murray AN, Mathur J, Earley TJ, Petrus MJ, Patapoutian A (2007) TRPM8 is required for cold sensation in mice *Neuron* 54, 371–378.

Dib-Hajj SD, Cummins TR, Black JA, Waxman SG (2010) Sodium channels in normal and pathological pain *Annu Rev Neurosci* 33, 325–347.

Dirks WG, Drexler HG (2013) STR DNA typing of human cell lines: detection of intra- and interspecies cross-contamination *Methods Mol Biol* 946, 27–38.

Dreser N, Madjar K, Holzer A-K, Kapitza M, Scholz C, Kranaster P, Gutbier S, Klima S, Kolb D, Dietz C, Trefzer T, Meisig J, van Thriel C, Henry M, Berthold MR, Blüthgen N, Sachinidis A, Rahnenführer J, Hengstler JG, Waldmann T, Leist M (2020) Development of a neural rosette formation assay (RoFA) to identify neurodevelopmental toxicants and to characterize their transcriptome disturbances *Arch Toxicol* 94, 151–171.

Dreser N, Zimmer B, Dietz C, Sügis E, Pallocca G, Nyffeler J, Meisig J, Blüthgen N, Berthold MR, Waldmann T, Leist M (2015) Grouping of histone deacetylase inhibitors and other toxicants disturbing neural crest migration by transcriptional profiling *Neurotoxicology* 50, 56–70.

Duan W, Zhang Y-P, Hou Z, Huang C, Zhu H, Zhang C-Q, Yin Q (2016) Novel Insights into NeuN: from Neuronal Marker to Splicing Regulator *Mol Neurobiol* 53, 1637–1647.

Dubin AE, Patapoutian A (2010) Nociceptors: the sensors of the pain pathway *J Clin Invest* 120, 3760–3772.

Edwards SM (2020) Freshing Up your 'ggplot2' Plots. R package lemon version 0.4.5. https://cran.r-project.org/web/packages/lemon/index.html.

Ehrsson H, Wallin I, Yachnin J (2002) Pharmacokinetics of Oxaliplatin in Humans *Med Oncol* 19, 261–266.

Eldridge S, Scuteri A, Jones EMC, Cavaletti G, Guo L, Glaze E (2021) Considerations for a Reliable In Vitro Model of Chemotherapy-Induced Peripheral Neuropathy *Toxics* 9, 300.

Elshazzly M, Lopez MJ., Reddy V, Caban O (2021) Embryology, Central Nervous System. StatPearls Publishing, Treasure Island (FL).

Ewertz M, Qvortrup C, Eckhoff L (2015) Chemotherapy-induced peripheral neuropathy in patients treated with taxanes and platinum derivatives *Acta Oncol* 54, 587–591.

Fattorelli N, Martinez-Muriana A, Wolfs L, Geric I, Strooper B de, Mancuso R (2021) Stem-cell-derived human microglia transplanted into mouse brain to study human disease *Nat Protoc* 16, 1013–1033.

Ferguson DR, Kennedy I, Burton TJ (1997) ATP is released from rabbit urinary bladder epithelial cells by hydrostatic pressure changes--a possible sensory mechanism? *J Physiol* 505 (Pt 2), 503–511.

Ferretti E, Hadjantonakis A-K (2019) Mesoderm specification and diversification: from single cells to emergent tissues *Curr Opin Cell Biol* 61, 110–116.

Ferrier J, Bayet-Robert M, Pereira B, Daulhac L, Eschalier A, Pezet D, Moulinoux J-P, Balayssac D (2013) A polyamine-deficient diet prevents oxaliplatin-induced acute cold and mechanical hypersensitivity in rats *PLoS One* 8, e77828.

Finkbeiner S, Greenberg ME (1998) Ca2+ channel-regulated neuronal gene expression *J Neurobiol* 37, 171–189.

Fischer BD, Ho C, Kuzin I, Bottaro A, O'Leary ME (2017) Chronic exposure to tumor necrosis factor in vivo induces hyperalgesia, upregulates sodium channel gene expression and alters the cellular electrophysiology of dorsal root ganglion neurons *Neurosci Lett* 653, 195–201.

Flury F (1921) Über Kampfgasvergiftungen I. Über Reizgase *Z Gesamte Exp Med* 13, 1–15.

Franck MCM, Stenqvist A, Li L, Hao J, Usoskin D, Xu X, Wiesenfeld-Hallin Z, Ernfors P (2011) Essential role of Ret for defining non-peptidergic nociceptor phenotypes and functions in the adult mouse *Eur J Neurosci* 33, 1385–1400.

Fujii Y, Ozaki N, Taguchi T, Mizumura K, Furukawa K, Sugiura Y (2008) TRP channels and ASICs mediate mechanical hyperalgesia in models of inflammatory muscle pain and delayed onset muscle soreness *Pain* 140, 292–304.

Fuller GN, Jacobs JM, Guiloff RJ (1993) Nature and incidence of peripheral nerve syndromes in HIV infection *J Neurol Neurosurg Psychiatry* 56, 372–381.

Gabella G (2001) Autonomic Nervous System *eLS* Wiley.

García-León JA, García-Díaz B, Eggermont K, Cáceres-Palomo L, Neyrinck K, Da Madeiro Costa R, Dávila JC, Baron-Van Evercooren A, Gutiérrez A, Verfaillie CM (2020) Generation of oligodendrocytes and establishment of an all-human myelinating platform from human pluripotent stem cells *Nat Protoc* 15, 3716–3744.

García-León JA, Kumar M, Boon R, Chau D, One J, Wolfs E, Eggermont K, Berckmans P, Gunhanlar N, Vrij F de, Lendemeijer B, Pavie B, Corthout N, Kushner SA, Dávila JC, Lambrichts I, Hu W-S, Verfaillie CM (2018) SOX10 Single Transcription Factor-Based Fast and Efficient Generation of Oligodendrocytes from Human Pluripotent Stem Cells *Stem Cell Reports* 10, 655–672.

Geden MJ, Deshmukh M (2016) Axon degeneration: context defines distinct pathways *Curr Opin Neurobiol* 39, 108–115.

Geden MJ, Romero SE, Deshmukh M (2019) Apoptosis versus axon pruning: Molecular intersection of two distinct pathways for axon degeneration *Neurosci Res* 139, 3–8.

Gever JR, Soto R, Henningsen RA, Martin RS, Hackos DH, Panicker S, Rubas W, Oglesby IB, Dillon MP, Milla ME, Burnstock G, Ford APDW (2010) AF-353, a novel, potent and orally bioavailable P2X3/P2X2/3 receptor antagonist *Br J Pharmacol* 160, 1387–1398.

Gill JS, Windebank AJ (1998) Cisplatin-induced apoptosis in rat dorsal root ganglion neurons is associated with attempted entry into the cell cycle *J Clin Invest* 101, 2842–2850.

Goodman EC, Iversen LL (1986) Calcitonin gene-related peptide: Novel neuropeptide *Life Sci* 38, 2169–2178.

Gornstein EL, Schwarz TL (2017) Neurotoxic mechanisms of paclitaxel are local to the distal axon and independent of transport defects *Exp Neurol* 288, 153–166.

Govoni V, Granieri E, Casetta I, Tola MR, Paolino E, Fainardi E, Monetti VC (1996) The incidence of Guillain-Barré syndrome in Ferrara, Italy: Is the disease really increasing? *J Neurol Sci* 137, 62–68.

Gramowski A, Stuewe S, Juegelt K, Schiffmann D, Weiss DG (2006) Detecting neurotoxicity through electrical activity changes of neuronal networks on multielectrode neurochips *ALTEX* 23 Suppl, 410–415.

Grapin-Botton A, Melton DA (2000) Endoderm development: from patterning to organogenesis *Trends Genet* 16, 124–130.

Gregg RW, Molepo JM, Monpetit VJ, Mikael NZ, Redmond D, Gadia M, Stewart DJ (1992) Cisplatin neurotoxicity: the relationship between dosage, time, and platinum concentration in neurologic tissues, and morphologic evidence of toxicity *J Clin Oncol* 10, 795–803.

Grynkiewicz G, Poenie M, Tsien RY (1985) A new generation of Ca2+ indicators with greatly improved fluorescence properties *J Biol Chem* 260, 3440–3450.

Guimarães MZP, Vecchi R de, Vitória G, Sochacki JK, Paulsen BS, Lima I, Da Rodrigues Silva F, Da Costa RFM, Castro NG, Breton L, Rehen SK (2018) Generation of iPSC-Derived Human Peripheral Sensory Neurons Releasing Substance P Elicited by TRPV1 Agonists *Front Mol Neurosci* 11, 277.

Gunthorpe MJ, Rami HK, Jerman JC, Smart D, Gill CH, Soffin EM, Luis Hannan S, Lappin SC, Egerton J, Smith GD, Worby A, Howett L, Owen D, Nasir S, Davies CH, Thompson M, Wyman PA, Randall AD, Davis JB (2004) Identification and characterisation of SB-366791, a potent and selective vanilloid receptor (VR1/TRPV1) antagonist *Neuropharmacology* 46, 133–149.

Gustafsson H, Runesson J, Lundqvist J, Lindegren H, Axelsson V, Forsby A (2010) Neurofunctional endpoints assessed in human neuroblastoma SH-SY5Y cells for estimation of acute systemic toxicity *Toxicol Appl Pharmacol* 245, 191–202.

Haber F (1924) Zur Geschichte des Gaskrieges *Fünf Vorträge aus den Jahren 1920–1923* Springer Berlin Heidelberg, 76–92.

Hamill OP, Marty A, Neher E, Sakmann B, Sigworth FJ (1981) Improved patch-clamp techniques for high-resolution current recording from cells and cell-free membrane patches *Pflugers Arch* 391, 85–100.

Harjuhaahto S, Rasila TS, Molchanova SM, Woldegebriel R, Kvist J, Konovalova S, Sainio MT, Pennonen J, Torregrosa-Muñumer R, Ibrahim H, Otonkoski T, Taira T, Ylikallio E, Tyynismaa H (2020) ALS and Parkinson's disease genes CHCHD10 and CHCHD2 modify synaptic transcriptomes in human iPSC-derived motor neurons *Neurobiol Dis* 141, 104940.

Hartung T (2008) Food for thought… on animal tests *ALTEX* 25, 3–16.

Hartung T, Leist M (2008) Food for thought … on the evolution of toxicology and the phasing out of animal testing *ALTEX* 25, 91–102.

Hayashi H, Miyata H (1994) Fluorescence imaging of intracellular Ca2+ *J Pharmacol Toxicol Methods* 31, 1–10.

Heidari A, Shahrabi M, Shahrabi MS, Ghandehari M, Rahbar P (2017) Comparison of the Level of Substance P and Neurokinin A in Gingival Crevicular Fluid of Sound and Symptomatic Carious Primary Teeth by ELISA *J Dent (Tehran)* 14, 173–179.

Herkenham M, Little MD, Bankiewicz K, Yang S-C, Markey SP, Johannessen JN (1991) Selective retention of MPP+ within the monoaminergic systems of the primate brain following MPTP administration: An in vivo autoradiographic study *Neuroscience* 40, 133–158.

Herzig S, Martinou J-C (2008) Mitochondrial dynamics: to be in good shape to survive *Curr Mol Med* 8, 131–137.

Hoelting L, Klima S, Karreman C, Grinberg M, Meisig J, Henry M, Rotshteyn T, Rahnenführer J, Blüthgen N, Sachinidis A, Waldmann T, Leist M (2016) Stem Cell-Derived Immature Human Dorsal Root Ganglia Neurons to Identify Peripheral Neurotoxicants *Stem Cells Transl Med* 5, 476–487.

Hofrichter M, Nimtz L, Tigges J, Kabiri Y, Schröter F, Royer-Pokora B, Hildebrandt B, Schmuck M, Epanchintsev A, Theiss S, Adjaye J, Egly J-M, Krutmann J, Fritsche E (2017) Comparative performance analysis of human iPSC-derived and primary neural progenitor cells (NPC) grown as neurospheres in vitro *Stem Cell Res* 25, 72–82.

Honore P, Kage K, Mikusa J, Watt AT, Johnston JF, Wyatt JR, Faltynek CR, Jarvis MF, Lynch K (2002) Analgesic profile of intrathecal P2X3 antisense oligonucleotide treatment in chronic inflammatory and neuropathic pain states in rats *Pain* 99, 11–19.

Honore P, Wismer CT, Mikusa J, Zhu CZ, Zhong C, Gauvin DM, Gomtsyan A, El Kouhen R, Lee C-H, Marsh K, Sullivan JP, Faltynek CR, Jarvis MF (2005) A-425619 1-isoquinolin-5-yl-3-(4-trifluoromethyl-benzyl)-urea, a novel transient receptor potential type V1 receptor antagonist, relieves pathophysiological pain associated with inflammation and tissue injury in rats *J Pharmacol Exp Ther* 314, 410–421.

Horwitz SB (1994) Taxol (paclitaxel): mechanisms of action *Ann Oncol* 5 Suppl 6, S3-6.

House JS, Grimm FA, Jima DD, Zhou Y-H, Rusyn I, Wright FA (2017) A Pipeline for High-Throughput Concentration Response Modeling of Gene Expression for Toxicogenomics *Front. Genet.* 8, 168.

Hrstka SCL, Ankam S, Agac B, Klein JP, Moore RA, Narapureddy B, Schneider I, Hrstka RF, Dasari S, Staff NP (2021) Proteomic analysis of human iPSC-derived sensory neurons implicates cell stress and microtubule dynamics dysfunction in bortezomib-induced peripheral neurotoxicity *Exp Neurol* 335, 113520.

Hulme AJ, McArthur JR, Maksour S, Miellet S, Ooi L, Adams DJ, Finol-Urdaneta RK, Dottori M (2020) Molecular and Functional Characterization of Neurogenin-2 Induced Human Sensory Neurons *Front Cell Neurosci* 14, 600895.

Immke DC, Gavva NR (2006) The TRPV1 receptor and nociception *Semin Cell Dev Biol* 17, 582–591.

Isensee J, Schild C, Schwede F, Hucho T (2017) Crosstalk from cAMP to ERK1/2 emerges during postnatal maturation of nociceptive neurons and is maintained during aging *J Cell Sci* 130, 2134–2146.

Ishchenko Y, Shakirzyanova A, Giniatullina R, Skorinkin A, Bart G, Turhanen P, Määttä JA, Mönkkönen J, Giniatullin R (2017) Selective Calcium-Dependent Inhibition of ATP-Gated P2X3 Receptors by Bisphosphonate-Induced Endogenous ATP Analog ApppI *J Pharmacol Exp Ther* 361, 472–481.

Israel MR, Tanaka BS, Castro J, Thongyoo P, Robinson SD, Zhao P, Deuis JR, Craik DJ, Durek T, Brierley SM, Waxman SG, Dib-Hajj SD, Vetter I (2019) NaV 1.6 regulates excitability of mechanosensitive sensory neurons *J Physiol* 597, 3751–3768.

Jagannath S, Barlogie B, Berenson J, Siegel D, Irwin D, Richardson PG, Niesvizky R, Alexanian R, Limentani SA, Alsina M, Adams J, Kauffman M, Esseltine D-L, Schenkein DP, Anderson KC (2004) A phase 2 study of two doses of bortezomib in relapsed or refractory myeloma *Br J Haematol* 127, 165–172.

Jancsó N, Jancsó-Gábor A, Szolcsányi J (1967) Direct evidence for neurogenic inflammation and its prevention by denervation and by pretreatment with capsaicin *Br J Pharmacol Chemother* 31, 138–151.

Jang JH, Nam TS, Paik KS, Leem JW (2004) Involvement of peripherally released substance P and calcitonin gene-related peptide in mediating mechanical hyperalgesia in a traumatic neuropathy model of the rat *Neurosci Lett* 360, 129–132.

Jarvis MF (2003) Contributions of P2X3 homomeric and heteromeric channels to acute and chronic pain *Expert Opin Ther Targets* 7, 513–522.

Jarvis MF (2010) The neural-glial purinergic receptor ensemble in chronic pain states *Trends Neurosci* 33, 48–57.

Jarvis MF, Burgard EC, McGaraughty S, Honore P, Lynch K, Brennan TJ, Subieta A, van Biesen T, Cartmell J, Bianchi B, Niforatos W, Kage K, Yu H, Mikusa J, Wismer CT, Zhu CZ, Chu K, Lee C-H, Stewart AO, Polakowski J, Cox BF, Kowaluk E, Williams M, Sullivan J, Faltynek C (2002) A-317491, a novel potent and selective non-nucleotide antagonist of P2X3 and P2X2/3 receptors, reduces chronic inflammatory and neuropathic pain in the rat *Proc Natl Acad Sci U S A* 99, 17179–17184.

Jarvis MF, Honore P, Shieh C-C, Chapman M, Joshi S, Zhang X-F, Kort M, Carroll W, Marron B, Atkinson R, Thomas J, Liu D, Krambis M, Liu Y, McGaraughty S, Chu K, Roeloffs R, Zhong C, Mikusa JP, Hernandez G, Gauvin D, Wade C, Zhu C, Pai M, Scanio M, Shi L, Drizin I, Gregg R, Matulenko M, Hakeem A, Gross M, Johnson M, Marsh K, Wagoner PK, Sullivan JP, Faltynek CR, Krafte DS (2007) A-803467, a potent and selective Nav1.8 sodium channel blocker, attenuates neuropathic and inflammatory pain in the rat *Proc Natl Acad Sci U S A* 104, 8520–8525.

Jennings P (2015) "The future of in vitro toxicology" *Toxicol In Vitro* 29, 1217–1221.

Jeon I, Lee N, Li J-Y, Park I-H, Park KS, Moon J, Shim SH, Choi C, Chang D-J, Kwon J, Oh S-H, Shin DA, Kim HS, Do JT, Lee DR, Kim M, Kang K-S, Daley GQ, Brundin P, Song J (2012) Neuronal properties, in vivo effects, and pathology of a Huntington's disease patient-derived induced pluripotent stem cells *Stem Cells* 30, 2054–2062.

Jeong NY, Shin YH, Jung J (2013) Neuropathic pain in hereditary peripheral neuropathy *J Exerc Rehabil* 9, 397–399.

Ji R-R, Samad TA, Jin S-X, Schmoll R, Woolf CJ (2002) p38 MAPK Activation by NGF in Primary Sensory Neurons after Inflammation Increases TRPV1 Levels and Maintains Heat Hyperalgesia *Neuron* 36, 57–68.

Jones I, Yelhekar TD, Wiberg R, Kingham PJ, Johansson S, Wiberg M, Carlsson L (2018) Development and validation of an in vitro model system to study peripheral sensory neuron development and injury *Sci Rep* 8, 15961.

June CH, Moore JS (2004) Measurement of intracellular ions by flow cytometry *Curr Protoc Immunol* Chapter 5, 5.5.1-5.5.20.

Kanat O, Ertas H, Caner B (2017) Platinum-induced neurotoxicity: A review of possible mechanisms *World J Clin Oncol* 8, 329–335.

Kane RC, Bross PF, Farrell AT, Pazdur R (2003) Velcade: U.S. FDA approval for the treatment of multiple myeloma progressing on prior therapy *Oncologist* 8, 508–513.

Kanzawa-Lee GA, Knoerl R, Donohoe C, Bridges CM, Smith EML (2019) Mechanisms, Predictors, and Challenges in Assessing and Managing Painful Chemotherapy-Induced Peripheral Neuropathy *Semin Oncol Nurs* 35, 253–260.

Karam C, Dyck PJB (2015) Toxic Neuropathies *Semin Neurol* 35, 448–457.

Karashima Y, Talavera K, Everaerts W, Janssens A, Kwan KY, Vennekens R, Nilius B, Voets T (2009) TRPA1 acts as a cold sensor in vitro and in vivo *Proc Natl Acad Sci USA* 106, 1273–1278.

Karreman C, Klima S, Holzer A-K, Leist M (2020) CaFFEE: A program for evaluating time courses of Ca2+ dependent signal changes of complex cells loaded with fluorescent indicator dyes *ALTEX* 37, 332–336.

Kim CH, Oh Y, Chung JM, Chung K (2001) The changes in expression of three subtypes of TTX sensitive sodium channels in sensory neurons after spinal nerve ligation *Mol Brain Res* 95, 153–161.

Kleckner IR, Jusko TA, Culakova E, Chung K, Kleckner AS, Asare M, Inglis JE, Loh KP, Peppone LJ, Miller J, Melnik M, Kasbari S, Ossip D, Mustian KM (2021) Longitudinal study of inflammatory, behavioral, clinical, and psychosocial risk factors for chemotherapy-induced peripheral neuropathy *Breast Cancer Res Treat* 189, 521–532.

Klein R, Nanduri V, Jing SA, Lamballe F, Tapley P, Bryant S, Cordon-Cardo C, Jones KR, Reichardt LF, Barbacid M (1991) The trkB tyrosine protein kinase is a receptor for brain-derived neurotrophic factor and neurotrophin-3 *Cell* 66, 395–403.

Klima S, Brüll M, Spreng A-S, Suciu I, Falt T, Schwamborn JC, Waldmann T, Karreman C, Leist M (2021a) A human stem cell-derived test system for agents modifying neuronal N-methyl-D-aspartate-type glutamate receptor Ca2+-signalling *Arch Toxicol* 95, 1703–1722.

Klima S, Suciu I, Hoelting L, Gutbier S, Waldmann T, Dietrich DR, Leist M (2021b) Examination of microcystin neurotoxicity using central and peripheral human neurons *ALTEX* 38, 73–81.

Klose J, Pahl M, Bartmann K, Bendt F, Blum J, Dolde X, Förster N, Holzer A-K, Hübenthal U, Keßel HE, Koch K, Masjosthusmann S, Schneider S, Stürzl L-C, Woeste S, Rossi A, Covaci A, Behl M, Leist M, Tigges J, Fritsche E (2021) Neurodevelopmental toxicity assessment of flame retardants using a human DNT in vitro testing battery *Cell Biol Toxicol*.

Kole AJ, Annis RP, Deshmukh M (2013) Mature neurons: equipped for survival *Cell Death Dis* 4, e689.

Konishi S, Tsunoo A, Yanaihara N, Otsuka M (1980) Peptidergic excitatory and inhibitory synapses in mammalian sympathetic ganglia: roles of substance P and enkephalin *Biomed Res* 1, 528–536.

Kortuem KM, Stewart AK (2013) Carfilzomib *Blood* 121, 893–897.

Koshimizu TA, van Goor F, Tomić M, Wong AO, Tanoue A, Tsujimoto G, Stojilkovic SS (2000) Characterization of calcium signaling by purinergic receptor-channels expressed in excitable cells *Mol Pharmacol* 58, 936–945.

Kramer I, Sigrist M, Nooij JC de, Taniuchi I, Jessell TM, Arber S (2006) A role for Runx transcription factor signaling in dorsal root ganglion sensory neuron diversification *Neuron* 49, 379–393.

Kraus D, Boyle V, Leibig N, Stark GB, Penna V (2015) The Neuro-spheroid--A novel 3D in vitro model for peripheral nerve regeneration *J Neurosci Methods* 246, 97–105.

Krebs A, van Vugt-Lussenburg BMA, Waldmann T, Albrecht W, Boei J, Braak B ter, Brajnik M, Braunbeck T, Brecklinghaus T, Busquet F, Dinnyes A, Dokler J, Dolde X, Exner TE, Fisher C, Fluri D, Forsby A, Hengstler JG, Holzer A-K, Janstova Z, Jennings P, Kisitu J, Kobolak J, Kumar M, Limonciel A, Lundqvist J, Mihalik B, Moritz W, Pallocca G, Ulloa APC, Pastor M, Rovida C, Sarkans U, Schimming JP, Schmidt BZ, Stöber R, Strassfeld T, van de Water B, Wilmes A, van der Burg B, Verfaillie CM, Hellfeld R von, Vrieling H, Vrijenhoek NG, Leist M (2020) The EU-ToxRisk method documentation, data processing and chemical testing pipeline for the regulatory use of new approach methods *Arch Toxicol* 94, 2435–2461.

Krishan A (1975) Rapid flow cytofluorometric analysis of mammalian cell cycle by propidium iodide staining *J Cell Biol* 66, 188–193.

Krug AK, Balmer NV, Matt F, Schönenberger F, Merhof D, Leist M (2013) Evaluation of a human neurite growth assay as specific screen for developmental neurotoxicants *Arch Toxicol* 87, 2215–2231.

Krug AK, Gutbier S, Zhao L, Pöltl D, Kullmann C, Ivanova V, Förster S, Jagtap S, Meiser J, Leparc G, Schildknecht S, Adam M, Hiller K, Farhan H, Brunner T, Hartung T, Sachinidis A, Leist M (2014) Transcriptional and metabolic adaptation of human neurons to the mitochondrial toxicant MPP(+) *Cell Death Dis* 5, e1222.

Kuegler P, Zimmer B, Waldmann T, Baudis B, Ilmjärv S, Hescheler J, Gaughwin P, Brundin P, Mundy W, Bal-Brice AK, Schrattenholz A, Krause K-H, van Thriel C, Rao MS, Kadereit S, Leist M (2010) Markers of murine embryonic and neural stem cells, neurons and astrocytes: reference points for developmental neurotoxicity testing *ALTEX* 27, 16–42.

Kwan KY, Allchorne AJ, Vollrath MA, Christensen AP, Zhang D-S, Woolf CJ, Corey DP (2006) TRPA1 contributes to cold, mechanical, and chemical nociception but is not essential for hair-cell transduction *Neuron* 50, 277–289.

La Roche J de, Eberhardt MJ, Klinger AB, Stanslowsky N, Wegner F, Koppert W, Reeh PW, Lampert A, Fischer MJM, Leffler A (2013) The molecular basis for species-specific activation of human TRPA1 protein by protons involves poorly conserved residues within transmembrane domains 5 and 6 *J Biol Chem* 288, 20280–20292.

Lallemend F, Ernfors P (2012) Molecular interactions underlying the specification of sensory neurons *Trends Neurosci* 35, 373–381.

Lasek RJ, Garner JA, Brady ST (1984) Axonal transport of the cytoplasmic matrix *J Cell Biol* 99, 212s-221s.

Leeuw SM de, Davaz S, Wanner D, Milleret V, Ehrbar M, Gietl A, Tackenberg C (2021) Increased maturation of iPSC-derived neurons in a hydrogel-based 3D culture *J Neurosci Methods* 360, 109254.

Legha SS (1986) Vincristine neurotoxicity. Pathophysiology and management *Med Toxicol* 1, 421–427.

Lehky TJ, Leonard GD, Wilson RH, Grem JL, Floeter MK (2004) Oxaliplatin-induced neurotoxicity: acute hyperexcitability and chronic neuropathy *Muscle Nerve* 29, 387–392.

Lehmann HC, Staff NP, Hoke A (2020) Modeling chemotherapy induced peripheral neuropathy (CIPN) in vitro: Prospects and limitations *Exp Neurol* 326, 113140.

Leist M, Efremova L, Karreman C (2010) Food for thought … considerations and guidelines for basic test method descriptions in toxicology *ALTEX* 27, 309–317.

Leist M, Nicotera P (1998) Calcium and neuronal death *Rev Physiol Biochem Pharmacol* 132, 79–125.

Levanon D, Brenner O, Negreanu V, Bettoun D, Woolf E, Eilam R, Lotem J, Gat U, Otto F, Speck N, Groner Y (2001) Spatial and temporal expression pattern of Runx3 (Aml2) and Runx1 (Aml1) indicates non-redundant functions during mouse embryogenesis *Mech Dev* 109, 413–417.

Levine JD, Alessandri-Haber N (2007) TRP channels: targets for the relief of pain *Biochim Biophys Acta* 1772, 989–1003.

Li C, Deng T, Shang Z, Di Wang, Xiao Y (2018) Blocking TRPA1 and TNF-α Signal Improves Bortezomib-Induced Neuropathic Pain *Cell Physiol Biochem* 51, 2098–2110.

Li L, Shao J, Wang J, Liu Y, Zhang Y, Zhang M, Zhang J, Ren X, Su S, Li Y, Cao J, Zang W (2019) MiR-30b-5p attenuates oxaliplatin-induced peripheral neuropathic pain through the voltage-gated sodium channel Nav1.6 in rats *Neuropharmacology* 153, 111–120.

Lilja J, Forsby A (2004) Development of a sensory neuronal cell model for the estimation of mild eye irritation *Altern Lab Anim* 32, 339–343.

Lin JH (1995) Species similarities and differences in pharmacokinetics *Drug Metab Dispos* 23, 1008–1021.

Ling B, Coudoré-Civiale M-A, Balayssac D, Eschalier A, Coudoré F, Authier N (2007) Behavioral and immunohistological assessment of painful neuropathy induced by a single oxaliplatin injection in the rat *Toxicology* 234, 176–184.

Livak KJ, Schmittgen TD (2001) Analysis of relative gene expression data using real-time quantitative PCR and the 2(-Delta Delta C(T)) Method *Methods* 25, 402–408.

Lock JT, Parker I, Smith IF (2015) A comparison of fluorescent Ca^{2+} indicators for imaging local Ca^{2+} signals in cultured cells *Cell Calcium* 58, 638–648.

Loser D, Grillberger K, Hinojosa MG, Blum J, Haufe Y, Danker T, Johansson Y, Möller C, Nicke A, Bennekou SH, Gardner I, Bauch C, Walker P, Forsby A, Ecker GF, Kraushaar U, Leist M (2021a) Acute effects of the imidacloprid metabolite desnitro-imidacloprid on human nACh receptors relevant for neuronal signaling *Arch Toxicol* 95, 3695–3716.

Loser D, Hinojosa MG, Blum J, Schaefer J, Brüll M, Johansson Y, Suciu I, Grillberger K, Danker T, Möller C, Gardner I, Ecker GF, Bennekou SH, Forsby A, Kraushaar U, Leist M (2021b) Functional alterations by a subgroup of neonicotinoid pesticides in human dopaminergic neurons *Arch Toxicol* 95, 2081–2107.

Loser D, Schaefer J, Danker T, Möller C, Brüll M, Suciu I, Ückert A-K, Klima S, Leist M, Kraushaar U (2021c) Human neuronal signaling and communication assays to assess functional neurotoxicity *Arch Toxicol* 95, 229–252.

Love MI, Huber W, Anders S (2014) Moderated estimation of fold change and dispersion for RNA-seq data with DESeq2 *Genome Biol* 15, 550.

Ludman T, Melemedjian OK (2019) Bortezomib-induced aerobic glycolysis contributes to chemotherapy-induced painful peripheral neuropathy *Mol Pain* 15, 1-17.

Ly CV, Verstreken P (2006) Mitochondria at the synapse *Neuroscientist* 12, 291–299.

Ma Q, Chen Z, Del Barrantes IB, La Luis de Pompa J, Anderson DJ (1998) neurogenin1 Is Essential for the Determination of Neuronal Precursors for Proximal Cranial Sensory Ganglia *Neuron* 20, 469–482.

Ma Q, Fode C, Guillemot F, Anderson DJ (1999) Neurogenin1 and neurogenin2 control two distinct waves of neurogenesis in developing dorsal root ganglia *Genes Dev* 13, 1717–1728.

Ma Q, Ye L, Liu H, Shi Y, Zhou N (2017) An overview of Ca2+ mobilization assays in GPCR drug discovery *Expert Opin Drug Discov* 12, 511–523.

Macko P, Palosaari T, Whelan M (2021) Extrapolating from acute to chronic toxicity in vitro *Toxicol In Vitro* 76, 105206.

Marmigère F, Ernfors P (2007) Specification and connectivity of neuronal subtypes in the sensory lineage *Nat Rev Neurosci* 8, 114–127.

Marrs TC, Maynard RL (2013) Neurotranmission systems as targets for toxicants: a review *Cell Biol Toxicol* 29, 381–396.

Masjosthusmann S, Blum J, Bartmann K, Dolde X, Holzer A-K, Stürzl L-C, Keßel EH, Förster N, Dönmez A, Klose J, Pahl M, Waldmann T, Bendt F, Kisitu J, Suciu I, Hübenthal U, Mosig A, Leist M, Fritsche E (2020) Establishment of an a priori protocol for the implementation

and interpretation of an in-vitro testing battery for the assessment of developmental neurotoxicity *EFSA Support Publ* 17, 1938E.

Mattson MP (1992) Calcium as sculptor and destroyer of neural circuitry *Exp Gerontol* 27, 29–49.

McLeod JG (1995) Investigation of peripheral neuropathy *J Neurol Neurosurg Psychiatry* 58, 274–283.

McMahon SB, Armanini MP, Ling LH, Phillips HS (1994) Expression and coexpression of Trk receptors in subpopulations of adult primary sensory neurons projecting to identified peripheral targets *Neuron* 12, 1161–1171.

Meregalli C, Chiorazzi A, Carozzi VA, Canta A, Sala B, Colombo M, Oggioni N, Ceresa C, Foudah D, La Russa F, Miloso M, Nicolini G, Marmiroli P, Bennett DL, Cavaletti G (2014) Evaluation of tubulin polymerization and chronic inhibition of proteasome as citotoxicity mechanisms in bortezomib-induced peripheral neuropathy *Cell Cycle* 13, 612–621.

Miltenburg NC, Boogerd W (2014) Chemotherapy-induced neuropathy: A comprehensive survey *Cancer Treat Rev* 40, 872–882.

Mols F, Beijers T, Vreugdenhil G, van de Poll-Franse L (2014) Chemotherapy-induced peripheral neuropathy and its association with quality of life: a systematic review *Support Care Cancer* 22, 2261–2269.

Mondal B, Jin H, Kallappagoudar S, Sedkov Y, Martinez T, Sentmanat MF, Poet GJ, Li C, Fan Y, Pruett-Miller SM, Herz H-M (2020) The histone deacetylase complex MiDAC regulates a neurodevelopmental gene expression program to control neurite outgrowth *Elife* 9, e57519.

Morgan JP (1982) The Jamaica ginger paralysis *JAMA* 248, 1864–1867.

Morrison G, Liu C, Wing C, Delaney SM, Zhang W, Dolan ME (2016) Evaluation of inter-batch differences in stem-cell derived neurons *Stem Cell Res* 16, 140–148.

Mosmann T (1983) Rapid colorimetric assay for cellular growth and survival: Application to proliferation and cytotoxicity assays *J Immunol Methods* 65, 55–63.

Mudge AW (1984) Schwann cells induce morphological transformation of sensory neurones in vitro *Nature* 309, 367–369.

Murray D, Wigglesworth M (2016) Chapter 1. HTS Methods: Assay Design and Optimisation *High Throughput Screening Methods* Royal Society of Chemistry (Chemical Biology), 1–15.

Nakamura F, Strittmatter SM (1996) P2Y1 purinergic receptors in sensory neurons: contribution to touch-induced impulse generation *Proc Natl Acad Sci U S A* 93, 10465–10470.

Namer B, Schick M, Kleggetveit IP, Ørstavik K, Schmidt R, Jorum E, Torebjörk E, Handwerker H, Schmelz M (2015) Differential sensitization of silent nociceptors to low pH stimulation by prostaglandin E2 in human volunteers *Eur J Pain* 19, 159–166.

Narahashi T (1996) Neuronal ion channels as the target sites of insecticides *Pharmacol Toxicol* 79, 1–14.

Nickolls AR, Lee MM, Espinoza DF, Szczot M, Lam RM, Wang Q, Beers J, Zou J, Nguyen MQ, Solinski HJ, AlJanahi AA, Johnson KR, Ward ME, Chesler AT, Bönnemann CG (2020) Transcriptional Programming of Human Mechanosensory Neuron Subtypes from Pluripotent Stem Cells *Cell Rep* 30, 932-946.e7.

Nicolini G, Monfrini M, Scuteri A (2015) Axonal Transport Impairment in Chemotherapy-Induced Peripheral Neuropathy *Toxics* 3, 322–341.

Nikasa P, Tricot T, Mahdieh N, Baharvand H, Totonchi M, Hejazi MS, Verfaillie CM (2021) Patient-Specific Induced Pluripotent Stem Cell-Derived Hepatocyte-Like Cells as a Model to Study Autosomal Recessive Hypercholesterolemia *Stem Cells Dev* 30, 714–724.

Nikolopoulou E, Galea GL, Rolo A, Greene NDE, Copp AJ (2017) Neural tube closure: cellular, molecular and biomechanical mechanisms *Development* 144, 552–566.

Nimtz L, Hartmann J, Tigges J, Masjosthusmann S, Schmuck M, Keßel E, Theiss S, Köhrer K, Petzsch P, Adjaye J, Wigmann C, Wieczorek D, Hildebrandt B, Bendt F, Hübenthal U, Brockerhoff G, Fritsche E (2020) Characterization and application of electrically active neuronal networks established from human induced pluripotent stem cell-derived neural progenitor cells for neurotoxicity evaluation *Stem Cell Res* 45, 101761.

Niwa S, Takahashi H, Hirokawa N (2013) β-Tubulin mutations that cause severe neuropathies disrupt axonal transport *EMBO J* 32, 1352–1364.

North RA (2002) Molecular physiology of P2X receptors *Physiol Rev* 82, 1013–1067.

North RA (2003) The P2X3 subunit: a molecular target in pain therapeutics *Curr Opin Investig Drugs* 4, 833–840.

North RA (2004) P2X3 receptors and peripheral pain mechanisms *J Physiol* 554, 301–308.

Nyffeler J, Dolde X, Krebs A, Pinto-Gil K, Pastor M, Behl M, Waldmann T, Leist M (2017) Combination of multiple neural crest migration assays to identify environmental toxicants from a proof-of-concept chemical library *Arch Toxicol* 91, 3613–3632.

OECD (2018) Guidance Document on Good In Vitro Method Practices (GIVIMP). OECD Series on Testing and Assessment, No. 286, OECD Publishing, Paris.

O'Rahilly R, Müller F (2010) Developmental stages in human embryos: revised and new measurements *Cells Tissues Organs* 192, 73–84.

Orozco OE, Walus L, Sah DW, Pepinsky RB, Sanicola M (2001) GFRalpha3 is expressed predominantly in nociceptive sensory neurons *Eur J Neurosci* 13, 2177–2182.

Orrenius S, Zhivotovsky B, Nicotera P (2003) Regulation of cell death: the calcium-apoptosis link *Nat Rev Mol Cell Biol* 4, 552–565.

Pamies D, Bal-Price A, Chesné C, Coecke S, Dinnyes A, Eskes C, Grillari R, Gstraunthaler G, Hartung T, Jennings P, Leist M, Martin U, Passier R, Schwamborn JC, Stacey GN, Ellinger-Ziegelbauer H, Daneshian M (2018) Advanced Good Cell Culture Practice for human primary, stem cell-derived and organoid models as well as microphysiological systems *ALTEX* 35, 353–378.

Pamies D, Sogorb MA, Fabbri M, Gribaldo L, Collotta A, Scelfo B, Vilanova E, Harris G, Bal-Price A (2014) Genomic and phenotypic alterations of the neuronal-like cells derived from human embryonal carcinoma stem cells (NT2) caused by exposure to organophosphorus compounds paraoxon and mipafox *Int J Mol Sci* 15, 905–926.

Papandreou CN, Daliani DD, Nix D, Yang H, Madden T, Wang X, Pien CS, Millikan RE, Tu S-M, Pagliaro L, Kim J, Adams J, Elliott P, Esseltine D, Petrusich A, Dieringer P, Perez C, Logothetis CJ (2004) Phase I trial of the proteasome inhibitor bortezomib in patients with

advanced solid tumors with observations in androgen-independent prostate cancer *J Clin Oncol* 22, 2108–2121.

Parish ST, Aschner M, Casey W, Corvaro M, Embry MR, Fitzpatrick S, Kidd D, Kleinstreuer NC, Lima BS, Settivari RS, Wolf DC, Yamazaki D, Boobis A (2020) An evaluation framework for new approach methodologies (NAMs) for human health safety assessment *: RTP* 112, 104592.

Park SB, Goldstein D, Krishnan AV, Lin CS-Y, Friedlander ML, Cassidy J, Koltzenburg M, Kiernan MC (2013) Chemotherapy-induced peripheral neurotoxicity: a critical analysis *CA Cancer J Clin* 63, 419–437.

Park SB, Krishnan AV, Lin CS-Y, Goldstein D, Friedlander M, Kiernan MC (2008) Mechanisms underlying chemotherapy-induced neurotoxicity and the potential for neuroprotective strategies *Curr Med Chem* 15, 3081–3094.

Partanen J, Niskanen L, Lehtinen J, Mervaala E, Siitonen O, Uusitupa M (1995) Natural history of peripheral neuropathy in patients with non-insulin-dependent diabetes mellitus *N Engl J Med* 333, 89–94.

Peier AM, Moqrich A, Hergarden AC, Reeve AJ, Andersson DA, Story GM, Earley TJ, Dragoni I, McIntyre P, Bevan S, Patapoutian A (2002) A TRP Channel that Senses Cold Stimuli and Menthol *Cell* 108, 705–715.

Perner C, Flayer CH, Zhu X, Aderhold PA, Dewan ZNA, Voisin T, Camire RB, Chow OA, Chiu IM, Sokol CL (2020) Substance P Release by Sensory Neurons Triggers Dendritic Cell Migration and Initiates the Type-2 Immune Response to Allergens *Immunity* 53, 1063-1077.e7.

Pinho-Ribeiro FA, Verri WA, Chiu IM (2017) Nociceptor Sensory Neuron-Immune Interactions in Pain and Inflammation *Trends Immunol* 38, 5–19.

Piva R, Ruggeri B, Williams M, Costa G, Tamagno I, Ferrero D, Giai V, Coscia M, Peola S, Massaia M, Pezzoni G, Allievi C, Pescalli N, Cassin M, Di Giovine S, Nicoli P, Feudis P de, Strepponi I, Roato I, Ferracini R, Bussolati B, Camussi G, Jones-Bolin S, Hunter K, Zhao H, Neri A, Palumbo A, Berkers C, Ovaa H, Bernareggi A, Inghirami G (2008) CEP-18770: A novel, orally active proteasome inhibitor with a tumor-selective pharmacologic profile competitive with bortezomib *Blood* 111, 2765–2775.

Portanova JP, Zhang Y, Anderson GD, Hauser SD, Masferrer JL, Seibert K, Gregory SA, Isakson PC (1996) Selective neutralization of prostaglandin E2 blocks inflammation, hyperalgesia, and interleukin 6 production in vivo *J Exp Med* 184, 883–891.

Poruchynsky MS, Sackett DL, Robey RW, Ward Y, Annunziata C, Fojo T (2008) Proteasome inhibitors increase tubulin polymerization and stabilization in tissue culture cells: a possible mechanism contributing to peripheral neuropathy and cellular toxicity following proteasome inhibition *Cell Cycle* 7, 940–949.

R Core Team (2020) R: A language and environment for statistical computing *R Foundation for Statistical Computing, Vienna, Austria.* https://www.R-project.org.

Radio NM, Mundy WR (2008) Developmental neurotoxicity testing in vitro: models for assessing chemical effects on neurite outgrowth *Neurotoxicology* 29, 361–376.

Ramirez CN, Antczak C, Djaballah H (2010) Cell viability assessment: toward content-rich platforms *Expert Opin Drug Discov* 5, 223–233.

Ramsey IS, Delling M, Clapham DE (2006) An introduction to TRP channels *Annu Rev Physiol* 68, 619–647.

Rana P, Luerman G, Hess D, Rubitski E, Adkins K, Somps C (2017) Utilization of iPSC-derived human neurons for high-throughput drug-induced peripheral neuropathy screening *Toxicol In Vitro* 45, 111–118.

Raudvere U, Kolberg L, Kuzmin I, Arak T, Adler P, Peterson H, Vilo J (2019) g:Profiler: a web server for functional enrichment analysis and conversions of gene lists (2019 update) *Nucleic Acids Res* 47, W191-W198.

Reece DE, Sullivan D, Lonial S, Mohrbacher AF, Chatta G, Shustik C, Burris H, Venkatakrishnan K, Neuwirth R, Riordan WJ, Karol M, Moltke LL von, Acharya M, Zannikos P, Keith Stewart A (2011) Pharmacokinetic and pharmacodynamic study of two doses of bortezomib in patients with relapsed multiple myeloma *Cancer Chemother Pharmacol* 67, 57–67.

Rempel E, Hoelting L, Waldmann T, Balmer NV, Schildknecht S, Grinberg M, Das Gaspar JA, Shinde V, Stöber R, Marchan R, van Thriel C, Liebing J, Meisig J, Blüthgen N, Sachinidis A, Rahnenführer J, Hengstler JG, Leist M (2015) A transcriptome-based classifier to identify developmental toxicants by stem cell testing: design, validation and optimization for histone deacetylase inhibitors *Arch Toxicol* 89, 1599–1618.

Richardson PG, Barlogie B, Berenson J, Singhal S, Jagannath S, Irwin D, Rajkumar SV, Srkalovic G, Alsina M, Alexanian R, Siegel D, Orlowski RZ, Kuter D, Limentani SA, Lee S, Hideshima T, Esseltine D-L, Kauffman M, Adams J, Schenkein DP, Anderson KC (2003) A phase 2 study of bortezomib in relapsed, refractory myeloma *N Engl J Med* 348, 2609–2617.

Richardson PG, Briemberg H, Jagannath S, Wen PY, Barlogie B, Berenson J, Singhal S, Siegel DS, Irwin D, Schuster M, Srkalovic G, Alexanian R, Rajkumar SV, Limentani S, Alsina M, Orlowski RZ, Najarian K, Esseltine D, Anderson KC, Amato AA (2006) Frequency, characteristics, and reversibility of peripheral neuropathy during treatment of advanced multiple myeloma with bortezomib *J Clin Oncol* 24, 3113–3120.

Richardson PG, Xie W, Mitsiades C, Chanan-Khan AA, Lonial S, Hassoun H, Avigan DE, Oaklander AL, Kuter DJ, Wen PY, Kesari S, Briemberg HR, Schlossman RL, Munshi NC, Heffner LT, Doss D, Esseltine D-L, Weller E, Anderson KC, Amato AA (2009) Single-agent bortezomib in previously untreated multiple myeloma: efficacy, characterization of peripheral neuropathy, and molecular correlations with response and neuropathy *J Clin Oncol* 27, 3518–3525.

Riva B, Dionisi M, Potenzieri A, Chiorazzi A, Cordero-Sanchez C, Rigolio R, Carozzi VA, Lim D, Cavaletti G, Marmiroli P, Distasi C, Genazzani AA (2018) Oxaliplatin induces pH acidification in dorsal root ganglia neurons *Sci Rep* 8, 15084.

Rizzuto R, Pinton P, Carrington W, Fay FS, Fogarty KE, Lifshitz LM, Tuft RA, Pozzan T (1998) Close contacts with the endoplasmic reticulum as determinants of mitochondrial Ca2+ responses *Science* 280, 1763–1766.

Ronzhina M, Cmiel V, Janoušek O, Kolářová J, Nováková M, Babula P, Provazník I (2013) Application of the optical method in experimental cardiology: action potential and intracellular calcium concentration measurement *Physiol Res* 62, 125–137.

Roopa, Kumar N, Kumar M, Bhalla V (2019) Design and Applications of Small Molecular Probes for Calcium Detection *Chem Asian J* 14, 4493–4505.

Rossi AM, Taylor CW (2020) Reliable measurement of free Ca2+ concentrations in the ER lumen using Mag-Fluo-4 *Cell Calcium* 87, 102188.

Rostock C, Schrenk-Siemens K, Pohle J, Siemens J (2018) Human vs. Mouse Nociceptors - Similarities and Differences *Neuroscience* 387, 13–27.

Russell W, Burch R (1959) The Principles of Humane Experimental Technique, Methuen & Co. Ltd., London.

Saito-Diaz K, Street JR, Ulrichs H, Zeltner N (2021) Derivation of Peripheral Nociceptive, Mechanoreceptive, and Proprioceptive Sensory Neurons from the same Culture of Human Pluripotent Stem Cells *Stem Cell Rep* 16, 446–457.

San Miguel JF, Schlag R, Khuageva NK, Dimopoulos MA, Shpilberg O, Kropff M, Spicka I, Petrucci MT, Palumbo A, Samoilova OS, Dmoszynska A, Abdulkadyrov KM, Schots R, Jiang B, Mateos M-V, Anderson KC, Esseltine DL, Liu K, Cakana A, van de Velde H, Richardson PG (2008) Bortezomib plus melphalan and prednisone for initial treatment of multiple myeloma *N Engl J Med* 359, 906–917.

Sanchez-Ramos J, Song S, Cardozo-Pelaez F, Hazzi C, Stedeford T, Willing A, Freeman TB, Saporta S, Janssen W, Patel N, Cooper DR, Sanberg PR (2000) Adult bone marrow stromal cells differentiate into neural cells in vitro *Exp Neurol* 164, 247–256.

Scelfo B, Politi M, Reniero F, Palosaari T, Whelan M, Zaldívar J-M (2012) Application of multielectrode array (MEA) chips for the evaluation of mixtures neurotoxicity *Toxicology* 299, 172–183.

Schildknecht S, Karreman C, Pöltl D, Efrémova L, Kullmann C, Gutbier S, Krug A, Scholz D, Gerding HR, Leist M (2013) Generation of genetically-modified human differentiated cells for toxicological tests and the study of neurodegenerative diseases *ALTEX* 30, 427–444.

Schinke C, Fernandez Vallone V, Ivanov A, Peng Y, Körtvelyessy P, Nolte L, Huehnchen P, Beule D, Stachelscheid H, Boehmerle W, Endres M (2021) Modeling chemotherapy induced neurotoxicity with human induced pluripotent stem cell (iPSC) -derived sensory neurons *Neurobiol Dis* 155, 105391.

Schlafer D, Shah KS, Panjic EH, Lonial S (2017) Safety of proteasome inhibitors for treatment of multiple myeloma *Expert Opin Drug Saf* 16, 167–183.

Schmidt BZ, Lehmann M, Gutbier S, Nembo E, Noel S, Smirnova L, Forsby A, Hescheler J, Avci HX, Hartung T, Leist M, Kobolák J, Dinnyés A (2017) In vitro acute and developmental neurotoxicity screening: an overview of cellular platforms and high-throughput technical possibilities *Arch Toxicol* 91, 1–33.

Scholz D, Pöltl D, Genewsky A, Weng M, Waldmann T, Schildknecht S, Leist M (2011) Rapid, complete and large-scale generation of post-mitotic neurons from the human LUHMES cell line *J Neurochem* 119, 957–971.

Schrenk-Siemens K, Wende H, Prato V, Song K, Rostock C, Loewer A, Utikal J, Lewin GR, Lechner SG, Siemens J (2015) PIEZO2 is required for mechanotransduction in human stem cell-derived touch receptors *Nat Neurosci* 18, 10–16.

Schwartzentruber J, Foskolou S, Kilpinen H, Rodrigues J, Alasoo K, Knights AJ, Patel M, Goncalves A, Ferreira R, Benn CL, Wilbrey A, Bictash M, Impey E, Cao L, Lainez S, Loucif AJ, Whiting PJ, Gutteridge A, Gaffney DJ (2018) Molecular and functional variation in iPSC-derived sensory neurons *Nat Genet* 50, 54–61.

Schwiebert LM, Rice WC, Kudlow BA, Taylor AL, Schwiebert EM (2002) Extracellular ATP signaling and P2X nucleotide receptors in monolayers of primary human vascular endothelial cells *Am J Physiol Cell Physiol* 282, C289-301.

Selleck MA, Bronner-Fraser M (1995) Origins of the avian neural crest: the role of neural plate-epidermal interactions *Development* 121, 525–538.

Seretny M, Currie GL, Sena ES, Ramnarine S, Grant R, MacLeod MR, Colvin LA, Fallon M (2014) Incidence, prevalence, and predictors of chemotherapy-induced peripheral neuropathy: A systematic review and meta-analysis *Pain* 155, 2461–2470.

Serrano A, Mo G, Grant R, Paré M, O'Donnell D, Yu XH, Tomaszewski MJ, Perkins MN, Séguéla P, Cao CQ (2012) Differential expression and pharmacology of native P2X receptors in rat and primate sensory neurons *J Neurosci* 32, 11890–11896.

Shafer TJ (2019) Application of Microelectrode Array Approaches to Neurotoxicity Testing and Screening *Adv Neurobiol* 22, 275–297.

Shah A, Hoffman EM, Mauermann ML, Loprinzi CL, Windebank AJ, Klein CJ, Staff NP (2018) Incidence and disease burden of chemotherapy-induced peripheral neuropathy in a population-based cohort *J Neurol Neurosurg Psychiatry* 89, 636–641.

Sharma S, Lagisetti C, Poliks B, Coates RM, Kingston DGI, Bane S (2013) Dissecting paclitaxel-microtubule association: quantitative assessment of the 2'-OH group *Biochemistry* 52, 2328–2336.

Sheahan TD, Valtcheva MV, McIlvried LA, Pullen MY, Baranger DAA, Gereau RW (2018) Metabotropic Glutamate Receptor 2/3 (mGluR2/3) Activation Suppresses TRPV1 Sensitization in Mouse, But Not Human, Sensory Neurons *eNeuro* 5, e0412-17.2018 1–11.

Sherrington CS (1903) Qualitative difference of spinal reflex corresponding with qualitative difference of cutaneous stimulus *J Physiol* 30, 39–46.

Shih P-Y, Kreir M, Kumar D, Seibt F, Pestana F, Schmid B, Holst B, Clausen C, Steeg R, Fischer B, Pita-Almenar J, Ebneth A, Cabrera-Socorro A (2021) Development of a fully human assay combining NGN2-inducible neurons co-cultured with iPSC-derived astrocytes amenable for electrophysiological studies *Stem Cell Res* 54, 102386.

Shimozuma K, Ohashi Y, Takeuchi A, Aranishi T, Morita S, Kuroi K, Ohsumi S, Makino H, Katsumata N, Kuranami M, Suemasu K, Watanabe T, Hausheer FH (2012) Taxane-induced peripheral neuropathy and health-related quality of life in postoperative breast cancer patients undergoing adjuvant chemotherapy: N-SAS BC 02, a randomized clinical trial *Support Care Cancer* 20, 3355–3364.

Shinde V, Hoelting L, Srinivasan SP, Meisig J, Meganathan K, Jagtap S, Grinberg M, Liebing J, Bluethgen N, Rahnenführer J, Rempel E, Stoeber R, Schildknecht S, Förster S, Godoy P, van Thriel C, Gaspar JA, Hescheler J, Waldmann T, Hengstler JG, Leist M, Sachinidis A (2017) Definition of transcriptome-based indices for quantitative characterization of chemically disturbed stem cell development: introduction of the STOP-Toxukn and STOP-Toxukk tests *Arch Toxicol* 91, 839–864.

Siau C, Bennett GJ (2006) Dysregulation of cellular calcium homeostasis in chemotherapy-evoked painful peripheral neuropathy *Anesth Analg* 102, 1485–1490.

Siau C, Xiao W, Bennett GJ (2006) Paclitaxel- and vincristine-evoked painful peripheral neuropathies: loss of epidermal innervation and activation of Langerhans cells *Exp Neurol* 201, 507–514.

Siegel D, Martin T, Nooka A, Harvey RD, Vij R, Niesvizky R, Badros AZ, Jagannath S, McCulloch L, Rajangam K, Lonial S (2013) Integrated safety profile of single-agent carfilzomib: experience from 526 patients enrolled in 4 phase II clinical studies *Haematologica* 98, 1753–1761.

Siegel DS (2013) From clinical trials to clinical practice: single-agent carfilzomib adverse events and their management in patients with relapsed and/or refractory multiple myeloma *Ther Adv Hematol* 4, 354–365.

Sietsema WK (1989) The absolute oral bioavailability of selected drugs *Int J Clin Pharmacol Ther Toxicol* 27, 179–211.

Simpson AWM (2006) Fluorescent measurement of Ca2+c: basic practical considerations *Methods Mol Biol* 312, 3–36.

Sleeper AA, Cummins TR, Dib-Hajj SD, Hormuzdiar W, Tyrrell L, Waxman SG, Black JA (2000) Changes in Expression of Two Tetrodotoxin-Resistant Sodium Channels and Their Currents in Dorsal Root Ganglion Neurons after Sciatic Nerve Injury But Not Rhizotomy *J Neurosci* 20, 7279–7289.

Smirnova L, Harris G, Delp J, Valadares M, Pamies D, Hogberg HT, Waldmann T, Leist M, Hartung T (2016) A LUHMES 3D dopaminergic neuronal model for neurotoxicity testing allowing long-term exposure and cellular resilience analysis *Arch Toxicol* 90, 2725–2743.

Smith JA, Slusher BS, Wozniak KM, Farah MH, Smiyun G, Wilson L, Feinstein S, Jordan MA (2016) Structural Basis for Induction of Peripheral Neuropathy by Microtubule-Targeting Cancer Drugs *Cancer Res* 76, 5115–5123.

Snider WD, McMahon SB (1998) Tackling Pain at the Source: New Ideas about Nociceptors *Neuron* 20, 629–632.

Snijders KE, Fehér A, Táncos Z, Bock I, Téglási A, van den Berk L, Niemeijer M, Bouwman P, Le Dévédec SE, Moné MJ, van Rossom R, Kumar M, Wilmes A, Jennings P, Verfaillie CM, Kobolák J, Braak B ter, Dinnyés A, van de Water B (2021) Fluorescent tagging of endogenous Heme oxygenase-1 in human induced pluripotent stem cells for high content imaging of oxidative stress in various differentiated lineages *Arch Toxicol* 95, 3285–3302.

Snyder C, Yu L, Ngo T, Sheinson D, Zhu Y, Tseng M, Misner D, Staflin K (2018) In vitro assessment of chemotherapy-induced neuronal toxicity *Toxicol In Vitro* 50, 109–123.

Souslova V, Cesare P, Ding Y, Akopian AN, Stanfa L, Suzuki R, Carpenter K, Dickenson A, Boyce S, Hill R, Nebenuis-Oosthuizen D, Smith AJ, Kidd EJ, Wood JN (2000) Warm-coding deficits and aberrant inflammatory pain in mice lacking P2X3 receptors *Nature* 407, 1015–1017.

St Germain DC, O'Mara AM, Robinson JL, Torres AD, Minasian LM (2020) Chemotherapy-induced peripheral neuropathy: Identifying the research gaps and associated changes to clinical trial design *Cancer* 126, 4602–4613.

Stacey P, Wassermann AM, Kammonen L, Impey E, Wilbrey A, Cawkill D (2018) Plate-Based Phenotypic Screening for Pain Using Human iPSC-Derived Sensory Neurons *SLAS Discov* 23, 585–596.

Staff NP, Cavaletti G, Islam B, Lustberg M, Psimaras D, Tamburin S (2019) Platinum-induced peripheral neurotoxicity: From pathogenesis to treatment *JPNS* 24 Suppl 2, S26-S39.

Staff NP, Grisold A, Grisold W, Windebank AJ (2017) Chemotherapy-induced peripheral neuropathy: A current review *Ann Neurol* 81, 772–781.

Staff NP, Podratz JL, Grassner L, Bader M, Paz J, Knight AM, Loprinzi CL, Trushina E, Windebank AJ (2013) Bortezomib alters microtubule polymerization and axonal transport in rat dorsal root ganglion neurons *Neurotoxicology* 39, 124–131.

Starkus J, Jansen C, Shimoda LMN, Stokes AJ, Small-Howard AL, Turner H (2019) Diverse TRPV1 responses to cannabinoids *Channels* 13, 172–191.

Stephan G, Huang L, Tang Y, Vilotti S, Fabbretti E, Yu Y, Nörenberg W, Franke H, Gölöncsér F, Sperlágh B, Dopychai A, Hausmann R, Schmalzing G, Rubini P, Illes P (2018) The ASIC3/P2X3 cognate receptor is a pain-relevant and ligand-gated cationic channel *Nat Commun* 9, 1354.

Stiegler NV, Krug AK, Matt F, Leist M (2011) Assessment of chemical-induced impairment of human neurite outgrowth by multiparametric live cell imaging in high-density cultures *Toxicol Sci* 121, 73–87.

Strickland JD, Martin MT, Richard AM, Houck KA, Shafer TJ (2018) Screening the ToxCast phase II libraries for alterations in network function using cortical neurons grown on multi-well microelectrode array (mwMEA) plates *Arch Toxicol* 92, 487–500.

Summers DW, DiAntonio A, Milbrandt J (2014) Mitochondrial dysfunction induces Sarm1-dependent cell death in sensory neurons *J Neurosci* 34, 9338–9350.

Takaku S, Yanagisawa H, Watabe K, Horie H, Kadoya T, Sakumi K, Nakabeppu Y, Poirier F, Sango K (2013) GDNF promotes neurite outgrowth and upregulates galectin-1 through the RET/PI3K signaling in cultured adult rat dorsal root ganglion neurons *Neurochem Int* 62, 330–339.

Terron A, Bennekou SH (2018) Towards a regulatory use of alternative developmental neurotoxicity testing (DNT) *Toxicol Appl Pharmacol* 354, 19–23.

Terryn J, Welkenhuysen M, Krylychkina O, Firrincieli A, Andrei A, Reumers V, van Damme P, Braeken D, Verfaillie C (2018) Topographical Guidance of PSC-Derived Cortical Neurons *J Nanomater* 2018, 1–10.

Tessarollo L, Tsoulfas P, Martin-Zanca D, Gilbert DJ, Jenkins NA, Copeland NG, Parada LF (1993) trkC, a receptor for neurotrophin-3, is widely expressed in the developing nervous system and in non-neuronal tissues *Development* 118, 463–475.

Toma K, Wang T-C, Hanashima C (2016) Encoding and decoding time in neural development *Dev Growth Differ* 58, 59–72.

Tominaga M, Caterina MJ, Malmberg AB, Rosen TA, Gilbert H, Skinner K, Raumann BE, Basbaum AI, Julius D (1998) The Cloned Capsaicin Receptor Integrates Multiple Pain-Producing Stimuli *Neuron* 21, 531–543.

Tomita S, Sekiguchi F, Deguchi T, Miyazaki T, Ikeda Y, Tsubota M, Yoshida S, Du Nguyen H, Okada T, Toyooka N, Kawabata A (2019) Critical role of Cav3.2 T-type calcium channels in the peripheral neuropathy induced by bortezomib, a proteasome-inhibiting chemotherapeutic agent, in mice *Toxicology* 413, 33–39.

Trevisan G, Materazzi S, Fusi C, Altomare A, Aldini G, Lodovici M, Patacchini R, Geppetti P, Nassini R (2013) Novel therapeutic strategy to prevent chemotherapy-induced persistent sensory neuropathy by TRPA1 blockade *Cancer Res* 73, 3120–3131.

Tsien RW, Tsien RY (1990) Calcium channels, stores, and oscillations *Annu Rev Cell Biol* 6, 715–760.

Tsien RY (1981) A non-disruptive technique for loading calcium buffers and indicators into cells *Nature* 290, 527–528.

Tsien RY (1992) Intracellular signal transduction in four dimensions: from molecular design to physiology *Am J Physiol* 263, C723-C728.

Ursu D, Knopp K, Beattie RE, Liu B, Sher E (2010) Pungency of TRPV1 agonists is directly correlated with kinetics of receptor activation and lipophilicity *Eur J Pharmacol* 641, 114–122.

Usoskin D, Furlan A, Islam S, Abdo H, Lönnerberg P, Lou D, Hjerling-Leffler J, Haeggström J, Kharchenko O, Kharchenko PV, Linnarsson S, Ernfors P (2015) Unbiased classification of sensory neuron types by large-scale single-cell RNA sequencing *Nat Neurosci* 18, 145–153.

Valensi-Kurtz M, Lefler S, Cohen MA, Aharonowiz M, Cohen-Kupiec R, Sheinin A, Ashery U, Reubinoff B, Weil M (2010) Enriched population of PNS neurons derived from human embryonic stem cells as a platform for studying peripheral neuropathies *PLoS One* 5, e9290.

Valentine WM (2020) Toxic Peripheral Neuropathies: Agents and Mechanisms *Toxicol Pathol* 48, 152–173.

van Steenwinckel J, Noghero A, Thibault K, Brisorgueil M-J, Fischer J, Conrath M (2009) The 5-HT2A receptor is mainly expressed in nociceptive sensory neurons in rat lumbar dorsal root ganglia *Neuroscience* 161, 838–846.

Varga A, Németh J, Szabó A, McDougall JJ, Zhang C, Elekes K, Pintér E, Szolcsányi J, Helyes Z (2005) Effects of the novel TRPV1 receptor antagonist SB366791 in vitro and in vivo in the rat *Neurosci Lett* 385, 137–142.

Velasco R, Alberti P, Bruna J, Psimaras D, Argyriou AA (2019) Bortezomib and other proteosome inhibitors-induced peripheral neurotoxicity: From pathogenesis to treatment *JPNS* 24 Suppl 2, S52-S62.

Velasco R, Petit J, Clapés V, Verdú E, Navarro X, Bruna J (2010) Neurological monitoring reduces the incidence of bortezomib-induced peripheral neuropathy in multiple myeloma patients *J Peripher Nerv Syst* 15, 17–25.

an Verheyen, Diels A, Dijkmans J, Oyelami T, Meneghello G, Mertens L, Versweyveld S, Borgers M, Buist A, Peeters P, Cik M (2015) Using Human iPSC-Derived Neurons to Model TAU Aggregation *PLoS One* 10, e0146127.

Vogl DT, Martin TG, Vij R, Hari P, Mikhael JR, Siegel D, Wu KL, Delforge M, Gasparetto C (2017) Phase I/II study of the novel proteasome inhibitor delanzomib (CEP-18770) for relapsed and refractory multiple myeloma *Leuk Lymphoma* 58, 1872–1879.

Volbracht C, Leist M, Nicotera P (1999) ATP controls neuronal apoptosis triggered by microtubule breakdown or potassium deprivation *Mol Med* 5, 477–489.

Waldmann T, Grinberg M, König A, Rempel E, Schildknecht S, Henry M, Holzer A-K, Dreser N, Shinde V, Sachinidis A, Rahnenführer J, Hengstler JG, Leist M (2017) Stem Cell Transcriptome Responses and Corresponding Biomarkers That Indicate the Transition from Adaptive Responses to Cytotoxicity *Chem Res Toxicol* 30, 905–922.

Waldmann T, Rempel E, Balmer NV, König A, Kolde R, Gaspar JA, Henry M, Hescheler J, Sachinidis A, Rahnenführer J, Hengstler JG, Leist M (2014) Design principles of concentration-dependent transcriptome deviations in drug-exposed differentiating stem cells *Chem Res Toxicol* 27, 408–420.

Wang M, Wang J, Tsui AYP, Li Z, Zhang Y, Zhao Q, Xing H, Wang X (2021) Mechanisms of peripheral neurotoxicity associated with four chemotherapy drugs using human induced pluripotent stem cell-derived peripheral neurons *Toxicol In Vitro* 77, 105233.

Wang X-M, Lehky TJ, Brell JM, Dorsey SG (2012) Discovering cytokines as targets for chemotherapy-induced painful peripheral neuropathy *Cytokine* 59, 3–9.

Webster RG, Brain KL, Wilson RH, Grem JL, Vincent A (2005) Oxaliplatin induces hyperexcitability at motor and autonomic neuromuscular junctions through effects on voltage-gated sodium channels *Br J Pharmacol* 146, 1027–1039.

Wheeler HE, Wing C, Delaney SM, Komatsu M, Dolan ME (2015) Modeling chemotherapeutic neurotoxicity with human induced pluripotent stem cell-derived neuronal cells *PLoS One* 10, e0118020.

White DM, Cousins MJ (1998) Effect of subcutaneous administration of calcium channel blockers on nerve injury-induced hyperalgesia *Brain Res* 801, 50–58.

Wickham H (2016) ggplot2. Elegant graphics for data analysis, Springer international publishing, New York.

Wilke CO (2020) Streamlined Plot Theme and Plot Annotations for 'ggplot2'. R package cowplot version 1.1.1. https://cran.r-project.org/web/packages/cowplot/index.html.

Wilson RH, Lehky T, Thomas RR, Quinn MG, Floeter MK, Grem JL (2002) Acute oxaliplatin-induced peripheral nerve hyperexcitability *J Clin Oncol* 20, 1767–1774.

Winer EP, Berry DA, Woolf S, Duggan D, Kornblith A, Harris LN, Michaelson RA, Kirshner JA, Fleming GF, Perry MC, Graham ML, Sharp SA, Keresztes R, Henderson IC, Hudis C, Muss H, Norton L (2004) Failure of higher-dose paclitaxel to improve outcome in patients with metastatic breast cancer: cancer and leukemia group B trial 9342 *J Clin Oncol* 22, 2061–2068.

Wing C, Komatsu M, Delaney SM, Krause M, Wheeler HE, Dolan ME (2017) Application of stem cell derived neuronal cells to evaluate neurotoxic chemotherapy *Stem Cell Res* 22, 79–88.

Wood JN, Boorman JP, Okuse K, Baker MD (2004) Voltage-gated sodium channels and pain pathways *J Neurobiol* 61, 55–71.

Woolf CJ, Ma Q (2007) Nociceptors--noxious stimulus detectors *Neuron* 55, 353–364.

Xiong C, Chua KC, Stage TB, Priotti J, Kim J, Altman-Merino A, Chan D, Saraf K, Canato Ferracini A, Fattahi F, Kroetz DL (2021) Human Induced Pluripotent Stem Cell Derived Sensory Neurons are Sensitive to the Neurotoxic Effects of Paclitaxel *Clin Transl Sci* 14, 568–581.

Yam MF, Loh YC, Tan CS, Khadijah Adam S, Abdul Manan N, Basir R (2018) General Pathways of Pain Sensation and the Major Neurotransmitters Involved in Pain Regulation *Int J Mol Sci* 19, 2164.

Yin K, Baillie GJ, Vetter I (2016) Neuronal cell lines as model dorsal root ganglion neurons: A transcriptomic comparison *Mol Pain* 12, 1–17.

Yong K, Gonzalez-McQuire S, Szabo Z, Schoen P, Hajek R (2018) The start of a new wave: Developments in proteasome inhibition in multiple myeloma *Eur J Haematol* 101, 220–236.

Young GT, Gutteridge A, Fox H de, Wilbrey AL, Cao L, Cho LT, Brown AR, Benn CL, Kammonen LR, Friedman JH, Bictash M, Whiting P, Bilsland JG, Stevens EB (2014) Characterizing human stem cell-derived sensory neurons at the single-cell level reveals their ion channel expression and utility in pain research *Mol Ther* 22, 1530–1543.

Yousuf MS, Maguire AD, Simmen T, Kerr BJ (2020) Endoplasmic reticulum-mitochondria interplay in chronic pain: The calcium connection *Mol Pain* 16, 1-20.

Yu Y-Q, Chen X-F, Yang Y, Yang F, Chen J (2014) Electrophysiological identification of tonic and phasic neurons in sensory dorsal root ganglion and their distinct implications in inflammatory pain *Physiol Res* 63, 793–799.

Zerboni L, Arvin A (2015) Neuronal Subtype and Satellite Cell Tropism Are Determinants of Varicella-Zoster Virus Virulence in Human Dorsal Root Ganglia Xenografts In Vivo *PLoS Pathog* 11, e1004989.

Zhang HY, Zheng LF, Yi XN, Chen ZB, He ZP, Zhao D, Zhang XF, Ma ZJ (2010) Slit1 promotes regenerative neurite outgrowth of adult dorsal root ganglion neurons in vitro via binding to the Robo receptor *J Chem Neuroanat* 39, 256–261.

Zhang X, Huang J, McNaughton PA (2005) NGF rapidly increases membrane expression of TRPV1 heat-gated ion channels *EMBO J* 24, 4211–4223.

Zhang Z-N, Freitas BC, Qian H, Lux J, Acab A, Trujillo CA, Herai RH, Nguyen Huu VA, Wen JH, Joshi-Barr S, Karpiak JV, Engler AJ, Fu X-D, Muotri AR, Almutairi A (2016) Layered hydrogels accelerate iPSC-derived neuronal maturation and reveal migration defects caused by MeCP2 dysfunction *Proc Natl Acad Sci USA* 113, 3185–3190.

Zheng H, Xiao WH, Bennett GJ (2012) Mitotoxicity and bortezomib-induced chronic painful peripheral neuropathy *Exp Neurol* 238, 225–234.

Zwick M, Davis BM, Woodbury CJ, Burkett JN, Koerber HR, Simpson JF, Albers KM (2002) Glial Cell Line-Derived Neurotrophic Factor is a Survival Factor for Isolectin B4-Positive, but not Vanilloid Receptor 1-Positive, Neurons in the Mouse *J Neurosci* 22, 4057–4065.